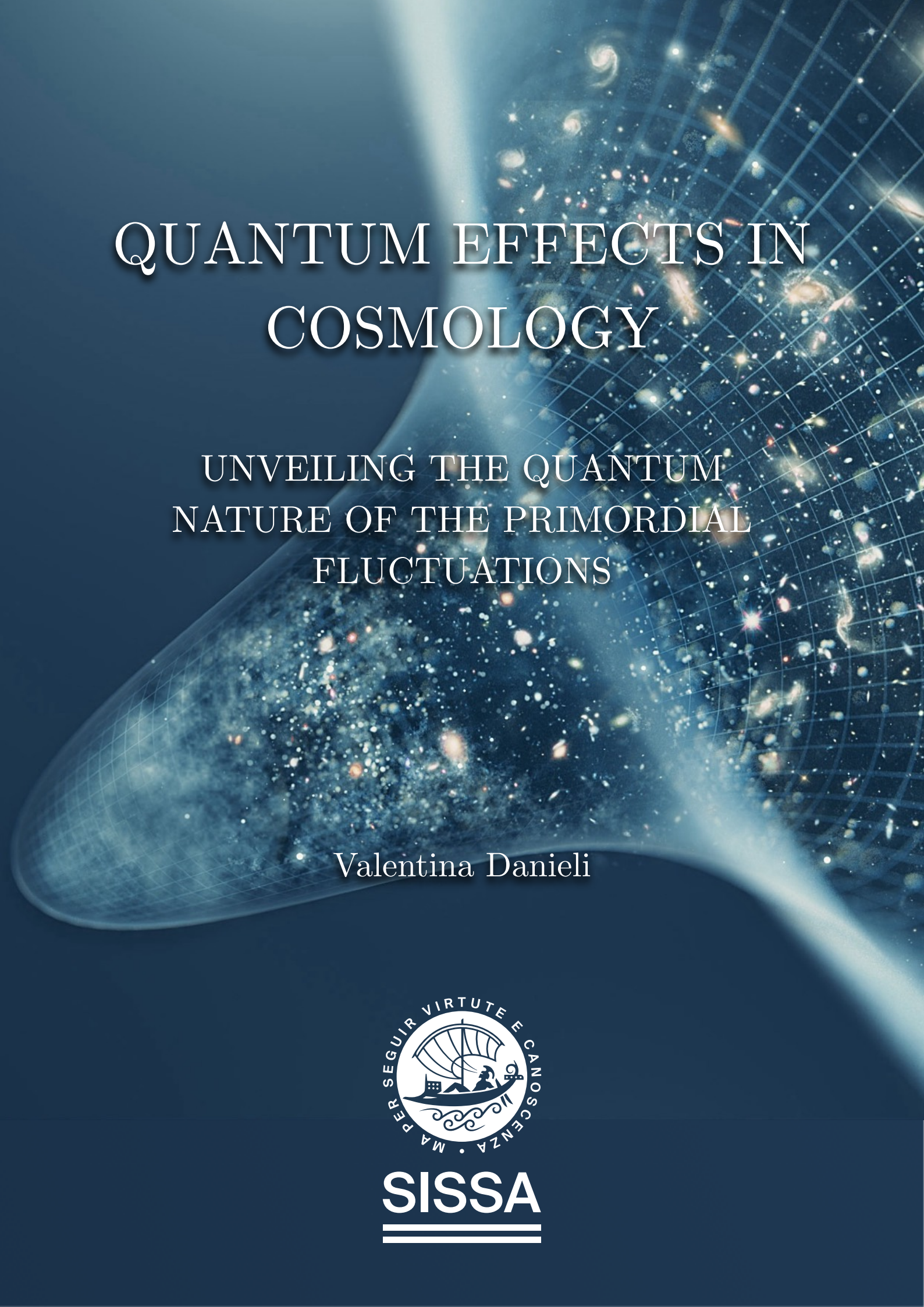


QUANTUM EFFECTS IN COSMOLOGY

UNVEILING THE QUANTUM NATURE OF THE PRIMORDIAL FLUCTUATIONS

Valentina Danieli

SISSA

The cover is taken from a picture by

Mike Zeng, for *Quanta Magazine*, an editorially independent online publication launched by the Simons Foundation in 2012
www.quantamagazine.org

INTERNATIONAL SCHOOL FOR ADVANCED STUDIES

PHYSICS AREA - PHD COURSE IN ASTROPARTICLE PHYSICS

PHD THESIS

QUANTUM EFFECTS IN COSMOLOGY

UNVEILING THE QUANTUM NATURE OF THE PRIMORDIAL FLUCTUATIONS

CANDIDATE:

VALENTINA DANIELI

CO-SUPERVISORS:

TAKESHI KOBAYASHI
SABINO MATARRESE
MATTEO VIEL

ACADEMIC YEAR 2023-2024



"We are not only the witnesses of the universe,
but its participants."

— Carl Sagan

ABSTRACT

It is commonly accepted in cosmology that a period of inflation took place in the Early Universe. This period of accelerated expansion provides the seeds for structure formation through vacuum fluctuations of the inflaton scalar field. These fluctuations get stretched by the quasi-exponential expansion of the Universe and become squeezed. The generation of perturbations out of the vacuum is a purely quantum phenomenon, however the Cosmological Microwave Background (CMB) measurements are analyzed within a classical framework, via ensemble averages of temperature anisotropies. Indeed, the two-point correlation functions of a squeezed Gaussian state can be obtained even with a classical stochastic description. Therefore the question of whether these fluctuations are really quantum mechanical or classical thermal fluctuations arises.

In this thesis, we explore the quantum effects in cosmology, focusing on the understanding of the quantum nature of the primordial fluctuations. We start with an overview of Big Bang cosmology and inflation. The work then delves into cosmological perturbation theory. Additionally, we interpret the amplification of the fluctuations in terms of cosmological particle creation, employing Bogoliubov transformations and the squeezing parameters to describe the dynamics of the system in an expanding Universe. We show how pairs of particles with opposite momenta are generated. The physical meaning and the geometrical interpretation of the squeezing parameters is provided.

The thesis then examines several criteria which can be used to test the "quantumness" of the inflationary perturbations, such as non-separability and quantum discord. After reviewing these criteria, the thesis focuses on the violation of Bell-like inequalities, which have been computed in the context of inflationary perturbations. My work contributes to the investigation of the origin of the cosmological perturbations by addressing the problem of the observability of the quantum features in a Bell type experiment on the Cosmic Microwave Background (CMB). In order to overcome some difficulties linked to the feasibility of such an experiment, the Leggett-Garg inequalities are studied. The Leggett-Garg inequalities give the correlations between the spin of the same system but measured at different times and they are computed for the cosmological perturbations.

Going beyond the Gaussian states description and introducing interactions, the quantum nature of the perturbations can be further tested by measuring the bispectrum, i.e. the three-point function. Indeed, the absence of poles in the bispectrum is shown to be an undeniable proof of the quantum mechanical mechanism generating the fluctuations. This work specifically takes into account the bispectrum of tensor perturbations generated during a de Sitter phase of inflation. The bispectrum computed considering the fluctuations to be quantum mechanical is compared with the classical three-point correlation function in order to find a difference between the two approaches.

The study performed in this thesis then extends to the treatment of axion perturbations, exploring their quantum mechanical description and evolution. Axions (or axion-like particles) are good candidates to test the quantumness of the perturbations, since they are produced via misalignment mechanism, possibly avoiding decoherence effects during the reheating phase after inflation. Moreover they naturally encode self-interactions thanks to their cosine potential. The consequences that a non-trivial evolution of the background axion field has on the squeezing of the perturbations are studied in details. This is the first step towards the analysis of the full bispectrum for the axion field, which could potentially provide a way to access the information on the quantumness of the perturbations.

Therefore, this thesis naturally aligns with the research programme of the quantum effects in cosmology.

PUBLICATIONS

The thesis is based on the following publications.

[P1] Valentina Danieli, Takeshi Kobayashi, Nicola Bartolo, Sabino Matarrese and Matteo Viel. 'Anharmonic effects on the squeezing of axion perturbations'. JCAP **04** (2024), p. 058. arXiv:2309.13112.

[P2] Valentina Danieli, Nicola Bartolo, Sabino Matarrese, Angelo Ricciardone and Matteo Viel. *Quantum Signatures in Graviton Bispectrum*. In preparation. 2024.

[P3] Valentina Danieli and Jerôme Martin. *Leggett-Garg Inequality Violation for the Cosmological Perturbations*. In preparation. 2024.

ACKNOWLEDGMENTS

This Thesis would not have been possible without the support of many people.

Firstly and foremost, I would like to express my deepest gratitude to my supervisors, Sabino Matarrese, Matteo Viel and Takeshi Kobayashi, whose support and guidance throughout the Ph.D. have been invaluable. Each of them gave me something unique, based on their different personalities and experiences in academia. Sabino's expertise, dedication, and seriousness have played a pivotal role in guiding my research endeavours and shaping my academic development. Matteo's insight illuminated the importance of fostering discussions and cultivating academic relationships and taught me the importance of believing in myself and in my work. Takeshi's deep commitment to academic excellence and meticulous attention to detail have significantly shaped my research.

I am very grateful to many people with whom I have had the opportunity to discuss the topics in this thesis as well as other related physics topics. Nicola Bartolo, who always found the time to discuss new ideas even if so busy, and who always give insightful advises; Angelo Ricciardone, who contributed with his numerical expertise; Jérôme Martin, who welcomed me in Paris and was always excited about every new step forward in our project; Vincent Vennin, always kind and willing to discuss the possible developments and progresses in our field of research. A special thanks to Amaury Micheli, a friend and an amazing physicist whom I had the luck to meet in a summer school. He helped me delving into the fascinating topic of the quantum effects in cosmology and this thesis would not be the same without our insightful discussions.

An honourable mention goes to SISSA and INFN. The collaborations that I had the opportunity to start with people abroad would not have been possible without their financial support. I am so grateful for all the schools, workshops and conferences I could attend; in particular the conference in Kyoto allowed me to meet Antonio De Felice, with whom I started a project recently and whom I thank for having been patient with me while I was writing this manuscript.

I wish to devote special thanks to all the people in Trieste, whom I know since I was a little child; among all Giorgia, Massimo and Filippo. Without your constant help my life in Trieste would have been harder. Thank you for making me feel at home.

These years were enriched by the amazing people I met in SISSA and in Trieste, and who have turned into incredibly warm and supportive friends. A special thanks to my "APP" fellows, Vania, Delpo, Daniele and Diego. Working in academia can be tough sometimes, but going through this journey with them has made it easier. I am also infinitely thankful to the girls with whom I shared one of the most amazing trips in my life: besides the already mentioned Vania, also Maria Vittoria and Fabiana. My experience in Iceland was so incredible also thanks to them. Moreover, I would be remiss in not mentioning my

volleyball teammates: Isabella, Dario, Franci, Jack, Alessio, Emma, Tadeo, Po, Costi, Carlos, Andrea and others. I am so grateful for having had the chance to play the sport I love with them in these years (and having defeated Amicici). Even if I left SISSA frustrated or demotivated sometimes, playing with them and laughing together always cheered me up. Many other people contributed in making this journey so special: Giulio, Fraga, Max, Cristiano, Stephane, Andrea, Giovanni, Giuà and many others. They were part of my life in these four years and I truly wish them the best for the future. A huge thank you also to Beatrice, the friend of a lifetime; the long phone calls with you made me smile even in the heaviest moments.

Last but not least, my family. All of this would not have been possible without the support, encouragement and love from my parents. Dad, you are always ready to downsize my anxieties and worries, reminding me what is really important. You are a solid pillar, always present and available, being of comfort whatever happens. Mom, you have always faced the difficulties you encountered head on, teaching me the meaning of the word resilience. You have always helped me with your rational way of dealing with problems. Sometimes misunderstood, but you were always there when I needed you. For this, and much more, thank you.

RICONOSCIMENTI

Questa tesi non sarebbe stata possibile senza il supporto di molte persone.

Innanzitutto, desidero esprimere la mia più profonda gratitudine ai miei relatori, Sabino Matarrese, Matteo Viel e Takeshi Kobayashi, il cui sostegno e la cui guida durante il dottorato sono stati inestimabili. Ognuno di loro mi ha dato qualcosa di unico, basato sulle loro diverse personalità ed esperienze accademiche. L'esperienza, la dedizione e la serietà di Sabino hanno svolto un ruolo fondamentale nell'orientare i miei sforzi di ricerca e plasmare il mio sviluppo accademico. La visione di Matteo ha sottolineato l'importanza di favorire discussioni e coltivare relazioni accademiche, e mi ha insegnato l'importanza di credere in me stessa e nel mio lavoro. Il profondo impegno di Takeshi verso l'eccellenza accademica e la meticolosa attenzione ai dettagli hanno significativamente influenzato la mia ricerca.

Sono molto grata a tante persone con le quali ho avuto l'opportunità di discutere i temi trattati in questa tesi, così come altri argomenti legati alla fisica. Nicola Bartolo, che ha sempre trovato il tempo per discutere nuove idee nonostante i suoi impegni, e che mi ha sempre dato consigli preziosi; Angelo Ricciardone, che ha contribuito con la sua competenza numerica; Jérôme Martin, che mi ha accolto a Parigi e che era sempre entusiasta per ogni nuovo progresso nel nostro progetto; Vincent Vennin, sempre gentile e disponibile a discutere i possibili sviluppi e progressi nel nostro campo di ricerca. Un ringraziamento speciale va ad Amaury Micheli, un amico e un fisico straordinario che ho avuto la fortuna di incontrare in una scuola estiva. Mi ha aiutata ad approfondire l'affascinante tema degli effetti quantistici in cosmologia e questa tesi non sarebbe la stessa senza le nostre illuminanti discussioni.

Una menzione d'onore va alla SISSA e all'INFN. Le collaborazioni che ho avuto l'opportunità di avviare con persone all'estero non sarebbero state possibili senza il loro supporto finanziario. Sono molto grata per tutte le scuole, i workshop e le conferenze a cui ho potuto partecipare; in particolare la conferenza a Kyoto mi ha permesso di incontrare Antonio De Felice, con cui ho recentemente avviato un progetto e che ringrazio per la sua pazienza durante la stesura di questo scritto.

Desidero dedicare un ringraziamento speciale a tutte le persone di Trieste, che conosco sin da quando ero bambina; tra tutti, Giorgia, Massimo e Filippo. Senza il vostro costante aiuto la mia vita a Trieste sarebbe stata più difficile. Grazie per avermi fatta sentire a casa.

Questi anni sono stati arricchiti dalle persone straordinarie che ho incontrato in SISSA e a Trieste, e che sono diventate amici affezionati su cui poter contare. Un riconoscimento speciale va ai miei compagni di "APP", Vania, Delpo, Daniele e Diego. Lavorare in ambito accademico può essere difficile a volte, ma affrontare questo percorso con loro lo ha reso più facile. Sono anche infinitamente grata alle ragazze con cui ho condiviso uno dei viaggi più belli della mia vita: oltre alla già menzionata Vania, anche Maria Vittoria e Fabiana. La mia es-

perienza in Islanda è stata così incredibile anche grazie a loro. Inoltre, sarebbe una mancanza non menzionare i miei compagni di squadra di pallavolo: Isabella, Dario, Franci, Jack, Alessio, Emma, Tadeo, Po, Costi, Carlos, Andrea e altri. Sono molto grata di aver avuto la possibilità di giocare lo sport che amo con loro in questi anni (e di aver sconfitto gli Amicici). Anche se a volte uscivo dalla SISSA frustrata o demotivata, giocare con loro e ridere insieme mi ha sempre sollevato il morale. Molte altre persone hanno contribuito a rendere questo percorso così speciale: Giulio, Fraga, Max, Cristiano, Stephane, Andrea, Giovanni, Giuà e molti altri. Sono stati parte della mia vita in questi quattro anni e auguro loro il meglio per il futuro. Un enorme grazie anche a Beatrice, l'amica di una vita; le lunghe telefonate con te mi hanno fatta sorridere anche nei momenti più difficili.

Ultima, ma non meno importante, la mia famiglia. Tutto questo non sarebbe stato possibile senza il supporto, l'incoraggiamento e l'amore dei miei genitori. Papà, sei sempre pronto a ridimensionare le mie ansie e preoccupazioni, ricordandomi ciò che è veramente importante. Sei un pilastro solido, sempre presente e disponibile, di conforto qualunque cosa accada. Mamma, hai sempre affrontato le difficoltà che hai incontrato a testa alta, insegnandomi il significato della parola resilienza. Mi hai sempre aiutata con il tuo modo razionale di affrontare i problemi. A volte incompresa, ma sei sempre stata lì quando avevo bisogno di te. Per questo, e molto altro, grazie.

CONTENTS

1 INTRODUCTION 1

I BACKGROUND 7

2 FROM THE BIG BANG COSMOLOGY TO INFLATION 9
- 2.1 Spacetime Geometry and Dynamics . . . 9
- 2.2 The Homogeneous Universe . . . 10
  - 2.2.1 Cosmological Distances and Conformal Time . . . 11
  - 2.2.2 Friedmann equations . . . 14
  - 2.2.3 Standard Model of Big Bang Cosmology . . . 16
    - 2.2.3.1 Thermal History of the Universe . . . 18
    - 2.2.3.2 Experimental Confirmations and Limits of the ΛCDM model . . . 20
- 2.3 Big Bang Puzzles . . . 23
  - 2.3.1 Horizon Problem . . . 23
  - 2.3.2 Flatness Problem . . . 23
  - 2.3.3 Monopoles Problem . . . 25
- 2.4 Cosmic Inflation . . . 25
  - 2.4.1 A Solution to the Big Bang Puzzles . . . 26
    - 2.4.1.1 Horizon Problem . . . 26
    - 2.4.1.2 Flatness Problem . . . 28
    - 2.4.1.3 Monopoles Problem . . . 29
  - 2.4.2 de Sitter Inflation . . . 29
  - 2.4.3 Single Field Slow-Roll Inflation . . . 30
  - 2.4.4 Reheating . . . 33

3 COSMOLOGICAL PERTURBATIONS THEORY 35
- 3.1 SVT Decomposition of Metric Perturbations . . . 36
- 3.2 Gauge - Invariant Variables . . . 36
- 3.3 Coupling with the Inflaton Perturbations . . . 37
- 3.4 Evolution of the Inflationary Perturbations . . . 39
- 3.5 Quantum Initial Conditions . . . 42
- 3.6 Link with the Observables . . . 44

4 PARTICLE CREATION AND SQUEEZING 49
- 4.1 Bogoliubov Transformations . . . 49
- 4.2 Particle Creation in an Expanding Background . . . 50
  - 4.2.1 Cosmological Perturbations in a Hydrodynamical Era . . . 51
  - 4.2.2 Number of Particles and Energy Density . . . 52
- 4.3 Squeezed States Formalism . . . 53
  - 4.3.1 Squeezing Parameters . . . 53
  - 4.3.2 Physical Interpretation of the Squeezing Parameters . . . 53
    - 4.3.2.1 Wave Function of a Two-Mode Squeezed State . . . 55
    - 4.3.2.2 Squeezed State in Phase Space . . . 55
  - 4.3.3 Link with the Observables . . . 57

II UNDERSTANDING THE NATURE OF THE COSMOLOGICAL PERTURBATIONS 59
5 CLASSICALITY CRITERIA 61
5.1 Classicality of the Two-point Correlation Functions 61
5.1.1 Partitions 62
5.1.2 Covariance Matrix 63
5.1.3 Classical Stochastic Description and Wigner Function . . 65
5.1.4 Wave Function of a Two-Mode Squeezed State 67
5.1.5 Two-Point Correlation Functions 68
5.2 Classicality Criteria 69
5.2.1 Positivity of the Wigner Function 70
5.2.2 Quantum Separability 71
5.2.3 Quantum Discord 71
6 COSMOLOGICAL BELL INEQUALITIES 75
6.1 Bell Inequality in Quantum Mechanics 75
6.2 Bell Inequality Violation for Different Pseudo-Spin Operators . . 77
6.2.1 Banaszek-Wodkiewicz (BW) Spin Operators 77
6.2.2 Gour-Khanna-Mann-Revzen (GKMR) Spin Operators . . . 78
6.2.3 Larsson Spin Operators 79
6.3 Bell Inequality Violation and the Positivity of the Wigner Function 81
6.4 Measurability of the Pseudo-Spin Operators 81
6.5 Leggett-Garg Inequalities 82
6.6 Leggett-Garg Inequalities for the Cosmological Perturbations . . 84
7 NON-GAUSSIANITIES 91
7.1 Non - Gaussianity in the Inflationary Perturbations 91
7.2 Computational Tools for the Bispectrum 94
7.2.1 In-In Formalism 94
7.2.2 Green's Function Method 96
7.3 Quantum Signatures in Scalar Bispectrum 99
7.3.1 Gaussian Fields 101
7.3.2 Non-gaussianities 101
7.4 Quantum Signatures in Graviton Bispectrum 102
7.4.1 Gaussian Fields 103
7.4.2 Non-gaussianities 104
7.4.2.1 Quantum Approach 105
7.4.2.2 Classical Approach 107
8 SQUEEZING OF AXIONS PERTURBATIONS 111
8.1 Quantization of Axions Fluctuations 112
8.1.1 Setup 112
8.1.2 Canonical Quantization 113
8.1.3 Bogoliubov Coefficients 115
8.1.4 Squeezing Parameters 115
8.2 Background Evolution 116
8.3 Evolution of Axions Fluctuations 117
8.3.1 Mode Functions 117
8.3.2 Bogoliubov Coefficients 119
8.3.2.1 Adiabaticity Condition 121

8.3.2.2 Enhancement in the Number of Particles 122
8.3.2.3 Parameter Dependence 123
8.3.2.4 Alternative Calculation for $|\beta_k|^2$ 124
8.3.3 Squeezing Parameters 127
8.4 Summary of the Main Results 127
8.5 Appendix A: Quadratic Potential 129
8.5.1 Mode Functions 130
8.5.2 Asymptotic $|\beta_k|^2$ 131
8.6 Appendix B: More Realistic Models for the Evolution of the Universe 132
8.6.1 Smooth Reheating 132
8.6.2 Single Field Inflation 134
9 CONCLUSIONS AND OUTLOOK 135

BIBLIOGRAPHY 139

Figure 1 Time evolution of the energy density. 17
Figure 2 Graphical representation of the horizon problem. 24
Figure 3 Graphical representation of the solution to the horizon problem. 27
Figure 4 Evolution of the comoving Hubble radius in time. 28
Figure 5 CMB map as measured by the satellite Planck. 35
Figure 6 Time evolution of the curvature perturbations. 41
Figure 7 Squeezing of the vacuum state. 56
Figure 8 Squeezing of a coherent state. 56
Figure 9 Non-separability and discord for mixed states. 73
Figure 10 Setup for a Bell experiment. 76
Figure 11 Bell inequality violation. 79
Figure 12 Relevant triangle configurations for the bispectrum. . . . 93
Figure 13 Correlations from a quantum vacuum or a thermal bath. 100
Figure 14 Time evolution of the background axion field and of the background energy density. 117
Figure 15 Asymptotic value of the energy density of the background axion field. 118
Figure 16 Evolution in time of the amplitude of the mode functions of the axion perturbations. 119
Figure 17 Evolution in time of the modulus square of the β_k - coefficient of the axion perturbations. 119
Figure 18 Asymptotic value of $|\beta_k|^2$. 123
Figure 19 Asymptotic value of the Bogoliubov coefficient $|\beta_k|^2$ in function of the parameters. 124
Figure 20 Time evolution of the squeezing parameters. 128
Figure 21 Time evolution of $|\beta_k|^2$ for instantaneous reheating and smooth reheating. 133
Figure 22 Time evolution of $|\beta_k|^2$ in a quasi de Sitter inflationary background. 133

ACRONYMS

GR	General Relativity
SR	Special Relativity
WEP	Weak Equivalence Principle
EEP	Einstein Equivalence Principle
FLRW	Friedmann-Lemaître-Robertson-Walker
dS	de Sitter
QFT	Quantum Field Theory
CMB	Cosmic Microwave Background
LSS	Last Scattering Surface
ΛCDM	Lambda Cold Dark Matter
CDM	Cold Dark Matter
SM	Standard Model
GUT	Grand Unified Theory
DM	Dark Matter
BBN	Big Bang Nucleosynthesis
BSM	Beyond the Standard Model
DE	Dark Energy
ALPs	axion-like particles
LGI	Leggett-Garg Inequality
BW	Banaszek-Wodkiewicz
GKMR	Gour-Khanna-Mann-Revzen
BD	Bunch-Davies
WKB	Wentzel–Kramers–Brillouin

1 INTRODUCTION

The field of cosmology stands at the intersection of observational astronomy and theoretical physics, aiming to understand the origins, evolution, and ultimate fate of the universe. Over the past few decades, significant strides have been made in this domain, particularly with the advent of precision cosmology. These advances have enabled us to explore the very earliest moments of the universe with unprecedented clarity. Central to this exploration is the study of the inflationary scenario. The current version of the standard cosmological model assumes that the Universe underwent a period of inflation, a rapid exponential expansion in its earliest stage, which solves several puzzles of the Big Bang cosmological scenario. Inflation also provides a mechanism for the generation of primordial fluctuations as a combination of the perturbations of spacetime geometry, i.e. the metric, and of the scalar field driving inflation, the inflaton field. These fluctuations get stretched by the rapid expansion of spacetime and become the seeds of all structures in the universe, from galaxies to the CMB anisotropies. In most inflationary models, these fluctuations have a quantum origin, however the CMB sky we observe today is analyzed with purely classical techniques. Therefore the question about the quantum or classical origin of the initial perturbations and how to probe it arises. Is it quantum mechanics really necessary to explain the anisotropies in the CMB or is a classical analysis enough, thereby questioning the quantum origin of the fluctuations? What specific properties would be overlooked if the analysis were conducted entirely within a classical description?

The classicalization of a quantum perturbation has been a subject of active research (see for example [1–6]). In [1] it has been shown how inflation itself provides an explanation for the classicalization of the originally quantum perturbations: they are squeezed due to the fast expansion of the Universe. A squeezed state is a special quantum state for which one variable has an arbitrarily small uncertainty, while its conjugate counterpart has a very big uncertainty, correspondingly. The authors argued how in the limit of large squeezing the commutators between the position and momentum of the perturbations vanish, hinting at a classicalization of the perturbations. However this conclusion is misleading and it has been proved in [7] how assuming the state to be classical would lead to some mathematical inconsistencies. Indeed, since squeezed states are associated with a huge uncertainty in one variable, they are highly quantum mechanical states [8]. Their quantum behaviour cannot be fully accounted for with a classical description.

It is however true that, considering the primordial fluctuations as stochastic rather than quantum, results in nearly identical outcomes. It has been shown in [9] that the correlation functions of the two-mode squeezed state describing the Gaussian cosmological perturbations of opposite momenta are exactly reproduced by a classical stochastic distribution, up to corrections which are in

practice negligible. It turns out the power spectrum, i.e. the two-point function, computed in a quantum framework is exactly the same as the one computed in a classical stochastic framework. Higher order (even) correlators depend instead on the amount of squeezing; the more squeezed the state is, the smaller are the deviations from the quantum results. In the cosmological framework the perturbations are highly squeezed, so that the deviations tend to vanish.

How can we then prove the quantum nature of the perturbations? This question is especially pertinent now, as recent advancements in quantum information theory provide new methods directly applicable to this issue. One example is provided by quantum discord [10–12]. It is defined as the difference between two alternative ways of computing the correlations between two sub-systems of a Hilbert space. Classically, these two ways coincide and the quantum discord vanishes, while for a quantum mechanical system the two ways are different and the quantum discord is then different from zero. Quantum discord is not the only criterion which relies on the splitting of the Hilbert space into two-subsystems. Another example is provided by quantum separability [13]: a state in the Hilbert space is said to be separable if its density matrix can be written as the product of the density matrices of the two subsystems. Non-separability is an intrinsic quantum mechanical feature. Splitting the Hilbert space into sub-systems is not the only way the classical or quantum nature can be tested. An alternative method is to make use of the phase-space description of quantum mechanics. In this picture, the evolution of the states can be described using the so-called *Wigner function*, i.e. a probability density function given by the Weyl transform of the density matrix. Interference terms, which are typical of a quantum mechanical system, induce oscillations in the Wigner function, causing it to be negative for some values of the field and its momentum. Therefore one "classicality" criterion often used is the positivity of the Wigner function. All these criteria assess the quantum nature of the perturbations and some of them have been compared in [14]. Specifically, non-separability and quantum discord have been compared in a simple class of Gaussian perturbations. The authors discovered that these criteria, although not always equivalent, attest the quantum nature of the fluctuations in the large squeezing limit, which is the case in the cosmological context.

Albeit hinting at the quantum nature of the fluctuations, the aforementioned criteria do not have a direct way to be measured. There is however another extremely useful criterion to test the cosmological perturbations, the well known Bell inequalities [15–17]. Bell inequalities have been extensively studied in the literature in the context of cosmological perturbations [18–24]. In the cosmological context, an analogous of spin operators can be defined from a field, like the scalar perturbation, and its conjugate momentum. The Bell operator can then be constructed from the correlators between two spins, related to two different subsystems of the Hilbert space. In both [19] and [23] the authors found that the Bell inequality is violated for some values of the squeezing parameters, i.e. those parameters giving the amount of squeezing of the state. The question of the measurability of these spin operators is also addressed. In fact, in order to compute the Bell inequality the knowledge of the spin operators along two different components is required. However, in the cosmological

context, we have access to only one spin operator. This is linked to the fact we can perform measurements of just one Universe, and we cannot measure ζ'_k, being it vanishing. One alternative is to design an experiment which relies only on the measurements of one spin component. This is what is done in the Leggett-Garg Inequality (LGI) [25–27], for which the correlators are built within the same spin operator but measured at different times. The analysis of the violation of such inequalities in the context of the cosmological perturbations is a relevant step in the study of their quantum nature and have been addressed in my work [28].

All the aforementioned criteria have been applied on Gaussian, i.e. free, states, but this investigation could be extended to non-Gaussian states. When interaction terms are taken into account, the behaviour of the system under quantum criteria is different. For example, assuming the state to be pure, the Wigner function is necessarily non-positive [29]. Furthermore, non-Gaussian states have non-vanishing odd higher-order correlation functions. The bispectrum, i.e. the three-point function, could provide an undeniable signature of the quantum nature of the perturbations. It has been shown in [30] for scalar perturbations that the absence of poles in the physical momenta is a typical characteristic of vacuum fluctuations; assuming locality to hold, no classical theory can reproduce the same results. In this thesis the computation of the bispectrum of tensor perturbations is reported from my work [31], where a comparison between the quantum result and the classical result has been carried out.

Notice that up to this point a minimal setup with a single scalar field generating inflation was considered. In principle there could be more complicated situations, such as multi-field inflation [32]. In this case isocurvature perturbations could source the curvature perturbations, changing the results here mentioned. Furthermore, the coupling with other scalar fields leads to decoherence effects, which cause effectively the classicalization of the system [33–36]. Notice that also the thermal bath produced during the reheating by the decay of the inflaton field leads to the decoherence of the inflationary perturbations [37]. Another source of decoherence is provided by gravitational interactions, which couple super-Hubble cosmological fluctuations with unobserved shorter-wavelength scalar and tensor modes. This effect is already present during inflation driven by a single scalar field and it turns out it fully classicalizes the system if the perturbations stay outside the horizon for at least more or less 10 e-folds [38]. The decoherence can be taken into account studying the quantumness criteria in function of the purity, a variable quantifying the amount of mixing of the state. The analysis of quantum discord in the presence of decoherence is addressed for example in [24]. The authors found there is no simple relationship between discord and decoherence. There are indeed two competing effects which have to be taken into account: the increasing of the squeezing amplitude and the decreasing of the purity due to the decoherence effects. In principle it is possible to have a decohered and non-discordant state, as well as a decohered but still discordant state. Therefore, even though decoherence might influence our capability to detect quantum correlations in a specific quantum system, this impact cannot be straightfor-

wardly measured by just examining the degree of decoherence, i.e. the purity of the state. Nonetheless, if the classicalization process is effective, a detection of quantum signatures becomes surely more cumbersome. One possible simplification consists in studying spectator fields, which do not couple to the inflaton field and hence are no subject to decoherence due to the interaction terms. The classicalization due to the gravitational interactions in these circumstances is still under study and it is not clear whether it is effective for a spectator field as it is for the inflaton field.

In this framework axions and axion like particles are potentially good candidates to test the quantumness of the perturbations. Being produced via misalignment mechanism, they could evade the decoherence due to the coupling with the thermal bath produced during the reheating phase. Furthermore they naturally encompass self-interactions, thus providing a fruitful setup to analyze the bispectrum. These are the reasons why in [39] we analyzed the time evolution of axion perturbations in the presence of self-interactions. The effect of a non-trivial background on the squeezing of the perturbations has been studied and the first steps into the understanding of quantum features in spectator fields have been moved.

This thesis is devoted to the study of the quantumness of the cosmological perturbations. My original work has been integrated into the existing literature on this subject. Specifically, my paper [28] is presented as the natural continuation on the topic of cosmological Bell inequalities in Chapter 6; my work [31] on the gravitons non-Gaussianity is reported as an extension of [30] in Chapter 7; finally, the article [39] on the evolution of axion perturbations in the presence of a non-trivial background due to the self-interaction terms is presented as a first step in the analysis of axion fields as quantum tracers in Chapter 8.

The thesis comprises two parts: Part i collects background material on the topic of Lambda Cold Dark Matter (ΛCDM) model and inflation and explains the generation of cosmological perturbations, as well as their evolution in time. In particular the amplification of the fluctuations during inflation is explained in terms of particle creation by an expanding spacetime. Part ii is devoted to the analysis of several "quantumness" criteria, such as the non-positivity of the Wigner function, the non-separability of the states and quantum discord. Particular attention is paid to the cosmological Bell inequalities. Furthermore the effect of interactions, i.e. non-Gaussianities, on the detection of quantum signatures in the fluctuations is discussed.

Specially, Chapter 2 reviews the homogeneous Universe. The Hot Big Bang model is introduced, starting from the Friedmann equations and the dynamics of the Universe. It then delves into the thermal history of the Universe and the experimental confirmations of the ΛCDM model. The Big Bang puzzles are then presented, in order to show why cosmic inflation has been firstly introduced. The chapter closes with a discussion on single-field inflation and the reheating phase.

Chapter 3 introduces the anisotropies on the CMB. The inflationary perturbations are presented in a gauge invariant formalism; their evolution during a de Sitter (dS) and and quasi - de Sitter expansions is then studied. The fluc-

tuations are enhanced when their wavelength is stretched on super-Hubble scales, while the curvature perturbations remain constant. The chapter then proceeds with the description of the quantum initial conditions, presenting the Bunch-Davies (BD) vacuum. It closes providing a link between the power spectrum of the curvature perturbations at the end of inflation and the two-point correlation functions in the temperature anisotropies of the CMB.

Chapter 4 looks at the time evolution of the perturbations under a different perspective. The amplification of the modes outside the horizon is interpreted in terms of cosmological particle creation. Pair of particles with opposite momenta are created due to the expansion of spacetime. The concepts of Bogoliubov coefficients and squeezing parameters are introduced. It is shown how the Hilbert space of cosmological perturbations can be split into sub-spaces of particles with opposite momenta. The state describing these sub-systems evolves from a vacuum state to a two-mode squeezed state. The description in phase space of the time evolution of the system is provided, as well as a physical interpretation of the squeezing parameters.

Chapter 5 opens Part ii by explaining the different partitions with which one can split the Hilbert space and how the physical quantities introduced so far depend on the choice of partition. The classical stochastic description in terms of the Wigner function is then presented, together with the reason why the two-point functions of the quantum perturbations can be perfectly mimicked with the classical stochastic formalism. The positivity of the Wigner function, the non-separability and the quantum discord are then analyzed in order to address the problem of detecting quantum signatures.

Chapter 6 expands the study of the quantumness of the perturbations by discussing the cosmological Bell inequalities. The concept of pseudo-spin operators for continuous variable systems is introduced and a violation of the Bell inequality is found for certain values of the squeezing parameters. This chapter presents then the LGI as a way to overcome the observational difficulties linked with the Bell inequalities. My original work [28] analysing the violation of the LGI for the cosmological perturbations is reported.

Chapter 7 goes beyond the Gaussian (free) fields studied until Chapter 6 and studies the effect of interactions. The concepts of non-Gaussianities and bispectrum are presented, first as a general theory for the cosmological perturbations and then as useful tools for the detection of quantum signatures. It is shown how the absence of poles in the bispectra is a clear hint of the quantum origin of the cosmological perturbations. The computation for the bispectrum of the primordial gravitational waves carried out in my work [31] is given in details.

The following Chapter 8 is focused on the results of my article [39], i.e. the evolution of axion-like particles in an expanding Universe. Being useful tools for the detection of quantum traces, a careful analysis of the effect of the self-interaction on their evolution is required. This chapter delves into the consequences that a non-trivial evolution of the background axion field has on the squeezing of the perturbations. An enhancement of the squeezing amplitude in function of the initial misalignment angle for the axion field is found. This effect is crucial and has to be taken into account when trying to evaluate the full bispectrum of axion-like particles.

Finally, Chapter 9 collects our final comments and closes the thesis.

CONVENTIONS The convention we use for the signature of the metric is $(-,+,+,+)$. Spacetime indices run from 0 to 3 and are denoted with Greek letters $\mu, \nu, \ldots$, while space indices run from 1 to 3 and are denoted with Latin letters $i, j, \ldots$. We use "geometrodynamics units" in which $c = G = k_B = 1$. Other conventions will be specified in the text when needed.

ON COMPUTER ALGEBRA SOFTWARE Some of the results in this thesis have been obtained using the Wolfram *Mathematica* software.

Part I

BACKGROUND

2

FROM THE BIG BANG COSMOLOGY TO INFLATION

We begin our discussion with an introduction on Cosmology and specifically on Inflation. This is a standard introduction, based on several textbooks [40–44].

2.1 SPACETIME GEOMETRY AND DYNAMICS

Cosmology studies the origin and the evolution of the Universe, spanning from the Big Bang to the present day and on into the future. The physical foundation of cosmology is General Relativity (GR), the theory of gravity formulated by Einstein [45] that best agrees with the observations and has been tested in a large number of situations that range from laboratory up to astrophysical distances. This section is devoted to the introduction of the elements of GR that will be useful to understand the discussion in this manuscript.

General Relativity is based on the Equivalence Principle. There is a variety of different formulations of the Equivalence Principle, the first of which is the Weak Equivalence Principle (WEP), stating the universality of free fall. Einstein generalized the WEP to what is known as the Einstein Equivalence Principle (EEP), asserting that the laws of physics are equivalent to those of Special Relativity (SR) in sufficiently small regions of spacetime. This implies that locally spacetime is flat and the metric $g_{\mu\nu}$, i.e. the mathematical object transforming spacetime coordinates $x^\mu = (t, x^i)$ into the invariant line element

$$ds^2 = g_{\mu\nu} x^\mu x^\nu \,, \tag{1}$$

is locally the Minkowski metric $\eta_{\mu\nu} = \mathrm{diag}(-1, 1, 1, 1)$. The metric $g_{\mu\nu}$ is in general coordinates dependent. Spacetime is thus a mathematical structure that resembles locally the Minkowski space but exhibits nontrivial curvature over extended regions. The object that possesses these properties is a Lorentzian manifold $\mathcal{M}$, i.e. a set of points such that in each point of $\mathcal{M}$ one can define an open neighbourhood which has a continuous one-to-one map onto an open set of $\mathbb{R}^4$. A manifold $\mathcal{M}$ equipped with a metric $g_{\mu\nu}$ encodes all the information about the geometry of spacetime. The metric is a dynamical object and its evolution depends on the matter content of spacetime. The field equations governing its dynamics are the Einstein equations given by

$$G_{\mu\nu} = 8\pi T_{\mu\nu} \,, \tag{2}$$

where $T_{\mu\nu}$ is the stress-energy tensor describing the matter distribution, while $G_{\mu\nu}$ is the Einstein tensor

$$G_{\mu\nu} = R_{\mu\nu} - \frac{1}{2} g_{\mu\nu} R \,, \tag{3}$$

$R = R^{\mu}{}_{\nu}$ is the Ricci scalar and $R_{\mu\nu} = R^{\alpha}{}_{\mu\alpha\nu}$ the Ricci tensor. The Riemann tensor $R^{\alpha}{}_{\mu\beta\nu}$ is given in terms of the Levi-Civita connection $\Gamma^{\alpha}{}_{\mu\nu}$ which is built with the first derivatives of the metric $g_{\mu\nu}$:

$$R^{\alpha}{}_{\mu\beta\nu} = \partial_{\beta}\Gamma^{\alpha}{}_{\nu\mu} - \partial_{\nu}\Gamma^{\alpha}{}_{\beta\mu} + \Gamma^{\alpha}{}_{\beta\lambda}\Gamma^{\lambda}{}_{\nu\mu} - \Gamma^{\alpha}{}_{\nu\lambda}\Gamma^{\lambda}{}_{\beta\mu}\,, \tag{4}$$

$$\Gamma^{\alpha}_{\mu\nu} = \frac{1}{2}g^{\alpha\sigma}\left(\partial_{n}ug_{\sigma\mu} + \partial_{\mu}g_{\sigma\nu} - \partial_{\sigma}g_{\mu\nu}\right)\,. \tag{5}$$

A formal derivation of the Einstein field equations relies on the variational principle, i.e. varying an action with respect to the dynamical fields. The total action is given by

$$S = S_{EH} + S_{m}\,, \tag{6}$$

where S_{EH} is the Einstein-Hilbert action for gravity

$$S_{EH} = \frac{1}{16\pi}\int d^{4}x\sqrt{-g}R\,, \tag{7}$$

with g the determinant of the metric and S_m the action describing the matter-energy content:

$$S_{m} = \int d^{4}x\sqrt{-g}\mathcal{L}_{m}\,. \tag{8}$$

Einstein field equations are obtained upon defining the stress-energy tensor $T_{\mu\nu}$ as:

$$T_{\mu\nu} = -\frac{2}{\sqrt{-g}}\frac{\delta S_{m}}{\delta g^{\mu\nu}}\,. \tag{9}$$

Once the matter-energy content of the spacetime is known, one can solve equation (2) to get the metric $g_{\mu\nu}$. The geodesic equation

$$\frac{d^{2}x^{\mu}}{du^{2}} + \Gamma^{\mu}{}_{\alpha\beta}\frac{dx^{\alpha}}{du}\frac{dx^{\beta}}{du} = 0\,, \tag{10}$$

with u an affine parameter, is then used to compute the paths of particles and radiation (geodesics) within the derived spacetime geometry.

2.2 THE HOMOGENEOUS UNIVERSE

Having introduced the necessary tools of GR, we proceed to derive and solve the equations that describe the large scale structures and the evolution of the Universe. Cosmology is based on the so called *Cosmological Principle* [46], stating that the Universe on scales larger than ~ 150 Mpc is homogeneous and isotropic. This postulate is an extension of the Copernican principle to the whole Universe and it is supported for example by observations of the local density of matter. As we consider increasingly larger scales, the density decreases until it levels off at a constant value at scales larger than the homogeneity scale.

Moreover at scales larger than $\sim$ 150 Mpc we do not observe any privileged direction.

The metric which implements mathematically the conditions of homogeneity and isotropy is the Friedmann-Lemaître-Robertson-Walker (FLRW) metric. In spherical *co-moving* coordinates it reads:

$$ds^2 = -dt^2 + a(t)^2 \left(\frac{dr^2}{1 - \mathcal{K} r^2} + r^2 d\theta^2 + r^2 \sin^2\theta \, d\phi^2 \right) , \tag{11}$$

where $a(t)$ is called *scale factor* and $\mathcal{K}$ sets the curvature, and therefore the size, of the spatial surfaces. Depending on the value of $\mathcal{K}$, the spacetime could be open ($\mathcal{K} = -1$), flat ($\mathcal{K} = 0$), or closed ($\mathcal{K} = 1$). Specifically, in the case $\mathcal{K} = -1$, the line element of the spatial section in (11) corresponds to a hyperboloid with negative curvature; in the case $\mathcal{K} = 0$, it is the same of a three-dimensional euclidean space; finally, in the case $\mathcal{K} = 1$, it is the same as of a three-dimensional sphere. Notice that with this parametrization of the metric the scale factor has units of distances, while the radial coordinate r is dimensionless.

2.2.1 *Cosmological Distances and Conformal Time*

Given the spacetime metric, we want to understand how to properly describe and measure time intervals and distances. Measuring distances in cosmology is quite cumbersome. Various definitions of distance exist, depending on what one wants to measure. Before entering into these details, let us highlights some important features of the FLRW metric. First of all, it is invariant under simultaneous rescaling of $a(t) \to a(t)/\lambda$, $r \to \lambda r$, $\mathcal{K} \to \mathcal{K}/\lambda^2$. This freedom can be used to set the value of the scale factor today: $a(t = t_0) = 1$. Moreover, notice that the co-moving coordinate r is not a physical observable. We therefore define the *physical coordinate* $r_{\rm phys} = a(t) r$.

Given this definition, we can now make the first important distinction between the *co-moving distance* d_C, constant in time, and the *physical distance* d_P, which changes in time due to the cosmological expansion. The co-moving distance between two points located at fixed co-moving coordinates r_1 and r_2 is simply given by $d_C = |r_2 - r_1|$; while the physical distance is instead given by integrating the three-dimensional metric on a $t =$ constant hypersurface:

$$d_P = \int_{r_1}^{r_2} \sqrt{g_{ij} dx^i dx^j} = a(t) |r_2 - r_1| = a(t) d_C \, . \tag{12}$$

By differentiating with respect to time we find

$$\dot{d}_P = \frac{\dot{a}}{a} d_P = H(t) d_P \, , \tag{13}$$

where we have introduced the *Hubble parameter* $H = \dot{a}/a$, i.e. the rate of expansion of the Universe. Evaluated today, equation (13) gives the famous Hubble law: $v = H_0 d$, where H_0 is the value of the Hubble parameter today. Notice that this law holds only in the recent times, since in general the scale factor $a(t)$ is time dependent.

In cosmology, distances are often measured in terms of redshift, i.e. a shift in the frequencies of photons reaching the observer. To calculate this shift, one has

to solve the geodesic equation (10) using the FLRW metric (11). If we consider a photon coming to us along the radial direction and reaching us today at t_0, we can trace back its evolution until a generic earlier time t. In particular one gets:

$$\frac{\nu(t_0)}{\nu(t)} = \frac{a(t)}{a(t_0)}\,, \tag{14}$$

where ν is the frequency of the incoming photon. From (14) we can define the redshift as:

$$1 + z = \frac{\nu(t)}{\nu(t_0)} = \frac{a(t_0)}{a(t)}\,. \tag{15}$$

Notice that if the scale factor is increasing in time we can properly talk about redshift, while if $a(t)$ decreases in time we actually have a blueshift (corresponding to a negative value of z).

The comoving distance can be expressed in terms of redshift. Assuming that t_0 is today, so that $z_0 = 0$:

$$d_C = \frac{1}{a_0}\int_0^z \frac{dz'}{H(z')}\,, \tag{16}$$

where we used $a_0 = a(t_0)$ for brevity. Expanding for small redshifts

$$d_C = \frac{1}{a_0 H_0}(z + \dots)\,. \tag{17}$$

Setting $a_0 = 1$, we recover the Hubble law, with $v = cz$ [1] the recession speed. Hence for small values of redshift the comoving distance coincides with the physical distance.

Unfortunately, even the physical distance cannot be measured, since it is the distance between two objects at a fixed time. Observables in cosmology rely on the measure of the lights emitted by far away sources. Therefore a more feasible way to define distance needs to consider that the Universe is expanding and that light takes a finite time to travel to us. The *luminosity distance* does exactly this. Given a source of electromagnetic emissions with an observed flux Φ, the luminosity distance is defined as

$$d_L = \sqrt{\frac{L_s}{4\pi\Phi}}\,, \tag{18}$$

where L_s is the absolute luminosity of the source. Hence, knowing L_s and measuring Φ we can infer the distance to the source. The luminosity distance is something we could measure, since there are some astrophysical sources whose absolute luminosities are known. For example, in 1929 Hubble used Cepheids to measure the luminosity distance and discovered the expansion of the Universe [47]. The definition (18) comes from the fact that in flat space the ratio between the flux and the luminosity of a source located at a distance d is given by one over the area centered around the emitter: $\Phi/L_s = 1/(4\pi d^2)$.

1 We restored the velocity of light c to make the relation clearer.

However, in a FLRW Universe this result has to be modified to keep into account the expansion of the spacetime. First of all, the area of the sphere centered around the source when the photons reach the Earth is $4\pi r^2 a^2(t_0)$ [2]. Moreover the luminosity is defined as the energy emitted per unit time $L = \Delta E/\Delta t$; therefore it will diminish by a factor $(1+z)^2$. Indeed, the energy of the photons will be redshifted by a factor $(1+z)$, while the time spent for the photons to reach us will increase by the same factor. The luminosity distance in a FLRW spacetime is thus defined as:

$$d_L = r\, a(t_0)\,(1+z)\,. \tag{19}$$

It is straightforward to prove that in the limit of small redshift $d_L \sim d_c \sim d_P$.

Another useful definition is the *angular diameter distance*, that is the distance deduced from the proper and observed size of an object. It is defined as:

$$d_A = \frac{R}{\delta\theta}\,, \tag{20}$$

where R is the intrinsic size of the object and $\delta\theta$ is its angular size. This definition is particularly useful since in astrophysics there are standard rulers, i.e. objects of known physical size, which can be used to compute distances. A particularly interesting example is provided by the CMB; the typical size of hot and cold spots in the CMB is theoretically predicted, so that the observed angular size gives us information about the distance to the Last Scattering Surface (LSS). The definition (20) must be modified to take into account the expansion of spacetime. In particular, the physical size of the object changes in time according to $R = ra(t)\delta\theta$, with t the time of emission. Therefore one can rewrite

$$d_A = r\, a(t) = r\,\frac{a(t_0)}{(1+z)} = \frac{d_L}{(1+z)^2}\,, \tag{21}$$

where in the last equation we used relation (19). Since the different definitions of distances are all related, they can be measured independently and used as a test of the FLRW framework.

We conclude this section introducing the concept of *conformal time* and *comoving (or particle) horizon*. Since light travels a distance $dr = dt/a(t)$ in a time dt, it is often convenient to introduce the notion of conformal time as $dt = a(\tau)d\tau$, or

$$\tau = \int \frac{dt}{a(t)}\,. \tag{22}$$

The FLRW metric in conformal time simplifies to

$$ds^2 = a^2(\tau)\left(-d\tau^2 + g_{ij}x^i x^j\right)\,. \tag{23}$$

2 Notice that we are assuming $\mathcal{K} = 0$ today, since we know from the observations that we are living in an almost flat spacetime. If this is not the case one has to substitute r with the metric distance, computed from the general metric (11).

If we assume the spacetime to be flat ($\mathcal{K} = 0$), this metric is conformally Minkowski, hence the name "conformal" time. The comoving (particle) horizon is defined as the maximum comoving distance light can propagate between an initial time t_i and some later time t:

$$\chi_P(\tau) = \tau - \tau_i = \int_{t_i}^{t} \frac{dt'}{a(t')} \,. \tag{24}$$

This quantity marks the boundary beyond which no information can arrive to the observer. Considering as initial time the Big Bang, the particle horizon defines the observable Universe. Indeed, as we will see, the standard Big Bang scenario predicts the "beginning" of the Universe at a certain time in the past, after which information started propagating. This limits the distance over which different spacetime patches could have been in causal contact and it is at the basis of the "*Big Bang puzzles*".

An important distinction has to be made between the comoving horizon and the *Hubble horizon (or sphere)*, that is the boundary between particles moving slower than the speed of light from those moving faster, as observed at a specific moment in time. The Hubble radius is expressed in terms of the Hubble rate as $\chi_H(t) = 1/H(t)$; moreover one can define the *comoving Hubble radius* as $\chi_H(t) = 1/(a(t)\,H(t))$. The particle horizon coincides with the Hubble sphere in the standard Big Bang model. However they differ if one takes into account inflation, that is a period of accelerated expansion of the Universe in its earliest stages. This expansion made objects recede from each other at velocities exceeding that of light.

Notice furthermore that the particle horizon differs from the *event horizon*. The particle horizon is the maximum comoving distance light could have travelled to reach the observer by a specific time, while the cosmic event horizon gives the furthest comoving distance from which a signal sent today will never be received by an observer in the future. Mathematically it is given by

$$\chi_e = \int_{\tau_0}^{\tau_{max}} d\tau = \tau_{max} - \tau_0 \,. \tag{25}$$

2.2.2 *Friedmann equations*

The FLRW metric (11) is defined for any value of the scale factor $a(t)$. All the concepts previously introduced do not rely on any assumption about the dynamics of the cosmological expansion. The next step is to apply Einstein field equations to derive the time evolution of the scale factor. The left-hand side of (2) is evaluated computing the Levi-Civita connection and then the contractions of the Riemann tensor from the FLRW metric (11). For the right-hand side we need to consider a suitable source of matter-energy which respects the cosmological principle. We therefore choose to model matter and energy by a perfect fluid, whose stress-energy tensor is given by

$$T_{\mu\nu} = (\rho + p)\, u_\mu u_\nu + p g_{\mu\nu} \,, \tag{26}$$

where ρ is the energy-density of the fluid, p its pressure and $u^\mu = (1,0,0,0)$ its comoving four-velocity. Clearly the fluid is isotropic, i.e. at rest with

a comoving observer. With one index raised, equation (26) takes the form $T^{\mu}{}_{\nu} = \mathrm{diag}(-\rho, p, p, p)$. This expression is particularly convenient since the conservation of the 0-component of the stress-energy tensor $\nabla_{\mu} T^{\mu}{}_{\nu} = 0$ gives immediately the equation

$$\dot{\rho} + 3H(\rho + p) = 0\,. \tag{27}$$

At this point, we can choose an equation of state linking the pressure to the energy-density. In cosmology it is convenient to parametrize the barotropic equation of state according to $p = w\rho$. If w is a constant, substituting this relation into (27) we get the solution

$$\rho = \rho_0 \left(\frac{a(t)}{a_0} \right)^{-3(1+w)}\,, \tag{28}$$

with ρ_0 and a_0 the energy density and scale factor respectively evaluated today. Depending on the value of w we can identify three different types of fluid:

- $w = 0$. This case corresponds to a pressureless fluid, or at least with a pressure negligible with respect to the energy density. This is the case of non-relativistic particles, for which the energy density scales as $\rho_m \propto a(t)^{-3}$. This dilution reflects the fact that the volume of space is increasing as $a(t)^3$, with the comoving energy density remaining constant. This type of fluid describes the behaviour of ordinary matter and *dark matter*.

- $w = 1/3$. In this scenario the Universe is filled with relativistic particles (or radiation), whose energy density scales as $\rho_r \propto a(t)^{-4}$. The different behaviour with respect to the non-relativistic particles reflects the fact the energy of radiation redshifts as $a(t)^{-1}$. Radiation comprises photons, neutrinos, ultra-light particles (e.g. ultra-light axions), gravitons, and other massless particles in general.

- $w = -1$. In this case the energy density ρ_Λ is constant and the pressure is negative. This fluid describes what is called *dark energy*. One possibility for the dark energy is given by a non-zero *vacuum energy*, present due to the expansion of spacetime itself. The presence of the vacuum energy is predicted by Quantum Field Theory (QFT), however the theoretical value predicted by the theory exceeds by far the observed value. Another "quantity" described by this equation of state is the so called *cosmological constant*, introduced by Einstein to describe a static Universe. It enters into the lhs of Einstein equations as $\Lambda g_{\mu\nu}$, with $\Lambda > 0$, however it is customary to move this term to the rhs and include it in the stress-energy tensor in the form of a fluid with $w = -1$. The corresponding spacetime is called dS spacetime and in this case the scale factor behaves as $a(t) \propto \exp\{Ht\}$, with H constant. As we will see, this solution is particularly useful in cosmology, since it provides in first approximation an inflationary period of the Universe.

From the 00-component of the Einstein equation, provided with the stress-energy tensor (26), one gets

$$H^2 = \frac{8\pi}{3}\rho - \frac{\mathcal{K}}{a^2}\,, \tag{29}$$

while from the ij-component

$$\dot{H} + H^2 = -\frac{4\pi}{3}(\rho + 3p)\,. \tag{30}$$

These two equations are called *Friedmann equations*, and together with (27) they form a system of three non-independent equations. Knowing the dependence of ρ from the scale factor one can find the time evolution of $a(t)$ from the *first Friedmann equation* (29), while the *second Friedmann equation* (30) is superfluous.

In the presence of different independent fluids the first Friedmann equation takes the form

$$H^2 = \frac{8\pi}{3}\sum_i \rho_i - \frac{\mathcal{K}}{a^2}\,, \tag{31}$$

with each ρ_i satisfying an independent conservation equation (27).

Another useful quantity is the *density parameter*

$$\Omega_i = \frac{8\pi}{3H^2}\rho_i = \frac{\rho_i}{\rho_{cr}}\,, \tag{32}$$

with ρ_{cr} the *critical density* defined as

$$\rho_{cr} = \frac{3H^2}{8\pi}\,. \tag{33}$$

The Friedmann equation (29) can be rewritten in terms of these quantities as

$$\Omega - 1 = \frac{\mathcal{K}}{a^2H^2}\,, \tag{34}$$

where $\Omega = \sum_i \Omega_i$. This relation links the density parameter to the spatial curvature of spacetime: if $\Omega < 1$, then the Universe is open ($\mathcal{K} < 0$); if $\Omega = 1$, the Universe is flat ($\mathcal{K} = 0$); while if $\Omega > 1$, the Universe is closed ($\mathcal{K} > 0$). This result has been used to infer the spatial curvature of our spacetime from measures of Ω coming from the CMB anisotropies using the angular diameter distance. These observations led us to think the Universe is very close to be flat and, as we will see, are at the basis of one of the Big Bang puzzles, i.e. the flatness problem.

2.2.3 *Standard Model of Big Bang Cosmology*

In the standard model of Big Bang cosmology the Universe is assumed to be composed by baryonic (or ordinary) matter, Cold Dark Matter (CDM), radiation and dark energy (in the form of a cosmological constant Λ). For this reason it is often referred to as the ΛCDM model. The time evolution of the

energy densities of these components determines the evolution of the Universe. From equation (34) one can reconstruct the history of the Universe in the past given the initial conditions today. Indeed, each component Ω_i scales differently in time, and the Universe has been characterized by periods when one specific component dominated above the others. The transition periods are identified by the *equality epochs*, i.e. the instants when two components contributed equally to the total density of the Universe. The evolution in time of the energy densities of the different components in terms of the scale factor $a(t)$ is shown in Figure 1. The values of Ω_i have been obtained from the CMB

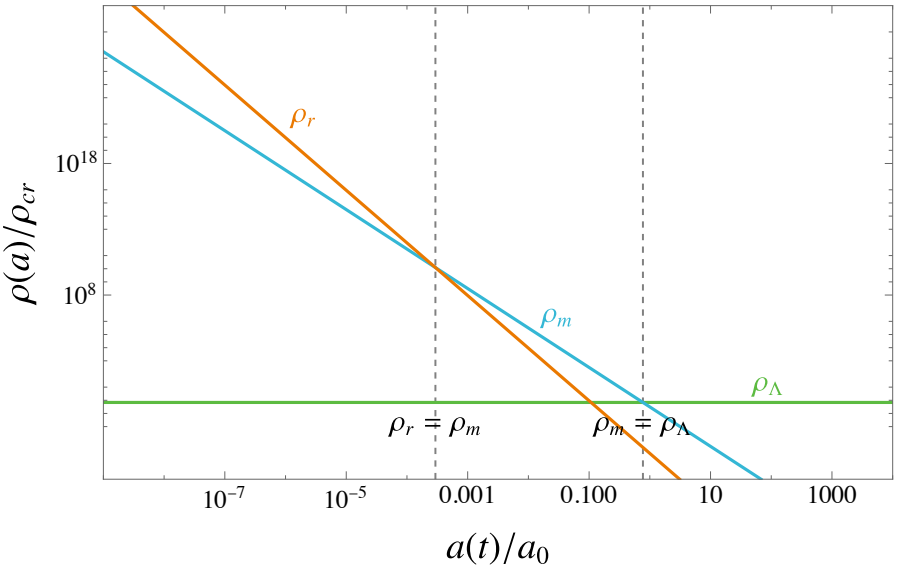


Figure 1: Time evolution of the energy density. The different components are normalized to the critical density ρ_{cr} and are shown in function of the scale factor $a(t)$, normalized by the scale factor today.

from the results of the *Planck mission* [48]. Today

$$\Omega_b^{(0)} \approx 0.049\,, \quad \Omega_{cdm}^{(0)} \approx 0.264\,, \quad \Omega_r^{(0)} \approx 9.21 \cdot 10^{-5}\,, \quad \Omega_\Lambda^{(0)} \approx 0.685\,,$$

where $\Omega_m = \Omega_b + \Omega_{cdm}$, being the pressureless fluid composed of baryonic matter and cold dark matter.

From Figure 1 we can distinguish clearly the three different epochs: first we have the present dark energy-dominated era; going back in time, we had a matter-dominated era; even further in the past, we had a radiation-dominated era. The equality times can be computed easily imposing the equality between the energy densities. For the matter - dark energy equality one has to impose

$$\frac{\rho_m(t)}{\rho_\Lambda} = \frac{\rho_m^{(0)}}{a^3(t)\rho_\Lambda} = 1\,, \tag{35}$$

from which the scale factor at equality can be computed, corresponding to a redshift $z_{m\Lambda} = 1/a - 1 \sim 0.297$. The matter - radiation equality can be computed in the same way, and it happens at a redshift $z_{rm} \sim 3400$.

One could be interested in expressing the evolution of the composition of the Universe in terms of cosmic time t, instead of the scale factor a. Since our Universe seems to be flat, we restrict to the case with $\mathcal{K} = 0$. Inserting the solution (28) for ρ into the Friedmann equation (29), one can solve for the scale factor $a(t)$. Assuming the Universe as a collection of fluids where just one dominates in each epoch, and further assuming the transitions between the eras to be instantaneous, one gets a piece-wise solution for the scale factor:

$$\frac{a(t)}{a_0} = \begin{cases} e^{-H_0(t_0-t)} & \text{for } t > t_{m\Lambda}\,, \\ \frac{1}{1+z_{m\Lambda}}\left[1+\frac{3}{2}H_0(t-t_{m\Lambda})\right]^{2/3} & \text{for } t_{m\Lambda} > t > t_{rm}\,, \\ \frac{1}{1+z_{rm}}\left[1+2H_0\left(\frac{1+z_{rm}}{1+z_{m\Lambda}}\right)^{3/2}(t-t_{rm})\right]^{1/2} & \text{for } t_{rm} > t > t_{\mathrm{BB}}\,, \end{cases} \tag{36}$$

where t_0 is today, $t_{m\Lambda}$ the time of matter - dark energy equality and t_{rm} the time of matter - radiation equality; H_0 is the value of the Hubble parameter today; t_{BB} is the time when the scale factor vanishes $a(T_{BB}) = 0$ and corresponds to the time of Big Bang. The age of the Universe can therefore be computed as $t_{BB} - t_0$. Inserting (36) into (28) one gets the evolution of the energy density in terms of the cosmic time t.

2.2.3.1 *Thermal History of the Universe*

As we have seen in the previous section, going back in time the energy density of the Universe increases; therefore, earlier epochs are associated to higher energies. Specifically, for $t = t_{BB}$ the scale factor goes to zero; correspondingly, the energy density blows up as $\rho \propto a^{-2}$. This initial singularity is known as the Big Bang singularity, from which the Universe is created. Of course, at such high energies, classical general relativity is not expected to accurately depict nature; quantum gravity becomes relevant in this regime. In order to describe the evolution of the Universe we introduce an energy scale E as $E = \rho^{1/4} = (3H^2M_{Pl}^2)$, with M_{Pl} the Planck mass. As the energy of the Universe decreases, we expect the gravitational interaction to decouple from the other forces; we are then in the regime of Grand Unified Theory (GUT), an extension of the Standard Model (SM) that predicts the unification of strong and electroweak interactions. At this energies other particles with respect to the SM particles could be present. In this epoch the baryon asymmetry of the Universe may have originated through a dynamical mechanism, called *Baryogenesis*. At the GUT scale ($\sim 10^{16}$ GeV) the strong interaction is expected to decouple from the electroweak interaction, leaving the Universe filled with a quark-gluon plasma. In this period, a Dark Matter (DM) formation mechanism may have occurred. At ~ 100 GeV the electroweak symmetry breaking happened. At this scale the Higgs takes a vev and the gauge bosons, as well as the SM fermions, acquire a mass.

Up to this temperature, we can assume all the particles to be in local equilibrium among each other. This is because the typical time-scale of collisions is much smaller than the cosmic time of expansion. Before the electroweak phase transition scale, where all the particles are massless, the electroweak

and strong interactions are enough to keep the plasma of quarks, leptons and gauge bosons in local equilibrium. Below this scale, the particles gradually become non-relativistic (when $m > T$) and decouple from the plasma; the energy scale of decoupling depends on the interactions these particles are subject to, and specifically their scattering rate. The decoupling of particles from the thermal equilibrium is called *freeze out* mechanism. If those particles are still relativistic at decoupling, they are called *hot relics*; on the contrary, if they are non-relativistic they are called *cold relics*. After the decoupling phase, the temperature of the decoupled species starts to differ from that of the thermal plasma.

In general, the energy density at a given reference temperature T is dominated by the effective number of degrees of freedom $g_*(T)$ that are ultra-relativistic at that temperature [3]:

$$\rho = \frac{\pi^2}{30} g_*(T) T^4 \,. \tag{37}$$

The effective number of degrees of freedom can be written as:

$$g_*(T) = \sum_b g_b \left(\frac{T_b}{T}\right)^4 + \frac{7}{8} \sum_f g_f \left(\frac{T_f}{T}\right)^4 \,, \tag{38}$$

where "b" stands for bosons and "f" stands for fermions and the sums run over the particles that are relativistic at the temperature T. Each species has a temperature T_i, that in general may differ from the reference temperature T, which is taken to be the temperature of photons.

For most of its history, the Universe is in thermal equilibrium, i.e. all species share the same temperature $T_i = T$. It can be shown indeed that all the SM particles decoupled when non-relativistic, so that their contribution to the total energy density of the Universe was negligible. Equation (38) then reduces to the counting of the number of relativistic degrees of freedom [4]. For example, $g_\gamma = 2$, since photons has two polarizations, $g_{e^-} = 2$, since electrons have two spin states, and so on. The number of relativistic degrees of freedom changes in time, since the Universe expands and the temperature drops.

Thanks to equation (37) we can link the temperature of the plasma to the scale factor $a(t)$. Indeed, the energy density for relativistic particles scales as $\rho \propto a^{-4}$; therefore, $T \propto a^{-1}$. The energy scale E, used to describe the evolution of the Universe is instead proportional to the temperature T.

Below the electroweak energy scale, we are left with a plasma of SM particles, i.e. leptons, gauge bosons and free quarks and gluons. When the temperature of the Universe drops below $\sim$ 200 MeV, the QCD phase transition occurs and the quark-gluon plasma hadronizes to form hadronic matter (mesons and baryons). As the temperature further decreases, the heaviest particles stop being produced and we are only left with neutrons, protons, electrons, positrons, photons, neutrinos and anti-neutrinos. Initially, neutrinos are trapped via weak

3 The non-relativistic degrees of freedom, for which $m \ll T$, are exponentially suppressed by a factor $\sim exp(-m/T)$.

4 The only particles which decoupled when still relativistic are neutrinos. After neutrino decoupling (at $\sim$ 1 MeV), the temperature dependence in (38) has to be taken into account.

interaction; however, at $T \simeq 1$ MeV, the leptons annihilation reactions become inefficient and neutrinos decouple from the plasma. After decoupling, neutrinos free-stream in the Universe, giving us a cosmic neutrino background. Shortly after neutrino decoupling, the temperature drops below the electron mass. At this point e^+e^- can annihilate into two photons. The energy density of electrons and protons is then transferred to the photons, which warm up with respect to the decoupled neutrinos. Specifically, it turns out $T_\nu = (4/11)^{1/3} T_\gamma$. The temperature of the cosmic neutrino background can then be computed in function of the photons temperature. The temperature of neutrinos background today (computed from the CMB) is $T_\nu^{(0)} \simeq 1.96\,K$.

At the time of neutrinos decoupling, neutrons and protons are kept in equilibrium by bremsstrahlung, elastic scattering and Compton effect. The equilibrium is broken by the expansion of the Universe when the temperature goes below $T \simeq 0.8$ MeV. After that temperature the neutron to proton ratio freezes out. After some time, neutrons start decaying and their number with respect to protons diminish. When the Universe cools down until $T \simeq 0.3$ MeV, the nuclei of light elements (up to Lithium) start to be formed. This is the so called Big Bang Nucleosynthesis (BBN). The abundances of the light nuclei are predicted by the theory and they are in a remarkably good agreement with the observed ones. It is the earliest probe of the Universe.

After BBN, the plasma mostly consists of photons, electrons, positrons, and light nuclei. At low enough temperatures, the processes of electron capture from the nuclei become favourable; therefore, nuclei start to trap electrons and become electrically neutral atoms. This process is called *recombination*. Before recombination, photons were interacting with free electrons via Thompson scattering. As the number of electrons drops, the photons decouple and the Universe becomes transparent to radiation (at $T \simeq 0.25$ eV). These left photons constitute the CMB radiation we observe today.

After recombination, the Universe undergoes a long period known as the *dark ages*, where the structures we know today gradually formed thanks to gravitational instabilities. The name of this period comes from the fact that there are no visible stars yet to light up the Universe.

2.2.3.2 *Experimental Confirmations and Limits of the ΛCDM model*

Several predictions of the ΛCDM model have been confirmed by the observations. First of all, the measure of distances in cosmology proved the expansion of the Universe. The first to use observational data to extract the rate of expansion was Lemaître in 1927 [49]. In 1929 Hubble [47] analyzed the motion of the Sun with respect to the extra-galactic nebulae and theorised the Hubble law (13). Later on, his relation was checked using more accurate data. The expansion of the Universe is the first confirmed prediction of GR-based cosmology.

Another fundamental validation of the ΛCDM model comes from the observation of the CMB, whose name arises from the fact the observed wavelength of the photons lies in the microwave region. The Big Bang model indeed predicts the existence of a background thermal radiation, which was emitted when the photons decoupled from the plasma, right after the Universe became

neutral. The first detection of the CMB has been done by Penzias and Wilson in 1965 [50, 51]. The study of the background radiation improved through various missions, and reached its peak with the observations made by the Planck satellite. The first results have been published in 2015 [52] and subsequently updated in 2018 [48, 53, 54]. The measured temperature is $T_{CMB} \simeq 2.7\,K$, in accordance with the prediction of the Big Bang model. The CMB provides the most optimal insight into the state of the early Universe, and it will be revisited frequently throughout this work.

Actually, the ΛCDM model predicts another background thermal radiation made of neutrinos, which decoupled earlier with respect to photons. Unfortunately the Cosmic Neutrino Background has not been detected yet. Indeed, it is quite cumbersome to observe them, since neutrinos interact only via weak interaction; furthermore, their predicted temperature is below the temperature of the CMB.

The thermal history of the Universe is characterized by another fundamental moment, the BBN. The theoretically predicted abundances of the light elements have been compared with the measured ones and are in very good agreement [55]. The only mismatch with the data comes from the abundance of the Lithium; this is known as the *cosmological Lithium problem*. The BBN abundances can be used to constraint alternative scenarios with respect to the standard ΛCDM. For example, a Beyond the Standard Model (BSM) theory would in general change the effective number of degrees of freedom $g_*(T)$; this would change in turn the Hubble rate H and the time of neutron freeze-out. From upper bounds on the Helium abundance it is possible to constraint extra contributions to $g_*(T)$. Even the lifetime of extra particles is bounded to $\tau < 300\,s$, so that possible new particles decay before the onset of the BBN.

Despite its successes, the Big Bang scenario still has some mysteries and unexplained observational facts. We already briefly touched the cosmological Lithium problem, but there are others it is worth to mention. First of all, the ΛCDM model relies on the introduction of two unknown fluids: dark matter and dark energy.

The ordinary baryonic matter content in the Universe is predicted by the cosmological nucleosynthesis, however its theoretical value differ from the observed one. This led to the conclusion there is some form of *dark* matter, in the sense that it is subject to gravitational interaction only. Its existence can be inferred from observations at different scales [56]. The first evidence for DM comes from the observed rotation curves of galaxies. In 1933 the astronomer Fritz Zwicky [57] found that the total mass of the stars in the Coma galaxy cluster accounted for merely one percent of the mass required to prevent the galaxies from leaving the cluster's gravitational pull. The presence of this "missing mass" was confirmed by the observations of Vera Rubin and W. Kent Ford in the 1970s. It was found that the orbital velocity of the stars around the centre of the galaxy remained more or less constant after a certain distance. From the observed mass, on the contrary, the orbital velocity should have decreased. In order to account for this phenomenon, the mass inside the

orbit of the stars in the galaxy must increase with the distance of the stars from the galaxy's centre. This issue is solved by introducing additional matter, which acts like a pressure-less fluid and interacts only gravitationally with baryonic matter. After this discovery, other proofs of the existence of DM came from the strong gravitational lensing of background objects by galaxy clusters. However, the most compelling evidence is found at cosmological scales: the measure of the CMB spectra allowed to separate the contribution of ordinary baryonic matter from that of DM and infer their abundances independently.

There are several candidates for dark matter, but its nature is still a mystery. However, it can be categorised according to its properties at the time of matter-radiation equality. Whether the DM is relativistic or non-relativistic at this time changes the clustering properties during the matter dominated period, and therefore it affects the structure formation. We can identify three types of DM: *hot dark matter*, which becomes non-relativistic at matter-radiation equality; *cold dark matter*, which becomes non-relativistic long before that time; *warm dark matter*, which becomes non-relativistic before the equality, but has a free-streaming length much higher with respect to cold dark matter. As regards structure formation, different DM types give rise to different scenarios: hot dark matter makes that large structures already present fragment into smaller structures, while cold dark matter makes that smaller objects merge into bigger structures hierarchically. A comparison of cosmological observations with theoretical predictions excludes hot dark matter. Warm dark matter is instead still a valid candidate, but it is strongly constrained by Ly-α data. The DM considered in the ΛCDM model is CDM.

Concerning Dark Energy (DE), the first observational evidence comes from Type IA Supernovae [58, 59], which are very good standard candles. A comparison between their luminosity distance and their redshift showed that the expansion of the Universe is accelerating. Before this observation, it was thought that the gravitational attraction of matter and energy would result in a deceleration of the Universe's expansion in time. In order to explain the expansion, some fluid behaving as a cosmological constant had to be introduced. Since the first discovery, several independent evidences supported the existence of DE, coming from the Large Scale Structures and the CMB. There are several theories trying to explain the nature of DE, like vacuum energy, quintessence, or modified theories of gravity; however it still remains a mystery.

Besides these two unknown components, there are other unsolved problems of the ΛCDM model. Two that is worth to mention are the *Hubble tension* and the S_8 *tension*. The former is a difference in the measured Hubble rate as inferred from the CMB with respect to that derived from the astronomical distance measurements. The latter is a discrepancy between early (CMB) and late (weak gravitational lensing events) time measurements of the S_8 parameter, quantifying the amplitude of matter fluctuations in the late Universe. These two tensions could imply the ΛCDM model is incomplete.

Last but not least, the hot Big Bang model cannot be valid up to arbitrarily high energies. After a scale set by the Planck mass, we expect the structure of spacetime to change dramatically and quantum gravity effects to become relevant. The Big Bang theory starts to be reliable at energies below the Planck

scale. We conventionally set the initial time of validity of the model at the GUT scale, i.e. $T \simeq 10^{16}$ GeV.

2.3 BIG BANG PUZZLES

The limitations listed in the previous section are still unsolved mysteries in cosmology, but there are other problems in the Big Bang scenario which are solved by the so called *inflation*, a period of accelerated expansion of the Universe in its earliest stages. These problems go under the name of *Big Bang puzzles*.

2.3.1 *Horizon Problem*

Observations coming from the CMB tell us the Universe is very close to be homogeneous and isotropic, thus confirming the cosmological principle. This implies any two points on the sky are causally-connected or at least have been in causal contact at a certain time. The size of causally-connected regions in space is given by the maximum distance over which light can be observed. As introduced in Section 2.2.1, the particle horizon (24) defines the greatest comoving distance from which an observer at time t will be able to receive light signals coming from an initial time t_i. Choosing as initial time the Big Bang time $t_i = t_{BB}$, one can determine which are the regions in the sky that are in causal contact today. We can visualise the horizon problem as in Figure 2a. An observer today can see events lying within the intersections of its past light-cone with the spacelike surface at the recombination time τ_{rec}, i.e. the LSS. Two regions in space are causally connected if their past light-cones intersects at the spacelike surface at τ_{BB}. As we can see from Figure 2a, we don't expect all the patches of the observable Universe to be in causal contact.

To better understand the problem, let's consider the geometry represented in Figure 2b. We can compute the angle $\delta\theta$ below which we expect two points in the sky to be causally connected as

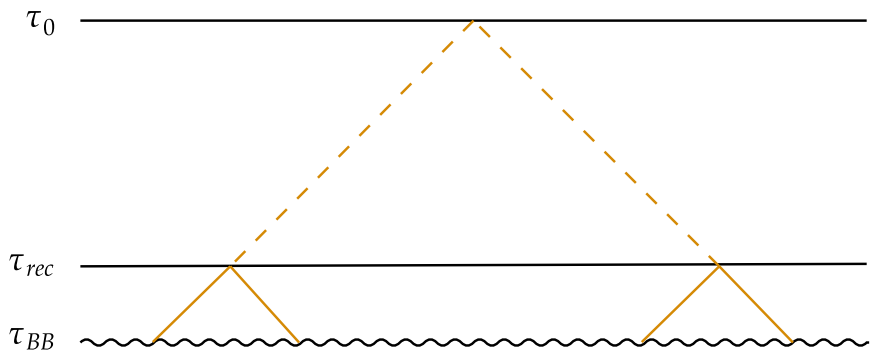
$$\delta\theta < \arctan\left[\frac{d_c(t_{LSS})}{2\chi_p(t_{LSS})}\right] . \tag{39}$$

This expression can be computed taking into account the evolution of the scale factor in time. It turns out $\delta\theta \simeq 2^\circ$. The CMB observations are in contrast with this result.

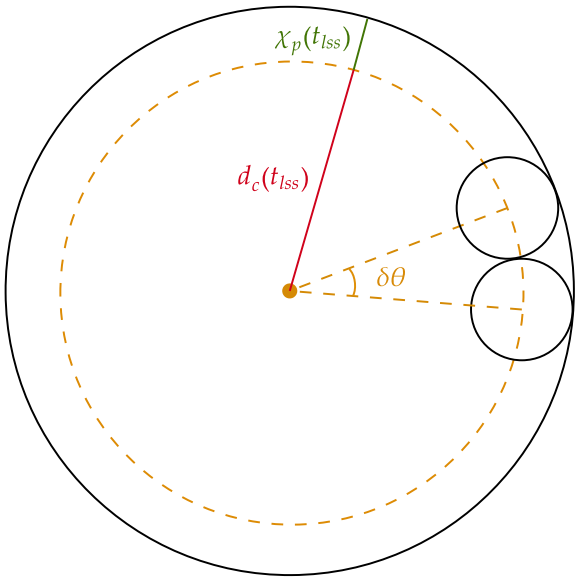
2.3.2 *Flatness Problem*

A second puzzle comes from the low value of the spatial curvature density parameter $\Omega_\mathcal{K}$. Measuring the density parameters of the other components of the Universe today, the value of $\Omega_\mathcal{K}$ can be computed from (34). Specifically we have

$$\Omega_\mathcal{K}^{(0)} = -\frac{\mathcal{K}}{a_0^2 H_0^2} = 0.0007 \pm 0.0019\,, \tag{40}$$



(a) The light-cones of photons coming to us from the LSS are shown. Since they were not in causal contact at the LSS, we do not expect to observe an homogeneous sky.



(b) The singularity is given by the solid black circle, while the last-scattering surface is given by the dashed orange circle. The red line gives the comoving distance of us from the LSS and the green line represents the particle horizon at the LSS.

Figure 2: Graphical representation of the horizon problem.

that is compatible with zero. However, looking at the scale factor dependence of the curvature component, we expect its contribution to the energy budget of the Universe to grow in time. This implies the value of $\Omega_{\mathcal{K}}$ at the beginning of the Universe had to be much smaller, giving rise to a fine-tuning problem. Ignoring the short period of dark-energy domination, we can compute the Hubble rate during matter domination from (36) and use the result to compute the curvature density during matter domination:

$$\Omega_{\mathcal{K}}(t) = \frac{\Omega_{\mathcal{K}}^{(0)}}{\Omega_m^{(0)}} \frac{a^2(t)}{a(t) + a(t_{rm})} \qquad \text{for} \qquad t_{rm} < t < t_0 \,. \tag{41}$$

At earlier times, the Universe underwent a period of radiation domination. Keeping into account the different evolution of the scale factor we get:

$$\Omega_{\mathcal{K}}(t) = 2\Omega_{\mathcal{K}}(t_{rm}) \left(\frac{a(t)}{a(t_{rm})}\right)^2 \qquad \text{for} \qquad t_{BB} < t < t_{rm}\,. \tag{42}$$

As an example, evaluating it at the GUT time one gets $\Omega_{\mathcal{K}}(t_{GUT}) \approx 10^{-58}$. It could be argued that the curvature is simply zero $\mathcal{K} = 0$, treating it as another initial condition. Nonetheless, it would be more satisfactory to see the flatness of the Universe emerging as the result of a physical process.

2.3.3 *Monopoles Problem*

Although not predicted in the SM, topological defects, such as monopoles, are present in several extensions, e.g. the GUT. These defects are produced whenever a (first or second order) phase transition occurs. Since the Universe cools down as the expansion proceeds, these phase transitions are natural consequences of symmetry breaking processes that occur in particle physics. Monopoles are expected to be produced in high quantities. Since the only way monopoles can be annihilated is by interacting with anti-monopoles, and these processes are suppressed by the expansion of the Universe, we expect the number of monopoles to be conserved until today. Their present abundance can be computed in function of their mass. In the case of the GUT extension of the SM, for a GUT scale of $\sim 10^{16}$ GeV, the predicted mass is around $\sim 10^{17} - 10^{18}$ GeV. With this value, the predicted abundance is $\Omega^{(0)}_{mono} \approx 10^{20}$; they would then dominate the energy content of the Universe, contrary to what is observed. Moreover, besides not governing the evolution of the Universe today, these monopoles have never been observed. The hot Big Bang scenario is then in contrast with the GUT and many other BSM theories.

2.4 COSMIC INFLATION

Among the three issues introduced in the previous section, the most serious is the horizon problem. The flatness problem could be solved simply assuming that the Universe is and has always been flat; while the monopole problem does not arise if we assume the BSM models predicting their existence to be wrong. Instead, the horizon problem suggests there was a period before the standard scenario in which all the different regions of space were in causal contact, thus explaining the homogeneity of the Universe. Then, some mechanism moved these regions far away, causing them to no longer be in causal contact. In 1980 Guth [60] realized that a sufficiently long period of accelerated expansion of the Universe does exactly this. Shortly after, Linde [61] and Albrecht and Steinhardt [62] proposed a *new inflation* model aimed at addressing some issues associated with the end of inflation in Guth's original formulation.

A period of accelerated expansion can be obtained in several ways. The minimum requirement is that $\ddot{a}(t) > 0$. Using the second Friedmann equation

(30) and the equation of state $p = w\rho$, the condition of accelerated expansion implies

$$\ddot{a} > 0 \quad \Longleftrightarrow \quad w < -\frac{1}{3}\,. \tag{43}$$

Hence inflation is an epoch in the early Universe, before the electroweak symmetry breaking, when the energy-density was dominated by a fluid whose parameter w is smaller than $-1/3$. Notice that the condition $\ddot{a} > 0$ leaves three possibilities for the Hubble rate:

- $\dot{H} < 0$, $-1 < w < -1/3$. This situation corresponds to a *power-law inflation*, with $a(t) \propto t^p$, $p > 1$ [63]. It can be obtained with a single scalar field with an exponential potential (see Section 2.4.3 for further details).
- $\dot{H} = 0$, $-1 < w < -1/3$. This case represents a phase of dark-energy dominated Universe. We then talk of *de Sitter inflation* (see Section 2.4.2).
- $\dot{H} > 0$, $w < -1$. For these values of w the scale factor goes like $a(t) \propto (t - t_{bounce})^{-n}$, with $n > 0$. In this scenario the evolution of the scale factor leads to a singularity. This behaviour is exploited in the so called *Big Bounce hypothesis*, a cosmological model for the origin of the known Universe. We will not treat this topic in this work.

2.4.1 *A Solution to the Big Bang Puzzles*

We now review the Big Bang puzzles in light of a period of accelerated expansion of the Universe.

2.4.1.1 *Horizon Problem*

The intuitive reason why an accelerated expansion solves the horizon problem is that starting from a locally homogeneous Universe over small regions and expanding any of these regions until the size of our observable Universe makes that it appears homogeneous.

Let us express this concept in a more formal way. Consider the particle horizon (24); it can be rewritten in the following way:

$$\chi_p(\tau) = \int_{a_i}^{a} \frac{da}{a\dot{a}} = \int_{\ln a_i}^{\ln a} \frac{1}{aH}\, d\ln a\,, \tag{44}$$

in function of the *comoving Hubble radius* $1/aH$. The Hubble radius can be rewritten in terms of the parameter w using the first Friedmann equation as

$$\frac{1}{aH} \propto \frac{1}{H_i} a^{\frac{1}{2}(1+3w)}\,. \tag{45}$$

The qualitative behaviour then depends on the sign of the exponent. In the standard Big Bang scenario $(1 + 3w) > 0$ always, therefore the Hubble radius increases monotonically with time. The integral in (44) is then dominated by

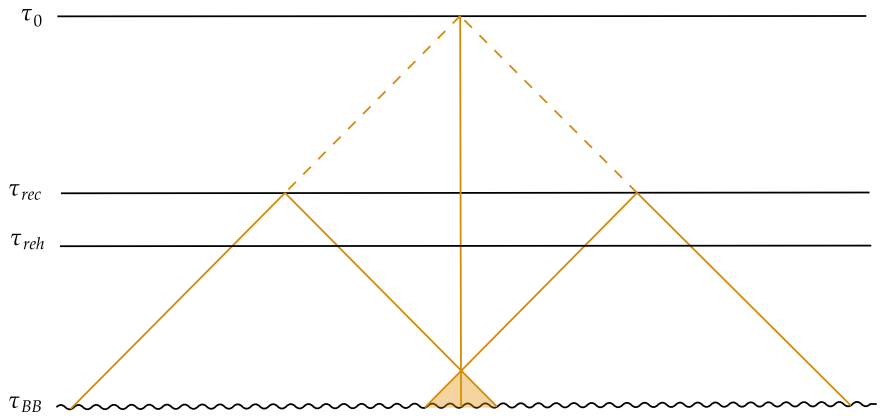


Figure 3: Graphical representation of the solution to the horizon problem. The light-cones of photons coming to us from the LSS did overlap in the far past thanks to a period of accelerated expansion of the Universe.

the late time contributions ($a \ll a_i$) and it is more or less equal to the Hubble radius itself: $\chi_p \approx 1/aH$.

What happens if we have instead a period in which $\ddot{a} > 0$? It can be proved using the second Friedmann equation that $\ddot{a} > 0$ is equivalent to the condition $d/dt(1/aH) < 0$, i.e. having a decreasing Hubble radius. Furthermore, it has been shown in the previous section that $\ddot{a} > 0$ is also equivalent to say that $w < -1/3$. In this case we indeed see from (45), that $1/aH$ decreases in time. If the Hubble radius shrinks, the particle horizon receives most of its contribution from early times. Indeed we can write:

$$\chi_p(\tau) = \tau - \tau_i = \frac{2H_0^{-1}}{(1+3w)}\left[a^{\frac{1}{2}(1+3w)} - a_i^{\frac{1}{2}(1+3w)}\right] \xrightarrow{a_i \to 0,\, w<-1/3} -\infty\,. \quad (46)$$

The singularity has then been "pushed" towards $-\infty$, so that there is much more conformal time between the singularity and the recombination time. The point $\tau = 0$ becomes a turnover: it is the time conventionally chosen for the end of inflation. As we will see in Section 2.4.4, this phase is called *reheating*, and it is the moment when the scalar field driving inflation decays into the SM particles we know. In Figure 3, the schematics of this new scenario is reported. If the period of accelerated expansion lasts a sufficient amount of time, then even points widely separated in space had been in causal contact at the beginning of the Universe.

The question now is which is the minimum required duration for inflation in order to solve the horizon problem. The minimum constraint is that the fluctuations we observe were all inside the Hubble radius at the beginning of inflation. Mathematically, the requirement is that the observable Universe was smaller then the comoving Hubble radius at the beginning of inflation (see Figure 4), i.e.

$$(a_0 H_0)^{-1} < (a_i H_i)^{-1}\,. \quad (47)$$

Notice that we used the Hubble radius as a measure of causality instead of the particle horizon, which is a more restrictive criterion, since the particle horizon

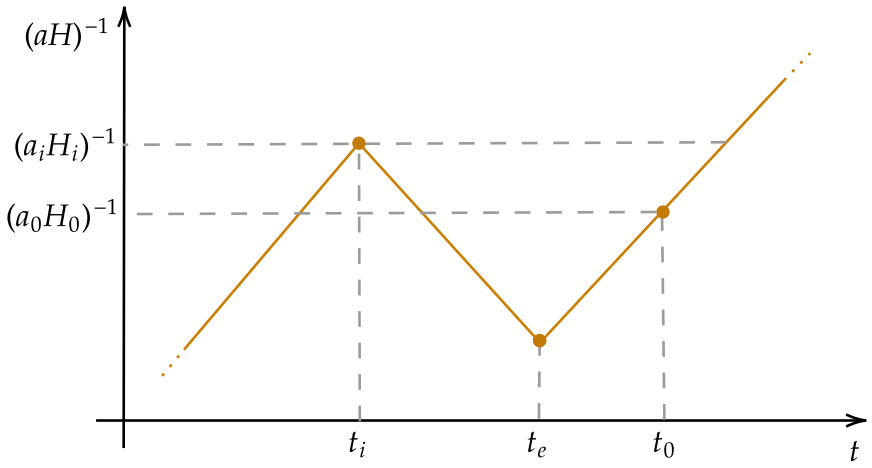


Figure 4: Evolution of the comoving Hubble radius in time in the presence of a period of inflation starting at t_i and ending at t_e. In order for inflation to solve the horizon problem we need the Hubble radius at the present time to be smaller than that at t_i.

at the beginning of inflation was larger than the Hubble radius. As we will see in the following sections, during inflation the Hubble rate can be assumed to be almost constant, that is $H_i \approx H_e$. Hence an estimate of the minimum duration of inflation could be given by an estimate of the minimum required increase in the scale factor. This concept is enclosed into the *e-foldings number*, defined as $N = \ln a$. The total duration of inflation is then given by:

$$N_{tot} = N_e - N_i = \ln\left(\frac{a_e}{a_i}\right) . \tag{48}$$

To evaluate the inequality (47) one has to relate the Hubble radius today to the one at the end of inflation. We can give an estimate assuming an instantaneous reheating such that the end of inflation coincides with the beginning of the radiation domination, and furthermore neglecting the periods of matter and dark energy domination. It can be shown [41] that

$$N_{tot} > 64 + \ln\left(\frac{T_R}{10^{15}\,\text{GeV}}\right) , \tag{49}$$

where T_R is the reheating temperature and 10^{15} GeV a reference scale. Of course if T_R is smaller the required e-foldings number would be smaller.

2.4.1.2 *Flatness Problem*

We have shown how going backwards in time up to the GUT scale the contribution of the curvature to the energy-density of the Universe is expected to become more and more negligible. We can express the curvature density parameter at any time in terms of its value at a given scale using its definition, given in (40), as

$$\frac{\Omega_\mathcal{K}(t)}{\Omega_\mathcal{K}(t_i)} = \frac{(a_iH_i)^2}{(aH)^2} . \tag{50}$$

Choosing the reference time t_i as the beginning of inflation, implies that the curvature density parameter at an arbitrary time t during inflation will be smaller. Indeed the Hubble sphere is shrinking, making the rhs of (50) smaller than one.

To understand this phenomenon intuitively, let us consider the Universe before inflation to be generically curved, but locally it can approximated to be flat. Inflation expands the regions of spacetime until one of these regions becomes the size of our observable Universe. The Universe is flattened by the rapid expansion of spacetime exactly like a balloon is locally flattened while inflated.

How long inflation has to last in order to flatten our Universe enough? Setting as initial condition the present curvature density parameter and going backwards in time assuming an early period dominated by a fluid with $w = -1$ for simplicity, the number of e-foldings can be computed to be $N_{tot} \approx 66$. For this computation the GUT scale has been assumed as the starting time for inflation. We see that the required duration of inflation is more or less the same as the one needed to solve the horizon problem.

2.4.1.3 *Monopoles Problem*

A period of accelerated expansion makes that the monopoles (or particles / topological defects in general) get diluted. An estimate of the present abundance of monopoles can be given in function of their mass as before. Assuming a period of inflation characterized by a fluid with $w = -1$, one can compute the minimum number of e-folds in order to satisfy the current observations on the upper bound of monopole abundance. It turns out that $N_{tot} > 25$. The result of these computations is then that the three Big-bang puzzles can be simultaneously addressed assuming an early epoch of inflation lasting for roughly 60 e-folds.

2.4.2 *de Sitter Inflation*

As introduced before, a period of accelerated expansion characterized by $w = -1$ is called de Sitter inflation. In this case the energy density is constant and the first Friedmann equation (29) contains only a dark-energy fluid (or a cosmological constant term). The Hubble rate is then a constant too, so that we can write during inflation $H = H_i$. Solving for the scale factor we find:

$$a(t) = a_i \, e^{H(t-t_i)} \, . \tag{51}$$

The Universe expands exponentially, just as in the latest stage of the standard Big Bang scenario. The geometry of spacetime is then given by a de Sitter spacetime, that is the maximally symmetric vacuum solution of Einstein field equations with a positive cosmological constant[5]. The simple scenario described by a de Sitter inflation is particularly useful since, as we are going to

5 For a negative value of Λ one gets an anti-de Sitter spacetime, while for $\Lambda = 0$ the solution to the Einstein equations is a Minkowski spacetime.

see in the next section, it is the limiting case of a more general situation, in which inflation is driven by a scalar filed with arbitrary potential.

2.4.3 *Single Field Slow-Roll Inflation*

Besides setting artificially $w = -1$, there is a more natural way to introduce inflation and to realise a fluid with $w < -1/3$. This fluid can be adequately described by a scalar field φ, called *inflaton*, whose potential $V(\varphi)$ is almost flat [61, 62]. This scenario is called *single-field slow roll inflation*, since the field is "slowly-rolling" down its potential. There are other inflationary scenarios, driven by more than one field (see [64] for a comprehensive review), however single-field inflation is the simplest one and it is still compatible with all the observations. In this work we will focus on this model.

Let us consider the following action for a scalar field minimally coupled to gravity:

$$S_\varphi = -\int d^4x\sqrt{-g}\left[\frac{1}{2}g^{\mu\nu}\partial_\mu\varphi\partial_\nu\varphi + V(\varphi)\right]. \tag{52}$$

The stress-energy tensor associated to this fluid is given by:

$$T_{\mu\nu} = \partial_\mu\varphi\partial_\nu\varphi - g_{\mu\nu}\left[\frac{1}{2}g^{\alpha\beta}\partial_\alpha\varphi\partial_\beta\varphi + V(\varphi)\right]. \tag{53}$$

The conditions for homogeneity and isotropy make that the spatial derivatives vanish. Assuming a FLRW metric, the 00 and ij-components of the stress-energy tensor then read:

$$T_{00} = \frac{\dot\varphi^2}{2} + V(\varphi)\,, \qquad T_{ij} = a^2(t)\,\delta_{ij}\,\frac{\dot\varphi^2}{2} + V(\varphi)\,. \tag{54}$$

Making a comparison with the stress-energy tensor for a perfect fluid one identifies:

$$\rho = \frac{\dot\varphi^2}{2} + V(\varphi)\,, \tag{55}$$

$$p = \frac{\dot\varphi^2}{2} - V(\varphi)\,. \tag{56}$$

The dynamics of the energy-density is governed by equation (27). Substituting the expression in (55) one gets the equation of motion for the inflaton field φ:

$$\ddot\varphi + 3H\dot\varphi + V'(\varphi) = 0\,, \tag{57}$$

where a prime denotes a derivative with respect to the scalar field. This equation is equivalent to the Klein-Gordon equation [65, 66] in curved spacetime $\Box\varphi = V'(\varphi)$, where the d'Alembertian operator in curved spacetime is given by $\Box = -1/\sqrt{-g}\,\partial_\mu(\sqrt{-g}g^{\mu\nu}\partial_\nu)$. The friction term in (57) accounts for the expansion of the Universe. Notice that equation (57) is a second-order differential equation, hence the evolution of the system is fully determined if the values of

the initial field and its time derivative φ_i, $\dot{\varphi}_i$ are given. The subsequent evolution can be represented in a $(\varphi, \dot{\varphi})$ - plane.

Since we are assuming the scalar field dominates the energy-density of the Universe, the first Friedmann equation (29) reduces to:

$$H^2 = \frac{8\pi}{3}\left[\frac{\dot{\varphi}^2}{2} + V(\varphi)\right] . \tag{58}$$

This equation, together with the equation of motion for the scalar field (57), forms a closed system of equations which completely determines the dynamics of the scalar field and of the expansion once the potential $V(\varphi)$ is given.

In order to get an accelerated expansion of the Universe we must impose the condition $\rho + 3p < 0$. Using equations (55) and (56) for the energy density and the pressure of the scalar field, this condition translates into a relation between the time derivative and the potential:

$$\dot{\varphi}^2 < V(\varphi) . \tag{59}$$

We can also define the equation of state parameter w as

$$w = \frac{p}{\rho} = \frac{\dot{\varphi}^2/2 - V(\varphi)}{\dot{\varphi}^2/2 + V(\varphi)} . \tag{60}$$

The condition in (59) is equivalent to require $w < -1/3$. In the limiting case of $\dot{\varphi}^2 \ll V(\varphi)$, it is clear from (60) that $w \sim -1$. This condition for the scalar field then reproduces a *quasi - de Sitter inflation*, quite well approximated by a de Sitter expansion with $H \approx \sqrt{8\pi V(\varphi)/3}$ constant. The main difference with the pure de Sitter case is that a de Sitter inflation never ends, while in the quasi - de Sitter scenario inflation ends at a finite time, when the inflaton field oscillates around the minimum of its potential, thus starting the reheating phase (see Section 2.4.4).

We now focus on the latter case of a quasi - de Sitter expansion, whose deviation from the de Sitter case is parametrized by what are called *slow-roll parameters*. Equations (57) and (58) can be combined into an expression for the evolution of the Hubble parameter:

$$\dot{H} = -\frac{1}{2}\frac{\dot{\phi}^2}{M_{Pl}} . \tag{61}$$

Taking the ratio between this expression and (58) one gets:

$$\varepsilon_1 \equiv -\frac{\dot{H}}{H^2} = \frac{\frac{3}{2}\dot{\varphi}^2}{\frac{1}{2}\dot{\varphi}^2 + V(\varphi)} . \tag{62}$$

The condition $\dot{\varphi}^2 \ll V(\varphi)$ translates into the requirement that $\varepsilon_1 \ll 1$. ε_1 is the first slow-roll parameter. Notice that since $\dot{H} < 0$, then $\varepsilon_1 > 0$. Moreover, since inflation happens for $\ddot{a} > 0$, it is easy to show using the Friedmann equations that $\varepsilon_1 < 1$. The condition to be close to de Sitter is then stronger than requiring inflation, as one would expect looking at the values of w. Inflation ends when $\varepsilon_1 = 1$. In order for slow-roll inflation to last enough, we need that ε_1 remains

small for a sufficient number of e-folds. We then define the second slow roll parameter as

$$\varepsilon_2 \equiv \frac{d \ln \varepsilon_1}{dN} = \frac{\dot{\varepsilon}}{H\varepsilon}, \tag{63}$$

and we require it to be much smaller than one. Substituting the previous result for ε_1 we get:

$$\varepsilon_2 = 2\frac{\ddot{\varphi}}{H\dot{\varphi}} - 2\frac{\dot{H}}{H^2} \ll 1. \tag{64}$$

Then, as one would expect, the second derivative of the scalar field has to be negligible. If this is the case, from equation (57) one gets:

$$\dot{\varphi} \approx -\frac{V'(\varphi)}{3H}. \tag{65}$$

This is a first order equation, then in this case the initial field value φ_i is enough to fully describe the system.

The slow-roll parameters ε_1 and ε_2 can be expressed in terms of the potential only; in particular:

$$\varepsilon_1 \approx \frac{1}{16\pi}\left(\frac{V'}{V}\right)^2, \tag{66}$$

$$\varepsilon_2 \approx \frac{1}{4\pi}\left[\left(\frac{V'}{V}\right)^2 - \frac{V''}{V}\right], \tag{67}$$

The slow-roll conditions $\varepsilon_1, \varepsilon_2 \ll 1$ then just tell us the potential has to be flat enough for slow-roll inflation to happen and last enough.

We can generalize the two definitions for the slow-roll parameters into the unique relation:

$$\varepsilon_{n+1} = \frac{d \ln |\varepsilon_n|}{dN}, \tag{68}$$

where $\varepsilon_0 = H_i/H \approx 1$ ($\varepsilon_0 = 1$ in the de Sitter case and all the higher order slow-roll parameters vanish identically). Slow-roll inflation requires the Hubble flow functions $\varepsilon_{n+1} \ll 1 \ \forall n$.

Notice that once specified the potential $V(\varphi)$, using equation (65) it is possible to iteratively build an analytic solution to the equations of motion that satisfies the slow-roll conditions (68). The series converges towards a unique trajectory in the $(\varphi, \dot{\varphi})$ - space, i.e. the slow-roll solution. An important feature of slow-roll inflation is that if the potential satisfies the slow-roll conditions, then the slow-roll solution is an attractor. Different trajectories in phase-space converge exponentially in the number of e-folds. The slow-roll approximation is then a good approximation of the dynamics of the field regardless of the initial conditions at the onset of inflation. This characteristic makes that slow-roll inflation does not suffer of fine-tuning problems in the initial conditions.

2.4.4 *Reheating*

We have seen how a period of inflation solves some of the major problems in the Big Bang model of cosmology. However, the standard succession of eras of the hot Big Bang model has lots of observational confirmations coming from the BBN and the CMB, as we have seen in Section 2.2.3.2. We then need to understand how to connect the period of accelerated expansion to the standard evolution in the Big Bang scenario.

During inflation, the energy-density of the Universe is dominated by the scalar field φ. Any form of matter that existed beforehand would have been significantly diluted by the expansion, hence the matter content of the Universe is expected to be produced after inflation [67, 68]. Therefore, at the end of inflation, the energy of the inflaton field has to be transferred, possibly through intermediaries, to SM particles. This process is called *reheating* [69] and it leads to the initial radiation domination of the standard Big Bang model. Since we do not want to spoil the BBN, we must require that the particles produced during the reheating thermalize at a temperature T_{reh} higher than the BBN temperature, i.e. $T_{reh} \geq 1$ MeV. Two relevant papers on this topic are [70, 71], while an interesting review is provided by [72]. Here we give just a basic overview of the main features.

There are two competing processes generating the SM particles during reheating. First, by perturbative decay of the inflaton field φ; second, by collective non-perturbative resonances, called *parametric resonances*.

Let us consider the perturbative decay of φ particles. Inflation ends when $\varepsilon_1 \simeq 1$, which means that the kinetic energy of the inflaton field starts to become relevant with respect to the potential energy. This happens when the potential steepens and the inflaton starts quickly rolling down towards the minimum. At this moment, the field starts oscillating around the minimum, and the amplitude of the oscillations diminishes thanks to the friction term $3H\dot{\varphi}$ in (57). When the oscillations are close to the minimum of the potential, we can approximate $V(\varphi) \approx 1/2\, m\varphi^2$, with m the mass of the inflaton. In this case the equation of motion simplifies to

$$\ddot{\varphi} + 3H\dot{\varphi} + m^2\varphi = 0\,. \tag{69}$$

This is the equation for a damped harmonic oscillator, whose solution can be written as

$$\phi(t) \simeq \Phi(t)\cos(mt)\left(1 + \frac{\sin(2mt)}{2mt}\right)\,, \tag{70}$$

with $\Phi(t) = M_{Pl}/\sqrt{3\pi}mt$. Taking (56), and averaging over one period of oscillations, one finds $\langle p\rangle = 0$. This result is obtained in the limit $m \gg H$, which is justified on timescales that are short compared to the expansion of spacetime. The oscillating field thus behaves like a pressureless fluid; hence the Universe during reheating expands like a matter dominated Universe.

The inflaton oscillations can be interpreted as a collection of independent scalar particles, each oscillating coherently at the same frequency m, i.e. a coherent wave of particles with zero momenta and particle density $n = \rho/m \sim$

a^{-3}. Each individual particle can be coupled to particles χ of other species, leading to a decrease of the oscillating amplitude which competes to the decrease due to the expansion of spacetime. Notice that those couplings exist even during inflation but play no role because, even if χ particles were produced, the exponential expansion would dilute them and nothing would be left at the end of inflation. There are several interaction terms one could consider, the simplest being a three-body interaction of the kind $\sigma\varphi\chi^2$, corresponding to the annihilation of φ-particles in pairs of χ particles. Here σ is a coupling constant, supposed to be small to avoid large radiative corrections. One way to treat this kind of perturbative decay processes is to add an effective decay rate into the equations of motion (57) [6]:

$$\ddot{\varphi} + 3H\dot{\varphi} + m^2\varphi = -\Gamma\dot{\varphi}\,, \tag{71}$$

whose generic solution is given by

$$\varphi(t) = \Phi(t)\,\sin(mt)\,. \tag{72}$$

Here $\Phi(t)$ has a different, more complicated expression with respect to the previous result, and it contains both H and Γ. Taking into account both the expansion of the Universe and the decay into χ particles, one can check that the amplitude of the oscillations decreases as

$$\Phi(t) = \Phi_0 \exp\left[-\frac{1}{2}(3H+\Gamma)t\right]\,. \tag{73}$$

Notice that Γ may include different decay processes, being the sum of different decay rates Γ_i. Initially $\Gamma \ll 3H$ and the energy and number densities of the inflaton particles decay like a matter fluid. Eventually, the Universe expands sufficiently that the decay rate becomes larger than the rate of expansion and the inflaton decays suddenly into χ particles. Assuming the mass of the decay products to be much smaller than the Hubble rate, $m_i \ll H$, we expect them to behave like radiation, i.e. having an energy density given by (37). After they are produced, the χ particles interact among themselves and soon thermalize to a common temperature. An estimate of the reheating temperature arises from equating the Hubble rate to the decay rate: $H \sim \Gamma$.

Perturbative calculations of reheating neglect the fact that the initially large oscillations of the inflaton field could trigger an exponential production of particles [68, 70]. This is the second way we can produce the SM particles, i.e. via parametric resonances. This method is much more efficient in transferring energy than the perturbative decays. The phase of non-perturbative resonances is called *preheating*. The preheating processes start to become inefficient when the oscillations of the inflaton are damped; at this point, perturbative decays finish the job and make the inflaton to totally decay. Notice that the particles produced via parametric amplifications are in a non-thermal state, then coupling with other particles are required to reach the thermalization.

The analysis of non-perturbative decays through parametric resonances is beyond the scope of this introduction. Interested readers can refer to [68, 70–72].

6 The effective decay rate arises from the imaginary part of the denominator of the QFT propagator; the real part is negligible thanks to the small coupling.

3

COSMOLOGICAL PERTURBATIONS THEORY

In the previous chapter, we have explained the physics of a homogeneous Universe; however, on small scales the Universe is clearly inhomogeneous. Indeed the Universe is made of galaxy clusters separated by cosmic voids. In order to understand cosmic structure formation, we have to introduce inhomogeneities and follow their evolution.

We expect the inhomogeneities in the early Universe to be small. Indeed in the CMB map generated by the Planck collaboration (see Figure 5) the anisotropies in the temperature are measured to be $\delta T/T \sim 10^{-5}$. These anisotropies directly reflect the small degree of inhomogeneities at LSS time [73]. The structures in the Universe are then generated via gravitational instabilities by small fluctuations in the early Universe. Right after the first works on inflation, it was realized that an accelerated expansion of spacetime also provides a mechanism to generate these small perturbations. In [74], it was proposed for the first time how small fluctuations enhanced by a de Sitter phase could explain inhomogeneities in the Universe. The analysis of matter inhomogeneities in the context of inflation was first done by [75–78], while the generation of cosmological gravitational waves was firstly discussed in [79].

In this chapter, we develop the theory of cosmological perturbations, by deriving the equations that govern their evolution in a full GR framework.

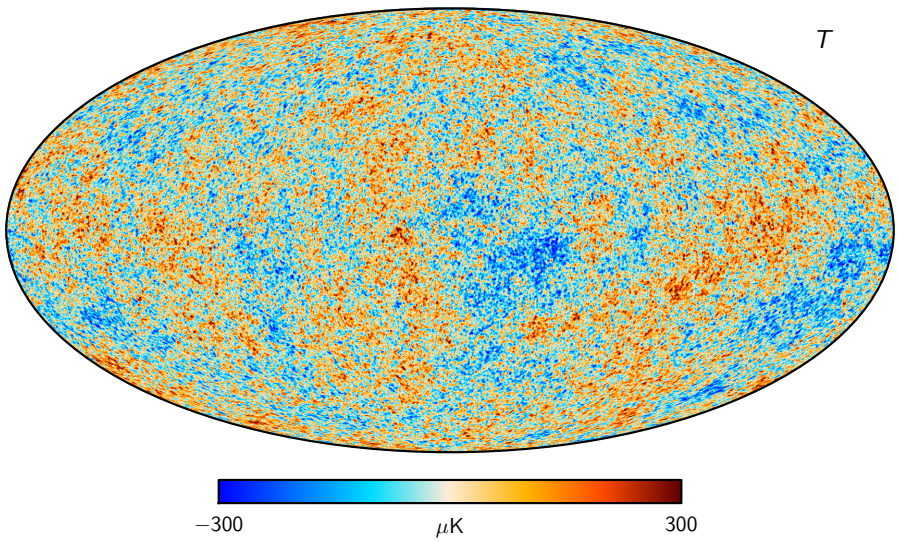


Figure 5: CMB map as measured by the satellite Planck [53]. In this map the dipole, attributed to our peculiar velocity with respect to the CMB, and the monopole, corresponding to the average thermal emission at $T_{CMB} = 2.72548 \pm 0.00057\,K$, have been subtracted. This map displays the anisotropies in the CMB, highlighting the inhomogeneities in the energy-matter distribution of the Universe at the moment of emission.

3.1 SVT DECOMPOSITION OF METRIC PERTURBATIONS

For the following discussion, we will primarily refer to [40, 41, 80, 81]. According to the standard model of structure formation, small primordial fluctuations give rise to the structures thanks to gravitational collapse. In this chapter we focus on the initial stage of this process, when the inhomogeneities remain small relative to the background densities, so that a perturbative analysis can be applied.

The problem of studying the growth of small perturbations in the GR framework reduces to solving the linearized Einstein equations around a FLRW background. We start considering the metric perturbations. Since the spatial curvature becomes negligible right after the onset of inflation, we will neglect it in this treatment, and set $\mathcal{K} = 0$. We can then write the generic perturbed line element as:

$$ds^2 = a^2(\tau)\left[-(1+2\phi)d\tau^2 + 2B_i dx^i d\tau + (\gamma_{ij} + E_{ij})dx^i dx^j\right] . \tag{74}$$

Here ϕ, B_i and E_{ij} are functions of (τ, x^i) and we will work with the conformal time τ. γ_{ij} is the Euclidean three-dimensional metric. It is convenient to perform a scalar-vector-tensor (SVT) decomposition. In this decomposition, one breaks down each of these terms into components that transform in a well-defined manner under the group of 3D spatial rotations, which is a symmetry of the (flat) background metric. It has been shown that, within this decomposition and considering linear theory, scalar, vector, and tensor perturbations evolve independently and can be analyzed separately [80, 82]. The SVT decomposition for vectors splits B_i into the gradient of a scalar and a divergenceless vector, according to

$$B_i = S_i - \partial_i B\,, \qquad \partial^i S_i = 0\,. \tag{75}$$

For tensors we have a similar decomposition, i.e.

$$E_{ij} = -2\psi\gamma_{ij} + 2\partial_i\partial_j E + 2\partial_{(i}F_{j)} + h_{ij}\,, \qquad \partial^i F_i = \partial^i h_{ij} = 0\,, \quad h^i_i = 0\,, \tag{76}$$

where $\partial_{(i}F_{j)} = (\partial_i F_j + \partial_j F_i)$ is the symmetrized derivative. Here F_i is divergenceless, and h_{ij} is divergenceless and traceless. The perturbations ϕ, B_i and E_{ij} have 10 components; after the SVT decomposition, we have four scalars (ϕ, ψ, B, E), two divergenceless vectors (S_i, F_i) and one divergenceless and traceless tensor (h_{ij}), i.e. again 10 components. Vector perturbations are not produced during inflation and, even if they were present initially, the expansion of the Universe would make them decay. For this reason, in the following we will consider only scalar and tensor perturbations, which give rise to density fluctuations and gravitational waves respectively in the late Universe.

3.2 GAUGE - INVARIANT VARIABLES

The definition of the variables here introduced is not unique, but it depends on the gauge choice, i.e. the specific coordinates chosen to describe the system.

This ambiguity arises from the fact that general covariance is broken in cosmology by choosing a specific foliation of spacetime, i.e. specific time slices and specific coordinates on those slices. A change in the coordinates affects the values of the perturbation variables. As an example, consider the FLRW metric in (23) with $\mathcal{K} = 0$ and perform a change of coordinates $x^i \mapsto \tilde{x}^i = x^i + \xi^i(\tau, x^i)$. Then we can write $dx^i = d\tilde{x}^i - \partial_\tau \xi^i d\tau - \partial_k \xi^i d\tilde{x}^k$. The line element consequently becomes

$$\begin{aligned} ds^2 &= a^2(\tau)\left[-d\tau^2 + \gamma_{ij}x^i x^j\right] \\ &= a^2(\tau)\left[-d\tau^2 - 2\xi_i' d\tilde{x}^i d\tau + (\gamma_{ij} - 2\partial_{(i}\xi_{j)})d\tilde{x}^i d\tilde{x}^j\right], \end{aligned} \tag{77}$$

where a prime indicates a derivative with respect to conformal time and we have neglected higher order terms in the perturbations. Comparing with (74), we see that this change of coordinates introduced fictitious perturbations $B_i = -2\xi_i'$ and $E_{ij} = -2\partial_{(i}\xi_{j)}$. These modes are spurious, since we can move back to the homogeneous metric (23) by restoring the old coordinates.

This simple example shows how the perturbations introduced in (74) are sensitive to the choice of coordinates. In order to avoid mistaking true perturbations of spacetime with spurious gauge degrees of freedom, one can introduce gauge-invariant variables. In order to construct these variables, one has to look at how each perturbation variable changes under a change of coordinates $x^\mu \mapsto \tilde{x}^\mu = x^\mu + \xi^\mu(x^\mu)$, with ξ^μ small. The computations of the gauge-invariant variables can be found in [41, 81]. It turns out there are two gauge invariant scalars called *Bardeen variables* [83], which can be constructed out of the previous variables as:

$$\Phi_B = \phi - \mathcal{H}(B - E') + (B - E')', \tag{78}$$

$$\Psi_B = \psi - \mathcal{H}(B - E'), \tag{79}$$

with $\mathcal{H} = a'/a$ the conformal Hubble radius. The tensor perturbations h_{ij} are instead already gauge-invariant.

3.3 COUPLING WITH THE INFLATON PERTURBATIONS

In order to study the evolution in time of the cosmological perturbations and how they give rise to structures in the Universe, one needs to perturb the stress-energy tensor $T_{\mu\nu}$ in the same way as we did for the metric, and then compute the perturbed Einstein equations. Indeed, as a general fact, the perturbations in the matter-energy content of the Universe backreact on the spacetime geometry, and metric and matter perturbations couple together through the Einstein equations. After inflation, the equations of motion for the perturbations are obtained considering the stress-energy tensor for a perfect fluid. The description of this general case is beyond the scope of this work. For a full treatment see [41, 80, 81]. We are instead interested in the perturbations during single-field inflation, where the energy-density of the Universe is dominated

by the inflaton field φ. Consequently the stress-energy tensor will be that of a scalar field, as seen in Section 2.4.3. We decompose the inflaton field as

$$\varphi(\tau, x^i) = \bar{\varphi}(\tau) + \delta\varphi(\tau, x^i)\,, \tag{80}$$

with $\bar{\varphi}$ the background field and $\delta\varphi$ the perturbations. Since we are considering a homogeneous and isotropic background metric, i.e. a FLRW metric, the background inflaton field has to be homogeneous too for consistency. Notice that the inflaton field only generates scalar perturbations.

The stress-energy tensor can be also decomposed into a background and a perturbed part as

$$T_{\mu\nu} = \bar{T}_{\mu\nu} + \delta T_{\mu\nu}\,. \tag{81}$$

At this point, one can compute the components of the background stress-energy tensor and of the perturbed one at first order in the perturbations using (53) and substituting (80) and (74). As done in the previous section, we want our results to be independent on the choice of coordinates. We then introduce the gauge-invariant inflaton perturbation

$$\delta\varphi_{gi} = \delta\varphi + \varphi_0'(B - E')\,. \tag{82}$$

In order to write down the gauge-invariant evolution equations for the cosmological perturbations, one has to rewrite the Einstein equations in a gauge invariant way (see equation (4.15) of [81]) and insert the gauge-invariant components of the stress-energy tensor, written in function of the new variable (82) and of the Bardeen variables (78) and (79). From the ij-components of the Einstein equations it follows that $\Phi_B = \Psi_B$. Imposing this equality in the remaining components of the Einstein equations one finds three different evolution equations for $\delta\varphi_{gi}$ and Φ_B, out of which only two are independent:

$$\begin{aligned} &\Phi_B' + \mathcal{H}\Phi_B = 4\pi\bar{\varphi}'\delta\varphi_{gi}\,,\\ &\Phi_B'' + \nabla^2\Phi_B = 8\pi\bar{\varphi}'\delta\varphi_{gi}'\,. \end{aligned} \tag{83}$$

These are the basic perturbation equations for a Universe dominated by a scalar field. It turns out that the evolution of the perturbations is more conveniently studied in terms of a single scalar quantity, called Mukanov-Sasaki variable [74, 82]:

$$v = a\left[\delta\varphi_{gi} + z\Phi_B\right]\,, \qquad z = \frac{a\bar{\varphi}'}{\mathcal{H}}\,. \tag{84}$$

The perturbed Einstein-Hilbert action (7) and the perturbed scalar field action (52) can then be gathered together into

$$S = \frac{1}{2}\int d^4x\left[(v')^2 - \gamma^{ij}\partial_i v\partial_j v + \frac{z''}{z}v^2\right]\,. \tag{85}$$

Moving to Fourier space:

$$S = \int d\tau \int_{R^{3+}} d^3k\left[v_{\mathbf{k}}'v_{-\mathbf{k}}' - k^2 v_{\mathbf{k}}v_{-\mathbf{k}} + \frac{z''}{z}v_{\mathbf{k}}v_{-\mathbf{k}}\right]\,, \tag{86}$$

where we have used the following convention for the Fourier transform:

$$v(\tau, \mathbf{x}) = \int \frac{d^3k}{(2\pi)^{3/2}} e^{i\mathbf{k}\cdot\mathbf{x}} v_{\mathbf{k}}(\tau) \,. \tag{87}$$

Notice that, since v is real, $v^*_{\mathbf{k}} = v_{-\mathbf{k}}$. Looking at the action (86), it is immediately clear that it is more convenient to work in Fourier space when studying the evolution of the perturbations; indeed the two modes $\pm\mathbf{k}$ evolve independently.

We now have all the ingredients to study in details the evolution of the cosmological perturbations. But before doing this, let us underline one thing. The gauge-invariant inflaton perturbation is well defined only during inflation. After this period, the inflaton field decays into the SM particles, as seen in Section 2.4.4, and its perturbations lose their meaning. The Mukhanov - Sasaki variable (84), although very useful, is then well defined only during inflation. A convenient quantity to work with is the curvature perturbation ζ:

$$\zeta = \frac{2}{3} \frac{\mathcal{H}^{-1}\Phi'_B + \Phi_b}{1+w} + \Phi_B \,, \tag{88}$$

with $w = \rho/p$ the equation of state parameter. The definition of ζ only involves Φ_B, which is related to the structure of spacetime, and not to the specific matter content considered. ζ is then useful since it is valid even after inflation, during both radiation-domination and matter-domination; moreover it easily related to the Mukhanov - Sasaki variable via:

$$\zeta = \frac{v}{z} \,. \tag{89}$$

One important property of ζ is that, as we are going to see in the next section, it is conserved on large scales [78, 81]. It allows then to link the evolution of the perturbations during inflation, and specifically of the Bardeen potentials, with observables at later times. One example is provided by the power spectrum, i.e. the two-point function, of ζ (see Section 3.6); it is directly related to the Bardeen potentials, which in turn are linked to the CMB temperature anisotropies via Sachs-Wolfe effect [73]. The details of the computations to connect the primordial perturbations to the CMB observables are beyond the scope of this work; further details can be found in [41, 43, 84].

As a last remark, the case of tensor perturbations is similar to that of scalar perturbations. One can decompose the tensor h_{ij} into two real scalar fields $h_\lambda(\tau, \mathbf{k})$, with $\lambda = \pm$, representing its two polarizations in helicity basis. The free action for the tensor modes decouples into a sum of two actions for the two polarizations, independent of each other. More details will be provided in Section 7.4, where also interactions will be considered.

3.4 EVOLUTION OF THE INFLATIONARY PERTURBATIONS

We now proceed to the study of the time evolution of the cosmological perturbations during inflation. The equation of motion for the Mukhanov-Sasaki variable is easily obtained from the action (86). In Fourier space it reads:

$$v''_{\pm\mathbf{k}} + \left(k^2 - \frac{z''}{z}\right) v_{\pm\mathbf{k}} = 0 \,. \tag{90}$$

Notice that this equation is valid on all scales and it does not rely on the slow-roll approximation. It is the equation of motion of an harmonic oscillator with time-dependent frequency

$$\omega_k^2 = k^2 - \frac{z''}{z}\,. \tag{91}$$

The behaviour of the perturbations depend on the sign of the frequency squared: if ω_k^2 is positive, the modes are expected to oscillate, while if ω_k^2 is negative, the modes get amplified. In order to understand the time evolution of ω_k^2, let us focus on the term z''/z. It can be expanded in terms of the slow-roll parameters as [1]

$$\frac{z''}{z} = \frac{a''}{a} + \frac{\varepsilon_2}{2}\left(\frac{a''}{a} + \mathcal{H}^2\right) + \frac{\mathcal{H}}{2}\left(\varepsilon_2\varepsilon_3 + \frac{\varepsilon_2^2}{2}\right)\,. \tag{92}$$

However let us consider for the moment the de Sitter case, for which one has

$$\frac{z''}{z} \approx \frac{a''}{a} \approx 2\mathcal{H}^2\,, \tag{93}$$

having used the fact that $a' = a^2 H$. This allows us to catch the qualitative behaviour of the perturbations. The slow-roll expansion will be considered in the next section.

The inverse of z''/z is then a measure of the comoving Hubble radius. Making a comparison between k^2 and $(aH)^2$ one can then understand the behaviour of the modes. This is equivalent to make a comparison between the physical size of the Hubble radius $1/aH$ and the wavelength $1/k$ of the mode. We have two possible regimes:

- $k \gg aH$. The wavelength is smaller than the Hubble radius and the mode is said to be *sub-Hubble* (or *sub-horizon*). In this case $\omega_k^2 > 0$ and the perturbation oscillates.
- $k \ll aH$. The wavelength is larger than the Hubble radius and the mode is said to be *super-Hubble* (or *super-horizon*). In this case $\omega_k^2 < 0$ and the perturbation is amplified.

We have already seen in Section 2.4.1.1 that the physical size of the Hubble radius decreases in time if the Universe is undergoing an accelerated expansion. Therefore, modes whose wavelength was smaller than the Hubble radius, as time goes by, will eventually become larger. We than say they *exit the horizon*. When this happens, they get amplified by the expansion of spacetime. After the end of inflation, the Hubble radius starts growing and the modes will eventually *re-enter the horizon* and they will start to oscillate again. Of course modes with different wavelengths will exit and re-enter the horizon at different times.

Let us now follow more in details the evolution of the cosmological perturbations. Suppose the mode under consideration has a wavelength smaller than

1 This expansion can be easily obtained noticing that one can rewrite $z \approx a\sqrt{2\varepsilon_1}\,M_{Pl}$ (combining its definition (62) and (61)) and then taking its second derivative with respect to the conformal time. The higher order slow-roll parameters appear thanks to higher derivatives of ε_1.

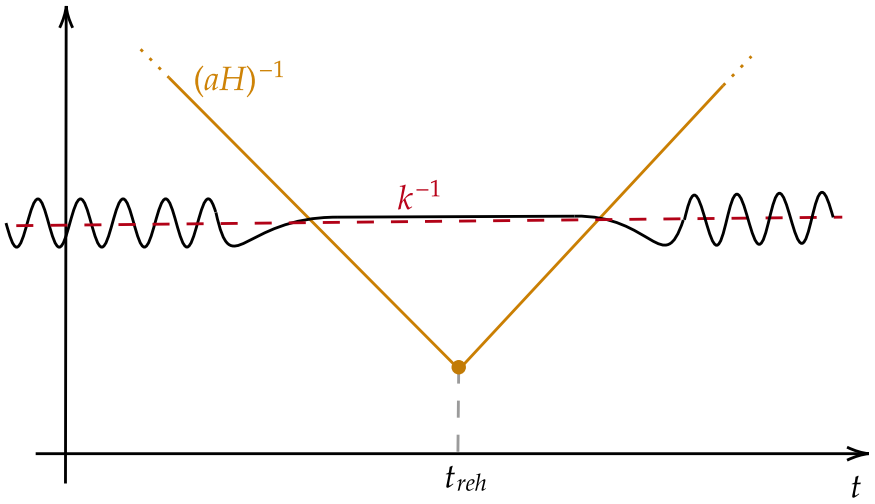


Figure 6: Schematic representation of the time evolution of the curvature perturbations. The initially oscillating mode is frozen on super-horizon scales. As soon as it re-enter the horizon it starts oscillating again.

the Hubble radius at the beginning of inflation, i.e. it is initially sub-horizon. In this regime we can neglect the scale factor dependent term in (91); this is equivalent to say that the perturbation "does not feel" the expansion of spacetime. We can then write the solution of (90) as

$$v_k(\tau) \approx A_k\, e^{ik\tau} + B_k\, e^{-ik\tau}\,. \tag{94}$$

The two constants A_k and B_k are fixed once the initial conditions for the modes are known. As time goes by, the Hubble radius shrinks and at a certain time the wavelength k^{-1} will overcome it. We then enter in the opposite regime. The perturbation starts "feeling" the expansion of spacetime, until the scale factor dependent term in (91) becomes dominant. At this point, the solution to (90) matches

$$v_k(\tau) \approx \alpha_k\, z(\tau) + \beta_k\, z(\tau) \int_\tau^0 \frac{d\tau'}{z^2(\tau')}\,. \tag{95}$$

α_k and β_k are two complex coefficients, which are determined by following the evolution of the perturbations in time. Since $z(\tau) > 0$, the first term, proportional to z, is called *growing mode*; while the second term, proportional to z, is instead called *decaying mode*.

Recall now the definition of the curvature perturbation ζ (88). At the end of inflation the Mukhanov - Sasaki variable loses his meaning; it is then useful to see which is the behaviour of ζ at that moment. Using the definition (89), we can divide by z equation (95) to get

$$\zeta_k(\tau) \approx \alpha_k + \beta_k \int_\tau^0 \frac{d\tau'}{z^2(\tau')}\,. \tag{96}$$

Since the second term is decaying, and can be neglected after few e-folds of inflation, the curvature perturbation on super-horizon scales can be approximated as $\zeta \approx \alpha_k$; it is therefore "frozen" on large scales (see Figure 6). This

fact is really helpful, since it implies that in order to connect the perturbations during inflation to the CMB observables we just need to compute the value of the constant α_k. This is done by fixing the initial conditions for the Mukhanov - Sasaki variable in (94) and joining the solution in the sub-horizon regime to that in the super-horizon regime at $k \sim aH$.

3.5 QUANTUM INITIAL CONDITIONS

To study the time evolution of the inflationary perturbations we need to fix the initial conditions. We already told that the beginning of inflation is set around the GUT scale. The starting point for the analysis of the perturbations, when they were sub-horizon, is then around that energy scale too. We then expect a description of the system in terms of quantum fields to be relevant. In order to fix the initial conditions for the evolution of the perturbations we then proceed to the canonical quantization of the system under consideration. Let's start from the action (86). We define the canonically conjugated variable, the momentum, as $p_{\pm k} = v'_{\pm k}$; we can then construct the Hamiltonian as

$$\mathcal{H} = \frac{1}{2}\int_{R^{3+}} d^3k \left[p_{\mathbf{k}} p^*_{\mathbf{k}} + \left(k^2 - \frac{z''}{z} \right) v_{\mathbf{k}} v^*_{\mathbf{k}} \right] . \tag{97}$$

We now proceed to the canonical quantization by promoting the fields v and p to operators $\hat{v}$ and $\hat{p}$ [2], imposing the following canonical commutations relations:

$$[v_{\mathbf{x}}, v_{\mathbf{x}'}] = [\pi_{\mathbf{x}}, \pi_{\mathbf{x}'}] = 0\,, \quad [v_{\mathbf{x}}, \pi_{\mathbf{x}'}] = i\delta(\mathbf{x} - \mathbf{x}')\,, \tag{98}$$

or equivalently in Fourier space:

$$[v_{\mathbf{k}}, v_{\mathbf{k}'}] = [\pi_{\mathbf{k}}, \pi_{\mathbf{k}'}] = 0\,, \quad [v_{\mathbf{k}}, \pi_{\mathbf{k}'}] = i\delta(\mathbf{k} - \mathbf{k}')\,. \tag{99}$$

At this point, we expand the field and its conjugate momentum in terms of creation and annihilation operators as

$$v_{\mathbf{k}} = u_k(\tau)\, a^0_{\mathbf{k}} + u^*_k(\tau)\, a^{0\dagger}_{-\mathbf{k}}\,, \tag{100}$$

$$\pi_{\mathbf{k}} = u'_k(\tau)\, a^0_{\mathbf{k}} + u^{*\prime}_k(\tau)\, a^{0\dagger}_{-\mathbf{k}}\,, \tag{101}$$

with $k = |\mathbf{k}|$. The ladder operators satisfy the following commutation relations:

$$\left[a_{\mathbf{k}}, a^\dagger_{\mathbf{k}'}\right] = \delta\left(\mathbf{k} - \mathbf{k}'\right)\,, \quad [a_{\mathbf{k}}, a_{\mathbf{k}'}] = \left[a^\dagger_{\mathbf{k}}, a^\dagger_{\mathbf{k}'}\right] = 0\,. \tag{102}$$

The label "0" indicates the ladder operators are considered at an initial time τ_0. In this way, instead of fixing the two initial conditions for $v_{\mathbf{k}}(\tau_0)$ and $\pi_{\mathbf{k}}(\tau_0)$,

2 From now on, we will drop the hat for simplicity.

we need to fix the initial ladder operators, while the time dependence is encoded in the two complex *mode functions* $u_k(\tau)$, which satisfy the classical equation of motion (90). The normalization condition for the mode functions is given by

$$u_k\, u_k^{*\prime} - u_k^*\, u_k' = i\,. \tag{103}$$

We have now reformulated the problem in a quantum framework and we are back to the problem of specifying the initial conditions. The simplest choice we can make is to assume there were only vacuum fluctuations at the beginning of inflation. The vacuum state is defined as the one annihilated by the annihilation operator $a_{\mathbf{k}}$, i.e. $a_{\mathbf{k}}|0\rangle = 0$, at the beginning of inflation. The starting point τ_0 is chosen such that the mode k considered was far inside the Hubble radius and did not feel the expansion of spacetime; this condition translates mathematically into $|k\tau| \ll 1$. To make the computations simpler we take the limit $\tau \to -\infty$. In this regime, the mode functions satisfy the equation (90) but neglecting the term z''/z. For each mode k we then choose as ground state that of an harmonic oscillator. The normalized mode functions are then given by

$$u_k(\tau) \xrightarrow{k\tau\to-\infty} \frac{1}{\sqrt{2k}}\, e^{-ik\tau}\,. \tag{104}$$

This choice for the initial vacuum state is called Bunch-Davies (BD) *vacuum*. Solving equation (90) in the de Sitter approximation leads to the BD *mode functions*

$$u_k(\tau) = \frac{1}{\sqrt{2k}}\left(1 - \frac{i}{k\tau}\right) e^{-ik\tau}\,. \tag{105}$$

In the sub-horizon limit we have already seen how this mode function leads to plane waves. In the super-horizon limit, i.e. taking $\tau \to 0$ we immediately see that $|\zeta_k| = |u_k|/a \to H/\sqrt{2k^3}$, having used $a \approx -1/H\tau$. The curvature perturbation ζ_k then approaches a constant at the end of inflation, as expected.

Let us now consider the more general case of slow-roll inflation. Looking at (92), we can write the time dependent part of ω_k^2 at leading order in the slow-roll parameters as

$$\frac{z''}{z} \approx \frac{a''}{a} + \frac{\varepsilon_2}{2}\left(\frac{a''}{a} + \mathcal{H}^2\right) \approx \frac{2 + 3\varepsilon_1 + \frac{3}{2}\varepsilon_2}{\tau^2}\,, \tag{106}$$

having used for the conformal Hubble parameter $\mathcal{H} \approx -1/\tau(1+\varepsilon_1)$ at leading order. The equation of motion (90) reduces then to

$$u_k'' + \left(k^2 - \frac{\nu^2 - 1/4}{\tau^2}\right) u_k = 0\,, \tag{107}$$

with

$$\nu^2 = \frac{9}{4} + 3\left(\varepsilon_1 + \frac{1}{2}\varepsilon_2\right)\,. \tag{108}$$

This equation has an exact solution given by

$$u_k(\tau) = \sqrt{-\tau}\left[c_1(k)\,\mathrm{H}_\nu^{(1)}(-k\tau) + c_2(k)\,\mathrm{H}_\nu^{(2)}(-k\tau)\right]\,, \tag{109}$$

where $H_\nu^{(1,2)}$ are the Hankel functions of the first and second kind. Considering the following asymptotic expansions for the Hankel functions [3]

$$\begin{aligned}\lim_{k\tau\to-\infty} H_\nu^{(1)}(-k\tau) &\approx \sqrt{\frac{2}{\pi}}\frac{1}{\sqrt{-k\tau}}e^{-\imath k\tau}\,,\\ \lim_{k\tau\to-\infty} H_\nu^{(2)}(-k\tau) &\approx \sqrt{\frac{2}{\pi}}\frac{1}{\sqrt{-k\tau}}e^{\imath k\tau}\,,\end{aligned} \tag{110}$$

and imposing the BD vacuum conditions (104), we can find the expressions for the coefficients in (109). It turns out $c_1(k) = \sqrt{\pi}/2$ and $c_2(k) = 0$, so that the final expression for the mode functions at leading order in slow-roll inflation is

$$u_k(\tau) = \frac{\sqrt{\pi}}{2}\sqrt{-\tau}H_\nu^{(1)}(-k\tau)\,. \tag{111}$$

We now have the exact expression for the mode function and we want to find the final value of the curvature perturbation ζ_k in a quasi - de Sitter expansion. We then take the limit of the Hankel function of the first kind for $k\tau \to 0^-$:

$$H_\nu^{(1)}(-k\tau) \approx -\frac{i}{\pi}\Gamma(\nu)\,2^\nu\,(-k\tau)^{-\nu}\,, \tag{112}$$

where $\Gamma(\nu)$ is the Gamma function. In order to get an expression for ζ_k we need to get an expression for $z(\tau)$ too. Using $\mathcal{H} \approx -1/\tau(1+\varepsilon_1)$, one can show that

$$z(\tau) \approx z_*\left(\frac{\tau}{\tau_*}\right)^{\frac{1}{2}-\nu}\,, \tag{113}$$

where τ_* is some reference time and z_* the value of $z(\tau)$ at that time. It is convenient to choose as a reference time the moment when the mode with wavenumber k_* crosses the horizon, that is $\eta_* = -k_*^{-1}$. It can be proved that $z_* \approx H_*/(\sqrt{2\varepsilon_{1*}}M_{Pl}k_*)$ at horizon crossing. Using (112) and (113) we then get

$$|\zeta_k| = \frac{|u_k|}{z} \approx \frac{H_*}{\sqrt{2\varepsilon_{1*}}M_{Pl}}\frac{1}{\sqrt{2k_*^3}}\left(\frac{k}{k_*}\right)^{-\nu}\,. \tag{114}$$

This result shows once again that the curvature perturbation is constant on super-horizon scales, even in the quasi - de Sitter case. Its value depends only on the specific mode k considered.

3.6 LINK WITH THE OBSERVABLES

An important quantity which can be constructed out of the mode functions is the two-point function, defined as:

$$\langle v(\mathbf{x},\tau)v(\mathbf{x},\tau)\rangle = \int\frac{d^3k}{(2\pi)^3}|u_k|^2 = \int\frac{dk}{k}\,P_k(k,\tau)\,, \tag{115}$$

3 In these expressions we removed the unphysical phases.

where

$$P_v(k,\tau) = \frac{k^3}{2\pi^2}\,|u_k|^2 \tag{116}$$

is the *power spectrum*. The average is over an ensemble of Universes, where in each Universe the states were prepared with the same initial conditions. Unfortunately, we have access only to our Universe. Still, under an ergodicity assumption [85], we can intend the average as over independent patches of the sky. From (89) we deduce the expression for the power spectrum of the curvature perturbation ζ_k:

$$P_\zeta(k,\tau) = \frac{k^3}{2\pi^2}\,\frac{|u_k|^2}{z^2}\,. \tag{117}$$

The power spectrum of ζ_k is directly related to the CMB anisotropies. Temperatures anisotropies $\delta T/T$ are seen as the result of a random process. They are measured along different directions $\hat{\mathbf{n}}$ and then compared. The result of this process is the two-point correlation function

$$C(\theta) \equiv \langle \Theta(\hat{\mathbf{n}})\,\Theta(\hat{\mathbf{n}}')\rangle\,, \tag{118}$$

where $\Theta(\hat{\mathbf{n}}) = \delta T/T(\hat{\mathbf{n}})$. The average is over independent patches of the sky, each one considered as an independent realisation of the process $\delta T/T(\hat{\mathbf{n}})$ [85]. We can decompose (118) into spherical harmonics as

$$C(\theta) = \sum_l \frac{2l+1}{4\pi}\,C_l\,P_l(\cos\theta)\,, \tag{119}$$

where C_l is the *angular power spectrum* and $\cos\theta = \hat{\mathbf{n}}\cdot\hat{\mathbf{n}}'$. C_l is related to the correlation functions of the curvature perturbation via a transfer function, which encodes the evolution of the fluctuations in the primordial plasma, the free streaming of photons after decoupling and the projection of the anisotropies on the sky:

$$C_l = 4\pi \int d\ln k\,\Theta_l^2(k)\,\Delta_\zeta^2(k)\,. \tag{120}$$

The transfer function $\Theta_l(k)$ then leads to all the non-trivial features of the CMB angular power spectrum (see [53]). We can identify three different regimes depending on the angles θ (or multipoles):

- Large angles ($\sim 5^\circ - 90^\circ$). These correlations derive from perturbations which were still outside the horizon at the moment of recombination.
- Intermediate angles ($\sim 0.1^\circ - 5^\circ$). At these angles the power spectrum is characterized by an oscillating behaviour. This is due to the fact that the perturbations in the baryon-photon fluid propagate as sound waves, whose frequency depends on the mode. Hence different modes are captured at different stages of their evolution.
- Small angles ($\sim 0.05^\circ - 0.1^\circ$). The power spectrum shows a damping due to the random diffusion of photons, which erases the density contrast in the plasma.

The large-angle correlations were still frozen at the moment of recombination. This part of the CMB spectrum, dominated by the Sachs-Wolfe effect, is then a direct probe of the primordial perturbations.

We now want to study the power spectrum for the CMB scales at the end of inflation. The pivot scale in (114) will then be among those observed in the CMB. For the de Sitter case, using that $u_k(\tau) \approx H/\sqrt{2k^3}$ at the end of inflation, we get for the power spectrum of the curvature perturbations

$$P_\zeta^{dS}(k) = \left(\frac{H}{2\pi}\right)^2 , \tag{121}$$

which is clearly scale invariant.

For a quasi - de Sitter inflation, we use instead the result in (114). The corresponding power spectrum is given by:

$$P_\zeta(k) = \frac{1}{2\varepsilon_{1*} M_{Pl}^2}\left(\frac{H_*}{2\pi}\right)^2 \left(\frac{k}{k_*}\right)^{3-2\nu} . \tag{122}$$

This expression is usually rewritten in function of two unknown parameters, which can be fit using the CMB data, as

$$P_\zeta(k) = A_S \left(\frac{k}{k_*}\right)^{n_S - 1} , \tag{123}$$

where [4]

$$A_S = \frac{H_*^2}{8\pi^2 \varepsilon_{1*} M_{Pl}^2} , \qquad n_S = 1 - 2\varepsilon_{1*} - \varepsilon_{2*} . \tag{124}$$

n_S is called *spectral index* and it is formally defined as

$$n_S = 1 + \frac{d\ln P_\zeta}{d\ln k} . \tag{125}$$

This way of writing the power spectrum is quite convenient since it parameterises the deviation from scale invariance, i.e. the departure from de Sitter. In particular a value for n_S different from one implies the power spectrum is not scale invariant.

We briefly mention here that a similar computation can be performed for tensor perturbations. In this case the mode functions for each polarization u_k^λ will be solutions of equation (90) with z''/z replaced by a''/a. The power spectrum for the gravitational waves h_{ij} will then be a rescaling of the power spectrum for scalar perturbations:

$$P_h(k,\tau) = 2\frac{4}{M_{Pl}^2} P_v(k,\tau) , \tag{126}$$

where the factor 2 comes from the fact we have two-polarizations. The tensor power spectrum is commonly parameterised as

$$P_h(k) = A_T \left(\frac{k}{k_*}\right)^{n_T} . \tag{127}$$

4 To get the expression for n_S we used (108) and Taylor expanded at lowest order the square root.

n_T is another spectral index, defined as

$$n_T = \frac{d \ln P_h}{d \ln k} \,. \tag{128}$$

Scale invariance corresponds to $n_S = 1$ and $n_T = 0$. Like n_S, n_T has an expansion in terms of the slow-roll parameters as

$$n_T = -2\varepsilon_{1*} \,. \tag{129}$$

The behaviour of the spectra thereby relies on the values of the slow-roll parameters, which change depending on the model. However, since $\varepsilon_1 > 0$ for any inflationary scenario, inflation generally forecasts a subtly red-tilted spectrum for tensor perturbations $n_T < 0$, meaning a spectrum whose amplitude decreases with k. Observational data on the power spectra constraint the values of the spectral indices n_S and n_T, thereby restricting the range of feasible inflationary models.

Another relevant parameter is provided by the ratio between the amplitudes of the two power spectra:

$$r = \frac{A_T}{A_S} \approx 16\varepsilon_{1*} \,, \tag{130}$$

which has been evaluated at leading order in the slow-roll parameters. This parameter is called *tensor-to-scalar ratio*.

So far, only the scalar perturbations have been detected. The strongest constraint to the tensor-to-scalar ratio has been found in [86], analysing all data coming from the BICEP2, Keck Array and BICEP3 CMB polarization experiments. They found an upper bound of $r < 0.036$ at 95% confidence level. The values of the spectral index n_S and of the amplitude A_S have been obtained from the latest measurements by the Planck satellite. It was found $n_S = 0.9649 \pm 0.0042$ and $A_S = 2.101^{+0.031}_{-0.034} \times 10^{-9}$ [87].

We close this chapter emphasising that the results here presented rely on the fact that the primordial perturbations originated from vacuum fluctuations, i.e. a purely quantum mechanism. Therefore, in principle, CMB measurements could be a probe of the quantum physics at the basis of the mechanism generating them. This feature is the premise of my whole research and it is for sure worth a deeper investigation. The analysis that is performed on the CMB relies indeed on classical statistics. Hence the question on when and how this quantum-to-classical transition happened arises. Moreover, although the predictions from inflation match the results from the CMB, they could be the result of a classical stochastic process (see Section 5.1 for further details). We will then study other quantities that could help us discerning between the classical or quantum nature of the perturbations in the following chapters. Before delving these topics, we will see in Chapter 4 how the amplification of the primordial fluctuations can be interpreted in terms of particle creation out of the vacuum thanks to the expansion of spacetime.

4

PARTICLE CREATION AND SQUEEZING

In the previous chapter we have introduced the theory of cosmological perturbations and we have seen how they evolve in time during and after inflation. In particular the fluctuations behave as plane waves when they are sub-horizon, while they start growing as soon as they go outside the horizon, i.e. their wavelength becomes bigger than the Hubble radius. We have also provided quantum initial conditions for their evolution, defining the BD vacuum. In this chapter we will see the evolution of these perturbations under a new perspective: particle creation out of the vacuum in an expanding Universe. We will also see that this process is equivalent to *squeezing* the vacuum state. But let us proceed gradually, introducing the basic formalism necessary to understand these concepts.

4.1 BOGOLIUBOV TRANSFORMATIONS

In Section 3.5 we introduced the canonical quantization of the cosmological perturbations. We report here the Hamiltonian of the system, written in terms of the fields $v_{\mathbf{k}}$ and its conjugate momentum $p_{\mathbf{k}}$:

$$H = \int_{R^{3+}} d^3k \left[\pi_{\mathbf{k}} \pi_{-\mathbf{k}} + \left(k^2 - \frac{z''}{z} \right) v_{\mathbf{k}} v_{-\mathbf{k}} \right] . \tag{131}$$

The fields were quantized introducing the ladder operators $a_{\mathbf{k}}$ and $a^{\dagger}_{-\mathbf{k}}$, whose commutation relations are written in (102), as

$$\begin{aligned} v_{\mathbf{k}} &= u_k(\tau)\, a^0_{\mathbf{k}} + u^*_k(\tau)\, a^{0\,\dagger}_{-\mathbf{k}} , \\ \pi_{\mathbf{k}} &= u'_k(\tau)\, a^0_{\mathbf{k}} + u^{*\,\prime}_k(\tau)\, a^{0\,\dagger}_{-\mathbf{k}} . \end{aligned} \tag{132}$$

These relations link the fields with the *time-independent* ladder operators, defined at an initial time τ_0, when the modes were far inside the horizon. However this is not the only way one can write the fields in terms of ladder operators; $v_{\mathbf{k}}$ and $p_{\mathbf{k}}$ can be written in terms of *time-dependent* ladder operators as

$$\begin{aligned} v_{\mathbf{k}} &= \frac{1}{\sqrt{2|\omega_k|}} \left(a_{\mathbf{k}}(\tau) + a^{\dagger}_{-\mathbf{k}}(\tau) \right) , \\ \pi_{\mathbf{k}} &= -i \sqrt{\frac{|\omega_k|}{2}} \left(a_{\mathbf{k}}(\tau) - a^{\dagger}_{-\mathbf{k}}(\tau) \right) , \end{aligned} \tag{133}$$

where ω_k is the frequency defined in (91). Notice that this way of expanding the field is particularly useful since the Hamiltonian becomes that of an harmonic oscillator with time dependent frequency ω_k. One should also note that the frequency ω_k can become imaginary thanks to the term due to the expansion of spacetime, hence we chose to normalize the fields with $|\omega_k|$ in (133).

The time evolution of the fields is now encoded in the time evolution of the ladder operators. $a_{\mathbf{k}}(\tau)$ and $a^{\dagger}_{-\mathbf{k}}(\tau)$ respect the same canonical commutation relations (102) and can be linked to the time-independent operators through a Bogoliubov transformation:

$$\begin{aligned} a_{\boldsymbol{k}}(\tau) &= \alpha_k(\tau)\, a^0_{\boldsymbol{k}} + \beta_k(\tau) a^{0\,\dagger}_{-\boldsymbol{k}}\,, \\ a^{\dagger}_{-\boldsymbol{k}}(\tau) &= \alpha^*_k(\tau)\, a^{0\,\dagger}_{-\boldsymbol{k}} + \beta^*_k(\tau) a^0_{\boldsymbol{k}}\,, \end{aligned} \tag{134}$$

with $a^0_{\boldsymbol{k}} = a_{\mathbf{k}}(\tau_0)$. From the commutation relations for the ladder operators, one finds the following relation among the Bogoliubov coefficients:

$$|\alpha_k|^2 - |\beta_k|^2 = 1\,. \tag{135}$$

Making a comparison between (133) and (132) one can find an expression for the Bogoliubov coefficients in terms of the mode functions. Indeed, rewriting (133) one gets

$$\begin{aligned} a_{\boldsymbol{k}} &= \sqrt{\frac{|\omega_k|}{2}}\,\chi_{\boldsymbol{k}} + \frac{i}{\sqrt{2\,|\omega_k|}}\,\pi_{\boldsymbol{k}}\,, \\ a^{\dagger}_{-\boldsymbol{k}} &= \sqrt{\frac{|\omega_k|}{2}}\,\chi_{\boldsymbol{k}} - \frac{i}{\sqrt{2\,|\omega_k|}}\,\pi_{\boldsymbol{k}}\,. \end{aligned} \tag{136}$$

Substituting (132), we then have

$$\alpha_k = \sqrt{\frac{|\omega_k|}{2}}\,u_k + \frac{i}{\sqrt{2\,|\omega_k|}}\,u_k'\,, \tag{137}$$

$$\beta_k = \sqrt{\frac{|\omega_k|}{2}}\,u_k^* + \frac{i}{\sqrt{2\,|\omega_k|}}\,u_k^{*\prime}\,. \tag{138}$$

With these definitions for the Bogoliubov coefficients, and using (103), we can compute the useful quantity:

$$|\beta_k|^2 = \frac{|\omega_k|}{2}\,|u_k|^2 + \frac{1}{2\,|\omega_k|}\,|u_k'|^2 - \frac{1}{2}\,. \tag{139}$$

Its physical meaning will be clarified in the following section.

4.2 PARTICLE CREATION IN AN EXPANDING BACKGROUND

Having introduced the Bogoliubov coefficients, we need to interpret these quantities in terms of physical observables. Their evolution can be understood in terms of particle creation by a spacetime-dependent background [7, 88–90]. Consider two sets of ladder operators $(a,a^{\dagger})$ and $(b,b^{\dagger})$ and their corresponding vacua defined through $a|0\rangle_a = 0$ and $b|0\rangle_b = 0$. These sets can be linked via a constant Bogoliubov transformation:

$$\begin{aligned} b &= A\,a + B\,a^{\dagger}\,, \\ b^{\dagger} &= A^*\,a^{\dagger} + B^*\,a\,. \end{aligned} \tag{140}$$

The two vacua $|0\rangle_a$ and $|0\rangle_b$ do not necessarily coincide. The expectation value of the number operator of one basis with respect to the vacuum of the other basis is given by $|B|^2$. In other words, an observer in the a-basis feels the vacuum as filled with b-particles.

In the cosmological case, where time-dependent Bogoliubov transformations have been introduced, the instantaneous vacuum defined by the time-dependent ladder operators $(a_k(\tau),\, a_k^\dagger(\tau))$ is filled with particles associated with the initial-time operators $(a_k^0,\, a_k^{\dagger 0})$. However, unlike in Minkowski spacetime, in a general curved spacetime there is no way to uniquely define the vacuum state, and the corresponding creation and annihilation operators. In Minkowski spacetime the vacuum state is found diagonalizing the Hamiltonian; the vacuum state is then defined as the minimum energy state. It is invariant under Poincaré transformations and it is the same for all inertial observers. In this case there is a preferred choice for the ladder operators, i.e. $a_{\mathbf{k}}$ is the one annihilating this unique vacuum state. In a general curved spacetime this procedure cannot be applied. Due to the expansion of the Universe, the frequency in the Hamiltonian (131) changes in time and can even become imaginary. The minimum of the Hamiltonian then changes in time and when the frequency becomes imaginary it cannot be properly defined. We have not anymore a physically preferred vacuum state. This ambiguity can be overcome if the effective spacetime seen by the fluctuations approaches Minkowski both in the far past and in the far future. As we have seen in Chapter 2, this happens when the perturbations are far sub-horizon. This requirement is equivalent to having adiabatic vacua asymptotically, such that the mode functions are given by plane waves. Having an adiabatic vacuum means the *adiabaticity conditions* are respected:

$$\left|\frac{\omega_k'}{\omega_k^2}\right|^2, \quad \left|\frac{\omega_k''}{\omega_k^3}\right| \ll 1\,. \tag{141}$$

When this happens, the fluctuations can be interpreted as particles, and the Bogoliubov coefficients relating the ladder operators in the asymptotic past and future give the final particle number as $|\beta_k|^2$. During inflation, the adiabaticity conditions (141) are not respected; we then need to follow further in time the evolution of the perturbations, deep into radiation domination.

4.2.1 *Cosmological Perturbations in a Hydrodynamical Era*

In order to interpret correctly $|\beta_k|^2$ we must make a digression on the evolution of the cosmological perturbations after the end of inflation, during an hydrodynamical era driven by radiation. A useful reference for this topic is [81]. During a hydrodynamical era with equation of state parameter w one can still use the Mukhanov-Sasaki variable, defined as $\zeta_{\mathbf{k}} = v_{\mathbf{k}}/\tilde{z}$, but now the Hamiltonian has a correction due to the different equation of state. In particular

$$\mathcal{H} = \frac{1}{2}\int_{R^{3+}} d^3k \left[\pi_{\mathbf{k}}\pi_{\mathbf{k}}^* + \left(c_s^2 k^2 - \frac{\tilde{z}''}{\tilde{z}}\right) v_{\mathbf{k}} v_{\mathbf{k}}^*\right], \tag{142}$$

where

$$\tilde{z} = \frac{a\sqrt{2\varepsilon_1}M_{Pl}}{c_s}\,. \tag{143}$$

c_s is the speed of sound, defined as $c_s = \delta p/\delta\rho = w = 1/3$ [1]. $\tilde{z}$ can then be rewritten in terms of the parameter of state only as

$$\tilde{z} = aM_{Pl}\sqrt{3\left(1+\frac{1}{w}\right)} = 2aM_{Pl}\,. \tag{144}$$

The equations of motion for the perturbations are then modified accordingly as

$$v''_{\pm\mathbf{k}} + \left(c_s^2k^2 - \frac{\tilde{z}''}{\tilde{z}}\right)v_{\pm\mathbf{k}} = 0\,. \tag{145}$$

We can therefore redefine the frequency squared as

$$\omega_k^2 = c_s^2k^2 - \frac{\tilde{z}''}{\tilde{z}}\,. \tag{146}$$

The solution to this equation is a sum of plane waves whose frequency is $\omega_k = c_sk$. Indeed during radiation domination $\frac{\tilde{z}''}{\tilde{z}} \propto \frac{a''}{a} = 0$. The coefficients of the positive and negative frequency modes are found matching the solution for the mode functions during inflation with the solution during radiation domination. The matching conditions are obtained imposing the continuity of $\zeta_{\mathbf{k}}$ and its first derivative $\zeta'_{\mathbf{k}}$. The expansion term inside ω_k^2 can be neglected right after inflation, hence the perturbations stop feeling the expansion of spacetime as soon as the Universe enters a radiation dominated period. Notice that we are here considering an instantaneous reheating.

4.2.2 *Number of Particles and Energy Density*

We have now all the ingredients to understand the process of particle creation during inflation. In order to do so, let us compute the expectation value of the Hamiltonian (142). Using (133), we can rewrite the Hamiltonian in terms of the ladder operators as

$$\begin{aligned}\mathcal{H} = \int \frac{d^3k}{2}\Bigg[&\left(\frac{|\omega_k|}{2}+\frac{\omega_k^2}{2\,|\omega_k|}\right)\left(2\,a_{\mathbf{k}}^\dagger a_{\mathbf{k}} + \left[a_{\mathbf{k}}, a_{\mathbf{k}}^\dagger\right]\right)\\ &-\left(\frac{|\omega_k|}{2}-\frac{\omega_k^2}{2\,|\omega_k|}\right)\left(a_{\mathbf{k}}^\dagger a_{-\mathbf{k}}^\dagger + a_{\mathbf{k}}a_{-\mathbf{k}}\right)\Bigg]\,.\end{aligned} \tag{147}$$

1 We are considering adiabatic perturbations. In general, the pressure could depend not only on the energy density, but also on the entropy per baryon ratio. This case is not considered here. Moreover we are dealing for simplicity with perturbations which re-enter the horizon during radiation domination. If they re-enter after the matter-radiation equality (but before recombination), one has to consider the evolution in a Universe filled with both matter and radiation. This general discussion is addressed in [81]. Here we present just a simple situation useful to our treatment.

Since we are interested in the late time limit of (147), we can simply drop the absolute value for ω_k and simplify the previous expression. Indeed during radiation domination the scale factor follows $a''/a = 0$, hence ω_k^2 becomes positive. Taking the expectation value over the initial vacuum, i.e. the vacuum annihilated by the initial time-independent annihilation operator, $a^0_{\boldsymbol{k}}|0\rangle = 0$ for all $\boldsymbol{k}$, we get:

$$\langle \mathcal{H} \rangle = \int d^3k\, \omega_k \, \langle a^\dagger_{\boldsymbol{k}} a_{\boldsymbol{k}} \rangle + (\text{vacuum energy}) \,, \tag{148}$$

with $\omega_k = c_s\, k$. The divergent vacuum energy can be removed by a normal ordering. The expectation value for the ladder operators can be computed from (134) as follows:

$$\langle a^\dagger_{\boldsymbol{k}} a_{\boldsymbol{k}} \rangle = |\beta_k|^2 \langle a^0_{-\boldsymbol{k}}\, a^{0\,\dagger}_{-\boldsymbol{k}} \rangle = |\beta_k|^2 \frac{V}{(2\pi)^3} \,, \tag{149}$$

where $V = \int d^3x = (2\pi)^3\, \delta^3(0)$ is the comoving volume. The expression for $|\beta_k|^2$ is given in terms of the mode functions, as in (139), keeping into account the full evolution until radiation domination. Notice that the particle interpretation is valid only when the perturbation mode does not feel the expansion, i.e. after the reheating phase. In this limit, ω_k is positive and can be interpreted as the frequency of the perturbation mode. $|\beta_k|^2$ can then be understood as the expectation value of the number of particles with comoving momentum k, created per comoving volume due to the time-dependent background. The divergent factor $\delta^3(0)$ arises because we are considering an infinite spatial volume, but the mean density of particles per comoving volume is finite. We therefore expect the norm of β_k to approach a constant after reheating.

4.3 SQUEEZED STATES FORMALISM

4.3.1 *Squeezing Parameters*

Thanks to the constraint (135), the two complex Bogoliubov coefficients can be parameterised by three real variables, the so-called *squeezing parameters*, as:

$$\begin{aligned} \alpha_k(\tau) &= e^{-i\vartheta_k(\tau)} \cosh r_k(\tau) \,, \\ \beta_k(\tau) &= e^{i[\vartheta_k(\tau) + 2\varphi_k(\tau)]} \sinh r_k(\tau) \,, \end{aligned} \tag{150}$$

where r_k is restricted to be non-negative. Inverting these relations yields the expressions for the squeezing parameters in terms of the Bogoliubov coefficients:

$$\begin{aligned} r_k &= \operatorname{arcsinh}|\beta_k| \,, \\ \vartheta_k &= -\arg(\alpha_k) \,, \\ \varphi_k &= \frac{1}{2} \arg(\alpha_k \beta_k) \,. \end{aligned} \tag{151}$$

4.3.2 *Physical Interpretation of the Squeezing Parameters*

The parameters here introduced have a clear physical interpretation. Indeed, the process of particle creation explained in Section 4.2 can be equivalently

described by means of the *squeezing formalism*. Its advantage is to give a clear phase space representation of the system's evolution. An introduction to the squeezing formalism can be found in [91, 92] (see also [9, 14, 93, 94]). The evolution in time of the ladder operators can be given in terms of an evolution operator U as

$$a_{\boldsymbol{k}}(\tau) = U(\tau)\, a^0_{\boldsymbol{k}}\, U^\dagger(\tau)\,, \qquad a^\dagger_{\boldsymbol{k}}(\tau) = U(\tau)\, a^{0\dagger}_{\boldsymbol{k}}\, U^\dagger(\tau)\,. \tag{152}$$

The form of this operator has been deduced by Parker in [95]. Using the language introduced by [96] in the context of quantum optics, it can be rewritten as $U = RS$, where

$$R(\vartheta_k) = \exp\left[i\vartheta_k \left(a^{0\dagger}_{\boldsymbol{k}} a^0_{\boldsymbol{k}} + a^{0\dagger}_{-\boldsymbol{k}} a^0_{-\boldsymbol{k}}\right)\right] \tag{153}$$

is the rotation operator, and

$$S(r_k, \varphi_k) = \exp\left[r_k \left(e^{-2i\varphi_k} a^0_{\boldsymbol{k}} a^0_{-\boldsymbol{k}} - e^{2i\varphi_k} a^{0\dagger}_{\boldsymbol{k}} a^{0\dagger}_{-\boldsymbol{k}}\right)\right] \tag{154}$$

is the two-mode squeeze operator. Here r_k, φ_k and ϑ_k are the squeezing parameters introduced in (150). Their time dependence in (153) and (154) have been made implicit to avoid clutter. The time evolution (152) thus corresponds to the application of a rotation with the parameter ϑ_k, followed by a squeezing with the parameters r_k and φ_k. The action of these two operators can be computed using the expansion $e^{\hat{A}}\, \hat{B}\, e^{-\hat{A}} = \hat{B} + [\hat{A}, \hat{B}] + 1/2\, [\hat{A}, [\hat{A}, \hat{B}]] + \dots$ as

$$\begin{aligned} U a^0_{\boldsymbol{k}}\, U^\dagger &= e^{-i\,\vartheta_k} \cosh r_k\, a^0_{\boldsymbol{k}} + e^{i\,(\vartheta_k + 2\,\varphi_k)} \sinh r_k\, a^{0\dagger}_{-\boldsymbol{k}}\,, \\ U a^{0\dagger}_{\boldsymbol{k}}\, U^\dagger &= e^{i\,\vartheta_k} \cosh r_k\, a^{0\dagger}_{\boldsymbol{k}} + e^{-i\,(\vartheta_k + 2\,\varphi_k)} \sinh r_k\, a^0_{-\boldsymbol{k}}\,. \end{aligned} \tag{155}$$

Rewriting the squeezing parameters in terms of the Bogoliubov coefficients using (151), we see that (155) matches with (134). These expressions also show that the modes $+\boldsymbol{k}$ and $-\boldsymbol{k}$ are mixed, hence a two-mode squeeze operator is needed to describe particle pairs in states $\pm\boldsymbol{k}$.

The rotation operator shifts the phase of the ladder operators as $R a^0_{\boldsymbol{k}}\, R^\dagger = e^{-i\vartheta_k} a^0_{\boldsymbol{k}}$, $R a^{0\dagger}_{\boldsymbol{k}}\, R^\dagger = e^{i\vartheta_k} a^{0\dagger}_{\boldsymbol{k}}$. The vacuum state is invariant under this rotation [92, 93], and hence the parameter ϑ_k is unphysical. Physical observables for a system starting in the vacuum state thus depend only on the parameters r_k and φ_k. Using (151), this in turn implies that the relevant combinations of the Bogoliubov coefficients are $|\beta_k|^2$ and $\arg(\alpha_k \beta_k)$. In particular, the squeezing parameter r_k is related to the number of particles created. The expectation value of the number operator in the vacuum annihilated by $a^0_{\boldsymbol{k}}$ follows from (155) as,

$$\frac{(2\pi)^3}{V} \langle a^\dagger_{\boldsymbol{k}} a_{\boldsymbol{k}} \rangle = \sinh^2 r_k = |\beta_k|^2, \tag{156}$$

as we have also derived in (149), and V is the spatial volume. Thus cosmological particle creation amounts to squeezing the vacuum, as observed by Grishchuk and Sidorov [2].

4.3.2.1 *Wave Function of a Two-Mode Squeezed State*

From the discussion in the previous section, it is clear that the Hilbert space of the system can be split into products of bipartite Hilbert sub-spaces for the modes $\mathbf{k}$ and $-\mathbf{k}$ as

$$\mathcal{H} = \prod_{\mathbf{k}\in R^{3+}} \mathcal{H}_{\mathbf{k}} \otimes \mathcal{H}_{-\mathbf{k}}\,.$$

Each subsystem evolves from an initial vacuum state $|0_{\mathbf{k}},\, 0_{-\mathbf{k}}\rangle$ into a two-mode squeezed state. The vacuum state is rotational invariant, hence the wave function of the bipartite system can be found applying only the squeezing operator. Using the operator ordering theorem, one can check that the wave function reduces to [9]

$$\begin{aligned} |\Psi\rangle_{2\text{sq}} &= S(r_k, \varphi_k) R(\vartheta_k) |0_{\mathbf{k}}, 0_{-\mathbf{k}}\rangle \\ &= \frac{1}{\cosh r_k} \sum_{n=0}^{\infty} e^{2in\varphi_k} (-1)^n \tanh^n r_k |n_{\mathbf{k}}, n_{-\mathbf{k}}\rangle\,. \end{aligned} \tag{157}$$

Here the sum is performed over the total number of particles produced by the expansion of spacetime. It is easy to check that this wave function cannot be written as $|\Psi\rangle_{2\text{sq}} = |\Psi\rangle_{\mathbf{k}} \otimes |\Psi\rangle_{-\mathbf{k}}$, hence the two modes $\mathbf{k}$ and $-\mathbf{k}$ are entangled. We will delve deeper into this topic in the following chapters.

4.3.2.2 *Squeezed State in Phase Space*

In order to understand better the physical meaning of the squeezing parameters we need to move to the phase space representation for a quadrature pair. A squeezed state is given by a quadrature pair for which the uncertainty in one variable is small, while the uncertainty in the other variable is correspondingly large, in order to respect the Heisenberg uncertainty principle. To see this explicitly, we introduce a set of operators:

$$x_k = \frac{1}{\sqrt{2}} \left(a_k + a_{-k}^\dagger\right), \quad y_k = -\frac{i}{\sqrt{2}} \left(a_k - a_{-k}^\dagger\right), \tag{158}$$

which are the same as v_k and π_k in (133), up to the normalization factor $\sqrt{|\omega_k|}$. These satisfy the commutation relation

$$\left[x_k, y_{k'}^\dagger\right] = i\delta^{(3)}(\boldsymbol{k} - \boldsymbol{k}'). \tag{159}$$

We further introduce a linear combination of the operators by rotating in the x_k - y_k plane by an angle ψ ($\in \mathbb{R}$):

$$\xi_k(\psi) = \cos\psi\, x_k + \sin\psi\, y_k. \tag{160}$$

The vacuum expectation value of a quadratic combination of ξ_k can be written as

$$\left| \frac{\langle \xi_k(\psi) \xi_k^\dagger(\psi) \rangle}{\frac{1}{2}[x_k,\, y_k^\dagger]} \right|^{1/2} = \{\cosh(2r_k) + \cos(2\psi - 2\varphi_k) \sinh(2r_k)\}^{1/2}\,. \tag{161}$$

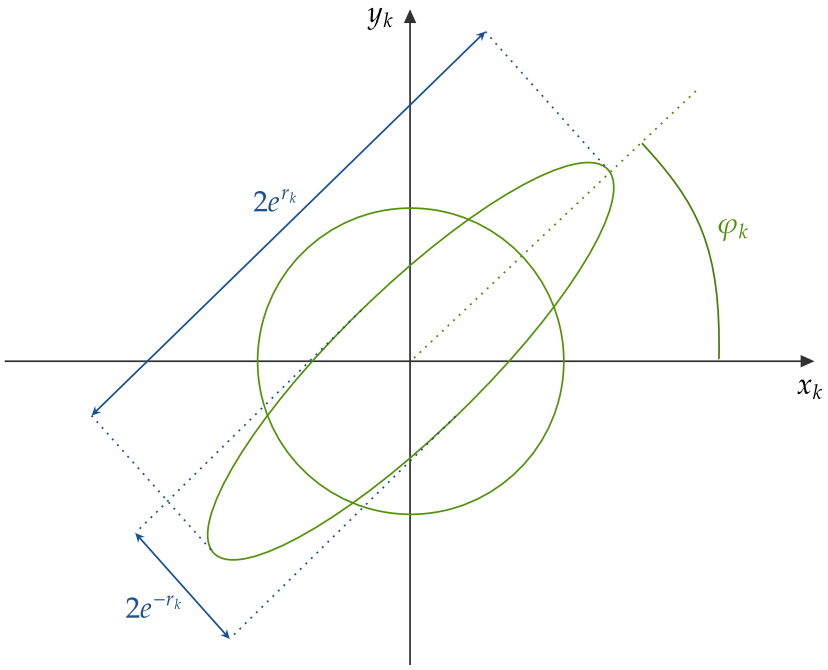


Figure 7: Squeezing mechanism in phase space for an initial state given by the vacuum state. The two parameters describing the physics of the evolution are r_k and φ_k; θ_k is instead unphysical since the vacuum state is rotationally invariant.

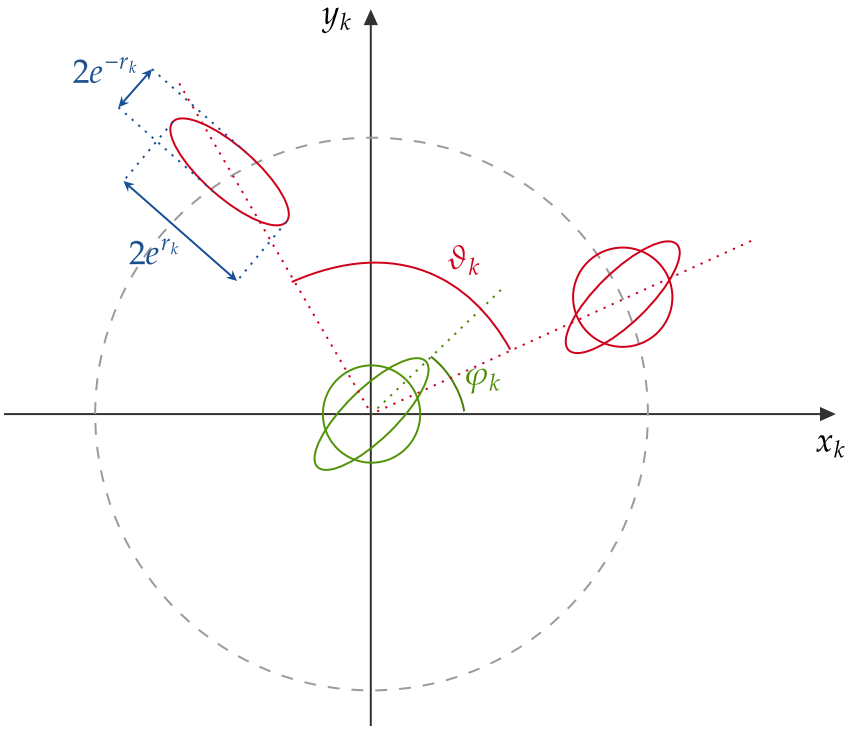


Figure 8: Squeezing mechanism in phase space for an initial state given by a coherent state. All the three squeezing parameters are physical; θ_k gives the rotation of the whole system in phase space.

The right-hand side takes the values e^{r_k} for $\psi = \varphi_k$ and e^{-r_k} for $\psi = \varphi_k + \frac{\pi}{2}$, moreover for $r_k = 0$ it becomes unity for all ψ. The quantity of (161) denotes the standard deviation of x_k and y_k along the ψ-direction, in units of half the quantum uncertainty (159). It also implies that the probability distribution in the x_k - y_k plane is an ellipse with semi-major axis e^{r_k} and semi-minor axis e^{-r_k} (normalized by the quantum uncertainty), with the major axis rotated by an angle φ_k, as illustrated in Figure 7. This can be understood by noting that when projecting this ellipse onto the ψ-axis, then its half length is given by the right-hand side of (161) [2]. When $r_k = 0$ the ellipse in phase space reduces to a circle; in this case, the state is the vacuum state of the system. The ϑ_k angle does not enter the discussion here since we are considering vacuum expectation values.

For the sake of completeness, we notice here that the squeezing parameter ϑ_k becomes physical if one consider the squeezing of a state which is not the vacuum. The phase ϑ_k represents the angle by which the whole system was rotated in phase space (see Figure 8). More details about the phase space representation using the squeezing parameters will be given in the following chapter and can be also found in [94, 97, 98].

Notice furthermore that for the cosmological fluctuations analyzed in this chapter, the parameters r_k and φ_k depend on time such that the ellipse in phase space becomes more and more squeezed, and also rotates as the Universe expands. These effects start to apply when the fluctuation's wave mode exits the Hubble horizon during inflation, that is when the mode starts feeling the expansion of spacetime. The squeezing continues until adiabaticity is recovered, right after the reheating phase.

4.3.3 *Link with the Observables*

The squeezing parameters are also linked to cosmological observables. We have seen in Section 4.2 that $|\beta_k|^2$ can be interpreted as the number of particles created by the expansion of spacetime. The parameter r_k is given in terms of this net number of particles, as shown in (151). The parameter φ_k is instead linked to the power spectrum of the field fluctuations. As explained in the previous section, the initial state we are working with, i.e. the vacuum state, is rotationally invariant; hence only one phase is physically meaningful. From the expectation value of the field fluctuations:

$$\langle v^2 \rangle = \int \frac{d^3k}{(2\pi)^3} |u_k|^2 = \int \frac{dk}{k} P_v(\mathbf{k}) \,, \tag{164}$$

2 The ellipse in an x - y plane is described by

$$e^{-2r_k}(\cos\varphi_k\, x + \sin\varphi_k\, y)^2 + e^{2r_k}(-\sin\varphi_k\, x + \cos\varphi_k\, y)^2 = 1. \tag{162}$$

To obtain the length of this ellipse projected along the ψ-axis, consider a line running through the origin with a polar angle ψ, and another line that is orthogonal to the first line and passes through a point $(\rho\cos\psi, \rho\sin\psi)$ with $\rho > 0$, i.e.,

$$y = -\frac{x}{\tan\psi} + \frac{\rho}{\sin\psi}. \tag{163}$$

This line is tangent to the ellipse if (162) and (163) admit only one set of solutions for (x, y). This requirement sets ρ as the projected half length, and reproduces the right-hand side of (161).

the power spectrum is written as

$$P_\zeta(\mathbf{k}) = \frac{k^3}{2\pi^2\,\tilde{z}^2}\,|u_k|^2\,. \tag{165}$$

Substituting the expression for $|u_k|^2$ in terms of the Bogoliubov coefficients (137) and (138), and exploiting the constraint (135), the power spectrum can be rewritten in terms of $|\beta_k|$ and $\arg(\alpha_k\beta_k)$:

$$\begin{aligned} P_k &= \frac{k^3}{2\pi^2\,\tilde{z}^2}\,\frac{\left|\alpha_k+\beta_k^*\right|^2}{2|\omega_k|} \\ &= \frac{k^3}{4\pi^2\,\tilde{z}^2\,|\omega_k|}\,\left[1+2|\beta_k|^2+2|\beta_k|\,\sqrt{1+|\beta_k|^2}\,\cos\left(\arg\left(\alpha_k\beta_k\right)\right)\right]\,. \end{aligned} \tag{166}$$

In terms of the squeezing parameters, $\arg(\alpha_k\beta_k)$ corresponds to φ_k, which is therefore a physical quantity.

Part II

UNDERSTANDING THE NATURE OF THE COSMOLOGICAL PERTURBATIONS

5 CLASSICALITY CRITERIA

We have shown in the previous chapter that the cosmological perturbations evolve from the vacuum state into a squeezed state. A squeezed state is a special quantum state for which one variable has an arbitrarily small uncertainty, while its conjugate counterpart has a very big uncertainty, correspondingly. Since squeezed states are associated with a huge uncertainty in one variable, they are highly quantum mechanical states [8]. In principle we should then be able to infer the quantum nature of the perturbations. However, the CMB data are analyzed within a classical framework. Indeed it turns out that from an observational point of view, a squeezed state is indistinguishable from a classical phase-space distribution, as soon as one works with Gaussian states. The two-point correlation functions can indeed be perfectly mimicked by ensemble averages weighted with a probability density function.

Unless these observational limitations, given the quantum nature of the system we are dealing with, we should be able to find a test for the quantum nature of the perturbations, without relying on the two-point correlation functions. These statement is at the basis of an active branch of research, trying to design experiments to measure quantum effects in cosmology, as well as trying to explain the possible quantum to classical transition of the perturbations via *decoherence* mechanism, i.e. the classicalization of the perturbations thanks to the interaction with other fields [1] [33–37].

In the recent years, several criteria to assess the quantum (or classical) nature of the cosmological perturbations have been studied. The aim of this chapter is to provide an overview of the most recent literature on this topic. In particular we will give a list of *classicality criteria*, i.e. a series of criteria used to determine whether the state considered presents classical or quantum characteristics (see [9, 14, 94, 99, 100] for further references). Decoherence effects can be taken into account when dealing with these criteria. Depending on the "amount" of decoherence, quantum effects could either be completely erased or persist in time; we will however neglect decoherence for simplicity.

5.1 CLASSICALITY OF THE TWO-POINT CORRELATION FUNCTIONS

Before delving into the several classicality criteria, we will explain why the two-point functions can be perfectly computed using a classical phase-space distribution. In order to do so, we have first to introduce the concepts of partitions and Wigner function.

1 The interactions could take place with other fields already present during inflation or with the thermal bath produced by the decay of the inflaton field during the reheating phase. Notice that decoherence effects could take place even between modes at different wavevectors due to gravitational interactions.

5.1.1 *Partitions*

The quantum fields $v_{\mathbf{k}}$ and $\pi_{\mathbf{k}}$ introduced so far are not Hermitian operators. Indeed, since v is a real field, one has $v_{\mathbf{k}}^{\dagger} = v_{-\mathbf{k}}$. This can be seen also from (133), which mixes creation and annihilation operators of the modes $\mathbf{k}$ and $-\mathbf{k}$. The physical quantities that will be introduced in this chapter are well defined for Hermitian operators. Hence we need to construct a set of Hermitian operators starting from the fields $v_{\mathbf{k}}$ and $\pi_{\mathbf{k}}$. There are several ways one can derive them, corresponding to the possible ways we have to factorise the Hilbert space of the two modes $\mathbf{k}$ and $-\mathbf{k}$ into two sub-systems. The Hermitian operators obtained from the quantum fields define a *partition*, i.e. a specific way of splitting the Hilbert space. The correlation properties, e.g. the entanglement, in Fourier space depend on the specific partition one chooses to work with. In general, there is no preferred partition, so one should test the quantum properties of the system in all possible partitions. One way to proceed is to define a generic partition

$$R_{1/2} = \left(k^{1/2}\, q_{\mathbf{k}}^{(1)},\ k^{-1/2}\, \pi_{\mathbf{k}}^{(1)},\ k^{1/2}\, q_{\mathbf{k}}^{(2)},\ k^{-1/2}\, \pi_{\mathbf{k}}^{(2)}\right)^{T}, \tag{167}$$

where the normalizations with the wavevector k have been introduced to make all the elements of the same dimension.

There are two special partitions that it is worth mentioning: the R/I partition and the $\pm\mathbf{k}$ partition. The first one is given by

$$R_{R/I} = \left(k^{1/2}\, v_{\mathbf{k}}^{R},\ k^{-1/2}\, \pi_{\mathbf{k}}^{R},\ k^{1/2}\, q_{\mathbf{k}}^{I},\ k^{-1/2}\, \pi_{\mathbf{k}}^{I}\right)^{T}, \tag{168}$$

where the Hermitian operators are obtained via canonical transformation [2] from the initial fields as

$$v_{\mathbf{k}}^{R} = \frac{v_{\mathbf{k}} + v_{\mathbf{k}}^{\dagger}}{\sqrt{2}}, \quad v_{\mathbf{k}}^{I} = \frac{v_{\mathbf{k}} - v_{\mathbf{k}}^{\dagger}}{\sqrt{2}i}, \quad \pi_{\mathbf{k}}^{R} = \frac{\pi_{\mathbf{k}} + \pi_{\mathbf{k}}^{\dagger}}{\sqrt{2}}, \quad \pi_{\mathbf{k}}^{I} = \frac{\pi_{\mathbf{k}} - \pi_{\mathbf{k}}^{\dagger}}{\sqrt{2}i}. \tag{169}$$

One can easily check that $[v_{\mathbf{k}}^{\lambda}, \pi_{\mathbf{k}}^{\lambda'}] = i\delta^{\lambda\lambda'}\,\delta(\mathbf{k}-\mathbf{k}')$ and $[v_{\mathbf{k}}^{\lambda}, v_{\mathbf{k}}^{\lambda'}] = [\pi_{\mathbf{k}}^{\lambda}, v_{\mathbf{k}}^{\lambda'}] = 0$, where $\lambda = R/I$. With this set of operators the Hamiltonian (131) reduces to

$$H = \int_{R^{3+}} d^3k \sum_{\lambda=R/I} \left[(\pi_{\mathbf{k}}^{\lambda})^2 + \omega_k^2\,(v_{\mathbf{k}}^{\lambda})^2\right], \tag{170}$$

which is sum separable. This implies that the two set of operators R and I are not correlated; hence if the initial state can be decomposed in this basis, the two sub-systems R and I evolve independently. This is indeed the case for the vacuum state of the cosmological perturbations.

The second relevant partition is given by

$$R_{\pm k} = \left(k^{1/2}\, q_{\mathbf{k}},\ k^{-1/2}\, p_{\mathbf{k}},\ k^{1/2}\, q_{-\mathbf{k}},\ k^{-1/2}\, p_{-\mathbf{k}}\right)^{T}, \tag{171}$$

2 A canonical transformation is a change of variables which preserves the structure of the commutators (98). Further details on the canonical transformations in the context of the cosmological perturbations can be found in [100].

where

$$q_{\mathbf{k}} = \frac{1}{\sqrt{2k}}(a_{\mathbf{k}} + a^{\dagger}_{\mathbf{k}}), \quad p_{\mathbf{k}} = \frac{1}{\sqrt{2k}}(a_{\mathbf{k}} - a^{\dagger}_{\mathbf{k}}), \tag{172}$$

and analogous definitions for the operators of the mode $-\mathbf{k}$. In this partition, the Hilbert space has been divided into a sub-system for the mode $+\mathbf{k}$ and a sub-system for the mode $-\mathbf{k}$.

It is easy to show that one can change partition applying a four-by-four matrix to a reference partition. We can choose the R/I partition as the reference one, since the computations in this partition are easier; each other partition is obtained as

$$R_{1/2} = T\, R_{R/I}, \tag{173}$$

where

$$T = \begin{pmatrix} \cos\alpha\cos\theta & -\sin\alpha\cos\theta & -\cos\delta\sin\theta & \sin\delta\sin\theta \\ \sin\alpha\cos\theta & \cos\alpha\cos\theta & -\sin\delta\sin\theta & -\cos\delta\sin\theta \\ \cos\beta\sin\theta & -\sin\beta\sin\theta & \cos(\alpha-\beta-\delta)\cos\theta & \sin(\alpha-\beta-\delta)\cos\theta \\ \sin\beta\sin\theta & \cos\beta\sin\theta & -\sin(\alpha-\beta-\delta)\cos\theta & \cos(\alpha-\beta-\delta)\cos\theta \end{pmatrix}. \tag{174}$$

This matrix depends on four angles which completely characterise a generic partition. The R/I partition corresponds to $\alpha = \beta = \delta = \theta = 0$, while the $\pm\mathbf{k}$ one to $\alpha = 0$, $\beta = -\pi$, $\delta = \pi/2$ and $\theta = -\pi/4$. To simplify the analysis, a one parameter family of partitions is often considered. The resulting matrix is

$$T = \begin{pmatrix} \cos\theta & 0 & 0 & \sin\theta \\ 0 & \cos\theta & -\sin\theta & 0 \\ \sin\theta\sin(2\theta) & \sin\theta\cos(2\theta) & \cos\theta\cos(2\theta) & -\cos\theta\sin(2\theta) \\ -\sin\theta\cos(2\theta) & \sin\theta\sin(2\theta) & \cos\theta\sin(2\theta) & \cos\theta\cos(2\theta) \end{pmatrix}. \tag{175}$$

In this case $\theta = 0$ gives the R/I partition, while $\theta = -\pi/4$ the $\pm\mathbf{k}$ one. This is enough to study how the properties of the system are affected by a change of partition; however the results could be extended to the more general case (174). Notice that the linear transformation (173) preserves the quadratic nature of the Hamiltonian (131).

5.1.2 *Covariance Matrix*

Since the Hamiltonian describing the system is quadratic (independently on the partition chosen), the Gaussianity of the initial vacuum state is preserved by the time evolution. The final state will then be a Gaussian state, which can be completely characterized by the two-point correlation functions. These functions are conventionally gathered into the *covariance matrix*

$$\gamma_{ab} = \langle \{R_a, R_b\} \rangle, \tag{176}$$

where a and b are two generic elements of the vector $R_{1/2}$, and $\{.\}$ is the anti-commutator. The covariance matrix is real and symmetric. Under a change of partition

$$\tilde{\gamma} = T\,\gamma\,T^T\,. \tag{177}$$

In the R/I partition the covariance matrix is block-diagonal:

$$\gamma^{R/I} = \begin{pmatrix} \gamma_{vv} & \gamma_{v\pi} & 0 & 0 \\ \gamma_{\pi v} & \gamma_{\pi\pi} & 0 & 0 \\ 0 & 0 & \gamma_{vv} & \gamma_{v\pi} \\ 0 & 0 & \gamma_{\pi v} & \gamma_{\pi\pi} \end{pmatrix}. \tag{178}$$

This reflects the fact that in the initial vacuum state the real and imaginary sub-systems are uncorrelated and that the Hamiltonian is sum-separable, so that the two sub-systems evolve independently. Notice that the two matrix elements $\gamma_{v\pi}$ and $\gamma_{\pi v}$ are equal. The elements of (178) are

$$\begin{aligned} \gamma_{vv} &= 2k\left\langle \left(v_{\mathbf{k}}^R\right)^2 \right\rangle = 2k\left\langle \left(v_{\mathbf{k}}^I\right)^2 \right\rangle = k\left\langle \left\{v_{\mathbf{k}}, v_{\mathbf{k}}^\dagger\right\} \right\rangle, \\ \gamma_{v\pi} &= \gamma_{\pi v} = \left\langle v_{\mathbf{k}}^R \pi_{\mathbf{k}}^R + \pi_{\mathbf{k}}^R v_{\mathbf{k}}^R \right\rangle = \left\langle v_{\mathbf{k}}^I \pi_{\mathbf{k}}^I + \pi_{\mathbf{k}}^I v_{\mathbf{k}}^I \right\rangle = \left\langle v_{\mathbf{k}} \pi_{\mathbf{k}}^\dagger + \pi_{\mathbf{k}} v_{\mathbf{k}}^\dagger \right\rangle, \\ \gamma_{\pi\pi} &= \frac{2}{k}\left\langle \left(\pi_{\mathbf{k}}^R\right)^2 \right\rangle = \frac{2}{k}\left\langle \left(\pi_{\mathbf{k}}^I\right)^2 \right\rangle = \frac{1}{k}\left\langle \left\{\pi_{\mathbf{k}}, \pi_{\mathbf{k}}^\dagger\right\} \right\rangle. \end{aligned} \tag{179}$$

Thanks to (177) the covariance matrix can be written in a generic partition of the θ-parameter family. In general it will not be a block-diagonal matrix; we can write it as

$$\gamma = \begin{pmatrix} \gamma_A & \gamma_C \\ \gamma_C & \gamma_B \end{pmatrix}, \tag{180}$$

where each γ_i is a two-by-two matrix. The expressions for the elements of γ in a generic partition can be found in [14]; here we report just the results for the the correlators in the $\pm\mathbf{k}$ partition:

$$\begin{aligned} 2\,k\,\langle q_{\mathbf{k}}^2\rangle &= \gamma_{A,11} + iJ_{11} = \frac{\gamma_{vv}+\gamma_{\pi\pi}}{4}, \\ \frac{2}{k}\langle p_{\mathbf{k}}^2\rangle &= \gamma_{A,22} + iJ_{22} = \frac{\gamma_{vv}+\gamma_{\pi\pi}}{4}, \\ \langle q_{\mathbf{k}} p_{\mathbf{k}}\rangle &= -\langle p_{\mathbf{k}} q_{\mathbf{k}}\rangle = \gamma_{A,12} + \frac{i}{2}J_{12} = \frac{i}{2}, \\ 2\,k\langle q_{\mathbf{k}} q_{-\mathbf{k}}\rangle &= \gamma_{C,11} + iJ_{13} = \frac{\gamma_{vv}-\gamma_{\pi\pi}}{4}, \\ \frac{2}{k}\langle p_{\mathbf{k}} p_{-\mathbf{k}}\rangle &= \gamma_{C,22} + iJ_{24} = -\frac{\gamma_{vv}-\gamma_{\pi\pi}}{4}, \\ \langle q_{\mathbf{k}} p_{-\mathbf{k}}\rangle &= \langle p_{\mathbf{k}} q_{-\mathbf{k}}\rangle = \langle q_{\mathbf{k}} p_{-\mathbf{k}}\rangle = \langle q_{\mathbf{k}} p_{-\mathbf{k}}\rangle = \langle p_{\mathbf{k}} q_{-\mathbf{k}}\rangle = \frac{1}{2}\gamma_{C,12} + \frac{i}{2}J_{14} = \frac{1}{2}\gamma_{v\pi}, \end{aligned} \tag{181}$$

where

$$J = \begin{pmatrix} 0 & 1 & 0 & 0 \\ -1 & 0 & 0 & 0 \\ 0 & 0 & 0 & 1 \\ 0 & 0 & -1 & 0 \end{pmatrix}, \tag{182}$$

and in this specific partition $\gamma_B = \gamma_A$. The first three lines in (181) give the correlators in the sub-system $+\mathbf{k}$; analogous expressions are found for the sub-system $-\mathbf{k}$. The last three lines give instead the correlation functions mixing the $+\mathbf{k}$ and the $-\mathbf{k}$ sectors. Notice that the correlators of the ladder operators (172) can also be expressed in terms of the elements of the covariance matrix as:

$$\begin{aligned} \left\langle \left\{ a_{\mathbf{k}}, a^{\dagger}_{\mathbf{k}} \right\} \right\rangle &= \left\langle \left\{ a_{-\mathbf{k}}, a^{\dagger}_{-\mathbf{k}} \right\} \right\rangle = \frac{\gamma_{vv} + \gamma_{\pi\pi}}{2} = N_k + 1 \,, \\ \langle \{ a_{\mathbf{k}}, a_{-\mathbf{k}} \} \rangle &= \frac{\gamma_{vv} - \gamma_{\pi\pi}}{2} + i\gamma_{v\pi} = 2C_k \,, \\ \left\langle \left\{ a_{-\mathbf{k}}, a^{\dagger}_{-\mathbf{k}} \right\} \right\rangle &= \frac{\gamma_{vv} - \gamma_{\pi\pi}}{2} - i\gamma_{v\pi} = 2C^*_k \,. \end{aligned} \tag{183}$$

Here N_k is the number of pairs $\pm\mathbf{k}$ created, while C_k gives the correlations between modes $\pm k$. We then find a link between the elements of the covariance matrix and some of the physical quantities introduced in Chapter 4. Furthermore, the elements of the covariance matrix can be linked to the Bogoliubov coefficients and the squeezing parameters. In particular for the Bogoliubov coefficients one can find the following relations:

$$\begin{aligned} \gamma_{vv}(\tau) &= |\alpha_k(\tau) + \beta^*_k(\tau)|^2 \,, \\ \gamma_{v\pi}(\tau) &= 2 \, \mathrm{Im}[\alpha_k(\tau)\beta_k(\tau)] \,, \\ \gamma_{\pi\pi}(\tau) &= |\alpha_k(\tau) - \beta^*_k(\tau)|^2 \,. \end{aligned} \tag{184}$$

For the squeezing parameters one has instead:

$$\begin{aligned} \gamma_{vv}(\tau) &= \cosh(2r_k) + \cos(2\varphi_k) \, \sinh(2r_k) \,, \\ \gamma_{v\pi}(\tau) &= \sin(2\varphi_k) \sinh(2r_k) \,, \\ \gamma_{\pi\pi}(\tau) &= \cosh(2r_k) - \cos(2\varphi_k) \sinh(2r_k) \,. \end{aligned} \tag{185}$$

From this expressions, using the results in (172), the relations in the $\pm\mathbf{k}$ partition can be easily found.

5.1.3 *Classical Stochastic Description and Wigner Function*

Until now, the description of the system was based on quantum mechanics. However, the quantum formalism can be ignored and the time evolution can be described in terms of a stochastic probability distribution [9, 94]. In an effective classical stochastic description, quantum averages are given by

$$\langle \hat{O} \rangle = \langle O \rangle_{\mathrm{stoch}} \,, \tag{186}$$

where

$$\langle O \rangle_{\text{stoch}} = \int \tilde{O}(R_{1/2})\, W(R_{1/2})\, d^4 R_{1/2}\,. \tag{187}$$

The "hat" indicates a quantum operator, whereas the "tilde" indicates the Weyl transform of the operator, defined as

$$\tilde{O}(R_{1/2}) = \int dq_1' dq_2' e^{-ip_1 q_1' - ip_2 q_2'} \left\langle q_1 + \frac{q_1'}{2}, q_2 + \frac{q_2'}{2} \middle| \hat{O} \middle| q_1 - \frac{q_1'}{2}, q_2 - \frac{q_2'}{2} \right\rangle . \tag{188}$$

Here $R_{1/2}$ has to be interpreted as the vector of the classical variables in phase space. The quantity $W(R_{1/2})$, called *Wigner function*, represents a probability density function and it is the Weyl transform of the density matrix $\hat{\rho}$ representing the quantum state of the perturbations [101–104]:

$$W(R_{1/2}) = \frac{\tilde{\rho}}{(2\pi)^2}\,. \tag{189}$$

The stochastic description works if three conditions are satisfied:

- the Wigner function is non-negative everywhere and normalized to unity, such that it can be viewed as a distribution function;
- it obeys the classical equations of motion;
- the quantum averages can be indeed reproduced by stochastic averages, as in (186).

Let us now analyse the Wigner function of our system. As explained in the previous chapter, the initial vacuum state is Gaussian. All the information on a Gaussian state is contained in the covariance matrix (176). The Wigner function in this case is then Gaussian and can be expressed in terms of γ as

$$W(R_{1/2}) = \frac{1}{\pi^2 \sqrt{\det \gamma}} \exp\left(-R_{1/2}^{\mathrm{T}} \gamma^{-1} R_{1/2}\right)\,. \tag{190}$$

Let us introduce the concept of *purity*; it is defined as $p = \mathrm{Tr}(\hat{\rho}^2)$ and it tells us whether a state is pure ($p = 1$), or mixed ($p < 1$). The purity of the state is linked to the determinant of the covariance matrix as [105]

$$p = \frac{1}{\sqrt{\det(\gamma)}}\,. \tag{191}$$

In this work we consider pure states, neglecting decoherence effects, hence $p = 1$ and then $\det(\gamma) = 1$. The explicit expression in terms of the phase space coordinates of course depends on the chosen partition. In the R/I partition the covariance matrix is block-diagonal, hence $W(R_{R/I})$ factorises as $W(R_{R/I}) = W^R(R_R)\, W^I(R_I)$. This partition is particularly useful for the geometrical interpretation of the squeezing parameters. We have already explained in Section 4.3.2 how a squeezed state can be seen as an ellipse in phase space. This result can be reinterpreted in terms of the Wigner function; indeed, given its Gaussian nature, the contours of $W(R_{1/2})$ are ellipses in phase space.

From the elements of the covariance matrix (179) and the expression (190) for the Wigner function, one can check that the semi-minor and the semi-major axes of the $\sqrt{2}-\sigma$ contours go like e^{-r_k} and e^{r_k} respectively, while the angle φ_k gives the rotation of the ellipses in phase space. A plot of the $\sqrt{2}-\sigma$ contour levels of the Wigner function W^i, with $i = R/I$ is reported in [94] for $\varphi_k = \pi/4$ and $r_k = 1$. Notice that for pure states the area of the ellipse is a constant; indeed it can be proved that the area is proportional to the determinant of the covariance matrix γ. If decoherence effects are at play, then the determinant of γ increases as the purity decreases; this implies the area of the ellipses in phase space increases with time. The contour levels of W^i in the case of $p < 1$ are reported in [94] too; a comparison between pure and mixed states is reported instead in [14].

5.1.4 *Wave Function of a Two-Mode Squeezed State*

Now that we have introduced the concepts of partitions of the Hilbert space and of Wigner function, we have all the ingredients to evaluate the wave function of a two-mode squeezed state in position space for a generic partition. In (157) we implicitly split up the Hilbert space in the $\pm\mathbf{k}$ partition; this expression can be rewritten in position space as

$$\begin{aligned}\Psi_{2sq}(q_1, q_2) &= \langle q_1, q_2|\Psi_{2sq}\rangle \\ &= \frac{1}{\cosh(r_k)}\sum_{n=0}^{\infty} e^{-2in\varphi_k}\tanh^2(r_k)\langle q_1|n_1\rangle\langle q_2|n_2\rangle\,,\end{aligned} \tag{192}$$

where $q_1 = k^{1/2}\,q_{\mathbf{k}}$ and $q_2 = k^{1/2}\,q_{-\mathbf{k}}$. It can be proved that

$$\Psi_n(q_1) = \langle q_1|\frac{(a^\dagger)^n}{\sqrt{n!}}|0\rangle = \frac{1}{\pi^{1/4}\sqrt{2^n\,n!}}e^{-q_1^2/2}\,H_n(q_1)\,, \tag{193}$$

where $H_n(q_{\mathbf{k}})$ are the Hermite polynomials. Performing then the sum over n as showed in [106] the wave function reduces to

$$\Psi_{2sq}(q_1, q_2) = \frac{\exp\left[\frac{1}{2}A(r_k,\varphi_k)\,(q_1^2+q_2^2) + B(r_k,\varphi_k)q_1q_2\right]}{\cosh r_k\sqrt{\pi}\sqrt{1-e^{-4i\varphi_k}\tanh^2 r_k}}\,, \tag{194}$$

with

$$A(r_k,\varphi_k) = -\frac{1+e^{-4i\varphi_k}\tanh^2 r_k}{1-e^{-4i\varphi_k}\tanh^2 r_k}\,,\quad B(r_k,\varphi_k) = \frac{2e^{-2i\varphi_k}\tanh r_k}{1-e^{-4i\varphi}\tanh^2 r_k}\,. \tag{195}$$

The wave function in (194) has been written in the $\pm\mathbf{k}$ partition. However this is not the only possibility. There is a simple way to find the wave function in a generic partition, that is using the Wigner function. Indeed, since the Wigner function is the Weyl transform of the density matrix, one can write

$$\Psi(q_{\mathbf{k}}^{(1)}, q_{\mathbf{k}}^{(2)}) \sim \int d\pi_{\mathbf{k}}^{(1)}d\pi_{\mathbf{k}}^{(2)}W\left(\frac{q_{\mathbf{k}}^{(1)}}{2}, \frac{q_{\mathbf{k}}^{(2)}}{2}, \pi_{\mathbf{k}}^{(1)}, \pi_{\mathbf{k}}^{(2)}\right) e^{iq_{\mathbf{k}}^{(1)}\pi_{\mathbf{k}}^{(1)}}\,e^{iq_{\mathbf{k}}^{(2)}\pi_{\mathbf{k}}^{(2)}}\,. \tag{196}$$

Substituting the expression in (190) and then normalizing the result one gets the normalized wave function for a generic partition. The final expression will depend on the elements of the covariance matrix in the reference partition R/I (179) and on the angle θ of the transformation matrix T in (175). As expected, in the R/I partition, i.e. setting $\theta = 0$, the wave function becomes separable:

$$\begin{aligned}\Psi(q^R_{\mathbf{k}}, q^I_{\mathbf{k}}) &= \Psi^R(q^R_{\mathbf{k}})\,\Psi^I(q^I_{\mathbf{k}}) \\ &= \left(\frac{k}{\pi\gamma_{vv}}\right)^{1/2} \exp\left\{-\frac{k}{2}\,\frac{1-i\,\gamma_{v\pi}}{\gamma_{vv}}\,\left[(q^R_{\mathbf{k}})^2 + (q^I_{\mathbf{k}})^2\right]\right\},\end{aligned} \tag{197}$$

where in order to get this expression we have used the fact that $\det\gamma = 1$ to rewrite $\gamma_{\pi\pi}$ in terms of γ_{vv} and $\gamma_{v\pi}$. For the $\pm\mathbf{k}$ partition, the wave function simplifies to

$$\begin{aligned}\Psi(q_{\mathbf{k}}, q_{-\mathbf{k}}) = \left(\frac{k}{\pi(1+\gamma_{v\pi})^{1/2}}\right)^{1/2} \exp\left\{-\frac{k}{4}\,\frac{1-i\gamma_{v\pi}}{\gamma_{vv}}\left(1+\frac{\gamma^2_{vv}}{(1-i\gamma_{v\pi})^2}\right)\cdot\right. \\ \left.\cdot\left[(q_{\mathbf{k}})^2 + (q_{-\mathbf{k}})^2 - 2q_{\mathbf{k}}q_{-\mathbf{k}}\frac{\gamma^2_{vv} - (1-i\gamma_{v\pi})^2}{\gamma^2_{vv} + (1-i\gamma_{v\pi})^2}\right]\right\}.\end{aligned} \tag{198}$$

Inserting equations (185) into (198) one can easily check that the wave function reduces to (194), up to the substitutions $q_1 = k^{1/2}\,q_{\mathbf{k}}$ and $q_2 = k^{1/2}\,q_{-\mathbf{k}}$ (and consequent normalization of the wave function).

These expressions for the wave functions will be useful to evaluate the expectation values when computing correlation functions. In particular equation (194) will be used in Chapter 6.

5.1.5 *Two-Point Correlation Functions*

The aim of this section is to show how the quantum two-point correlation functions of the cosmological perturbations derived in Section 3.6 can be obtained even in a classical stochastic description. The computations have been carried in [9]; we report here the main results. Notice that in this paper the definition of the momentum is different with respect to the conventions we use in this work; in particular they define it as

$$\pi_{\mathbf{k}} = v'_{\mathbf{k}} - \frac{z'}{z}\,v_{\mathbf{k}}\,. \tag{199}$$

With this definition of the momentum the Hamiltonian (131) changes as

$$H = \int_{R^{3+}} d^3k\left[\pi_{\mathbf{k}}\pi_{-\mathbf{k}} + k^2 v_{\mathbf{k}}v_{-\mathbf{k}} + \frac{z'}{z}\,(v_{\mathbf{k}}\pi_{-\mathbf{k}} + v_{-\mathbf{k}}\pi_{\mathbf{k}})\right]. \tag{200}$$

The different definition for the momentum and the corresponding Hamiltonian can be obtained from the original action for the Mukhanov - Sasaki variable performing an integration by parts in time. This form of H allows one to clearly see the effect on a simple harmonic oscillator of the spacetime evolution, which is encoded in the last term of (200). Moreover, with this definition

of the momentum the relation between the time derivative of $\zeta_{\mathbf{k}} = v_{\mathbf{k}}/z$ and the momentum $\pi_{\mathbf{k}}$ trivializes:

$$\zeta'_{\mathbf{k}}(\tau) = \frac{\pi_{\mathbf{k}}(\tau)}{z(\tau)}\,. \tag{201}$$

The different two-point functions for ζ and ζ' can then be found easily from those of $v_{\mathbf{k}}$ and $\pi_{\mathbf{k}}$. Notice that being ζ a well-defined observable, the correlators given in terms of ζ and ζ' do not depend on the definition chosen for π. The results are given at the first order in slow-roll and in terms of the squeezing parameters. In the quantum approach one finds

$$\begin{aligned}\langle\zeta(\tau,\mathbf{x})\zeta(\tau,\mathbf{y})\rangle =& \frac{4\pi}{(2\pi)^3}\frac{1}{a^2M_p^2\epsilon_1}\int_0^\infty \frac{dk}{k}\frac{\sin(k|\mathbf{x}-\mathbf{y}|)}{|\mathbf{x}-\mathbf{y}|}\frac{k^2}{2}\cdot\\ &\cdot\left[\cosh(2r_k)-\sinh(2r_k)\cos(2\varphi_k)\right]\,,\end{aligned} \tag{202}$$

$$\begin{aligned}\langle\zeta(\tau,\mathbf{x})\zeta(\tau,\mathbf{y})+\zeta(\tau,\mathbf{x})\zeta(\tau,\mathbf{y})\rangle =& -\frac{4\pi}{(2\pi)^3}\frac{1}{z^2(\tau)}\int_0^\infty \frac{dk}{k}\frac{\sin(k|\mathbf{x}-\mathbf{y}|)}{|\mathbf{x}-\mathbf{y}|}\cdot\\ &\cdot k^3\sinh(2r_k)\sin(2\varphi_k)\,,\end{aligned} \tag{203}$$

$$\begin{aligned}\langle\zeta'(\tau,\mathbf{x})\zeta'(\tau,\mathbf{y})\rangle =& \frac{4\pi}{(2\pi)^3}\frac{1}{z^2(\tau)}\int_0^\infty \frac{dk}{k}\frac{\sin(k|x-y|)}{|x-y|}\cdot\\ &\cdot\frac{k^4}{2}\left[\cosh(2r_k)+\sinh(2r_k)\cos(2\varphi_k)\right]\,.\end{aligned} \tag{204}$$

The correlators correctly depend on $|\mathbf{x}-\mathbf{y}|$, reflecting the homogeneity and isotropy of the Universe. The same two-point functions are computed in a classical stochastic description using (186) and (187). As it is shown in [9], the results for the correlators of ζ and ζ' are exactly the same as in the quantum description.

In the case of a Gaussian state, although the two-point functions encode all the information, higher-order (even) correlators can be computed. In Appendix F of [9] the authors computed the expectation value of an operator $\hat{A}$ Taylor expanded in terms of $q_{\mathbf{k}}$, $\pi_{\mathbf{k}}$, $q_{-\mathbf{k}}$ and $\pi_{-\mathbf{k}}$. Differences between the stochastic and the quantum approaches arise when computing the expectation values of $q_{\mathbf{k}}^{n_1}\,\pi_{\mathbf{k}}^{n_2}$, for arbitrary values of n_1 and n_2. This is due to the fact that $q_{\mathbf{k}}$ and $\pi_{\mathbf{k}}$ do not commute. However it is also shown that in the large squeezing limit the stochastic approach gives accurate results for these correlators too. Notice that the operator $\hat{A}$ considered in [9] is an analytic function of v and π. The computations for non-analytic functions of these variables could actually lead to non-trivial results. One examples is provided by the pseudo-spin operators used to construct the cosmological Bell inequalities. More details on this topic will be given in Chapter 6.

5.2 CLASSICALITY CRITERIA

We have shown how the quantum and stochastic approaches lead to the same result for the two-point functions, i.e. the power spectra. However the two-mode squeezed state characterizing the cosmological perturbations is an intrinsically quantum state. In principle there should be a way to prove the

quantum nature of the system, however unfortunately we have only access to few observables and we cannot perform repeated experiments, since we have only access to one realization of the system, i.e. our Universe. There are anyway some criteria one can use to try to discern among the classical or quantum approaches. We present in this section three of them.

5.2.1 *Positivity of the Wigner Function*

A system is considered classical if its Wigner function is positive. In fact interference terms, typical of a quantum behaviour, induce oscillations in the Wigner function, which make it negative for some values of the variables v and π. The cosmological perturbations are in a Gaussian state, hence the Wigner function is in turn Gaussian. This implies that it is always positive for every value of the position and momentum. It seems then from this criterion that our system is classical. However it turns out the classicality of the Wigner function does not exclude the presence of quantum characteristics. A typical signature of the quantum behaviour of a system is the violation of Bell inequality (see Chapter 6); it has been proved that Bell inequality violations can occur even in the presence of a non-negative Wigner function [23, 107]. This happens if one consider *improper dynamical variables*. In order to explain the difference between proper and improper dynamical variables, let us report here the example provided in [23], while a more detailed discussion can be found in [107]. Consider a general operator $\hat{A}$, which is a function of the coordinates $q_{\mathbf{k}}$ and $\pi_{\mathbf{k}}$. Notice that a one dimensional phase space is considered for simplicity, but the generalization to a two-dimensional phase space can be easily done. Its Wigner-Weyl representation is given by

$$W_{\hat{A}}(q_{\mathbf{k}}, \pi_{\mathbf{k}}) \equiv \int_R dx\, e^{-i\pi_{\mathbf{k}} x} \left\langle q_{\mathbf{k}} + \frac{x}{2} \middle| \hat{A}(q_{\mathbf{k}}, \pi_{\mathbf{k}}) \middle| q_{\mathbf{k}} - \frac{x}{2} \right\rangle . \tag{205}$$

Let us now consider a bounded function $\mathcal{F}$, giving the eigenvalues of an operator $\hat{F}$, defined as

$$\hat{F} = \int_{-\infty}^{+\infty} dq'_{\mathbf{k}} |q'_{\mathbf{k}}\rangle \mathcal{F}(q'_{\mathbf{k}}) \langle q'_{\mathbf{k}}| \, . \tag{206}$$

It is then easy to show that

$$W_{\hat{F}}(q_{\mathbf{k}}, \pi_{\mathbf{k}}) = \mathcal{F}(q_{\mathbf{k}}) \, , \tag{207}$$

i.e. the function $W_{\hat{F}}(q_{\mathbf{k}}, \pi_{\mathbf{k}})$ takes the eigenvalues of the operator $\hat{F}$. In this case $\hat{F}$ is said to be a *proper dynamical variable*. For this kind of variables, the spectrum of the quantum operator is well reproduced by a classical probability distribution function. The sets of pseudo-spin operators used to introduce the Bell inequality for the cosmological perturbations (see Chapter 6 for further details) have at least one improper dynamical variables (e.g. one component along x, y or z) [23]. In [107] it is shown a theorem stating that a violation of Bell inequality in the presence of a positive definite Wigner function can only occur for improper dynamical variables. We then conclude that a positive Wigner function, although hinting at a classical theory of the perturbations, it is not a definitive proof of their classicality.

5.2.2 *Quantum Separability*

A second criterion to understand whether a system is classical or quantum is the *separability*. It was discuss in a recent paper by Martin, Micheli and Vennin [14]. Given a partition of the Hilbert space into two sub-systems, a state is said to be separable in that partition if its density matrix can be written as a mixture of the products of the density matrices of the two sub-systems:

$$\hat{\rho} = \sum_i \alpha_i \hat{\rho}_1^i \otimes \hat{\rho}_2^i \,, \tag{208}$$

where α_i are real coefficients. Proving the separability of a system is in general a difficult task, however there are some simplifications if one works with Gaussian states, as it is our case. In particular, there is one criterion which applies in this context, i.e. the Peres - Horodecki criterion [108]. In the Appendix of [14] it was shown how the Peres - Horodecki criterion for a generic covariance matrix (180) can be written as

$$\begin{aligned} &\det\gamma_A \det\gamma_B + (|\det\gamma_C| - 1)^2 - \\ &\qquad - \mathrm{Tr}\left[\gamma_A J^{(1)} \gamma_C J^{(1)} \gamma_B J^{(1)} \gamma_C^T J^{(1)}\right] \geq \det\gamma_A + \det\gamma_B \,, \end{aligned} \tag{209}$$

where

$$J^{(1)} = \begin{pmatrix} 0 & 1 \\ -1 & 0 \end{pmatrix} . \tag{210}$$

After some manipulation, using the expressions for the elements of (180), which can be found in [14], the inequality (209) can be recast into an inequality for $\det\gamma_C$. For the R/I partition, setting $\theta = 0$ in the generic expression, one finds that the system is separable, as expected from the fact the Hamiltonian is sum-separable. For the $\pm\mathbf{k}$ partition the authors find that the state is separable if and only if

$$e^{-2r_k} \geq \sqrt{p} \,. \tag{211}$$

Restricting to the case with a pure state, this inequality reduces to $e^{-2r_k} \geq 1$. A simple manipulation leads to the condition $r_k \leq 0$ for the separability. The cosmological perturbations evolve from the vacuum state, for which $r_k = 0$, to a two-mode squeezed state, which has $r_k > 0$. Hence the system evolves into a non-separable state. If decoherence effects are taken into account, the state could become separable depending on the value of the purity compared to the squeezing amplitude r_k. A plot of the threshold for separability in function of the squeezing parameter $\tanh r_k$ and the purity p is reported in Figure 9.

5.2.3 *Quantum Discord*

The concept of quantum discord has been introduced in the context of quantum information theory by Henderson and Vedral [10] and Ollivier and Zurek [11]. Its computation in the context of cosmological perturbations can be

found in [9, 14, 94]. Quantum discord is defined as the difference between two ways of measuring the correlations between two sub-systems that coincide for a classical system, but differ for a quantum system.

The first measure is the *mutual information* $\mathcal{I}$, defined as the sum of the von-Neumann entropy of the two sub-systems minus the entropy of the total system:

$$\mathcal{I}_{1,2} = S[\hat{\rho}_1] + S[\hat{\rho}_2] - S[\hat{\rho}_{1,2}]\,, \tag{212}$$

where the entropy S is given by $S = -\mathrm{Tr}(\hat{\rho}\log_2\hat{\rho})$. The reduced density matrices $\hat{\rho}_1$ and $\hat{\rho}_2$ can be obtained by the density matrix of the whole system $\hat{\rho}_{1,2}$ by tracing over the degrees of freedom of the 2 or 1 sub-system respectively.

The second measure $\mathcal{J}$ is given by

$$\mathcal{J}_{1,2} = S[\hat{\rho}_1] - \sum_j p_j S\left[\hat{\rho}_{1,\hat{\Pi}_j}\right]\,, \tag{213}$$

where

$$\hat{\rho}_{1,\hat{\Pi}_j} = \mathrm{Tr}_2\left[\frac{\hat{\Pi}_j\hat{\rho}\hat{\Pi}_j}{p_j}\right] \tag{214}$$

is the entropy of the sub-system 1 when the sub-system 2 has been measured. $\hat{\Pi}_j$ is the projector, defined on $\mathcal{H}_2$, which transforms the state $\hat{\rho}$ into $\hat{\Pi}_j\hat{\rho}\,\hat{\Pi}_j/p_j$, with $p_j = \mathrm{Tr}\left(\hat{\rho}\hat{\Pi}_j\right)$ the probability of a measure j. Equation (213) takes into account the set of all possible measurements by summing over a complete set of projectors $\hat{\Pi}_j$. In general it can be proved that $\mathcal{J} \leq \mathcal{I}$; they coincide only if the system is classical, thanks to Bayes' theorem (see Appendix C.1 of [94] for more details). Quantum discord is defined as

$$\mathcal{D} = \min_{\{\hat{\Pi}_j\}}\left[\mathcal{I}_{1,2} - \mathcal{J}_{1,2}\right]\,, \tag{215}$$

minimizing over the set of possible measurements. This avoids that the result for the quantum discord is affected by the choice of the projector, i.e. of the measurement performed. In turn this implies that the deviation from classicality is not a spurious effect of the choice of the projector.

The computation of the precise form of (212) and (213) is beyond the scope of this work. The full derivation can be found in Appendices C.3 and C.4 of [94]; further details can be found also in [105, 109–111]. We report here just the main results. For Gaussian states, both $\mathcal{I}$ and $\mathcal{J}$ can be expressed in terms of the symplectic eigenvalues of the reduced covariance matrix, that is γ_A in (180). The symplectic eigenvalues of the covariance matrix are the quantities σ_i such that $\mathrm{Sp}(J\gamma) = \{i\sigma_1, -i\sigma_1, i\sigma_2, -i\sigma_2\}$. For a generic partition $R_{1/2}$ depending on θ, it can be proved that $\sigma(\theta)$, given by $\mathrm{Sp}(J^{(1)}\gamma_A) = \{i\sigma(\theta), -i\sigma(\theta)\}$, is enough to fully characterize $\mathcal{I}$ and $\mathcal{J}$. One then finds

$$\mathcal{D}(\theta) = f\left[\sigma(\theta)\right] - 2f\left[\sigma(0)\right] + f\left[\frac{\sigma(\theta)+\sigma^2(0)}{\sigma(\theta)+1}\right]\,, \tag{216}$$

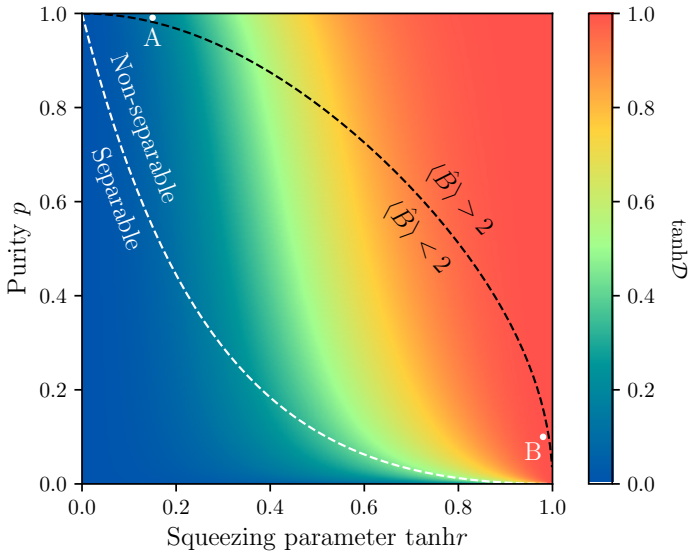


Figure 9: Quantum discord $\tanh \mathcal{D}$ as a function of the squeezing amplitude r_k and of the purity p. The white dashed line represents the threshold for separability. The black dashed line gives the threshold for Bell inequality violation. Bell inequality will be discussed in the following chapter. This figure has been taken from [14].

where

$$\sigma(\theta) = \sqrt{\cos^2(2\theta)\left(\gamma_{vv}\gamma_{\pi\pi} - \gamma_{v\pi}^2\right) + \left(\frac{\gamma_{vv} + \gamma_{\pi\pi}}{2}\right)^2 \sin^2(2\theta)}\,, \tag{217}$$

and

$$f(x) = \left(\frac{x+1}{2}\right)\log_2\left(\frac{x+1}{2}\right) - \left(\frac{x-1}{2}\right)\log_2\left(\frac{x-1}{2}\right)\,, \tag{218}$$

for $x \geq 1$. For $\theta = 0$ it is easy to see from (217) that $\sigma(0) = 0$. Therefore the quantum discord reduces to

$$\mathcal{D}(\theta) = f[\sigma(\theta)]\,. \tag{219}$$

In the R/I partition it is then clear that the quantum discord vanishes, reflecting the absence of correlations between the R and the I sub-systems. The symplectic eigenvalues $\sigma(\theta)$ can be expressed in terms of the Bogoliubov coefficients and in turn of the squeezing parameters by plugging (184) or (185) in (217). In particular

$$\sigma(\theta) = \sqrt{1 + 4|\alpha_k|^2|\beta_k|^2\sin^2(2\theta)} = \sqrt{1 + \sinh^2(2r_k)\sin^2(2\theta)}\,. \tag{220}$$

For a generic value of $\theta \neq 0$, the discord increases with the squeezing amplitude r_k. Moreover the discord is maximum for $\theta = -\pi/4$, that is in the $\pm\mathbf{k}$ partition.

Let us notice that in the case of a mixed state with $p \neq 1$, the expression for $\sigma(0)$ changes. Indeed, now the determinant of the covariance matrix

$\det\gamma = (\gamma_{vv}\gamma_{\pi\pi} - \gamma_{v\pi}^2)$ is given by (191), hence $\sigma(0) = p^{-1/2}$. It can be checked that in the $\pm\mathbf{k}$ partition $\sigma(\theta) = \cosh(2r_k)/\sqrt{p}$. A plot of $\tanh\mathcal{D}$ computed as a function of the squeezing amplitude $\tanh r_k$ and of the purity p is reported in Figure 9. It can be seen from the plot that for $p = 1$ the quantum discord is always different from zero; for $p < 1$ the quantum discord can vanish even for non-zero values of the squeezing amplitude r_k.

We conclude this chapter underlying how, although the two-point correlation functions of a two-mode squeezed state can be obtained even in a classical stochastic description, there are still some signatures stating the quantum nature of the cosmological perturbations. Indeed, even though the Wigner function is non-negative, we have seen how for a non-zero value of the squeezing amplitude r_k the system is non-separable and the quantum discord is different from zero. Another undeniable evidence of the quantum nature of the cosmological perturbations is provided by a violation of the Bell inequality. We will show in the following chapter how this violation occurs for some values of the squeezing parameters. Moreover we will discuss the observability of such violation.

6 COSMOLOGICAL BELL INEQUALITIES

Bell inequalities [112] are of crucial importance in Physics, since their experimental violation [113–115] shows that Nature cannot be fully explained by a theory that is both local and deterministic. Instead, it adheres to the principles of Quantum Mechanics, where such violations can occur when a system is in an entangled state. Cosmological Bell inequalities could then be an extremely useful instrument to test the quantum nature of the cosmological perturbations. In this chapter we review the main results obtained in the literature in this perspective. The first sections are a summary of the works [19] and [23], where a violation of the Bell inequality depending on the values of the squeezing parameters is reported. We furthermore discuss the observability of these violations. It turns out a measure of the correlators of the spin operators is in practice impossible, since it requires the measure of both the field $q_{\mathbf{k}}$ and its momentum $\pi_{\mathbf{k}}$, while we only know $q_{\mathbf{k}}$. This limitation is linked to the fact we cannot perform repeated experiments, since we have access only to our Universe. A possible way out to this problem is provided by the LGI, that are presented in Section 6.5. Measurements of the same spin operators at different times allow to construct inequalities, whose violation is a signature of the quantum nature of the system under consideration. A computation of the LGI for the cosmological perturbations is reported in Section 6.6. The results in this section are part of the article in preparation [28].

6.1 BELL INEQUALITY IN QUANTUM MECHANICS

Historically, a system consisting of two particles in a position-entangled state was first analyzed by Einstein, Podolsky, and Rosen (EPR) in [116]. Later works have addressed the problem using spin operators; with these discrete variables, the Bell inequalities assume the Clauser-Horne-Shimony-Holt (CHSH) form [16]. In this setup, the Hilbert space is split into two sub-systems as $\mathcal{H} = \mathcal{H}_A + \mathcal{H}_B$, where A and B are two particles whose spin along z is correlated. The state describing the system is

$$|\Psi\rangle = \frac{1}{\sqrt{2}}\left(|+,-\rangle + |-,+\rangle\right), \tag{221}$$

where $|+\rangle$ is an eigenstate of the spin along z, S_z, with eigenvalue $+1$, while $|-\rangle$ is an eigenstate with eigenvalue -1. The two particles are emitted in the same point and then travel in the positions A and B. These are measured along the directions $\mathbf{u}_A$ and $\mathbf{u_B}$ respectively (see Figure 10). A generic direction $\mathbf{u}$ can be written in terms of the polar and azimuthal angles as

$$\mathbf{u} = (\sin\theta\cos\varphi,\ \sin\theta\sin\varphi,\ \cos\theta)\,, \tag{222}$$

as shown by the green arrow in Figure 10. One can then compute the projection

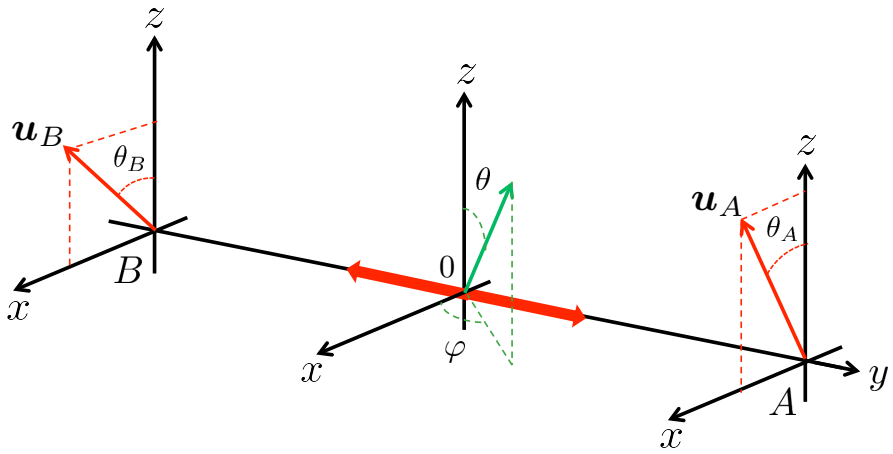


Figure 10: Setup for a Bell experiment. Two particles emitted in 0 travel towards A and B, where their spin is then measured along the directions $\mathbf{u}_A$ and $\mathbf{u}_B$ respectively. This figure has been taken from [23].

of the spin $\mathbf{S}$ along the direction $\mathbf{u}$ as $\mathbf{S}\cdot\mathbf{u}$, whose eigenstates will be linear combinations of those of S_z; in particular one as

$$\begin{aligned} |+\rangle_{\mathbf{u}} &= \cos\left(\frac{\theta}{2}\right) e^{-i\varphi/2}\,|+\rangle + \sin\left(\frac{\theta}{2}\right) e^{i\varphi/2}\,|-\rangle\,, \\ |-\rangle_{\mathbf{u}} &= -\sin\left(\frac{\theta}{2}\right) e^{-i\varphi/2}\,|+\rangle + \cos\left(\frac{\theta}{2}\right) e^{i\varphi/2}\,|-\rangle\,. \end{aligned} \tag{223}$$

The Bell operator is defined as

$$\begin{aligned} \hat{\mathcal{B}}_{\mathrm{CHSH}}(A,B) =& \mathbf{u}_A\cdot\mathbf{S}_A\otimes\mathbf{u}_B\cdot\mathbf{S}_B + \mathbf{u}_A\cdot\mathbf{S}_A\otimes\mathbf{u}'_B\cdot\mathbf{S}_B + \\ &+ \mathbf{u}'_A\cdot\mathbf{S}_A\otimes\mathbf{u}_B\cdot\mathbf{S}_B - \mathbf{u}'_A\cdot\mathbf{S}_A\otimes\mathbf{u}'_B\cdot\mathbf{S}_B\,, \end{aligned} \tag{224}$$

where $\mathbf{u}_A$, $\mathbf{u}_B$, $\mathbf{u}'_A$ and $\mathbf{u}'_B$ are four different unit vectors. The Bell inequality for the Bell operator (224) is $|\langle\hat{\mathcal{B}}_{\mathrm{CHSH}}(A,B)\rangle| \leq 2$. Any situation for which $2 < |\langle\hat{\mathcal{B}}_{\mathrm{CHSH}}(A,B)\rangle| \leq 2\sqrt{2}$ is a violation of the Bell inequality. The upper bound is called Cierl'son bound and it has been derived in [117]. For simplicity, and without loss of generality, one can set all the azimuthal angle φ_i to zero. We can then express the expectation value of the Bell operators as

$$\langle\hat{\mathcal{B}}_{\mathrm{CHSH}}(A,B)\rangle = E(\theta_A,\theta_B) + E(\theta_A,\theta'_B) + E(\theta'_A,\theta_B) - E(\theta'_A,\theta'_B)\,, \tag{225}$$

where

$$E(\theta_A,\theta_B) = \langle\mathbf{u}_A\cdot\mathbf{S}_A\otimes\mathbf{u}_B\cdot\mathbf{S}_B\rangle\,. \tag{226}$$

One can check that for the state (221), the correlator (226) reduces to $E(\theta_A,\theta_B) = -\cos(\theta_A-\theta_B)$. The polar angles θ_A, θ_B, θ'_A and θ'_B have to be carefully chosen in order to obtain a violation of the Bell inequality. The maximum violation can be obtain, in this simple system, by taking

$$\theta_A-\theta_B = \frac{\pi}{4}\,, \qquad \theta_A-\theta'_B = \theta'_A-\theta_B = -\frac{\pi}{4}\,, \qquad \theta'_A-\theta'_B = -\frac{3\pi}{4}\,.$$

We now want to design a similar setup in the case of the cosmological perturbations.

6.2 BELL INEQUALITY VIOLATION FOR DIFFERENT PSEUDO-SPIN OPERATORS

The wave function describing the inflationary perturbations is given by (157); in this chapter we use a slightly different convention, i.e.

$$|\Psi\rangle_{2\mathrm{sq}} = \frac{1}{\cosh r_k} \sum_{n=0}^{\infty} e^{-2in\varphi_k} (-1)^n \tanh^n r_k |n_{\mathbf{k}}, n_{-\mathbf{k}}\rangle \,. \tag{227}$$

This implies a redefinition of the squeezing angle $\varphi_k \to -(\varphi_k + \pi/2)$. The notation has been changed in order to recover the results of [23].

The aim is to construct a Bell operator like in (224) linking the two subsystems $\pm\mathbf{k}$, however we are now dealing with a continuous variables system. It has been shown how one can construct pseudo-spin operators starting from continuous position operators. Several definitions have been introduced: Banaszek-Wodkiewicz (BW) spin operators [15, 107, 118, 119], Gour-Khanna-Mann-Revzen (GKMR) spin operators [17, 107] and Larsson spin operators [19, 120]. We now study how to construct the pseudo-spin operators and in turn the Bell operators in all the three cases.

6.2.1 *Banaszek-Wodkiewicz (BW) Spin Operators*

The first set of pseudo-spin operators is defined by

$$\begin{aligned}
S_x(\mathbf{k}) &= \sum_{n=0}^{\infty} \left(|2n_{\mathbf{k}} + 1\rangle\langle 2n_{\mathbf{k}}| + |2n_{\mathbf{k}}\rangle\langle 2n_{\mathbf{k}} + 1| \right) , \\
S_y(\mathbf{k}) &= i \sum_{n=0}^{\infty} \left(|2n_{\mathbf{k}}\rangle\langle 2n_{\mathbf{k}} + 1| - |2n_{\mathbf{k}} + 1\rangle\langle 2n_{\mathbf{k}}| \right) , \\
S_z(\mathbf{k}) &= \sum_{n=0}^{\infty} \left(|2n_{\mathbf{k}} + 1\rangle\langle 2n_{\mathbf{k}} + 1| - |2n_{\mathbf{k}}\rangle\langle 2n_{\mathbf{k}}| \right) .
\end{aligned} \tag{228}$$

Analogous expressions for the spin of the mode $-\mathbf{k}$. The commutation relations

$$[S_x, S_y] = 2i\, S_z \,, \qquad [S_y, S_z] = 2i\, S_x \,, \qquad [S_x, S_z] = -2i\, S_y$$

are easily proved to be satisfied. We now define a unit vector $\mathbf{u}$ as in (222). It is not difficult to check that $(\mathbf{u}\cdot\mathbf{S})^2 = \mathbb{1}$, so that $(\mathbf{u}\cdot\mathbf{S})$ has eigenvalues ± 1. We can then introduce the Bell operator

$$\begin{aligned}
\hat{\mathcal{B}}_{\mathrm{BW}}(\mathbf{k}, -\mathbf{k}) =& \mathbf{u}_{\mathbf{k}} \cdot \mathbf{S}_{\mathbf{k}} \otimes \mathbf{u}_{-\mathbf{k}} \cdot \mathbf{S}_{-\mathbf{k}} + \mathbf{u}_{\mathbf{k}} \cdot \mathbf{S}_{\mathbf{k}} \otimes \mathbf{u}'_{-\mathbf{k}} \cdot \mathbf{S}_{-\mathbf{k}} + \\
&+ \mathbf{u}'_{\mathbf{k}} \cdot \mathbf{S}_{\mathbf{k}} \otimes \mathbf{u}_{-\mathbf{k}} \cdot \mathbf{S}_{-\mathbf{k}} - \mathbf{u}'_{\mathbf{k}} \cdot \mathbf{S}_{\mathbf{k}} \otimes \mathbf{u}'_{-\mathbf{k}} \cdot \mathbf{S}_{-\mathbf{k}} \,,
\end{aligned} \tag{229}$$

in analogy with the quantum mechanics case seen in the previous section. The expectation value over a two-mode squeezed state can then be computed, and we can write in analogy

$$\langle \Psi_{2\mathrm{sq}} | \hat{\mathcal{B}}_{\mathrm{BW}}(\mathbf{k}, -\mathbf{k}) | \Psi_{2\mathrm{sq}} \rangle = E(\theta_{\mathbf{k}}, \theta_{-\mathbf{k}}) + E(\theta_{\mathbf{k}}, \theta'_{-\mathbf{k}}) + E(\theta'_{\mathbf{k}}, \theta_{-\mathbf{k}}) - E(\theta'_{\mathbf{k}}, \theta'_{-\mathbf{k}}) \,, \tag{230}$$

with

$$\begin{aligned} E(\theta_{\mathbf{k}}, \theta_{-\mathbf{k}}) &= \langle \Psi_{2sq} | \mathbf{u}_{\mathbf{k}} \cdot \mathbf{S}_{\mathbf{k}} \otimes \mathbf{u}_{-\mathbf{k}} \cdot \mathbf{S}_{-\mathbf{k}} | \Psi_{2sq} \rangle \\ &= \sin\theta_{\mathbf{k}} \sin\theta_{-\mathbf{k}} \langle S_x^{\mathbf{k}} S_x^{-\mathbf{k}} \rangle + \cos\theta_{\mathbf{k}} \cos\theta_{-\mathbf{k}} \langle S_z^{\mathbf{k}} S_z^{-\mathbf{k}} \rangle \,. \end{aligned} \tag{231}$$

The last equation has been obtained thanks to the fact we set all the φ_i to zero for simplicity. Indeed, in this case $\mathbf{u} \cdot \mathbf{S} = \sin\theta\, S_x + \cos\theta\, S_z$; after some manipulations one can check that the correlators $\langle S_x \otimes S_z \rangle$ vanish for the two-mode squeezed state (227) (see Appendix A4 of [19] for the proof). In order to get the maximum violation of the Bell inequality $\hat{\mathcal{B}} < 2$ one can fix three out of four angles, and optimize over the last angle. In particular let us consider

$$\theta_{\mathbf{k}} = 0\,, \qquad \theta'_{\mathbf{k}} = \frac{\pi}{2}\,, \qquad \theta'_{-\mathbf{k}} = -\theta_{-\mathbf{k}}\,.$$

The maximum violation is then obtained for

$$\theta_{-\mathbf{k}}^{\mathrm{opt}} = \arctan\left[\frac{\langle \Psi_{2sq} | S_{\mathbf{k}}^x \otimes S_{-\mathbf{k}}^x | \Psi_{2sq} \rangle}{\langle \Psi_{2sq} | S_{\mathbf{k}}^z \otimes S_{-\mathbf{k}}^z | \Psi_{2sq} \rangle}\right]\,. \tag{232}$$

With this value for $\theta_{-\mathbf{k}}$, the expectation value of the Bell operator (229) reduces to

$$\langle \Psi_{2sq} | \hat{\mathcal{B}}_{\mathrm{BW}}(\mathbf{k}, -\mathbf{k}) | \Psi_{2sq} \rangle = 2\sqrt{\langle \Psi_{2sq} | S_{\mathbf{k}}^z \otimes S_{-\mathbf{k}}^z | \Psi_{2sq} \rangle^2 + \langle \Psi_{2sq} | S_{\mathbf{k}}^x \otimes S_{-\mathbf{k}}^x | \Psi_{2sq} \rangle^2}\,. \tag{233}$$

Using the two-mode squeezed state (227) to compute the expectation values, one can check that

$$\begin{aligned} &\langle \Psi_{2sq} | S_{\mathbf{k}}^z \otimes S_{-\mathbf{k}}^z | \Psi_{2sq} \rangle = 1\,, \\ &\langle \Psi_{2sq} | S_{\mathbf{k}}^x \otimes S_{-\mathbf{k}}^x | \Psi_{2sq} \rangle = \tanh(2r_k)\, \cos(2\varphi_k)\,. \end{aligned} \tag{234}$$

Looking at (236) we can immediately see that, as soon as $\varphi_k \neq \pi/4 \pm \pi/2$ and $r_k > 0$, the Bell inequality is violated. This can be seen in the left panel of Figure 11, where the Bell operator is plotted in function of the squeezing amplitude r_k for different values of the squeezing angle φ_k. Notice that the maximum violation, $\langle \hat{\mathcal{B}}_{\mathrm{BW}} \rangle = 2\sqrt{2}$ is obtained in the large r_k limit and for a value of the squeezing phase $\varphi_k = -\pi/2$. These are exactly the values that the squeezing parameters of the inflationary perturbations take in the super-Hubble limit, at the end of inflation.

6.2.2 *Gour-Khanna-Mann-Revzen (GKMR) Spin Operators*

An alternative set of pseudo-spin operators is given by the GKMR operators, defined as:

$$\begin{aligned} S_x(\mathbf{k}) &= \int_0^\infty dq_{\mathbf{k}} \left(|q_{\mathbf{k}}\rangle\langle q_{\mathbf{k}}| - |-q_{\mathbf{k}}\rangle\langle -q_{\mathbf{k}}| \right)\,, \\ S_y(\mathbf{k}) &= -\int_0^\infty dq_{\mathbf{k}} \left(|q_{\mathbf{k}}\rangle\langle -q_{\mathbf{k}}| - |-q_{\mathbf{k}}\rangle\langle q_{\mathbf{k}}| \right)\,, \\ S_z(\mathbf{k}) &= -\int_{-\infty}^\infty dq_{\mathbf{k}} |q_{\mathbf{k}}\rangle\langle -q_{\mathbf{k}}|\,. \end{aligned} \tag{235}$$

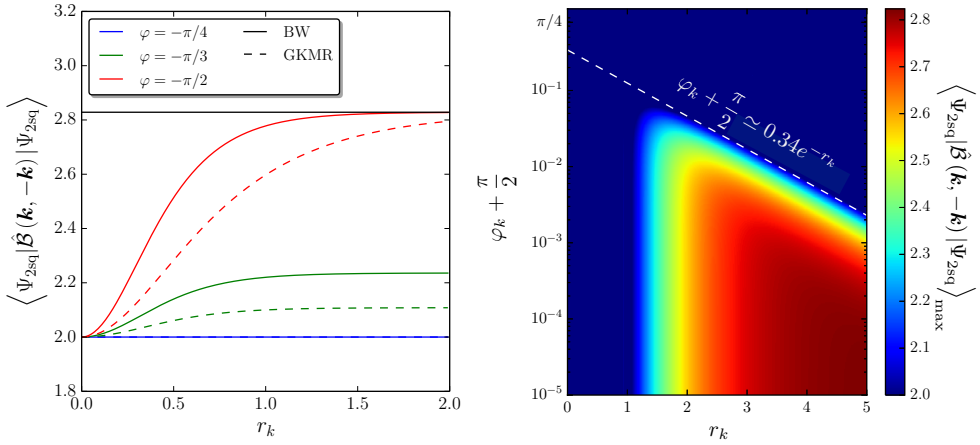


Figure 11: Left panel: Expectation value of the Bell operator in function of the squeezing amplitude r_k for three different values of the squeezing angle φ_k and for the BW (solid line) and the GKMR (dashed line) pseudo-spin operators. The horizontal black line represents the Cirel'son bound $2\sqrt{2}$. **Right panel**: maximum expectation value of the Bell operator in function of the squeezing amplitude r_k and the squeezing angle $\varphi_k + \pi/2$ for the Larsson pseudo-spin operators. The dashed white line sets the threshold for the Bell inequality violation. The figure has been taken from [23].

One can check that $S^z_{\text{GKMR}} = S^z_{\text{BW}}$ [23]. We can then proceed as in the previous section, introducing a Bell operator like (229), taking its expectation value over the state (227) and optimizing over the direction $\theta'_{-\mathbf{k}}$. The result is:

$$\langle \Psi_{2sq}|\hat{\mathcal{B}}_{\text{GKMR}}(\mathbf{k},-\mathbf{k})|\Psi_{2sq}\rangle = 2\sqrt{1+\langle \Psi_{2sq}|S^x_{\mathbf{k}}\otimes S^x_{-\mathbf{k}}|\Psi_{2sq}\rangle^2}\,. \tag{236}$$

The expectation value $\langle S^x_{\mathbf{k}}\otimes S^x_{-\mathbf{k}}\rangle$ can be computed as shown in Appendix A of [23]. The result is [14]

$$\langle \Psi_{2sq}|S^x_{\mathbf{k}}\otimes S^x_{-\mathbf{k}}|\Psi_{2sq}\rangle = -\frac{2}{\pi}\arcsin\left[\cos(2\varphi_k)\,\tanh(2r_k)\right]\,. \tag{237}$$

The behaviour of $\langle \Psi_{2sq}|\hat{\mathcal{B}}_{\text{GKMR}}(\mathbf{k},-\mathbf{k})|\Psi_{2sq}\rangle$ in function of r_k for three different values of φ_k is plotted in Figure 11. As for the BW operators, there is no violation for $\varphi_k = -\pi/4$. Moreover, although the violation is less strong with respect to the previous operators, it is still saturated in the large r_k limit for $\varphi_k = -\pi/2$.

6.2.3 *Larsson Spin Operators*

The construction of the Larsson pseudo-spin operators is carefully given in [19]. The idea is to divide the real axis in an infinite number of intervals $[n\ell,(n+1)\ell]$, with ℓ the length of the interval and n an integer number going from $-\infty$ to $+\infty$. We can then define the projector

$$P(n,\ell) = \int_{n\ell}^{(n+1)\ell} dq_{\mathbf{k}}|q_{\mathbf{k}}\rangle\langle q_{\mathbf{k}}|\,, \tag{238}$$

which projects a wave function defined over the whole real axis to the interval $[nl, (n+1)l]$. The spin operator along z is then defined as

$$S_z(\ell) = \sum_{n=-\infty}^{+\infty} (-1)^n \hat{P}(n,\ell) = \sum_{n=-\infty}^{\infty} (-1)^n \int_{n\ell}^{(n+1)\ell} dq_{\mathbf{k}} |q_{\mathbf{k}}\rangle\langle q_{\mathbf{k}}| \,. \tag{239}$$

The operators S_x and S_y are built from the raising and lowering operators S_+ and S_-, which can be built in turn in terms of the projector (238) (see [19]):

$$\begin{aligned} S_x(\ell) =& S_+(\ell) + S_-(\ell) \,, \\ S_y(\ell) =& -i\,[S_+(\ell) - S_-(\ell)] \,, \end{aligned} \tag{240}$$

where

$$S_+(\ell) = \sum_{n=-\infty}^{\infty} \int_{2n\ell}^{(2n+1)\ell} \mathrm{d}q_k |q_k\rangle\langle q_k + \ell| \,, \tag{241}$$

and $S_-(\ell) = S_+^\dagger(\ell)$. We have now all the ingredients to define again the Bell operator and take its expectation value. The optimization over the direction $\theta'_{-\mathbf{k}}$ proceeds as before and leads us to the relation (236) for the Larsson pseudo-spin operators. The expectation values of the spin correlators have no analytical expressions in this case, and one has to rely on the numerics. The numerical computations have been carried out in [19]; we report here the main results.

The expectation value of the Bell operator $\langle\hat{\mathcal{B}}\rangle$ can be computed for different values of the length ℓ, fixing the squeezing amplitude r_k and the squeezing phase φ_k. $\langle\hat{\mathcal{B}}\rangle$ approaches a plateau in the limit for large ℓ; the value of this plateau depends on the squeezing parameters φ_k and r_k. In the limit for low ℓ there is a second plateau, whose value is $\langle\hat{\mathcal{B}}\rangle = 2$ independently from the squeezing parameters. Between the two plateaus the structure is more complicated. Depending on the value of the phase φ_k one can identify a bump, for which $\langle\hat{\mathcal{B}}\rangle$ is maximum, or an oscillatory pattern below the threshold for the violation $\langle\hat{\mathcal{B}}\rangle < 2$. A plot of the value of $\langle\hat{\mathcal{B}}\rangle_{\max}$ in the (r_k, φ_k)-pl can then be obtained computing its value at the bump, where $\langle\hat{\mathcal{B}}\rangle$ reaches its maximum. Whenever the numerical result is below 2, $\langle\hat{\mathcal{B}}\rangle_{\max} = 2$ is set, since in the limit for small ℓ it approaches that value. The result of this numerical analysis is reported in the right panel of Figure 11. One can immediately notice that in order to get a violation of Bell inequality we need at least $r_k \gtrsim 1.12$; the higher the value of the squeezing amplitude r_k, the larger is the violation. Moreover, for a fixed value of r_k, the maximum violation is obtained for $\varphi_k = -\pi/2$ [1]; increasing the phase, the violation is milder. Moreover, increasing r_k the range of phases for which Bell inequality is violated decreases. It is proved in Appendix D of [19] that for large enough r_k Bell inequality is violated for

$$\varphi_k + \frac{\pi}{2} < 0.34\, e^{-r_k} \,. \tag{242}$$

This threshold is represented in Figure 11 with a dashed white line. To summarize, $\langle\hat{\mathcal{B}}\rangle_{\max} > 2$ if r_k is large enough and φ_k is sufficiently close to $-\pi/2$.

1 Notice that the convention on the phase φ_k in [19] is different. To get their results one has to change $\varphi_k \to \varphi_k + \pi/2$.

Notice however that during inflation on super-Hubble scales $\varphi_k \to -\pi/2$, while $r_k \to \infty$; it is then not so clear whether the condition (242) is satisfied. It has been showed in [23] how in slow-roll inflation the condition (242) is actually not respected, so that in this standard scenario a Bell inequality violation is not expected. The Larsson pseudo-spin operators are then not the best candidates to test it.

6.3 BELL INEQUALITY VIOLATION AND THE POSITIVITY OF THE WIGNER FUNCTION

We have already discussed in Section 5.2.1 how a violation of Bell inequality is not in contrast with the positivity of the Wigner function, if the operators considered are not proper dynamical variables. We hereby check that this is indeed the case for the pseudo-spin operators considered in this chapter, by computing their Wigner-Weyl representation. Let us start with the BW operators:

$$W_{S^z}(q_{\mathbf{k}}, \pi_{\mathbf{k}}) = \int_{-\infty}^{+\infty} e^{-i\pi_{\mathbf{k}} x} dx \left\langle q_{\mathbf{k}} + \frac{x}{2} \middle| S^z \middle| q_{\mathbf{k}} - \frac{x}{2} \right\rangle = -\pi\delta(q_{\mathbf{k}})\delta(\pi_{\mathbf{k}})\,. \quad (243)$$

Clearly $W_{S^z_{\rm BW}}(q_{\mathbf{k}}, \pi_{\mathbf{k}})$ does not reproduce the spectrum of S^z, i.e. the two eigenvalues ± 1. The same conclusion can be reached for the GKMR operator $S^z_{\rm GKMR}$, since it coincides with $S^z_{\rm BW}$. Interestingly, computing the Weyl transform of $S^x_{\rm GKMR}$ one gets $W_{S^x}(q_{\mathbf{k}}, \pi_{\mathbf{k}}) = \operatorname{sgn} q_{\mathbf{k}}$, showing it is a proper dynamical variable. Concerning $S^y_{\rm GKMR}$ one has instead $W_{S^y}(q_{\mathbf{k}}, \pi_{\mathbf{k}}) = -\delta(q_{\mathbf{k}})\,\mathcal{P}(1/\pi_{\mathbf{k}})$, with $\mathcal{P}$ the principal value; $S^y_{\rm GKMR}$ is then not proper. In the case of the Larsson spin operators one can check that S_z is a proper dynamical variable, while S_x and S_y are not (see [23]). Since each set of operators contains at least one improper dynamical variable, we have proved the consistency of these results [107].

6.4 MEASURABILITY OF THE PSEUDO-SPIN OPERATORS

We have shown how in principle the Bell inequality is violated for some values of the squeezing parameters and, at least for the BW and GKMR operators, $\langle \hat{\mathcal{B}} \rangle$ is saturated to $2\sqrt{2}$ for the values of r_k and φ_k corresponding to those of the cosmological perturbations in the super-Hubble regime. But are the pseudo-spin operators measurable? In [23] the authors showed how the temperature anisotropies in the CMB can be linked via Sachs-Wolfe effect to the value of the curvature perturbation $\zeta_{\mathbf{k}}$, provided the decaying mode $\zeta'_{\mathbf{k}}$ can be neglected. In particular, the eigenvectors of $\delta T/T$ are those of $\zeta_{\mathbf{k}} + \zeta^\dagger_{\mathbf{k}}$. The two-mode squeezed state, which is not an eigenstate of $\delta T/T$, collapsed onto a "CMB eigenstate", i.e. the Planck map, after the measurements had been performed. From the CMB measurements we have obtained $\zeta_{\mathbf{k}}$ (and it complex conjugate $\zeta_{-\mathbf{k}}$); using (172) and (133) one obtains $q_{\mathbf{k}}$ as

$$q_{\mathbf{k}} = \frac{z}{2}\left(\zeta_{\mathbf{k}} + \zeta_{-\mathbf{k}}\right) + \frac{z}{2k}\left(\zeta'_{\mathbf{k}} - \zeta'_{-\mathbf{k}}\right)\,, \quad (244)$$

Assuming $\zeta'_{\mathbf{k}}$ to be negligible, then from a measurement of $\zeta_{\mathbf{k}}$ we can infer the value of $q_{\mathbf{k}}$. We then have to understand whether the spin operators can be

computed from a measure of $q_{\mathbf{k}}$ only. Let us start from the BW operators; one can show that

$$\langle q_{\mathbf{k}}|[S^z_{\mathbf{k}}, q_{\mathbf{k}}]|q'_{\mathbf{k}}\rangle = 2q_{\mathbf{k}}\delta(q_{\mathbf{k}} + q'_{\mathbf{k}}) \neq 0\,. \tag{245}$$

Hence $S^z_{\mathbf{k}}$ does not commute with $q_{\mathbf{k}}$ and its value cannot be inferred from that of $q_{\mathbf{k}}$. Since in cosmology we cannot "repeat the experiment", we will never have access to the value of the spin along the z-direction. Analogous reasoning can be applied for S^x and S^y. They are indeed combinations of S^+ and S^-, which are in turn given in terms of $a_{\mathbf{k}}$ and $a^\dagger_{-\mathbf{k}}$; then S^x and S^y will be combinations of both $q_{\mathbf{k}}$ and $\pi_{\mathbf{k}}$. The same conclusion is reached when considering the GKMR pseudo-spin operators. However in this case, although S^z and S^y do not commute with $q_{\mathbf{k}}$, S^x does; in principle we have then access to one spin operator. Concerning the Larsson operators, S^z can be obtained from $q_{\mathbf{k}}$, but S^x and S^y cannot.

We conclude this section underlying how the knowledge of $\zeta_{\mathbf{k}}$, and in turn of $q_{\mathbf{k}}$, is not enough to determine two pseudo-spin operators and then measure the violation of Bell inequality. This is due to the fact that, contrary to what one would do in a laboratory, the experiments in cosmology cannot be repeated; we have access only to one Universe. Even if considering different patches of the sky, we have already measured ζ_k over the whole celestial sphere, making the wave function collapse into an eigenstate of ζ_k. Hence it is in a certain sense "too late" to measure another spin operator in the sky. We cannot then infer the values of two non-commuting observables.

Let us furthermore mention that this analysis has been carried out in Fourier space. The check of the Bell inequality violation in real space has been performed in [121]. The authors constructed Bell operators in real space and computed their expectation values as a function of the power spectra of the quantum fields. It turns out in real space there is no violation, although many pairs of entangled particles with opposite momenta are produced in momentum space. This is due to the fact that when considering two specific locations in space, one is implicitly tracing over the configurations of the field at every other location. It is a sort of decoherence effect, due to the fact we are tracing over a part of the Hilbert space. It seems then there is no possibility to detect a violation of Bell inequality in the sky. One way out is to design an experiment which involves the measurements of only one spin component. This is exactly what is done in the LGI; their investigation in real space has still to be done.

6.5 LEGGETT-GARG INEQUALITIES

The Leggett-Garg inequalities [26] examine the correlations within a single system observed at different times. This is possible since in general an observable does not commute with itself at a different time. Leggett-Garg inequalities are similar to Bell inequalities; however, while Bell inequalities rely on the principles of realism and locality, LGI rely on realism and noninvasive measurability. The former states that a measurement of the system will reveal a pre-determined value; the latter states that we are able to perform a measure-

ment without perturbing the system dynamics. These assumptions are clearly in conflict with quantum mechanics.

We now proceed to the construction of the LGI. Let us consider an observable $\mathcal{O}$ whose outcomes can be ± 1; let us then compute the correlation function E_{ij}, obtained from the joint probability $P_{ij}(\mathcal{O}_i, \mathcal{O}_j)$ of measuring $\mathcal{O}_i$ at time t_i and $\mathcal{O}_j$ at time t_j as

$$E_{ij} = \sum_{\mathcal{O}_i, \mathcal{O}_j = \pm 1} \mathcal{O}_i \mathcal{O}_j P_{ij}(\mathcal{O}_i, \mathcal{O}_j) \,. \tag{246}$$

The joint probability $P_{ij}(\mathcal{O}_i, \mathcal{O}_j)$ can be written as the marginal of a three-time probability distribution as

$$P_{ij}(\mathcal{O}_i, \mathcal{O}_j) = \sum_{\mathcal{O}_k, k \neq i,j} P_{ij}(\mathcal{O}_i, \mathcal{O}_j, \mathcal{O}_k) \,, \tag{247}$$

thanks to the fact the observable $\mathcal{O}$ has always a well-defined value at all times, assuming the hypothesis of realism to hold. If furthermore noninvasive measurability is assumed, measurements at different times do not affect the evolution of the system. Hence the probabilities $P_{ij}(\mathcal{O}_i, \mathcal{O}_j, \mathcal{O}_k)$ are equal $\forall i, j$; we can then drop the indices and write $P(\mathcal{O}_i, \mathcal{O}_j, \mathcal{O}_k)$. Keeping into account the dichotomy of the observable $\mathcal{O}$, and using the completeness relation $\sum_{i,j,k} P(\mathcal{O}_i, \mathcal{O}_j, \mathcal{O}_k) = 1$, one can compute the Leggett-Garg operator

$$K_3 = E_{21} + E_{32} - E_{31} = 1 - 4\left[P(+1, -1, +1) + P(-1, +1, -1)\right] . \tag{248}$$

It is then easy to check that $K_3^{\max} = 1$ and $K_3^{\min} = -3$. Indeed, $K_3 = 1$ for $P(+1, -1, +1) = P(-1, +1, -1) = 0$, while $K_3 = -3$ for $P(+1, -1, +1) + P(-1, +1, -1) = 1$. The Leggett-Garg inequality is then defined as

$$-3 \leq K_3 \leq 1 \,. \tag{249}$$

This is just an example of LGI. A family of inequalities can be computed by considering n measurements at n different times. Moreover, the Leggett-Garg inequalities possess some symmetry properties which can be used to derive further inequalities. For example, sending $\mathcal{O} \to -\mathcal{O}$ generates

$$-3 \leq K_3' \leq 1 \,, \qquad K_3' = -E_{21} - E_{32} - E_{31} \,. \tag{250}$$

Permutations of the time indices generate additional inequalities. In this work we restrict ourselves to the study of (248) and (250).

Given the inequalities, we need to understand how to properly construct the two-point correlation functions. The operator ordering prevents the classical correlations $E_{ij} = \langle \mathcal{O}(t_i)\mathcal{O}(t_j) \rangle$ from having a unique quantum analogue. The meaning of E_{ij} has then to be specified. In the original work [122], the correlations were obtained with projective measurements like in (246). It can be proved that the quantum expectation values of projective measurements can be written as [106, 123]:

$$E_{ij} = \frac{1}{2} \langle \{\mathcal{O}_i, \mathcal{O}_j\} \rangle \,. \tag{251}$$

This is the expression that will be used in the following sections.

6.6 LEGGETT-GARG INEQUALITIES FOR THE COSMOLOGICAL PERTURBATIONS

The Leggett-Garg inequalities have been computed in [27] for a one-mode squeezed state. The authors used the Larsson pseudo-spin operators introduced in the previous section and constructed the two-point correlation function of the spin component along z (239) as in (251). They then computed the LGI and made a plot of K_3 and K_3' in function of the squeezing parameters r_k and φ_k and found a violation of the LGI.

Although [27] shows how the LGI can be violated in a simple setup for a one-mode squeezed state, the question about its violation in the case of the cosmological perturbations is still unanswered. In this section I report the results of my original work [28], where the computations for the two-mode squeezed state of the inflationary fluctuations is performed. The aim is to compute the Leggett-Garg strings K_3 and K_3'; we then need to compute first the correlation functions of the spin along one direction evaluated at different times:

$$E(t_a, t_b) = \frac{1}{2}\langle 0_{\mathbf{k}}, 0_{-\mathbf{k}}|\{S^z_{\mathbf{k}}(t_a),\, S^z_{\mathbf{k}}(t_b)\}|0_{\mathbf{k}}, 0_{-\mathbf{k}}\rangle\,. \tag{252}$$

We chose to perform the calculation for the GKMR pseudo-spin operators (235) and we considered specifically the spin component along the z direction. Notice that the spin operator appearing in (252) is referred to the sub-system $\pm\mathbf{k}$. To be precise, one should instead write

$$E(t_a, t_b) = \frac{1}{2}\langle 0_{\mathbf{k}}, 0_{-\mathbf{k}}|\{(S^z_{\mathbf{k}}(t_a)\otimes \mathbb{1}_{-\mathbf{k}})(t_a),\, (S^z_{\mathbf{k}}(t_b)\otimes \mathbb{1}_{-\mathbf{k}})(t_b)\}|0_{\mathbf{k}}, 0_{-\mathbf{k}}\rangle\,. \tag{253}$$

The spin operators are written in the Heisenberg picture and their time evolution can be expressed in terms of the unitary evolution operator $U(t)$ (for the whole system) as

$$(S^z_{\mathbf{k}}(t)\otimes \mathbb{1}_{-\mathbf{k}}) = U^\dagger(t)(S^z_{\mathbf{k}}\otimes \mathbb{1}_{-\mathbf{k}})U(t)\,. \tag{254}$$

Plugging this expression into (253) leads to

$$E(t_a, t_b) = \mathrm{Re}\langle 0_{\mathbf{k}}, 0_{-\mathbf{k}}|U^\dagger(t_a)(S^z_{\mathbf{k}}\otimes \mathbb{1}_{-\mathbf{k}})U(t_a)U^\dagger(t_b)(S^z_{\mathbf{k}}\otimes \mathbb{1}_{-\mathbf{k}})U(t_b)|0_{\mathbf{k}}, 0_{-\mathbf{k}}\rangle\,. \tag{255}$$

The action of the evolution operator $U(t)$ on the vacuum state gives the two-mode squeezed state

$$|\Psi\rangle_{2\mathrm{sq}} = \frac{1}{\cosh r_k}\sum_{n=0}^{\infty} e^{-2in\varphi_k}(-1)^n \tanh^n r_k |n_{\mathbf{k}}, n_{-\mathbf{k}}\rangle\,. \tag{256}$$

As marked in Chapter 4, this state does not depend on the squeezing angle ϑ, which adds just an overall phase to the wave function, since the vacuum state is rotation independent. Although measurements performed at the same time are insensitive to a global phase, measurements at different times are not. The result is sensitive to the change in the global phase from time t_a to time t_b; in particular, as we are going to show, it depends on $\Delta\vartheta = \vartheta(t_a) - \vartheta(t_b)$. This is

related to the fact that measuring the spin along z of the system at a time t_a projects the state onto an eigenstate of the spin operator S^z. The eigenstates of S^z are not two-mode squeezed states and the resulting wave function is then not invariant under rotations anymore.

Substituting the expression (235) for the spin along z into (255) one gets

$$E(t_a,t_b)=\int_{-\infty}^{+\infty}dq_{\mathbf{k}}d\tilde{q}_{\mathbf{k}}\,\mathrm{Re}\langle\Psi_{2\mathrm{sq}}(t_a)|(|q_{\mathbf{k}}\rangle\langle -q_{\mathbf{k}}|\otimes\mathbb{1}_{-\mathbf{k}})U(t_a)\cdot \\ \cdot U^{\dagger}(t_b)(|\tilde{q}_{\mathbf{k}}\rangle\langle -\tilde{q}_{\mathbf{k}}|\otimes\mathbb{1}_{-\mathbf{k}})|\Psi_{2\mathrm{sq}}(t_b)\rangle\,. \tag{257}$$

We now insert twice the completeness relation

$$\mathbb{1}_{\mathbf{k}}\otimes\int dq_{-\mathbf{k}}|q_{-\mathbf{k}}\rangle\langle q_{-\mathbf{k}}|=1\,.$$

In this way the correlation function can be written as

$$E(t_a,t_b)=\int_{-\infty}^{+\infty}dq_{\mathbf{k}}d\tilde{q}_{\mathbf{k}}dq_{-\mathbf{k}}d\tilde{q}_{-\mathbf{k}}\,\mathrm{Re}\Big[\langle\Psi_{2\mathrm{sq}}(t_a)|-q_{\mathbf{k}},q_{-\mathbf{k}}\rangle\cdot \\ \cdot\langle q_{\mathbf{k}},q_{-\mathbf{k}}|U(t_a)U^{\dagger}(t_b)|\tilde{q}_{\mathbf{k}},\tilde{q}_{-\mathbf{k}}\rangle\langle -\tilde{q}_{\mathbf{k}},\tilde{q}_{-\mathbf{k}}|\Psi_{2\mathrm{sq}}(t_b)\rangle\Big]\,. \tag{258}$$

The two brakets with the two-mode squeezed state wave function give just the wave function written in position space and its complex conjugate. Its expression has been already derived in (194) and will be used later. We are then left with the computation of the matrix element

$$\langle q_{\mathbf{k}},q_{-\mathbf{k}}|U(t_a)U^{\dagger}(t_b)|\tilde{q}_{\mathbf{k}},\tilde{q}_{-\mathbf{k}}\rangle\,. \tag{259}$$

To proceed with its evaluation we insert three times the closure relation for a coherent state, i.e.

$$\int\frac{d\mathbf{u}}{(2\pi)^2}|\mathbf{u}\rangle\langle\mathbf{u}|=1\,. \tag{260}$$

Here the two-mode coherent state $|\mathbf{u}\rangle=|u_{\mathbf{k}},u_{-\mathbf{k}}\rangle$ is an eigenstate of the annihilation operators:

$$a_i|\mathbf{u}\rangle=u_i|\mathbf{u}\rangle\,, \tag{261}$$

with $i=\mathbf{k},-\mathbf{k}$. Each eigenvalue can be then decomposed into its real and imaginary part as

$$u_i=\frac{1}{\sqrt{2}}(u_i^R+iu_i^I)\,. \tag{262}$$

We then write the integration element as $d\mathbf{u}=du_{\mathbf{k}}^Rdu_{\mathbf{k}}^Idu_{-\mathbf{k}}^Rdu_{-\mathbf{k}}^I$. In this way the matrix element (259) can be expanded as

$$\langle q_{\mathbf{k}},q_{-\mathbf{k}}|U(t_a)U^{\dagger}(t_b)|\tilde{q}_{\mathbf{k}},\tilde{q}_{-\mathbf{k}}\rangle=\int\frac{d\mathbf{u}}{(2\pi)^2}\int\frac{d\mathbf{v}}{(2\pi)^2}\int\frac{d\mathbf{w}}{(2\pi)^2}\langle q_{\mathbf{k}},q_{-\mathbf{k}}|w_{\mathbf{k}},w_{-\mathbf{k}}\rangle\cdot \\ \cdot\langle w_{\mathbf{k}},w_{-\mathbf{k}}|U(t_a)|u_{\mathbf{k}},u_{-\mathbf{k}}\rangle\langle u_{\mathbf{k}},u_{-\mathbf{k}}|U^{\dagger}(t_b)|v_{\mathbf{k}},v_{-\mathbf{k}}\rangle\langle v_{\mathbf{k}},v_{-\mathbf{k}}|\tilde{q}_{\mathbf{k}},\tilde{q}_{-\mathbf{k}}\rangle\,. \tag{263}$$

The first and last brakets are just the coherent state and its complex conjugate in coordinate representation. We can expand for example the first braket as

$$\langle q_{\mathbf{k}}, q_{-\mathbf{k}}|w_{\mathbf{k}}, w_{-\mathbf{k}}\rangle = \langle q_{\mathbf{k}}|w_{\mathbf{k}}\rangle\langle q_{-\mathbf{k}}|w_{-\mathbf{k}}\rangle\,. \tag{264}$$

Each of these scalar products can be easily evaluated as follows:

$$\langle q_{\mathbf{k}}|w_{\mathbf{k}}\rangle = \exp\left\{-\frac{|w_{\mathbf{k}}|^2}{2}\right\}\sum_{n=0}^{\infty}\frac{w_{\mathbf{k}}^n}{\sqrt{n!}}\,\langle q_{\mathbf{k}}|n\rangle\,. \tag{265}$$

The scalar product in this expression is given in terms of Hankel functions as

$$\Psi_n(q_{\mathbf{k}}) = \frac{1}{\pi^{1/4}\sqrt{2^n n!}}e^{-q_{\mathbf{k}}^2/2}\,H_n(q_{\mathbf{k}})\,. \tag{266}$$

Expanding in terms of the real and imaginary parts (262):

$$\langle q_{\mathbf{k}}|w_{\mathbf{k}}\rangle = \pi^{-1/4}\exp\left\{-\frac{q_{\mathbf{k}}^2}{2}-\frac{\left(w_{\mathbf{k}}^R\right)^2}{2}+q_{\mathbf{k}}w_{\mathbf{k}}^R+iq_{\mathbf{k}}w_{\mathbf{k}}^I-\frac{i}{2}w_{\mathbf{k}}^Rw_{\mathbf{k}}^I\right\}\,. \tag{267}$$

We are left with the computation of the two matrix elements in (263). We start expanding the evolution operator U in terms of the rotation operator and squeezing operator as in (153) and (154). We then compute the action of $R(\vartheta)$ on

$$|\mathbf{u}\rangle = |u_{\mathbf{k}}\rangle|u_{-\mathbf{k}}\rangle = \exp\left\{-\frac{|u_{\mathbf{k}}|^2+|u_{-\mathbf{k}}|^2}{2}\right\}\sum_{n_{\mathbf{k}}=0}^{\infty}\sum_{n_{-\mathbf{k}}=0}^{\infty}\frac{(u_{\mathbf{k}})^{n_{\mathbf{k}}}}{\sqrt{n_{\mathbf{k}}!}}\frac{(u_{-\mathbf{k}})^{n_{-\mathbf{k}}}}{\sqrt{n_{-\mathbf{k}}!}}\,|n_{\mathbf{k}}, n_{-\mathbf{k}}\rangle\,. \tag{268}$$

After some tedious calculations one gets

$$R(\vartheta)|\mathbf{u}\rangle = |e^{i\vartheta}u_{\mathbf{k}}, e^{i\vartheta}u_{-\mathbf{k}}\rangle = |e^{i\vartheta}\mathbf{u}\rangle\,. \tag{269}$$

The next step consists in applying $S(r_k, \varphi_k)$ to the state just obtained. We start expanding $S(r_k, \varphi_k)$ using the operator ordering theorem as

$$\begin{aligned}S(r_k, \varphi_k) =& \exp\left\{e^{-2i\varphi_k}a_{-\mathbf{k}}^\dagger a_{\mathbf{k}}^\dagger\right\}\exp\left\{-\ln(\cosh r_k)\left(a_{\mathbf{k}}a_{\mathbf{k}}^\dagger + a_{-\mathbf{k}}^\dagger a_{\mathbf{k}}\right)\right\}\cdot\\ &\cdot\exp\left\{-e^{2i\varphi_k}a_{\mathbf{k}}a_{-\mathbf{k}}\right\}\,.\end{aligned} \tag{270}$$

Applying the first exponential on the bra and the last exponential on the ket, it is easy to show that the matrix element reduces to

$$\begin{aligned}\langle\mathbf{w}|U(t_a)|\mathbf{u}\rangle =& \exp\left\{e^{-2i\varphi_k}u_{\mathbf{k}}^*u_{-\mathbf{k}}^*\right\}\exp\left\{-e^{2i\varphi_k}e^{2i\vartheta_k}u_{\mathbf{k}}u_{-\mathbf{k}}\right\}\cdot\\ &\cdot\langle\mathbf{w}|\exp\left\{-\ln(\cosh r_k)\left(a_{\mathbf{k}}a_{\mathbf{k}}^\dagger + a_{-\mathbf{k}}^\dagger a_{\mathbf{k}}\right)\right\}|e^{i\vartheta_k}\mathbf{u}\rangle\,.\end{aligned} \tag{271}$$

The computation of the matrix element in (271) is quite tedious and we report here just the result:

$$\begin{aligned}&\langle\mathbf{w}|\exp\left\{-\ln(\cosh r_k)\left(a_{\mathbf{k}}a_{\mathbf{k}}^\dagger + a_{-\mathbf{k}}^\dagger a_{\mathbf{k}}\right)\right\}|e^{i\vartheta_k}\mathbf{u}\rangle = e^x\exp\left\{u_{\mathbf{k}}w_{\mathbf{k}}^*e^{i\vartheta_k}e^x\right\}\cdot\\ &\cdot\exp\left\{u_{-\mathbf{k}}w_{-\mathbf{k}}^*e^{i\vartheta_k}e^x\right\}\exp\left\{-\frac{|w_{\mathbf{k}}|^2}{2}-\frac{|w_{-\mathbf{k}}|^2}{2}-\frac{|u_{\mathbf{k}}|^2}{2}-\frac{|u_{-\mathbf{k}}|^2}{2}\right\}\,,\end{aligned} \tag{272}$$

This last expression has then to be expressed in real and imaginary variables as in (262) and plugged into (271). Then (271) has to be inserted into (263), together with its complex conjugate. The wave function in coordinate representation (264) and its complex conjugate, expressed in terms of (267), have also to be substituted into (263). The final expression is quite ugly, and there is no utility in writing it here. To simplify it, we introduce the following vectors:

$$\alpha^T = \left(w^R_{\mathbf{k}}, w^I_{\mathbf{k}}, w^R_{-\mathbf{k}}, w^I_{-\mathbf{k}}, u^R_{\mathbf{k}}, u^I_{\mathbf{k}}, u^R_{-\mathbf{k}}, u^I_{-\mathbf{k}}, v^R_{\mathbf{k}}, v^I_{\mathbf{k}}, v^R_{-\mathbf{k}}, v^I_{-\mathbf{k}}\right)^T , \tag{273}$$

$$J^T = (q_{\mathbf{k}}, iq_{\mathbf{k}}, q_{-\mathbf{k}}, iq_{-\mathbf{k}}, 0, 0, 0, 0, \tilde{q}_{\mathbf{k}}, -i\tilde{q}_{\mathbf{k}}, \tilde{q}_{-\mathbf{k}}, -i\tilde{q}_{-\mathbf{k}})^T . \tag{274}$$

Equation (263) then can be rewritten in terms of these vectors as

$$\begin{aligned}\langle q_{\mathbf{k}}, q_{-\mathbf{k}}|U(t_a)U^\dagger(t_b)|\tilde{q}_{\mathbf{k}}, \tilde{q}_{-\mathbf{k}}\rangle = \frac{1}{(2\pi)^6\,\pi\,\cosh(r_k(t_a))\cosh(r_k(t_b))}\cdot \\ \cdot \exp\left\{-\frac{q^2_{\mathbf{k}}}{2} - \frac{q^2_{-\mathbf{k}}}{2} - \frac{\tilde{q}^2_{\mathbf{k}}}{2} - \frac{\tilde{q}^2_{-\mathbf{k}}}{2}\right\}\int d^{12}\alpha \exp\left\{-\frac{1}{2}\alpha^T M\alpha + J^T\alpha\right\} ,\end{aligned} \tag{275}$$

where M is a twelve-by-twelve matrix whose elements depend just on the squeezing parameters r_k, φ_k and ϑ_k evaluated at the two different times t_a and t_b. The integration over α can be easily performed, since it is a Gaussian integral. One has to use the relation

$$\int d^n x e^{-\frac{1}{2}x^T Mx + J^T x} = \sqrt{\frac{(2\pi)^n}{\det M}} e^{\frac{1}{2}J^T M^{-1} J} . \tag{276}$$

Then (275) simplifies to

$$\begin{aligned}\langle q_{\mathbf{k}}, q_{-\mathbf{k}}|U(t_a)U^\dagger(t_b)|\tilde{q}_{\mathbf{k}}, \tilde{q}_{-\mathbf{k}}\rangle = \frac{1}{\pi\,\cosh(r_k(t_a))\cosh(r_k(t_b))}\cdot \\ \cdot \frac{1}{\sqrt{\det M}} \exp\left\{-\frac{q^2_{\mathbf{k}}}{2} - \frac{q^2_{-\mathbf{k}}}{2} - \frac{\tilde{q}^2_{\mathbf{k}}}{2} - \frac{\tilde{q}^2_{-\mathbf{k}}}{2}\right\} \exp\left\{-\frac{1}{2}J^T M^{-1} J\right\} .\end{aligned} \tag{277}$$

Notice that thanks to the structure of the vector J^T, whose central elements vanish, we can rewrite

$$J^T\left(M^{-1}\right)J = K^T\left(\tilde{M^{-1}}\right)K , \tag{278}$$

where

$$K^T = (q_{\mathbf{k}}, iq_{\mathbf{k}}, q_{-\mathbf{k}}, iq_{-\mathbf{k}}, \tilde{q}_{\mathbf{k}}, -i\tilde{q}_{\mathbf{k}}, \tilde{q}_{-\mathbf{k}}, -i\tilde{q}_{-\mathbf{k}})^T , \tag{279}$$

and $\tilde{M^{-1}}$ is an eight-by-eight matrix obtained from M^{-1} removing the four central horizontal and vertical lines. The matrix product (278) can be further simplified; indeed we can write

$$K^T = (G\cdot Q)^T , \tag{280}$$

where

$$Q^T = (q_{\mathbf{k}}, q_{-\mathbf{k}}, \tilde{q}_{\mathbf{k}}, \tilde{q}_{-\mathbf{k}})^T , \tag{281}$$

and

$$G = \begin{pmatrix} 1 & 0 & 0 & 0 \\ i & 0 & 0 & 0 \\ 0 & 1 & 0 & 0 \\ 0 & i & 0 & 0 \\ 0 & 0 & 1 & 0 \\ 0 & 0 & -i & 0 \\ 0 & 0 & 0 & 1 \\ 0 & 0 & 0 & -i \end{pmatrix} . \tag{282}$$

Therefore we can write

$$K^T \left(\tilde{M^{-1}}\right) K = Q^T \mathcal{M} Q \,, \tag{283}$$

with $\mathcal{M} = G^T(\tilde{M^{-1}})G$ a four-by-four matrix whose elements are lengthy and complicated expressions of r_k, φ_k and ϑ_k evaluated at t_a and t_b. The full matrix element then takes the simple form

$$\begin{aligned} \langle q_{\mathbf{k}}, q_{-\mathbf{k}} | U(t_a) U^\dagger(t_b) | \tilde{q}_{\mathbf{k}}, \tilde{q}_{-\mathbf{k}} \rangle = & \frac{1}{\pi \cosh(r_k(t_a)) \cosh(r_k(t_b))} \cdot \\ & \cdot \frac{1}{\sqrt{\det M}} \exp\left\{ -\frac{1}{2} Q^T (\mathbb{1} - \mathcal{M}) Q \right\} . \end{aligned} \tag{284}$$

It is interesting to point out that, as expected, the only combination of the squeezing angles ϑ_k appearing in this expression is $\Delta\vartheta_k = \vartheta_k(t_a) - \vartheta_k(t_b)$. To get the full correlator (258) the only thing left is to compute the product of the two wave functions in the coordinate representation. Using (194) one has:

$$\begin{aligned} \Psi^*_{2\mathrm{sq}}(-q_{\mathbf{k}}, q_{-\mathbf{k}}; t_a) \Psi_{2\mathrm{sq}}(-\tilde{q}_{\mathbf{k}}, \tilde{q}_{-\mathbf{k}}; t_b) = & \frac{1}{\pi \cosh(r_k(t_a)) \cosh(r_k(t_b))} \\ & \frac{1}{\sqrt{1 - e^{4i\varphi_k(t_a)} \tanh^2 r_k(t_a)} \sqrt{1 - e^{-4i\varphi_k(t_b)} \tanh^2 r_k(t_b)}} \exp\left\{ -\frac{1}{2} Q^T \mathcal{N} Q \right\} , \end{aligned} \tag{285}$$

where

$$\mathcal{N} = \begin{pmatrix} -A^*(t_a) & B^*(t_a) & 0 & 0 \\ B^*(t_a) & -A^*(t_a) & 0 & 0 \\ 0 & 0 & -A(t_b) & B(t_b) \\ 0 & 0 & B(t_b) & -A(t_b) \end{pmatrix} , \tag{286}$$

and where $A(t) = A(r_k(t), \varphi_k(t))$ and $B(t) = B(r_k(t), \varphi_k(t))$. The expressions for $A(t)$ and $B(t)$ are reported in (195). The full correlator (258) can then be finally written as

$$E(t_a,t_b) = \int_{-\infty}^{+\infty} dq_{\mathbf{k}} d\tilde{q}_{\mathbf{k}} dq_{-\mathbf{k}} d\tilde{q}_{-\mathbf{k}} \ \mathrm{Re}\left[\frac{1}{\pi^2 \cosh^2(r_k(t_a))\cosh^2(r_k(t_b))}\cdot\right.$$
$$\left.\cdot\frac{1}{\sqrt{\det M}}\frac{1}{\sqrt{1-e^{4i\varphi_k(t_a}\tanh^2(r(t_a))}}\frac{1}{\sqrt{1-e^{-4i\varphi_k(t_b}\tanh^2(r(t_b))}}\right]\cdot$$
$$\cdot\exp\left\{-\frac{1}{2}Q^T\left(\mathbb{1}-\mathcal{M}+\mathcal{N}\right)Q\right\}. \tag{287}$$

The Gaussian integral can be computed making use of expression (276) with a vanishing J. The result is the following:

$$E(t_a,t_b) = \mathrm{Re}\left[\frac{4}{\sqrt{\det\left(\mathbb{1}-\mathcal{M}+\mathcal{N}\right)}}\frac{1}{\cosh^2(r_k(t_a))\cosh^2(r_k(t_b))}\cdot\right.$$
$$\left.\frac{1}{\sqrt{\det M}}\frac{1}{\sqrt{1-e^{4i\varphi_k(t_a)}\tanh^2(r(t_a))}}\frac{1}{\sqrt{1-e^{-4i\varphi_k(t_b)}\tanh^2(r(t_b))}}\right]. \tag{288}$$

Notice that in the computations carried out in this section the positions $q_{\mathbf{k}}$, $q_{-\mathbf{k}}$, $\tilde{q}_{\mathbf{k}}$ and $\tilde{q}_{-\mathbf{k}}$ had a factor $k^{1/2}$ of difference with respect to (171). This is just a rescaling of the variables which can be taken into account in the last step, when integrating (287). The result (288) is then not affected by this rescaling. Having the expression for the correlation function, we can now compute the Leggett-Garg string as

$$K_3 = E(t_a,t_b) + E(t_b,t_c) - E(t_a,t_c)\,, \tag{289}$$

where t_a, t_b and t_c are in chronological order. Classical probability implies $-3 \leq K_3 \leq 1$; any deviation from this inequality is a sign of a quantum behaviour. The plots of K_3 as a function of the squeezing parameters at different times are under construction. We mention here as a preliminary result that the LGI are indeed violated for some values of the parameters.

As a final remark, we mention here an issue linked with the LGI, called *clumsiness loophole*. The LGI are indeed based on the assumption of noninvasive measurability, however proving conclusively that a physical measurement is genuinely noninvasive is not feasible. An observer cannot be completely sure he did not perturb the system classically and consequently affected its time evolution. Hence we cannot really say whether the deviation from classicality one observes is a genuine quantum mechanics effect or a "mistake" of the observer. The analogous of the clumsiness loophole for the Bell inequalities is the *communication loophole*. However in this case the issue can be solved by considering two space-like separated systems. Special relativity helps us closing this loophole. One possible way to avoid the clumsiness loophole is to consider the *temporal Bell inequalities*. They still rely on the measurement of one spin

component only, measured at different times, but now these measurements are performed on two different systems like in the standard Bell experiment. One recent article following this direction is [106], where Ando and Vennin showed that a two-mode squeezed state violates even the temporal Bell inequalities. Nevertheless, working with the LGI and testing non-invasiveness is still helpful in discerning between interpretations of quantum mechanics different from the Copenhagen interpretation, e.g. dynamical collapse theories.

7

NON-GAUSSIANITIES

So far, everything we discussed was based on the fact the perturbations we considered are Gaussian. Indeed the BD vacuum state giving the initial conditions for the evolution of the perturbations is a well-known Gaussian function. Moreover the Hamiltonian we always worked with is quadratic, hence it preserves the Gaussianity of the wave function. We can then deduce the statistical properties of the perturbations from the two-point function only, i.e. the power spectrum. The latest measurement of the CMB by Planck showed that the fluctuations are Gaussian within an excellent approximation [124]. Traces of non-Gaussianities were not found at the level of the Planck satellite precision. These observations are not surprising; slow-roll inflation indeed occurs when the potential is almost flat, so that the self-interactions of the scalar field are small. The odd n-point functions are thus expected to vanish. Small non-Gaussianities can nevertheless exist and would give us lots of information about the physics of inflation. Indeed, the process responsible for the generation of cosmological perturbations is not yet determined. Besides the single-field slow-roll models, there are indeed other inflationary scenarios which predict higher non-Gaussianities. In these models the curvature perturbations are sourced by a light scalar field (other than the inflaton), like for example the curvaton [125–130]. Moreover another source of strong primordial non–Gaussianity is provided by topological defects, in particular cosmic strings. Although topological defects have been ruled out as the primary source of non-Gaussianities, they could still contribute to part of them.

One other relevant aspect that has been pointed out in [30] is that a detection of primordial non-Gaussianities could help in discerning between the classical or quantum nature of the primordial fluctuations. In this chapter, we delve into this possibility, studying the shapes of the three-point function obtained from a quantum and a classical approach for the analysis of the perturbations. The case of curvature perturbations has been already analyzed in [30]; the study of gravitational waves carried out in Section 7.4 is instead my original contribution, which can be found in [31]. Before coming to this important question, let us introduce the concept of *bispectrum* for both the scalar and tensor perturbations generated during inflation. The necessary computational tools will also be presented.

7.1 NON - GAUSSIANITY IN THE INFLATIONARY PERTURBATIONS

Relevant works on the non-Gaussianities have been done by Bartolo, Matarrese and Riotto; among the others we mention one of the first papers on the topic [131] and one review [132]. In this section we give a general overview on the topic of primordial non-Gaussianities following [80, 132, 133].

The information about non-Gaussianities is encoded in (odd) higher-order correlation functions, which are sensitive to non-linear interactions, while the power spectrum is able to test only free theories. The first signature of non-Gaussianities relies in a non-vanishing three-point function. Its expression in Fourier space can be written as

$$\langle \zeta_{k_1}(\tau)\, \zeta_{k_2}(\tau)\, \zeta_{k_3}(\tau) \rangle = (2\pi)^3\, \delta^{(3)}(\mathbf{k}_1 + \mathbf{k}_2 + \mathbf{k}_3)\, \mathcal{B}_\zeta(k_1, k_2, k_3)\,, \tag{290}$$

where $\mathcal{B}_\zeta(k_1, k_2, k_3)$ is called the *bispectrum*. The delta function (enforcing momentum conservation) is a consequence of the homogeneity of the background. The delta function tells us the three wavevectors $\mathbf{k}_1$, $\mathbf{k}_2$ and $\mathbf{k}_3$ must form a closed triangle. Moreover rotational invariance reduces the number of independent variables from three to two, e.g. the ratios k_3/k_1 and k_2/k_1. For scale invariant fluctuations the bispectrum is a homogeneous function of degree -6:

$$\mathcal{B}_\zeta(\lambda k_1, \lambda k_2, \lambda k_3) = \lambda^{-6}\, \mathcal{B}_\zeta(k_1, k_2, k_3)\,. \tag{291}$$

A computation of the bispectrum requires a careful analysis of the time evolution of the perturbations keeping into account the interactions (either self-interactions or coupling with other fields, depending on the specific inflationary scenario). These kind of calculations will be explained in the following section. We can nevertheless present some general features for the bispectrum, independently on the precise result of the computation.

Different inflationary models predict a maximum in the bispectrum corresponding to different configurations for the triangle ($\mathbf{k}_1$, $\mathbf{k}_2$, $\mathbf{k}_3$). This characteristic is encoded in the shape function, defined as

$$\mathcal{S}_\zeta(k_1, k_2, k_3) = N_\zeta(k_1, k_2, k_3)^2\, \mathcal{B}_\zeta(k_1, k_2, k_3)\,, \tag{292}$$

where $N_\zeta(k_1, k_2, k_3)^2$ is an appropriate normalization factor. We can identify specifically three important configurations, which we now list (see Figure 12).

SQUEEZED CONFIGURATION It corresponds to values of the wavevectors where one is much smaller then the other two, e.g. $k_1 \approx k_2 \gg k_3$ (first picture in Figure 12). This configuration is the one predicted by one of the first ways to parameterize non-Gaussianity phenomenologically, the so called *local non-Gaussianity* [134]. It derives from the fact that one way to create a non-Gaussian field is to consider a small non-linear correction to the Gaussian field, as

$$\zeta(\mathbf{x}) = \zeta_g(\mathbf{x}) + \frac{3}{5}\, f_{\rm NL}^{\rm local} \left[\zeta_g^2(\mathbf{x}) - \langle \zeta_g^2(\mathbf{x}) \rangle \right], \tag{293}$$

where "g" stands for Gaussian. Moving to Fourier space, this assumption for $\zeta(\mathbf{x})$ leads to an expression for the bispectrum in terms of the power spectra for the wavevectors $\mathbf{k}_1$, $\mathbf{k}_2$ and $\mathbf{k}_3$:

$$\mathcal{B}_\zeta(k_1, k_2, k_3) = \frac{6}{5}\, f_{\rm NL}^{\rm local} \left[P_\zeta(k_1) P_\zeta(k_2) + P_\zeta(k_2) P_\zeta(k_3) + P_\zeta(k_3) P_\zeta(k_1) \right]. \tag{294}$$

If the power spectrum for ζ is scale invariant, i.e. $P_\zeta(k) = A\, k^{-3}$, then the bispectrum becomes

$$\mathcal{B}_\zeta(k_1, k_2, k_3) = \frac{6}{5} f_{NL}^{\rm local}\, A^2 \left[\frac{1}{(k_1 k_2)^3} + \frac{1}{(k_2 k_3)^3} + \frac{1}{(k_3 k_1)^3} \right]. \tag{295}$$

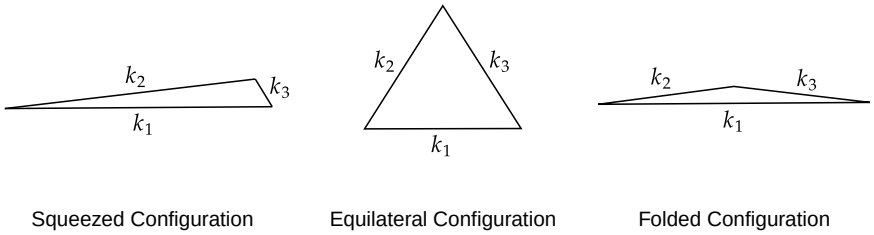


Figure 12: Relevant triangle configurations for the wavevectors in the bispectrum.

Assuming without loss of generality that $k_1 \geq k_2 \geq k_3$, we see that this configuration is peaked exactly for $k_1 \approx k_2 \gg k_3$.

The bispectrum is peaked for a squeezed configuration also for models with multiple light fields during inflation [131, 135–141] and in the curvaton scenario [141, 142]. However an interesting fact is that this shape cannot arise in single-field (not necessarily slow-roll) inflation. Indeed it has been proved by Creminelli and Zaldarriga [143] that in this case

$$\lim_{k_3 \to 0} \langle \zeta_{\mathbf{k}_1} \zeta_{\mathbf{k}_2} \zeta_{\mathbf{k}_3} \rangle = (2\pi)^3 \delta(\mathbf{k}_1 + \mathbf{k}_2 + \mathbf{k}_3) \, (1 - n_S) \, P_\zeta(k_1) P_\zeta(k_3) \, . \tag{296}$$

This result tells us that, in the context of single-field inflation, the squeezed limit of the three-point correlation function is suppressed by $1 - n_S$ and becomes zero for perturbations that are exactly scale-invariant. Hence, observing non-Gaussianity in the squeezed limit can invalidate the single-field inflation model.

EQUILATERAL CONFIGURATION In this scenario the values of the three wavevectors are all similar, that is $k_1 \approx k_2 \approx k_3$ (second picture in Figure 12). This configuration is peaked for example in single-field slow-roll inflation, when higher derivative corrections are introduced [1]. This kind of interaction is suppressed when one of the three modes considered is far outside the horizon; therefore one can intuitively guess that the maximum value for the bispectrum will be when the wavevectors are all comparable, i.e. the equilateral configuration. The specific shape depends on the interaction considered to compute the bispectrum, however there is a typical template shape that is used to analyse the CMB data which is a good approximation independently on the interaction close to the equilateral configuration [145].

FOLDED CONFIGURATION This configuration arises when one of the three wavevectors is given by the sum of the other two, e.g. $k_1 \approx k_2 + k_3$ (third picture in Figure 12). This shape for the bispectrum is obtained when one relaxes the initial conditions. Indeed in slow-roll inflation one usually assume the perturbations were generated out of the vacuum, so that the initial mode functions were described by the BD vacuum (104). However this is not the only option: the evolution of the perturbations could have started from an

1 These interactions can be classified using an Effective Field Theory approach. See [144] for further details.

excited state. The precise form of the bispectrum depends on how one models the initial excited state, however a common characteristic is that this scenario leads to correlations that are enhanced for folded triangles. A typical shape would be like

$$\mathcal{S}_\zeta^{\text{folded}} \propto \frac{1}{(k_1+k_2-k_3)^n} + \frac{1}{(k_1-k_2+k_3)^n} + \frac{1}{(-k_1+k_2+k_3)^n}\,, \tag{297}$$

where the power n depends on the interaction considered. The presence of these poles is due to the fact that in the initial state there are both positive and negative frequency waves; when correlating positive and negative frequency modes a minus sign comes out. The signal observed in the folded configuration serves as a fascinating examination of the quantum origins of the fluctuations [30]. We will deepen this topic in Section 7.3.

Having described the most relevant shapes of the bispectrum, we report here the result for the single-field slow-roll inflation. The bispectrum for this scenario of inflation was first obtained by Maldacena [146]. The result is

$$\mathcal{S}_\zeta^{\text{SR}}(k_1,k_2,k_3) \approx (2\varepsilon_1+\varepsilon_2)\,\mathcal{S}^{\text{local}}(k_1,k_2,k_3) + \frac{5}{3}\varepsilon_1 \mathcal{S}^{\text{equil}}(k_1,k_2,k_3)\,. \tag{298}$$

We see that the bispectrum for slow-roll inflation has an amplitude that is suppressed by slow-roll parameters, as expected. They indeed parameterise deviations from the free field case.

Lots of other inflationary scenarios have been studied in the literature. A careful analysis of the shapes of the bispectra in function of the inflationary model has been performed in [133]. For a summary of the main results see also [80].

7.2 COMPUTATIONAL TOOLS FOR THE BISPECTRUM

We now proceed to the precise computation of the bispectrum. There are two ways to compute it. The first one has been introduced by Acquaviva et al. in 2002 and it is based on the *Green's function method* [147]; the second one has been published a couple of months later by Maldacena and it relies on the *in-in formalism* [146]. Before these works, the problem of calculating the bispectrum of perturbations produced during inflation had been addressed differently: either by looking at the effect of inflaton self–interactions in a fixed de Sitter background [148] or using the so–called stochastic approach to inflation [149]. Since both the in-in formalism and the Green functions method will be used, we now give a brief overview on both of them.

7.2.1 *In-In Formalism*

The following discussion on the in-in formalism is based on [150, 151]. The goal of the in-in formalism is to compute fixed time correlators. Usually, in ordinary QFT one computes the transition probability, given by the S-matrix, between two asymptotically free states. These states are the $|\text{in}\rangle$ and the $|\text{out}\rangle$ states,

defined in the far past and in the far future, when the interacting particles are far away from each other so that the interaction can be neglected. In cosmology, one wants instead to compute expectation values of operators at a fixed time t. The in-in formalism is essentially standard QFT, modified to evaluate correlation functions at a fixed time, fixing the initial conditions rather than the asymptotic boundary conditions.

Let us suppose we want to compute a generic n-point function of the type

$$\langle \Omega | \zeta(t, \mathbf{x}_1) \cdots \zeta(t, \mathbf{x}_n) | \Omega \rangle \,, \tag{299}$$

with ζ quantized as presented in Section 3.5. $|\Omega\rangle$ is the interacting vacuum state, that is the vacuum state of the full-interacting theory. This expectation value has been written in the Heisenberg picture, where operators evolve in time, while the states do not. It turns out it is more convenient to work in the interaction picture, where both the operators and the states evolve in time. We work in the Hamiltonian formalism and we decompose the Hamiltonian of the system according to

$$H = H_0 + H_{\rm int} \,, \tag{300}$$

where H_0 is the free Hamiltonian, describing the evolution in the free theory, and we have included in $H_{\rm int}$ all the interaction terms. The operator in the Heisenberg picture evolves according to

$$\zeta^I(t) = U^{-1}(t, t_0)\, \zeta(t) U(t, t_0) \,, \tag{301}$$

where

$$U(t, t_0) = T \exp\left\{ -i \int_{t_0}^{t} H^I_{\rm int}(t') dt' \right\} . \tag{302}$$

The label "I" indicates the operator is represented in the interaction picture, and t_0 is some arbitrary initial time when we switch on the interaction. T gives the time-ordered product, while $H^I_{\rm int}$ is the interacting Hamiltonian in the interaction picture, which coincides with the one in the Heisenberg picture. Substituting the expression (301) into (299) one gets:

$$\langle \Omega | \left[\bar{T} \exp\left\{ i \int_{t_0}^{t} H_{\rm int}(t') dt' \right\} \right] \zeta^I(t, \mathbf{x}_1) \dots \zeta^I(t, \mathbf{x}_n) \left[T \exp\left\{ -i \int_{t_0}^{t} H_{\rm int}(t') dt' \right\} \right] | \Omega \rangle \,, \tag{303}$$

where $\bar{T}$ gives the anti-time-ordered product and we have dropped the label "I" on the interacting Hamiltonian.

The next step is to understand how to deal with the vacuum of the interacting theory. In ordinary QFT, i.e. Minkowski spacetime, the interacting vacuum is projected onto the free vacuum by deforming the integration contour in t'. In particular it is shifted in a slightly imaginary direction sending $t_0 \mapsto t_0(1 \pm i\varepsilon)$ (see [152] for further details). Fortunately we can apply a similar procedure in cosmology. Indeed we have shown in Section 3.5 that at early times, in the far sub-horizon limit, the perturbations do not feel the expansion of spacetime, which can be considered effectively Minkowski. Summing up, setting

$t_0 = -\infty(1 \pm i\varepsilon)$, we can substitute the interacting vacuum with the free vacuum, given by the BD vacuum (104). The n-point function will then be given by:

$$\begin{aligned}\langle\Omega|\zeta(t,\mathbf{x}_1)\cdots\zeta(t,\mathbf{x}_n)|\Omega\rangle = \langle 0|\left[\bar{T}\exp\left\{i\int_{-\infty(1\pm i\varepsilon)}^{t} H_{\rm int}(t')dt'\right\}\right]\cdot \\ \cdot\,\zeta^I(t,\mathbf{x}_1)\ldots\zeta^I(t,\mathbf{x}_n)\left[T\exp\left\{-i\int_{-\infty(1\pm i\varepsilon)}^{t} H_{\rm int}(t')dt'\right\}\right]|0\rangle\,.\end{aligned} \tag{304}$$

Replacing the interacting vacuum with the free one is crucial for the computations. It allows us to evaluate the expectation values of the operators expanded in terms of the ladder operators of the free theory. Equation (304) is telling us that, knowing the interaction terms in the Hamiltonian, we can compute the n-point correlation functions. The (anti) time-ordered exponentials can be expanded perturbatively; keeping only the first term of the expansion, i.e. considering only the tree level and neglecting loop effects, equation (304) simplifies to

$$\langle\Omega|\zeta(t,\mathbf{x}_1)\cdots\zeta(t,\mathbf{x}_n)|\Omega\rangle = -i\int_{-\infty(1\pm i\varepsilon)}^{t}\langle 0|\left[\zeta^I(t,\mathbf{x}_1)\ldots\zeta^I(t,\mathbf{x}_n), H_{\rm int}(t')\right]|0\rangle dt'\,. \tag{305}$$

This last equation is the starting point for the computation of the bispectrum. The following steps will be carried out in the case of the bispectrum of gravitational waves in a de Sitter expansion in Section 7.4.

7.2.2 *Green's Function Method*

We now illustrate how to compute the three-point function using the Green's function method. We consider for simplicity the case of a spectator scalar field χ evolving in a de Sitter background. The more complicated case of slow-roll inflation is treated in [147]. The equations of motion in conformal time are

$$\chi'' + 2\mathcal{H}\chi' - \nabla^2\chi + \frac{dV(\chi)}{d\chi} = 0\,, \tag{306}$$

where a prime denotes a derivative with respect to conformal time and $\mathcal{H}$ is the conformal Hubble radius. We can expand the field χ as

$$\chi(t,\mathbf{x}) = \bar{\chi}(t) + \delta\chi(t,\mathbf{x})\,, \tag{307}$$

and we further expand the perturbation $\delta\chi$ into

$$\delta\chi(t,\mathbf{x}) = \delta\chi^{(1)}(t,\mathbf{x}) + \delta\chi^{(2)}(t,\mathbf{x})\,, \tag{308}$$

where $\delta\chi^{(1)}$ is a first order perturbation, while $\delta\chi^{(2)}$ is a second order perturbation. $\delta\chi^{(1)}$ solves the free equation of motion (without the potential term), while $\delta\chi^{(2)}$ solves the interacting one (with the self-interacting potential taken into account). From now on we will drop the time and space dependencies in

the perturbations for simplicity. The potential term in (306) can be expanded in terms of the perturbations as

$$\begin{aligned} V'(\chi) =& V'(\bar{\chi}) + V''(\bar{\chi})\delta\chi^{(1)} + V''(\bar{\chi})\delta\chi^{(2)} + \\ &+ \frac{1}{2}V'''(\bar{\chi})\left(\delta\chi^{(1)}\right)^2 + \frac{1}{2}V'''(\bar{\chi})\left(\delta\chi^{(2)}\right)^2 + V'''(\bar{\chi})\delta\chi^{(1)}\delta\chi^{(2)}\,, \end{aligned} \tag{309}$$

up to second order in the perturbations. We have improperly used a prime to denote a derivative with respect to the field χ just for brevity of notation. The equation of motion (306) can be expanded perturbatively too and the different orders can be split. At 0-th order we have the equation for the background

$$\bar{\chi}'' + 2\mathcal{H}\bar{\chi}' - \nabla^2\bar{\chi} + \left.\frac{dV(\chi)}{d\chi}\right|_{\bar{\chi}} = 0\,. \tag{310}$$

At 1-st order

$$\delta\chi^{(1)\,\prime\prime} + 2\mathcal{H}\delta\chi^{(1)\,\prime} - \nabla^2\delta\chi^{(1)} + \left.\frac{d^2V(\chi)}{d\chi^2}\right|_{\bar{\chi}}\delta\chi^{(1)} = 0\,. \tag{311}$$

Finally at 2-nd order

$$\delta\chi^{(2)\,\prime\prime} + 2\mathcal{H}\delta\chi^{(2)\,\prime} - \nabla^2\delta\chi^{(2)} + \left.\frac{d^2V(\chi)}{d\chi^2}\right|_{\bar{\chi}}\delta\chi^{(2)} + \frac{1}{2}\left.\frac{d^3V(\chi)}{d\chi^3}\right|_{\bar{\chi}}\left(\delta\chi^{(1)}\right)^2 = 0\,. \tag{312}$$

Let us assume the potential to be negligible with respect to the expansion; we are indeed considering the interactions as small deviations with respect to the free Hamiltonian, i.e. the potential is almost flat, as for the inflaton field. In this case we can safely neglect the second derivative of the potential in both (311) and (312). We now solve the 1-st order equation of motion expanding the field in mode functions as it was done for the inflaton field in (100):

$$\delta\chi^{(1)} = u_k(\tau)a_{\mathbf{k}} + u_k^*(\tau)a^\dagger_{-\mathbf{k}}\,, \tag{313}$$

where the solution for the mode functions in this case is given in first approximation by the BD mode functions (105). $\delta\chi^{(1)}$ is then a Gaussian perturbation; the non-Gaussianity enters at second order, in $\delta\chi^{(2)}$. Here we do not specify intentionally anything about $a_{\mathbf{k}}$ and $a^\dagger_{-\mathbf{k}}$; they can be seen either as ladder operator as it was done in Section 3.5, or as stochastic parameters if we consider the perturbations to have a classical origin. We will see more in details these possibilities in the following section.

We now move to the 2-nd order equation of motion (312). Neglecting the second derivative of the potential, it can be written in Fourier space as

$$\delta\chi_k^{(2)\,\prime\prime} + 2\mathcal{H}\delta\chi_k^{(2)\,\prime} - \nabla^2\delta\chi_k^{(2)} = S(\mathbf{k},\tau)\,, \tag{314}$$

where

$$S(\mathbf{k},\tau) = -\frac{1}{2}\left.\frac{d^3V(\chi)}{d\chi^3}\right|_{\bar{\chi}}\left(\delta\chi^{(1)}\right)^2(\mathbf{k},\tau)\,. \tag{315}$$

The source term $S(\mathbf{k},\tau)$ can be written in Fourier space as the convolution of $\delta\chi^{(1)}(\mathbf{k}_1-\mathbf{k}_2,\tau)$ and $\delta\chi^{(1)}(\mathbf{k}_1,\tau)$. Let us assume without loss of generality the lowest correction to the Gaussian case coming from self-interaction, i.e. a cubic term for the potential of the type $V(\chi) = 1/3!\,\lambda\chi^3$. In this case $d^3V(\chi)/d\chi^3|_{\bar{\chi}} = \lambda$. The source term can then be evaluated simply as:

$$S(\mathbf{k},\tau) = -\frac{\lambda}{2\,(2\pi)^3}\int d^3k_2\,\delta\chi^{(1)}(\mathbf{k}_1-\mathbf{k}_2,\tau)\,\delta\chi^{(1)}(\mathbf{k}_2,\tau)\,. \tag{316}$$

We have now all the ingredients to solve the equation (314) applying the Green's function method. We can write the general solution as

$$\delta\chi^{(2)}(\mathbf{k},\tau) = \delta\chi^{(2)}_h(\mathbf{k},\tau) + \delta\chi^{(2)}_p(\mathbf{k},\tau)\,, \tag{317}$$

where $\delta\chi^{(2)}_h(\mathbf{k},\tau)$ is the homogeneous solution, i.e. the solution of the equation without the source term, and $\delta\chi^{(2)}_p(\mathbf{k},\tau)$ is the particular solution. The homogeneous equation is exactly equal to the 1-st order equation of motion; hence we already know the solution:

$$\delta\chi^{(2)}_h(\mathbf{k},\tau) = u_k(\tau)a_{\mathbf{k}} + u^*_k(\tau)a^\dagger_{-\mathbf{k}}\,. \tag{318}$$

The particular solution is instead found from the following ansatz:

$$\delta\chi^{(2)}_p(\mathbf{k},\tau) = c_1(\mathbf{k},\tau)\,u_k(\tau) + c_2(\mathbf{k},\tau)\,u^*_k(\tau)\,. \tag{319}$$

with $c_1(\mathbf{k},\tau)$ and $c_2(\mathbf{k},\tau)$ that have to be determined. We now compute the first and second derivatives of this expression and then insert them in (314); in this way one gets one equation for the two variables $c_1(\mathbf{k},\tau)$ and $c_2(\mathbf{k},\tau)$. We then have a second condition that we can impose on these functions. To simplify the computations we set

$$c_1'(\mathbf{k},\tau)u_k(\tau) + c_2'(\mathbf{k},\tau)u^*_k(\tau) = 0\,. \tag{320}$$

Substituting the first and second derivatives of (319) into (314) we find the equation

$$c_1'(\mathbf{k},\tau)u_k'(\tau) + c_2'(\mathbf{k},\tau)u^{*\prime}_k(\tau) = S(\mathbf{k},\tau)\,, \tag{321}$$

having used the fact that $u_k(\tau)$ and $u^*_k(\tau)$ solve the homogeneous equation. Equation (321), together with the constraint (320), leads to a system of first order differential equations for $c_1(\mathbf{k},\tau)$ and $c_2(\mathbf{k},\tau)$:

$$\begin{aligned} c_1'(\mathbf{k},\tau) &= \frac{u^*_k(\tau)}{u^{*\prime}_k(\tau)u_k(\tau) - u_k'(\tau)u^*_k(\tau)}S(\mathbf{k},\tau)\,,\\ c_2'(\mathbf{k},\tau) &= -\frac{u_k(\tau)}{u^{*\prime}_k(\tau)u_k(\tau) - u_k'(\tau)u^*_k(\tau)}S(\mathbf{k},\tau)\,. \end{aligned} \tag{322}$$

The particular solution will then be given by

$$\delta\chi^{(2)}_p(\mathbf{k},\tau) = \int_{-\infty}^{\tau}\frac{u_k(\tau)u^*_k(\tau') - u^*_k(\tau)u_k(\tau')}{W(k,\tau')}S(\mathbf{k},\tau)\,d\tau'\,, \tag{323}$$

with $S(\mathbf{k},\tau)$ given by (316) and where

$$W(k,\tau') = u_k^{*\prime}(\tau')u_k(\tau') - u_k'(\tau')u_k^*(\tau') \tag{324}$$

is the associated Wronskian. The 2-nd order perturbation is then given by

$$\delta\chi^{(2)}(\mathbf{k},\tau) = u_k(\tau)a_{\mathbf{k}} + u_k^*(\tau)a^\dagger_{-\mathbf{k}} + \int_{-\infty}^{\tau} \frac{u_k(\tau)u_k^*(\tau') - u_k^*(\tau)u_k(\tau')}{W(k,\tau')} S(\mathbf{k},\tau)\, d\tau' \,. \tag{325}$$

We can now proceed to the evaluation of the three-point function. The lowest order contribution is given by

$$\langle \delta\chi^{(1)}(\mathbf{k}_1,\tau)\, \delta\chi^{(1)}(\mathbf{k}_2,\tau)\, \delta\chi^{(2)}(\mathbf{k}_3,\tau)\rangle = (2\pi)^3\, \delta^{(3)}(\mathbf{k}_1+\mathbf{k}_2+\mathbf{k}_3)\, \mathcal{B}(k_1,k_2,k_3)\,. \tag{326}$$

Notice that the expectation value of three $a_{\mathbf{k}}$ or $a^\dagger_{-\mathbf{k}}$ vanishes, hence the lowest order contribution to the bispectrum reduces to the computation of

$$\langle \delta\chi^{(1)}(\mathbf{k}_1,\tau)\, \delta\chi^{(1)}(\mathbf{k}_2,\tau)\, \delta\chi^{(2)}_p(\mathbf{k}_3,\tau)\rangle \,.$$

We have now introduced all the mathematical tools necessary to compute a bispectrum, and these tools will be used in the following sections. We underline just one caveat. The in-in formalism is intrinsically quantum and it cannot be applied in a classical framework. Even if considering the ladder operators as stochastic parameters (see Section 7.3 for further details), equation (305) contains the commutator of operators which classically commute. On the contrary, the Green's function method allows to make computations with classical fields. An example of both a quantum and a classical calculation is reported in the case of gravitons (or gravitational waves) in Section 7.4.2.

7.3 QUANTUM SIGNATURES IN SCALAR BISPECTRUM

This section is mainly based on a paper published by Daniel Green and Rafael Porto in 2020 [30]. In their work they claimed that a detection of primordial non-Gaussianity would give a way to discern among the classical or quantum nature of the perturbations. The main reason is that vacuum fluctuations cannot be generated in a classical theory, where long-range correlations must originate from interactions between real particles in the initial state. The basic picture is illustrated in Figure 13. Higher-order correlators in the quantum case can be generated via particle production out of the vacuum state; instead in the classical case n-point functions are generated via decay ($1 \to 2$) or annihilation ($2 \to 1$) of preexisting particles in the initial state. The correlators generated in the two cases then will present different characteristics due to the different physical processes which generated the correlations themselves. In particular the classical bispectrum, as we will show in Section 7.3.2, presents poles in correspondence of physical momenta, as it happens in ordinary QFT. These poles are actually smoothed thanks to dissipative effects [153–156]. The presence of these poles is not a proof per se; they can indeed be generated also

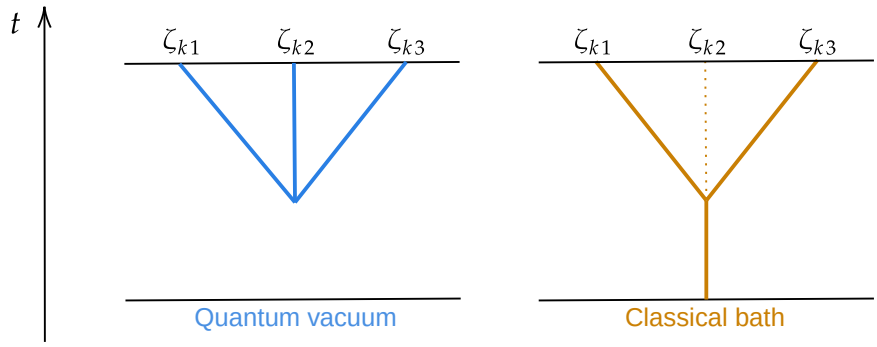


Figure 13: Schematic representation of the three-point correlations for two different initial configurations, i.e. a quantum vacuum and a thermal bath of particles.

by a quantum mechanical system whose initial state is an excited state (see the paragraph on the folded configuration of the bispectrum in Section 7.1). However the *absence of this signature* is a clear indication that the perturbations are intrinsically quantum. Notice that this statement holds if locality is assumed; if locality is violated, the quantum correlators could be reproduced even in a classical framework. However in the following we will assume that the locality principle holds.

We want to compare the predictions of quantum and classical physics for the statistics of the initial curvature perturbations. We will assume in the following that the non-Gaussianities are produced during the evolution, which is equivalent to require that the initial state is Gaussian. Moreover, for simplicity, let us assume the perturbations arise from a massless scalar field propagating in a de Sitter background. We then write the curvature perturbations as

$$\zeta(\mathbf{x},\tau) = \int \frac{d^3k}{(2\pi)^3}\frac{\Delta_\zeta}{\sqrt{k^3}}\, e^{i\mathbf{k}\cdot\mathbf{x}} \left[a_{\mathbf{k}}(1+ik\tau)e^{ik\tau} + a^\dagger_{-\mathbf{k}}(1-ik\tau)e^{ik\tau}\right], \qquad (327)$$

where Δ_ζ is a normalization factor. This form for the perturbations is equivalent to choose the BD mode functions in the initial state; indeed it can be proved they can be rewritten in this form up to some constants. The differences between the quantum and the classical approaches arise when we specify the statistics for the operators $a_{\mathbf{k}}$ and $a^\dagger_{-\mathbf{k}}$.

QUANTUM STATISTICS The $a_{\mathbf{k}}$ and $a^\dagger_{-\mathbf{k}}$ are annihilation and creation operators respectively, satisfying the standard commutation relations

$$[a_{\mathbf{k}}, a_{\mathbf{k}'}] = [a^\dagger_{-\mathbf{k}}, a^\dagger_{-\mathbf{k}'}] = 0\,, \qquad [a_{\mathbf{k}}, a^\dagger_{-\mathbf{k}'}] = \delta(\mathbf{k}-\mathbf{k}')\,. \qquad (328)$$

This implies that

$$\langle a_{\mathbf{k}}\, a^\dagger_{-\mathbf{k}'}\rangle = \delta(\mathbf{k}-\mathbf{k}')\,, \qquad \langle a^\dagger_{-\mathbf{k}'}\, a_{\mathbf{k}}\rangle = 0\,, \qquad (329)$$

with $\langle\cdot\rangle$ being an expectation value over the vacuum state.

CLASSICAL STATISTICS The $a_{\mathbf{k}}$ and $a^{\dagger}_{-\mathbf{k}}$ are classical stochastic parameters, which commute and obey the following statistical property:

$$\langle a_{\mathbf{k}}\, a^{\dagger}_{-\mathbf{k}'}\rangle = \langle a^{\dagger}_{-\mathbf{k}'}\, a_{\mathbf{k}}\rangle = \frac{1}{2}\delta(\mathbf{k}-\mathbf{k}')\,, \tag{330}$$

where now $\langle\cdot\rangle$ is an ensemble average.

We now proceed to the evaluation of the statistical correlators in the two approaches.

7.3.1 *Gaussian Fields*

At the level of Gaussian fields, the results obtained within a classical or a quantum approach are the same, as expected. The two-point function can be computed as in (115) and the result is

$$\langle\zeta(\mathbf{k},\tau)\,\zeta(\mathbf{k}',\tau)\rangle = (2\pi)^3\delta(\mathbf{k}+\mathbf{k}')\,\frac{\Delta^2_\zeta}{k^3}\,(1+k^2\tau^2)\,. \tag{331}$$

This result confirms that a measurement of the power spectrum alone is not enough to distinguish between the two possibilities.

7.3.2 *Non-gaussianities*

We now move to the results for the bispectrum. Let us choose a specific form of the interaction for the computations which is $H_{\rm int} = -\lambda/3!\,\dot\zeta^3$. We will see how changing the interaction could affect the form of the bispectrum, but this choice does not affect the main conclusions on the quantum nature of the fluctuations.

QUANTUM APPROACH The bispectrum in the quantum approach has been computed using the in-in formalism. Assuming as initial state the BD vacuum, the three-point function reads

$$\langle\zeta_{\mathbf{k}_1}\,\zeta_{\mathbf{k}_2}\,\zeta_{\mathbf{k}_3}\rangle = (2\pi)^3\,\delta(\mathbf{k}_1+\mathbf{k}_2+\mathbf{k}_3)\,\frac{4\lambda H^{-1}\Delta^6_\zeta}{(k_1+k_2+k_3)^3\,k_1k_2k_3}\,. \tag{332}$$

The bispectrum does not have poles in correspondence of physical momenta, but it has a pole in the total energy $k_1+k_2+k_3$. The order of the pole, i.e. the exponent of the pole, is related to the number of time derivatives in the interaction term. This correlation function is the result of the creation of three (virtual) particles out of the vacuum.

CLASSICAL APPROACH The classical bispectrum is calculated by solving perturbatively the equations of motion expanding $\zeta_{\mathbf{k}} \approx \zeta^{(1)}_{\mathbf{k}} + \zeta^{(2)}_{\mathbf{k}}$ and apply-

ing the Green's function method. The leading contribution to the bispectrum is found to be given by

$$\begin{aligned}\langle \zeta_{\mathbf{k}_1}\, \zeta_{\mathbf{k}_2}\, \zeta_{\mathbf{k}_3}\rangle =&(2\pi)^3\, \delta(\mathbf{k}_1+\mathbf{k}_2+\mathbf{k}_3)\, \frac{\lambda H^{-1}\Delta_\zeta^6}{3k_1k_2k_3}\left[\frac{3}{(k_1+k_2+k_3)^3}+\right.\\ &\left.+\frac{1}{(k_1+k_2-k_3)^3}+\frac{1}{(k_1-k_2+k_3)^3}+\frac{1}{(-k_1+k_2+k_3)^3}\right]\,.\end{aligned} \tag{333}$$

In addition to the pole in the total momentum, there are three more poles in correspondence of physical momenta. These new poles are present thanks to the interaction between classical fluctuations of real particles already present in the initial state. Examples of these processes are decays of initial particles for which $k_1 \to k_2 + k_3$ (and permutations of the momenta) or annihilations for which $k_1 + k_2 \to k_3$ (and permutations of the momenta). These poles give rise to a folded configuration for the bispectrum, which is actually present even in the quantum case if the initial state is not the vacuum, but an excited state. However the absence of poles at physical momenta is a unique signature of the quantum nature of the perturbations.

7.4 QUANTUM SIGNATURES IN GRAVITON BISPECTRUM

Until now we have considered only scalar perturbations. However tensor perturbations are interesting per se; their detection could provide information about the energy scale of inflation, and perhaps give us a signal of quantum gravity. In this section, based on my work [31], we aim at computing the bispectrum of gravitons (or gravitational waves) using both a quantum and a classical approach. Moreover, we will consider as initial state both the vacuum state and an excited state, contrary to what it was done in [30], where they chose to work with the vacuum state only. Before starting to compute the bispectra, let us introduce the formalism for tensor perturbations.

The framework we consider is a bit simpler with respect to the slow-roll scenario. In particular, we consider a de Sitter spacetime, with metric $ds^2 = a^2(\tau)\left(-d\tau^2 + d\boldsymbol{x}^2\right)$. The production of gravitational wave fluctuations is a generic prediction during an accelerated de Sitter expansion of the Universe, irrespective of the mechanism responsible for generating cosmological perturbations. We define the perturbations of the metric as

$$g_{\mu\nu} = a^2(\tau)\left(\eta_{\mu\nu} + h_{\mu\nu} + \frac{1}{2}h_{\mu\alpha}h^{\alpha}{}_{\nu} + \frac{1}{6}h_{\mu\alpha}h^{\alpha\beta}h_{\beta\nu}\right)\,, \tag{334}$$

Here the metric has been expanded up to third order, since we are interested in the interaction terms in the action. Splitting temporal and spatial components [2], we have:

$$\begin{aligned} &g_{00} = -a^2(\tau)\,, \qquad g_{0i} = 0\,,\\ &g_{ij} = a^2(\tau)\left(\eta_{ij} + h_{ij} + \frac{1}{2}h_{ik}h^{k}{}_{j} + \frac{1}{6}h_{ik}h^{kl}h_{lj}\right)\,. \end{aligned} \tag{335}$$

2 Both the metric and the perturbations are traceless and transverse in both the spacetime and spatial components, i.e. $\nabla^\mu g_{\mu\nu} = 0$ and $g^\mu{}_\mu = 0$.

The spatial metric perturbation can be decomposed using the polarization vectors e_{ij}^{λ} in Fourier space as [3]:

$$h_{ij}(\tau,\mathbf{x}) = \int \frac{d^3k}{(2\pi)^3} e^{i\mathbf{k}\cdot\mathbf{x}} \sum_{\lambda} h_{\lambda}(\tau,\mathbf{k}) e_{ij}^{\lambda}(\hat{k})\,. \tag{336}$$

At this point it is useful to redefine the field introducing the Mukhanov - Sasaki variable

$$v^{\lambda}(\tau,\mathbf{k}) = a\frac{M_{Pl}}{2} h^{\lambda}(\tau,\mathbf{k})\,. \tag{337}$$

The field $v^{\lambda}(\tau,\mathbf{k})$ is then expanded in terms of the mode functions $v_k^{\lambda}(\tau)$ as:

$$v_{\mathbf{k}}^{\lambda}(\tau) = v_k^{\lambda}(\tau) a_{\mathbf{k}}^{\lambda} + v_k^{\lambda *}(\tau) a_{-\mathbf{k}}^{\lambda\,\dagger}\,. \tag{338}$$

In this work we consider the most generic case of a non BD initial state. We want indeed to make a comparison between the classical computation and the quantum computation with an excited state as initial state. To this purpose we write the mode functions as:

$$v_k^{\lambda}(\tau) = \alpha_k^{\lambda} f_k(\tau) + \beta_k^{\lambda} f_k^{*}(\tau)\,, \tag{339}$$

where α_k^{λ} and β_k^{λ} are two complex numbers, the Bogoliubov coefficients, respecting the relation $|\alpha_k|^2 - |\beta_k|^2 = 1$. $f_k(\tau)$ are instead the BD mode functions

$$f_k(\tau) = \frac{1}{\sqrt{2k}}\left(1 - \frac{i}{k\tau}\right) e^{-ik\tau}\,, \tag{340}$$

where we have assumed a De Sitter spacetime, with a scale factor $a(\tau) \simeq -1/H\tau$. The BD mode functions are polarization independent. Therefore if the initial state for the system is BD, the two polarizations evolve independently. However in principle the Bogoliubov coefficients could depend on the polarization. We assume here for simplicity that the Bogoliubov coefficients do not depend on λ, so that the two polarizations evolve independently even in the case where the initial state is an excited state.

As introduced for the scalar perturbations, $a_{\mathbf{k}}^{\lambda}$ and $a_{-\mathbf{k}}^{\lambda\,\dagger}$ in (338) have different interpretations depending on whether we are working in a quantum or a classical framework. We now proceed to the computation of the bispectrum in the two different cases; but before delving into the computations, let us firstly briefly talk about the power spectrum.

7.4.1 *Gaussian Fields*

At the level of Gaussian fields, the results obtained within a classical or a quantum approach are the same. We can write the action for the gravitational field as:

$$S = S^{(free)} + S_{GR}^{(int)}\,. \tag{341}$$

3 The polarization vectors are symmetric, traceless, transverse, orthonormal and they respect the reality condition $e_{ij}^{\lambda}(\hat{k}) = e_{ik}^{*\lambda}(-\hat{k})$.

Splitting the metric as in (334), the perturbed free action becomes:

$$S^{(free)} = \frac{M_{pl}^2}{8}\int d^3x d\tau \left[(h'_{ij})^2 - (\nabla h_{ij})^2\right] . \tag{342}$$

Here a prime denotes a time derivative with respect to the conformal time, while the comma denotes a spatial derivative. The power spectrum can be computed through:

$$\langle h_{ij}(\tau,\mathbf{x})h^{ij}(\tau,\mathbf{x})\rangle = \int \frac{dk}{k}P_k\,, \tag{343}$$

and the result is

$$P_k = \frac{2k^3}{\pi^2 a^2 M_{Pl}^2}\sum_\lambda |v_k^\lambda|^2\,, \tag{344}$$

independently on the statistics chosen for the computation, whether classical or quantum. Here v_k^λ is given in (339) in terms of the BD mode functions. Notice that if v_k^λ are polarization dependent, the two polarizations do not sum up in a trivial way when computing the power spectrum. However, assuming the Bogoliubov coefficients to be polarization independent, the sum over the polarizations gives just a factor two in the final result.

7.4.2 *Non-gaussianities*

We now want to compute the bispectrum due to the interactions present in GR. In GR, the action describing the gravitational waves is the Einstein-Hilbert action. Splitting the metric as in (334) and perturbing the action up to third order in $h_{\mu\nu}$, one gets the free action in (342) plus the interacting action:

$$S^{(int)} = \frac{M_{pl}^2}{8}\int d^3x d\tau a^2 h^{ij}h^{lk}\left[h_{lk,ij} - 2h_{ik,jl}\right] . \tag{345}$$

From (345), we see that in GR we have two kind of possible interactions, for which we have to compute the bispectrum. The tensor bispectrum is defined in the following way:

$$\mathcal{B}_h(k_1,k_2,k_3) = \delta_{bc}\delta_{de}\delta_{fa}\mathcal{B}_{abcdef}(k_1,k_2,k_3)\,, \tag{346}$$

where $\mathcal{B}_{abcdef}(k_1,k_2,k_3)$ is the un-contracted bispectrum, defined from the three-point function as:

$$\langle h_{ab}(\tau,\mathbf{k_1})h_{cd}(\tau,\mathbf{k_2})h_{ef}(\tau,\mathbf{k_3})\rangle = (2\pi)^3\delta^{(3)}(\mathbf{k_1}+\mathbf{k_2}+\mathbf{k_3})\mathcal{B}_{abcdef}\,. \tag{347}$$

We now compute this bispectrum with the two different statistics for the ladder operators.

7.4.2.1 *Quantum Approach*

In computing the bispectrum with a quantum approach we make use of the in-in formalism. In this formalism the three-point function is computed starting from the interaction Hamiltonian as in (305):

$$\begin{aligned}\langle h_{ab}(t,\mathbf{k}_1)h_{cd}(t,\mathbf{k}_2)h_{ef}(t,\mathbf{k}_3)\rangle = \\ = -i\int_{\tau_0}^{\tau} d\tau' \langle \left[h_{ab}(\tau,\mathbf{k}_1)h_{cd}(\tau,\mathbf{k}_2)h_{ef}(\tau,\mathbf{k}_3), H_{int}(\tau')\right]\rangle .\end{aligned} \tag{348}$$

Here τ_0 is the initial time and τ the final time at which we compute the bispectrum. In our calculation we set $\tau_0 = -\infty(1 \pm i\varepsilon)$ and $\tau = 0$. We introduced the regularization parameter ε to take care of the divergences at $-\infty$.

The interaction Hamiltonian can be easily derived from the action (345) as

$$\begin{aligned}H_{int}(\tau) = -\frac{1}{M_{Pl}a(\tau)}\prod_i\left(\int\frac{d^3p_i}{(2\pi)^3}\right)(2\pi)^3\delta^{(3)}(\mathbf{p}_t)\cdot \\ \cdot\left(v_{ij}(\tau,\mathbf{p}_1)v_{kl}(\tau,\mathbf{p}_2)v_{kl}(\tau,\mathbf{p}_3)p_3^ip_3^j - 2v_{ij}(\tau,\mathbf{p}_1)v_{kl}(\tau,\mathbf{p}_2)v_{ik}(\tau,\mathbf{p}_3)p_3^jp_3^l\right) .\end{aligned} \tag{349}$$

Using equation (348), and inserting the interaction Hamiltonian (349), one gets:

$$\begin{aligned}\langle h_{ab}(t,\mathbf{k}_1)h_{cd}(t,\mathbf{k}_2)h_{ef}(t,\mathbf{k}_3)\rangle = i\frac{8}{M_{Pl}a^3(\tau)}\int_{-\infty(1\pm i\varepsilon)}^{\tau}d\tau'\frac{1}{a(\tau')}\cdot \\ \cdot\int\prod_i\left(\frac{d^3p_i}{(2\pi)^3}\right)(2\pi)^3\delta^{(3)}(\mathbf{p}_t)\langle\Big[v_{ab}(\tau,\mathbf{k}_1)v_{cd}(\tau,\mathbf{k}_2)v_{ef}(\tau,\mathbf{k}_3), \\ \left(v_{ij}(\tau',\mathbf{p}_1)v_{kl}(\tau',\mathbf{p}_2)v_{kl}(\tau',\mathbf{p}_3)p_3^ip_3^j - 2v_{ij}(\tau',\mathbf{p}_1)v_{kl}(\tau',\mathbf{p}_2)v_{ik}(\tau',\mathbf{p}_3)p_3^jp_3^l\right)\Big]\rangle .\end{aligned} \tag{350}$$

In computing the expectation values we make use of the Wick's theorem. There are two kinds of possible contractions between momenta: $\mathbf{k}_1 - \mathbf{p}_1$, $\mathbf{k}_2 - \mathbf{p}_2$, $\mathbf{k}_3 - \mathbf{p}_3$ or $\mathbf{k}_1 - \mathbf{k}_2$, $\mathbf{k}_3 - \mathbf{p}_1$, $\mathbf{p}_2 - \mathbf{p}_3$ plus all the possible permutations of momenta. The second type of contraction would give rise to a product of δ-functions of the type $\delta^{(3)}(\mathbf{k}_1 + \mathbf{k}_2)\delta^{(3)}(\mathbf{k}_3 + \mathbf{p}_1)\delta^{(3)}(\mathbf{p}_2 + \mathbf{p}_3)$. This product is in turn multiplied by the overall δ-function in (350). This would imply that $\mathbf{p}_1 = \mathbf{k}_3 = 0$, hence we would have two perturbations interacting while the third one would be uncorrelated. The cluster decomposition principle tells us that this kind of interactions do not enter into the three-point function. Analogous reasoning for all the permutations of momenta. Therefore the only contractions we have are of the type $\mathbf{k}_1 - \mathbf{p}_1$, $\mathbf{k}_2 - \mathbf{p}_2$, $\mathbf{k}_3 - \mathbf{p}_3$. In order to compute

explicitly these contractions we need the two-point functions. As an example, let us compute:

$$\begin{aligned}
&\langle v_{ab}(\tau,\mathbf{k}_1)v_{ij}(\tau',\mathbf{p}_1)\rangle = \\
&= \sum_{\alpha_1,\lambda_1} v_{k_1}(\tau)v^*_{p_1}(\tau')\langle a^{\alpha_1}_{\mathbf{k}_1} a^{\lambda_1\,\dagger}_{-\mathbf{p}_1}\rangle e^{\alpha_1}_{ab}(\hat{k}_1)e^{\lambda_1}_{ij}(\hat{p}_1) \\
&= \sum_{\alpha_1,\lambda_1} v_{k_1}(\tau)v^*_{p_1}(\tau')(2\pi)^3\delta^{\alpha_1\lambda_1}\delta^{(3)}(\mathbf{k}_1+\mathbf{p}_1)\cdot e^{\alpha_1}_{ab}(\hat{k}_1)e^{\lambda_1}_{ij}(\hat{p}_1) \\
&= \sum_{\alpha_1} v_{k_1}(\tau)v^*_{k_1}(2\pi)^3\delta^{(3)}(\mathbf{k}_1+\mathbf{p}_1)e^{\alpha_1}_{ab}(\hat{k}_1)e^{\alpha_1}_{ij}(\hat{k}_1)\,.
\end{aligned} \tag{351}$$

We can now use this expression for the two-point function to compute the Wick contractions. The result for the first term of the commutator in (350) is the following:

$$\begin{aligned}
&\langle v_{ab}(\tau,\mathbf{k}_1)v_{cd}(\tau,\mathbf{k}_1)v_{ef}(\tau,\mathbf{k}_1)\Big(v_{ij}(\tau',\mathbf{p}_1)v_{kl}(\tau',\mathbf{p}_2)v_{kl}(\tau',\mathbf{p}_3)p^i_3p^j_3- \\
&\quad 2v_{ij}(\tau',\mathbf{p}_1)v_{kl}(\tau',\mathbf{p}_2)v_{ik}(\tau',\mathbf{p}_3)p^j_3p^l_3\Big)\rangle = \\
&\quad = \sum_{\alpha_1\alpha_2\alpha_3}(2\pi)^9\delta^{(3)}(\mathbf{k}_1+\mathbf{p}_1)\delta^{(3)}(\mathbf{k}_2+\mathbf{p}_2)\delta^{(3)}(\mathbf{k}_3+\mathbf{p}_3)v_{k_1}(\tau)v_{k_2}(\tau)v_{k_3}(\tau) \\
&\qquad v^*_{k_1}(\tau')v^*_{k_2}(\tau')v^*_{k_3}(\tau')\Big[k^i_3k^j_3e^{\alpha_1}_{ab}(\hat{k}_1)e^{\alpha_1}_{ij}(\hat{k}_1)e^{\alpha_2}_{cd}(\hat{k}_2)e^{\alpha_2}_{kl}(\hat{k}_2)e^{\alpha_3}_{ef}(\hat{k}_3)e^{\alpha_3}_{kl}(\hat{k}_3)- \\
&\qquad -2k^j_3k^l_3e^{\alpha_1}_{ab}(\hat{k}_1)e^{\alpha_1}_{ij}(\hat{k}_1)e^{\alpha_2}_{cd}(\hat{k}_2)e^{\alpha_2}_{kl}(\hat{k}_2)e^{\alpha_3}_{ef}(\hat{k}_3)e^{\alpha_3}_{ik}(\hat{k}_3)\Big] + \text{perms}
\end{aligned} \tag{352}$$

Here "perms" refers to all the possible permutations of the momenta we could have. The second term of the commutator is easily obtained from the first one. Notice in fact that

$$\langle v_{ab}(\tau,\mathbf{k}_1)v_{ij}(\tau',\mathbf{p}_1)\rangle = \langle v_{ij}(\tau',\mathbf{p}_1)v_{ab}(\tau,\mathbf{k}_1)\rangle^*\,. \tag{353}$$

We can therefore write schematically

$$\langle[x,y]\rangle = 2i\,\mathrm{Im}\left\{\langle xy\rangle\right\}\,, \tag{354}$$

with x the product of the first three mode functions evaluated at τ and y the parenthesis in the second term of the commutator in (350). The three-point function then becomes

$$\begin{aligned}
&\langle h_{ab}(t,\mathbf{k_1})h_{cd}(t,\mathbf{k_2})h_{ef}(t,\mathbf{k_3})\rangle = \\
&= -\frac{16}{M^4_{Pl}a^3(\tau)}(2\pi)^3\delta^{(3)}\left(\mathbf{k}_t\right)\mathcal{I}(k_1,k_2,k_3;\tau)\mathcal{E}_{abcdef}(\hat{k}_1,\hat{k}_2,\hat{k}_3)\,,
\end{aligned} \tag{355}$$

where:

$$\begin{aligned}
\mathcal{I}(k_1,k_2,k_3;\tau) = &\int^{\tau}_{-\infty(1\pm i\varepsilon)} d\tau'\frac{1}{a(\tau')}\cdot \\
&\cdot\,\mathrm{Im}\left[v_{k_1}(\tau)v_{k_2}(\tau)v_{k_3}(\tau)v^*_{k_1}(\tau')v^*_{k_2}(\tau')v^*_{k_3}(\tau')\right]\,,
\end{aligned} \tag{356}$$

$$\mathcal{E}_{abcdef}(\hat{k}_1,\hat{k}_2,\hat{k}_3) = \sum_{\alpha_1\alpha_2\alpha_3} \Big\{ \Pi^{\alpha_1}_{ab,ij}(\hat{k}_1)\Pi^{\alpha_2}_{cd,kl}(\hat{k}_2)\cdot \\ \cdot \Big[k_3^i k_3^j \Pi^{\alpha_3}_{ef,kl}(\hat{k}_3) - 2k_3^j k_3^l \Pi^{\alpha_3}_{ef,ik}(\hat{k}_3)\Big] + 5 \text{ perms wrt } 1,2,3 \Big\}, \tag{357}$$

and we have introduced:

$$\Pi^{\alpha}_{ab,ij}(\hat{k}) = e^{\alpha}_{ab}(\hat{k}) e^{\alpha}_{ij}(-\hat{k}) \,. \tag{358}$$

The polarization term (357) can be simplified in the final expression (346) when contracting the spatial indices. Using the polarization identities, one can show that it reduces to

$$\begin{aligned} \mathcal{E} &= \delta_{bc}\,\delta_{de}\,\delta_{af}\,\mathcal{E}_{abcdef} \\ &= -\frac{1}{512\,k_1^6\,k_2^4\,k_3^4}\left(k_1^4+k_2^4+k_3^4-2\,k_1^2\,k_2^2-2\,k_1^2\,k_3^2-2\,k_2^2\,k_3^2\right)^2 \cdot \\ &\quad \cdot \Big(k_1^6+k_2^6+k_3^6+15\,k_1^4\,k_2^2+15\,k_1^2\,k_2^4+15\,k_1^4\,k_3^2+15\,k_1^2\,k_3^4+ \\ &\quad +15\,k_2^4\,k_3^2+15\,k_2^2\,k_3^4+90\,k_1^2\,k_2^2\,k_3^2\Big) \,. \end{aligned} \tag{359}$$

Let us now focus on the time integral in (356). Notice that up to now we have not specified the initial state, i.e. the mode function $v_k(\tau)$. We could use either BD mode functions, i.e. the vacuum state, or Bogoliubov mode functions, i.e. an excited state. The latter can be obtained from the former by means of a Bogoliubov transformation, as shown in (339), with the BD mode functions given in (340). We now consider the most general case of an excited state, out of which the simpler BD case can be extracted easily. Exploiting the relation $a(\tau) \simeq -1/H\tau$ during inflation, we can write for (356):

$$-\frac{1}{a^3(\tau)}\mathcal{I}(k_1,k_2,k_3;\tau) = H^4\tau^3 \int_{-\infty(1\pm i\varepsilon)}^{\tau} d\tau'\tau' \cdot \\ \cdot \,\mathrm{Im}\left[v_{k_1}(\tau)v_{k_2}(\tau)v_{k_3}(\tau)v^*_{k_1}(\tau')v^*_{k_2}(\tau')v^*_{k_3}(\tau')\right] \,. \tag{360}$$

In order to get a value for the bispectrum, we set conventionally the end of inflation at $\tau = 0$ and we perform the computations consequently. For the numerical computation one first has to perform the integral and then take the limit $\tau \to 0$. One could be tempted to take this limit before performing the integration, however this could lead to misleading results. The numerical integration of (360) is ongoing and the final results will be shown in [31] soon.

7.4.2.2 *Classical Approach*

To compute the bispectrum within the classical approach we apply the Green's method. In particular we construct the sourced solution solving the equation of motion obtained from (345):

$$h''_{ij} + 2\mathcal{H}h'_{ij} - \nabla^2 h_{ij} = 2h^{lk}h_{ik,jl} - h^{lk}h_{ij,lk} - \frac{1}{2}h^{lk}h_{lk,ij} + h_{ik,l}h_j{}^{lk} \,. \tag{361}$$

We rewrite equation (361) in a more compact form as:

$$h''_{ij} + 2\mathcal{H}h'_{ij} - \nabla^2 h_{ij} = S_{ij}\,, \tag{362}$$

where S_{ij} is the source term generated from the GR action expanded up to third order, given by the rhs of (361). Moving to Fourier space, the equation of motion becomes:

$$h''_{ij}(\tau,\mathbf{k}) + 2\mathcal{H}h'_{ij}(\tau,\mathbf{k}) + k^2 h_{ij}(\tau,\mathbf{k}) = S_{ij}(\tau,\mathbf{k})\,, \tag{363}$$

where

$$\begin{aligned} S_{ij}(\tau,\mathbf{k}) = \sum_{\delta\sigma}\int \frac{d^3q}{(2\pi)^3} h^{\delta}(\tau,\mathbf{q})h^{\sigma}(\tau,\mathbf{k}-\mathbf{q})\Big[-2(k-q)^j(k-q)^l e^{\lambda}_{lk}(\hat{q})\cdot \\ \cdot e^{\sigma}_{ik}(\hat{k}-\hat{q}) + (k-q)^l(k-q)^k e^{\lambda}_{lk}(\hat{q})e^{\sigma}_{ij}(\hat{k}-\hat{q}) + \frac{1}{2}(k-q)^i\cdot \\ \cdot(k-q)^j e^{\lambda}_{lk}(\hat{q})e^{\sigma}_{lk}(\hat{k}-\hat{q}) - q^l(k-q)^k e^{\lambda}_{ik}(\hat{q})e^{\sigma}_{jl}(\hat{k}-\hat{q})\Big]\,, \end{aligned} \tag{364}$$

where we have used the decomposition in terms of the polarization vectors introduced in (336).

We can find a solution to this sourced equation using the Green's method. We split the metric perturbation as $h_{ij} = h^{(1)}_{ij} + h^{(2)}_{ij}$. $h^{(1)}_{ij}$ solves the free equation of motion, while $h^{(2)}_{ij}$ solves the sourced one. The solution for $h^{(2)}_{ij}$ can be written as:

$$h^{(2)}_{ij} = \sum_{\lambda}\left(h_k a^{\lambda}_{\mathbf{k}} + h^*_k a^{\lambda\,\dagger}_{-\mathbf{k}}\right) e^{\lambda}_{ij}(\hat{k}) + f_{ij}(\tau,\mathbf{k})\,, \tag{365}$$

where the first term is the homogeneous solution, obtained solving the free equation of motion, while the second term is the particular solution. We can further decompose the particular solution as:

$$f_{ij}(\tau,\mathbf{k}) = \sum_{\lambda} f^{\lambda}(\tau,\mathbf{k}) e^{\lambda}_{ij}(\hat{k})\,. \tag{366}$$

It is indeed easier to find a solution for the Fourier components of the metric perturbation, removing the polarization vectors. Indeed using again the decomposition (336), the left hand side of (363) can be expanded as:

$$\sum_{\lambda} e^{\lambda}_{ij}(\hat{k})\left(h^{\lambda\,\prime\prime}(\tau,\mathbf{k}) + 2\mathcal{H}h^{\lambda\,\prime}(\tau,\mathbf{k}) + k^2 h^{\lambda}(\tau,\mathbf{k})\right)\,. \tag{367}$$

The equation of motion can then be rewritten in terms of the Fourier components only, as:

$$h^{\lambda\,\prime\prime}(\tau,\mathbf{k}) + 2\mathcal{H}h^{\lambda\,\prime}(\tau,\mathbf{k}) + k^2 h^{\lambda}(\tau,\mathbf{k}) = S^{\lambda}(\tau,\mathbf{k})\,, \tag{368}$$

where $S^{\lambda}(\tau,\mathbf{k})$ is given by $S_{ij}(\tau,\mathbf{k})e^{\lambda\,*}_{ij}$. The homogeneous solution of this equation is given by:

$$h^{\lambda\,(1)}(\tau,\mathbf{k}) = h_k a_{\mathbf{k}} + h^*_k a^{\lambda\,\dagger}_{-\mathbf{k}}\,, \tag{369}$$

while the particular solution is obtained as in (323):

$$f^{\lambda}(\tau,\mathbf{k}) = \int_{-\infty}^{\tau} d\tau' \, \frac{h_k(\tau)h_k^*(\tau') - h_k^*(\tau)h_k(\tau')}{h_k(\tau')h_k^{*\prime}(\tau') - h_k'(\tau')h_k^*(\tau')} \, S^{\lambda}(\tau,\mathbf{k}) \,. \tag{370}$$

The denominator in (370), i.e. the Wronskian, can be computed separately. In particular it reads:

$$\begin{aligned} W(\tau',k) &= h_k^{\lambda}(\tau')h_k^{*\prime}(\tau') - h_k'(\tau')h_k^*(\tau') \\ &= \frac{4i}{M_{pl}^2 a^2(\tau')}(|\alpha_k|^2 - |\beta_k|^2) = \frac{4i}{M_{pl}^2 a^2(\tau')} \end{aligned} \tag{371}$$

Writing h_k in terms of v_k, as in (337), we get a lengthy expression for $f^{\lambda}(\tau,\mathbf{k})$ which is proportional to the combinations of products of two ladder operators. From this expression we can built the metric up to second order as in (365), with $f_{ij}(\tau,\mathbf{k})$ given by (366). At this point we can compute the three-point function at the lowest order $\langle h_{ab}^{(1)}(\tau,\mathbf{k}_1)h_{cd}^{(1)}(\tau,\mathbf{k}_2)h_{ef}^{(2)}(\tau,\mathbf{k}_3)\rangle$. The expectation value of three stochastic parameters vanishes, hence the homogeneous solution in (365) is not entering in the computation of the bispectrum. Therefore we are left with the computation of $\langle h_{ab}^{(1)}(\tau,\mathbf{k}_1)h_{cd}^{(1)}(\tau,\mathbf{k}_2)f_{ef}(\tau,\mathbf{k}_3)\rangle$. Moreover only the terms with an equal number of stochastic parameters a and $a^{\dagger}$ give a non-vanishing contribution. Keeping this in mind, one can proceed with the computation of the three-point function which, after a cumbersome derivation, reduces to

$$\langle h_{ab}^{(1)}(\tau,\mathbf{k}_1)h_{cd}^{(1)}(\tau,\mathbf{k}_2)h_{ef}^{(2)}(\tau,\mathbf{k}_3)\rangle = \frac{8}{M_{Pl}^4 a^3(\tau)}\delta^{(3)}(\mathbf{k}_t)\mathcal{I}^{cl}(k_1,k_2,k_3;\tau)\mathcal{E}^{cl}_{abcdef} \,, \tag{372}$$

where:

$$\begin{aligned} \mathcal{I}^{cl}(k_1,k_2,k_3;\tau) = \int_{-\infty(1\pm i\varepsilon)}^{\tau} d\tau' \frac{1}{a(\tau')} \cdot \\ \cdot \Big\{ \mathrm{Im}\left[v_{k_1}(\tau)v_{k_2}(\tau)v_{k_3}(\tau)v_{k_1}^*(\tau')v_{k_2}^*(\tau')v_{k_3}^*(\tau')\right] + \\ + \mathrm{Im}\left[v_{k_1}(\tau)v_{k_2}^*(\tau)v_{k_3}(\tau)v_{k_1}^*(\tau')v_{k_2}(\tau')v_{k_3}^*(\tau')\right] + \\ + \mathrm{Im}\left[v_{k_1}^*(\tau)v_{k_2}^*(\tau)v_{k_3}(\tau)v_{k_1}(\tau')v_{k_2}(\tau')v_{k_3}^*(\tau')\right] + \\ + \mathrm{Im}\left[v_{k_1}^*(\tau)v_{k_2}(\tau)v_{k_3}(\tau)v_{k_1}(\tau')v_{k_2}^*(\tau')v_{k_3}^*(\tau')\right] \Big\} \,, \end{aligned} \tag{373}$$

$$\begin{aligned} \mathcal{E}^{cl}_{abcdef}(\hat{k}_1,\hat{k}_2,\hat{k}_3) = \sum_{\alpha,\beta\,\lambda} e_{ab}^{\alpha}(\hat{k}_1)e_{cd}^{\beta}(\hat{k}_2)e_{ef}^{\lambda}(\hat{k}_3)e_{ij}^{\lambda\,*}(\hat{k}_3) \Big\{ \Big[-2k_2^j k_2^l e_{lk}^{\alpha}(-\hat{k}_1)e_{ik}^{\beta}(-\hat{k}_2) + \\ + k_2^l k_2^k e_{lk}^{\alpha}(-\hat{k}_1)e_{ij}^{\beta}(-\hat{k}_2) + \frac{1}{2}k_2^i k_2^j e_{lk}^{\alpha}(-\hat{k}_1)e_{lk}^{\beta}(-\hat{k}_2) - k_1^l k_2^k e_{ik}^{\alpha}(-\hat{k}_1)e_{jl}^{\beta}(-\hat{k}_2) - \\ - 2k_1^j k_1^l e_{ik}^{\alpha}(-\hat{k}_1)e_{lk}^{\beta}(-\hat{k}_2) + k_1^l k_1^k e_{ij}^{\alpha}(-\hat{k}_1)e_{lk}^{\beta}(-\hat{k}_2) + \frac{1}{2}k_1^i k_1^j e_{lk}^{\alpha}(-\hat{k}_1)e_{lk}^{\beta}(-\hat{k}_2) - \\ - k_2^l k_1^k e_{jl}^{\alpha}(-\hat{k}_1)e_{ik}^{\beta}(-\hat{k}_2) \Big] \Big\} \,. \end{aligned} \tag{374}$$

The polarization term (374) can be again simplified after contracting the spatial indices as in (346). Concerning the integration in (373), we are solving it numerically and the final results will be shown together with the quantum results in [31] soon. We just mention here that we expect a different combination of k's in the denominator, since the combinations of mode functions appearing in the integrals are different. A complex conjugation changes indeed the sign of the corresponding wave vector appearing in the denominator after the integration. Hence, already at this level, we are able to predict roughly the different poles of the final bispectra looking at the integrands. The results will be of course non-trivial, since we are considering the most general case of a non-BD initial state; however the several products of mode functions can be rewritten in terms of products of BD mode functions multiplied by products of Bogoliubov coefficients α_k and β_k.

The quantum computation with a non-BD initial state produces a bispectrum in the folded configuration, i.e. it has poles in correspondence of physical momenta, as in the classical computation with a BD initial state. This is due to the fact that non-vanishing Bogoliubov coefficients give rise to other combinations of BD mode functions with respect to the one in (356), sourcing alternative combinations of momenta in the denominator after the integration is performed. However, in principle, the two approaches could lead to different behaviours of the bispectra far from the poles. A careful comparison between the two cases just mentioned is under study.

8

SQUEEZING OF AXIONS PERTURBATIONS

In the previous chapters, we have shown how it is in principle possible to detect a quantum signature of the cosmological perturbations by focusing on a Leggett-Garg type experiment in the CMB or by detecting non-Gaussianities. In this chapter we present our work on the squeezing of axions perturbations [39]. It is relevant in understanding the classical or quantum nature of the cosmological fluctuations for several reasons.

In general, to address the problem of the nature of the perturbations one has to take into account decoherence effects during reheating. In fact, in order for a squeezed fluctuation to maintain its quantum nature into the later Universe, it is necessary that it does not undergo decoherence through the interactions with the cosmological plasma. The phenomenon of decoherence has been widely discussed in the literature; see for example [18, 37, 157–159]. From this perspective, axion-like particles (ALPs) [160, 161] coupled to other matter fields only through gravitational interactions provide an ideal setup that can evade decoherence. In particular, axions can be produced non-thermally via the so-called *misalignment mechanism*. In this model ALPs are not required to directly interact with the thermal bath.

Another interesting feature of ALPs is that their fluctuations around the classical axion background source axion isocurvature perturbations, that can be directly linked with observables. Their correlators constitute in principle a promising way to investigate the quantum origin of the cosmological perturbations. Indeed axions may evade decoherence and their bispectrum could provide a way to discern among the quantum or classical nature of the perturbations (see [30, 162, 163]). One further advantage in working with axions is that several constraints are already present in the literature, giving rise to strong bounds on the cosmological observables. Also for the purpose of studying interacting fields, axions are useful since they necessarily have self-interactions due to their periodic potential. The effects induced by higher-order terms in the potential is often referred to as "anharmonic effects," and axions provide a computable setup for incorporating the effect of self-interactions. Indeed in the late Universe the axion field settles down to the minimum of its potential and thus the self-interaction switches off. Axions thus reduce to effectively free fields in the asymptotic future, which allows one to apply Bogoliubov computations for studying the evolution of the fluctuations.

In this chapter we study the effect of self-interactions on the squeezing of axion fluctuations, focusing on how the background evolution modifies the evolution of the perturbations themselves. We focus on ALPs (instead of QCD axions [164–166]), and consider a scenario where the Peccei-Quinn symmetry is broken during inflation. In this way the axion field gets homogenized, giving rise to a background axion condensate. We study the perturbations around this background. In previous works on axion squeezing [167, 168], only the

quadratic term has been considered. Here we go beyond these analyses, considering the effect of self-interactions. In particular we study the interaction between the perturbations and the zero-mode, i.e. the background axion field, neglecting the interactions among perturbations themselves. We will show that the interaction with a non-trivial background gives already interesting effects. In particular, it strongly enhances the squeezing of the perturbations, which is directly linked with the number of particles created due to the expansion of the background.

8.1 QUANTIZATION OF AXIONS FLUCTUATIONS

8.1.1 *Setup*

We fix the metric to a flat FRW, $ds^2 = a^2(\tau)\left(-d\tau^2 + d\boldsymbol{x}^2\right)$. Here τ is the conformal time, linked with the cosmic time via $dt = a(\tau)\, d\tau$. We consider the evolution of the Universe as simply given by a dS phase of inflation, followed by a period of radiation domination. We further assume, for simplicity, that the reheating phase is instantaneous [1]. In the simple scenario here introduced, the Hubble rate is given by:

$$H = \begin{cases} H_{\rm inf} & \text{de Sitter} \\ H_{\rm inf}\ (a/a_{\rm reh})^{-2} & \text{Radiation Domination} \end{cases} \tag{375}$$

Here $H_{\rm inf}$ is the constant Hubble scale during the de Sitter phase and $a_{\rm reh}$ is the value of the scale factor at the reheating. We consider the axion to have negligible effect on the cosmological evolution. It is assumed that the Peccei-Quinn symmetry is broken before inflation, and specifically that $f > \max(T_{\rm reh}, H_{\rm inf})$, where f is the symmetry breaking scale and $T_{\rm reh}$ is the reheating temperature. This ensures that the symmetry is not restored during the reheating phase. For our assumption of instantaneous reheating, $T_{\rm reh} \sim \sqrt{M_{Pl} H_{\rm inf}} > H_{\rm inf}$, hence it is enough to require $f > T_{\rm reh}$.

Let us now consider the axion potential, which can be written as

$$V(\phi) = f^2 m^2 \left[1 - \cos\left(\frac{\phi}{f}\right)\right], \tag{376}$$

where ϕ is the axion field. We assume that the axion mass is constant in time, and also that $m < H_{\rm inf}$; this ensures the axion mass becomes comparable with the Hubble rate during radiation domination, after reheating has occurred. After the time when $m \sim H_{\rm inf}$, the field starts oscillating around its minimum and the equation of motion becomes that of a damped oscillator.

We consider the axion field to be a homogeneous background plus vacuum fluctuations. The initial value of the axion field affects the subsequent evolution of the background. Specifically, if the starting point is near the hilltop of the potential then the field scans the full cosine potential as it rolls down.

1 The cases of non-instantaneous reheating and quasi-de Sitter inflation are considered in Appendix 8.6.

When deviations from the quadratic potential are considered, the perturbations are affected by the background evolution. These perturbation modes exit the horizon during inflation. After inflation has ended they re-enter the horizon. Small-scale modes re-enter the horizon before the axion field begins to oscillate; hence they propagate unaffected by the oscillations. On the contrary, large-scale modes feel the oscillations and their evolution in time is consequently affected. Since we focus on the effect of the oscillations on the evolution of the perturbations, we will focus on large-scale modes that re-enter the horizon after the onset of the oscillations.

8.1.2 *Canonical Quantization*

In order to compute the squeezing parameters describing the system, we first need to calculate the Bogoliubov coefficients for the axion field. We work with the full potential for the background field evolution, while considering only the first order expansion of the potential for the perturbations. The equation of motion for the axion field is then:

$$\ddot{\phi} + 3H\dot{\phi} - \frac{1}{a^2}\partial_i^2\phi + \frac{dV(\phi)}{d\phi} = 0\,. \tag{377}$$

Here the dot indicates a derivative with respect to the physical time t, and Latin letters are used to denote spatial indices. We split the axion field as

$$\phi(t,\boldsymbol{x}) = \bar{\phi}(t) + \delta\phi(t,\boldsymbol{x})\,, \tag{378}$$

where $\bar{\phi}$ is the homogeneous classical background field, and $\delta\phi$ is the small perturbation around it. We are going to expand the axion up to quadratic order in $\delta\phi$. The first derivative of the potential, up to linear order, can be written as

$$V'(\phi) = fm^2\left[\sin\left(\frac{\bar{\phi}}{f}\right) + \cos\left(\frac{\bar{\phi}}{f}\right)\left(\frac{\delta\phi}{f}\right)\right]. \tag{379}$$

The equation of motion for the homogeneous background field becomes

$$\ddot{\bar{\phi}} + 3H\dot{\bar{\phi}} + fm^2\sin\left(\frac{\bar{\phi}}{f}\right) = 0\,, \tag{380}$$

while at first order in the perturbations one has in Fourier space [2]

$$\delta\ddot{\phi}_{\boldsymbol{k}} + 3H\delta\dot{\phi}_{\boldsymbol{k}} + \left[\frac{k^2}{a^2} + m^2\cos\left(\frac{\bar{\phi}}{f}\right)\right]\delta\phi_{\boldsymbol{k}} = 0\,. \tag{381}$$

where $k = |\boldsymbol{k}|$. The corresponding quadratic action for the perturbations is

$$S = \int d^3x d\tau\, a^2\left[\frac{1}{2}\delta\phi'^2 - \frac{1}{2}(\partial_i\delta\phi)^2 - \frac{1}{2}m^2a^2\cos\left(\frac{\bar{\phi}}{f}\right)\delta\phi^2\right]. \tag{382}$$

2 The convention we use for the Fourier transform is

$$\delta\phi_{\boldsymbol{k}} = \int \frac{d^3x}{(2\pi)^{3/2}} e^{-i\,\boldsymbol{k}\cdot\boldsymbol{x}}\,\delta\phi\,.$$

Here the prime denotes a τ-derivative. One can now introduce a new variable $\chi = a\delta\phi$. Then the action can be rewritten as

$$S = \int d^3x d\tau \frac{1}{2}\left[\chi'^2 + \left(\frac{a'}{a}\right)^2 \chi^2 - 2\frac{a'}{a}\chi\chi' - (\partial_i\chi)^2 - m^2a^2\cos\left(\frac{\bar{\phi}}{f}\right)\chi^2\right]. \tag{383}$$

The mixed term $\chi\chi'$ can be removed by integrating by parts and dropping surface terms as

$$S = \int d^3x d\tau \frac{1}{2}\left[\chi'^2 - (\partial_i\chi)^2 - \left(m^2a^2\cos\left(\frac{\bar{\phi}}{f}\right) - \frac{a''}{a}\right)\chi^2\right]. \tag{384}$$

From this action we can construct the Hamiltonian as $\mathcal{H} = \int d^3x\,(p\chi' - \mathcal{L})$, where $p = \chi'$ and $\mathcal{L}$ is the Lagrangian. Writing in terms of the Fourier components, the Hamiltonian acquires the following form:

$$\mathcal{H} = \frac{1}{2}\int d^3k \left[p_k p_k^* + \left(k^2 + m_{\rm eff}^2\,a^2 - \frac{a''}{a}\right)\chi_k\chi_k^*\right], \tag{385}$$

where the effective mass $m_{\rm eff}^2$ is given by

$$m_{\rm eff}^2 = m^2\cos\left(\frac{\bar{\phi}}{f}\right). \tag{386}$$

Notice that the effective mass depends on time through the evolution of the background $\bar{\phi}$. Moreover it can become tachyonic, i.e. $m_{\rm eff}^2 < 0$, due to the cosine factor. We also introduce the time dependent frequency ω_k, defined as

$$\omega_k^2 = k^2 + m_{\rm eff}^2a^2 - \frac{a''}{a}. \tag{387}$$

We now proceed to the quantization of the fields in analogy to what was done in Section 4.1 for the inflaton perturbations. The main differences arise due to the different expression for the frequency ω_k. We introduce the time-dependent ladder operators:

$$\begin{aligned}\chi_k(\tau) &= \frac{1}{\sqrt{2|\omega_k(\tau)|}}\left(a_k(\tau) + a_{-k}^\dagger(\tau)\right),\\ p_k(\tau) &= -i\sqrt{\frac{|\omega_k(\tau)|}{2}}\left(a_k(\tau) - a_{-k}^\dagger(\tau)\right),\end{aligned} \tag{388}$$

respecting the canonical commutation relations [3]

$$\left[\chi(\tau,\boldsymbol{x}), p(\tau,\boldsymbol{x}')\right] = i\delta^{(3)}(\boldsymbol{x}-\boldsymbol{x}'), \qquad \left[a_k(\tau), a_{k'}^\dagger(\tau)\right] = \delta^{(3)}(\boldsymbol{k}-\boldsymbol{k}'). \tag{389}$$

All the other commutators vanish.

3 In Fourier space the commutation relation between the field $\chi_k(\tau)$ and its conjugate momentum $p_{k'}(\tau)$ is given by: $\left[\chi_k(\tau), p_{k'}^\dagger(\tau)\right] = i\delta^{(3)}(\boldsymbol{k}-\boldsymbol{k}')$.

8.1.3 *Bogoliubov Coefficients*

Introducing an 'initial' time τ_0 during inflation, when the wave modes of interest are still deep inside the Hubble horizon, we can link the time-dependent ladder operators at later times to those at τ_0 through the Bogoliubov transformation

$$\begin{aligned} a_{\boldsymbol{k}}(\tau) &= \alpha_k(\tau)\, a^0_{\boldsymbol{k}} + \beta_k(\tau) a^{0\dagger}_{-\boldsymbol{k}}\,, \\ a^{\dagger}_{-\boldsymbol{k}}(\tau) &= \alpha^*_k(\tau)\, a^{0\dagger}_{-\boldsymbol{k}} + \beta^*_k(\tau) a^0_{\boldsymbol{k}}\,, \end{aligned} \tag{390}$$

with $a^0_{\boldsymbol{k}} = a_{\boldsymbol{k}}(\tau_0)$. Defining the fields in terms of the mode functions directly, one can get an expression for the Bogoliubov coefficients in terms of the mode functions themselves:

$$\begin{aligned} \alpha_k &= \sqrt{\frac{|\omega_k|}{2}}\, u_k + \frac{i}{\sqrt{2\,|\omega_k|}}\, u_k'\,, \\ \beta_k &= \sqrt{\frac{|\omega_k|}{2}}\, u_k^* + \frac{i}{\sqrt{2\,|\omega_k|}}\, u_k^{*\prime}\,. \end{aligned} \tag{391}$$

The number of particles created due to the expansion of spacetime (see Section 4.2) is then given by:

$$\mathcal{N}_k = \langle a^{\dagger}_{\boldsymbol{k}} a_{\boldsymbol{k}} \rangle = \frac{V}{(2\pi)^3}\, |\beta_k|^2 = \frac{V}{(2\pi)^3} \left[\frac{|\omega_k|}{2}\, |u_k|^2 + \frac{1}{2\,|\omega_k|}\, |u_k'|^2 - \frac{1}{2} \right] . \tag{392}$$

There is however a relevant difference with the cosmological perturbations. $|\beta_k|^2$ acquires the physical meaning of number of particles when we can define an adiabatic vacuum for our system. In the case of inflaton perturbations that happens at the end of inflation; however in the case of a massive spectator field, whether the adiabaticity conditions are satisfied or not depends also on the mass of the scalar field considered, i.e. the axion in this case. More details on the adiabaticity conditions for the system considered in this chapter will be given in Section 8.3.2.1.

8.1.4 *Squeezing Parameters*

Starting from the Bogoliubov coefficients, the squeezing parameters can be introduced as

$$\begin{aligned} \alpha_k(\tau) &= e^{-i\vartheta_k(\tau)}\, \cosh r_k(\tau)\,, \\ \beta_k(\tau) &= e^{i[\vartheta_k(\tau) + 2\varphi_k(\tau)]}\, \sinh r_k(\tau)\,, \end{aligned} \tag{393}$$

The inverse relations give the evolution in time of the squeezing parameters in terms of that of the Bogoliubov coefficients as:

$$\begin{aligned} r_k &= \operatorname{arcsinh} |\beta_k|\,, \\ \vartheta_k &= -\arg\left(\alpha_k\right)\,, \\ \varphi_k &= \frac{1}{2} \arg\left(\alpha_k \beta_k\right)\,. \end{aligned} \tag{394}$$

8.2 BACKGROUND EVOLUTION

To study the evolution in time of the Bogoliubov coefficients and then in turn of the squeezing parameters, we first analyse the background field dynamics by numerically solving the homogeneous equation of motion (380). It is convenient to introduce the background displacement angle

$$\theta = \bar{\phi}/f, \tag{395}$$

and solve the equation in terms of this variable. In this way we do not need to specify the value of the symmetry breaking scale f. The equation of motion for the background angle in conformal time is given by:

$$\theta'' + 2aH\theta' + a^2 m^2 \sin\theta = 0\,. \tag{396}$$

We expect the axion background to start oscillating after the Hubble rate becomes comparable with the axion mass. Solving the equations of motion numerically for different initial field values during inflation, we obtain the results reported in Figure 14 (above). Here we considered the Hubble rate in equation (375) with $H_{\rm inf} = 10^8\,\text{GeV}$, and took the mass as $m = 10^2\,\text{GeV}$. Then the third term in (396) becomes relevant at around $\ln(a/a_{\rm reh}) = \ln(H_{\rm inf}/m)^{1/2} \approx 7$, as shown in Figure 14 (above). The different colours represent different initial angles as shown in the legend, while the vertical dashed line identifies when the mass of the axion field becomes comparable with the Hubble rate. If we choose as the initial field value $\theta_0 = 0.1\,\pi$, it is close enough to the minimum such that the axion potential is well approximated by a quadratic. Indeed, if we compute the background trajectory with a quadratic potential we find the same result. Looking at Figure 14 (above) we see that starting close to the minimum, the amplitude of the oscillations is reduced. A huge difference in both the amplitude of the oscillations and the time of the onset of the oscillations can be seen if we set the initial field value to be very close to the hilltop.

This behaviour can be further understood by looking at the energy density of the background field. The energy density can be obtained as

$$\bar{\rho} = \frac{\dot{\bar{\phi}}^2}{2} + V(\bar{\phi}) = \frac{f^2}{2a^2}\,\theta'^2 + V(\theta f). \tag{397}$$

Given the solution for the background field evolution, the energy density can be directly computed. The time evolution of the energy density normalized by f^2 is reported in Figure 14 (below), which zooms into the RD epoch around the time when the oscillations begin. The energy density is constant until the background field starts oscillating; thereafter it decays as a^{-3}. The vertical dashed lines in Figure 14 (below) show when the oscillations begin; this is obtained as the time when the energy densities extrapolated from the asymptotic behaviours in the past ($\bar{\rho} = \text{const.}$) and in the future ($\bar{\rho} \propto a^{-3}$) cross each other. The value of the energy density in the asymptotic future in terms of the initial displacement angle is reported in Figure 15. It has be computed at the final time $\ln(a/a_{\rm reh}) = 10$. The final numerical value of $\bar{\rho}/f^2$ itself is not relevant for our discussion. What is relevant is that the energy density becomes strongly enhanced towards the hilltop. This behaviour can be understood by noticing that the field starts oscillating later as one approaches the hilltop.

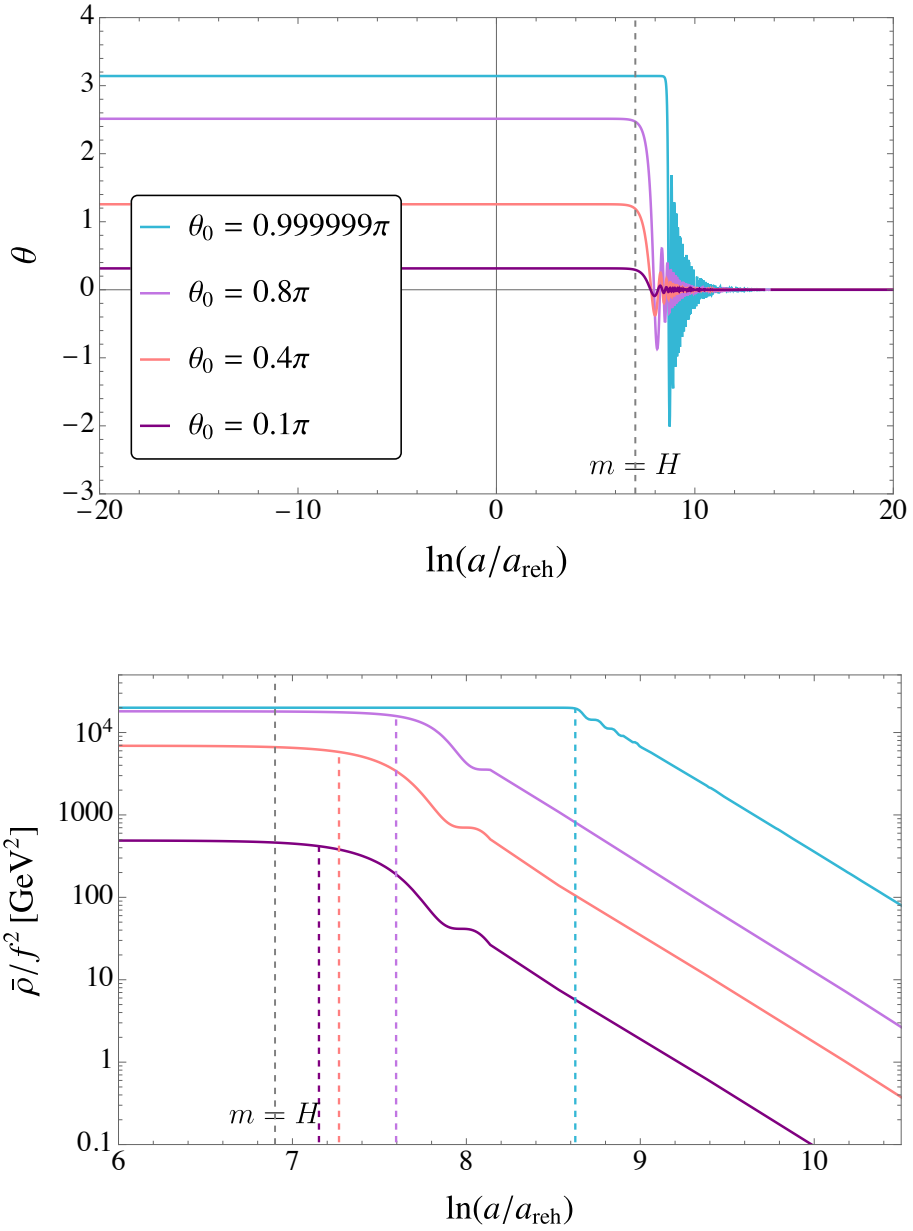


Figure 14: Time evolution of the background field (above) and of the background energy density (below) for different initial field values. The values of the initial angle are specified in the legend in the upper plot. The parameters chosen are $H_{\rm inf} = 10^8\,$GeV and $m = 10^2\,$GeV. The grey dashed vertical line shows the time when the axion mass becomes equal to the Hubble rate. Dashed vertical lines in other colours denote the onset of the axion oscillation for the different initial displacement angles.

8.3 EVOLUTION OF AXIONS FLUCTUATIONS

8.3.1 *Mode Functions*

In order to evaluate the evolution in time for the Bogoliubov coefficients and the squeezing parameters, we need firstly to solve the equation of motion for the mode functions, given by:

$$u_k'' + \left(k^2 + m_{\rm eff}^2 a^2 - \frac{a''}{a}\right) u_k = 0\,. \tag{398}$$

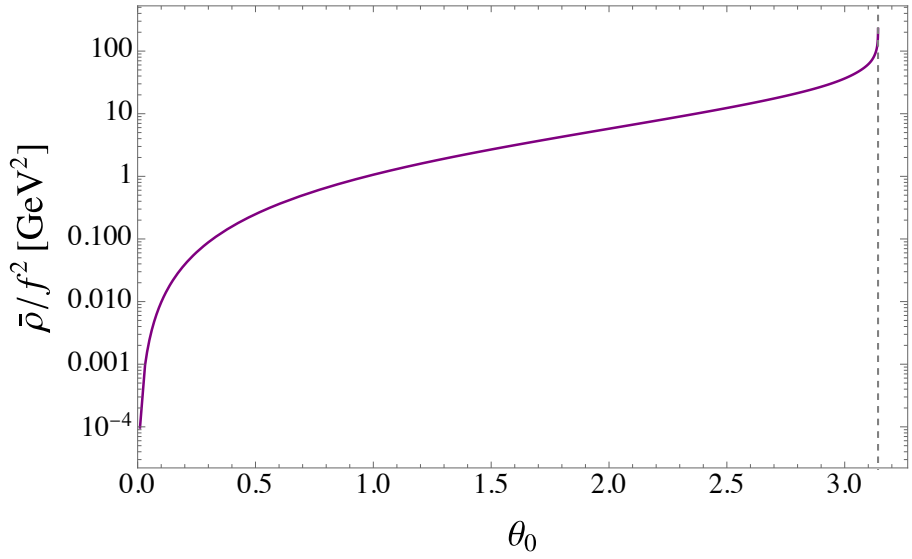


Figure 15: Asymptotic value of the energy density of the background field $\bar{\rho}$ as function of the initial displacement angle θ_0. The parameters used are $H_{\rm inf} = 10^8\,\text{GeV}$ and $m = 10^2\,\text{GeV}$.

If the potential has only the mass term, an analytical solution can be obtained, while if we work with the full cosine potential we have to rely on numerical computations. The analytical derivation for a mass term potential is reported in Appendix 8.5.1.

The time evolution of the amplitude of the mode functions is reported in Figure 16. It has been numerically computed for two different values of the initial background field during inflation: $\theta_0 = 0.1\,\pi$ and $\theta_0 = 0.999999\,\pi$. The initial condition for the mode function is set such that it starts as a positive-frequency Wentzel–Kramers–Brillouin (WKB) solution obeying the normalization condition (103), when the wave mode is deep inside the horizon during inflation. The parameters chosen for the evaluation are $H_{\rm inf} = 10^8\,\text{GeV}$, $m = 10^2\,\text{GeV}$ and $k/a_{\rm reh} = 10^2\,\text{GeV}$. These values have been chosen in order to consider a mode that leaves the horizon during inflation, and stays outside the horizon when the background field starts oscillating around the minimum, during radiation domination. The dashed vertical lines in Figure 16 indicate the time of the horizon exit, reheating and the onset of the oscillations of the background field.

Looking at Figure 16, we see that the mode function's amplitude stays constant until horizon exit, then grows outside the horizon until the background field starts to oscillate. This behaviour is more or less independent of the initial misalignment angle (and thus the lines overlap). Instead, at the onset of the oscillations the amplitude of the mode functions differ based on the value of the initial displacement angle. If the initial field is close to the minimum, then the approximation to the quadratic potential is enough to describe the system. The time evolution obtained from the analytical solution for a quadratic potential matches the time evolution for an initial field value $\theta_0 = 0.1\pi$. However, if the initial field is close to the hilltop an extra enhancement in the amplitude of the mode functions is observed due to the anharmonic effects.

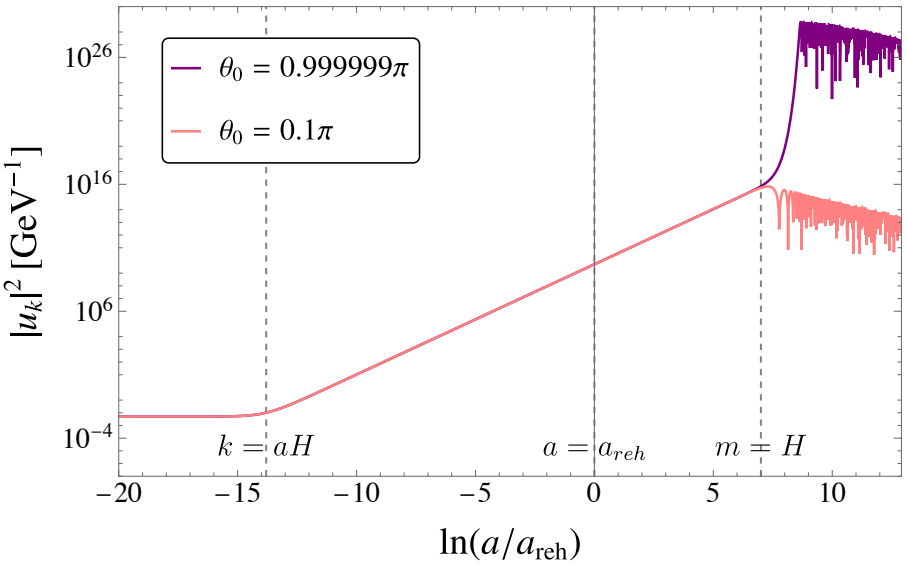


Figure 16: Evolution in time of the amplitude of the mode functions for a wave mode $k/a_{\rm reh} = 10^2\,\text{GeV}$, and for two different initial values of the background field. An increase in $|u_k|^2$ is observed approaching the hilltop of the potential. Dashed vertical lines denote when the mode exits the horizon, reheating and the onset of the oscillations, respectively. The values chosen for the Hubble rate and the axion mass are $H_{\rm inf} = 10^8\,\text{GeV}$ and $m = 10^2\,\text{GeV}$.

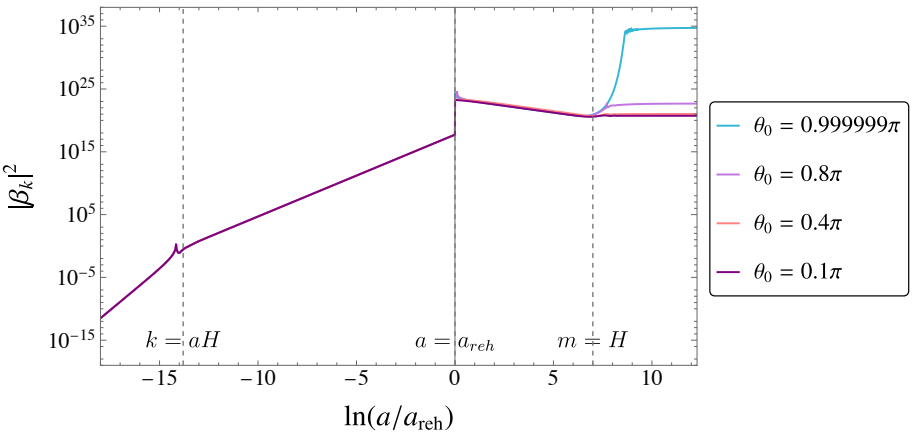


Figure 17: Evolution in time of the modulus square of the β_k-coefficient for few different initial values of the background field. The parameters chosen are the same as Figure 16. When θ_0 approaches the hilltop of the potential the final value of $|\beta_k|^2$ significantly increases. Dashed vertical lines denote when the mode exits the horizon, reheating and the onset of the oscillations, respectively.

8.3.2 *Bogoliubov Coefficients*

Exploiting relations (391) and (394), it is possible to evaluate the evolution in time of the Bogoliubov coefficients and in turn of the squeezing paramet-

ers. We start our analysis from the Bogoliubov coefficients, and specifically from $|\beta_k|^2$, which is directly linked with physical quantities, as explained in Section 4.1. The numerical results are reported in Figure 17, for the same values of parameters used in Figure 16 for the amplitude of the mode functions. The modulus square of the beta coefficient approaches zero in the asymptotic past, when the mode is far inside the horizon. Moreover it approaches a constant value in the asymptotic future, and specifically it becomes constant when the axion field starts oscillating. We further notice that the behaviour of $|\beta_k|^2$ changes depending on the initial field value. The evolution in time is more or less independent of the initial condition while the axion field is frozen by the Hubble friction; however, when the potential term becomes comparable with the Hubble rate, the field dynamics right before the onset of the oscillations affects the asymptotic value of the Bogoliubov coefficients. We see in Figure 17 that, approaching the hilltop of the potential, the asymptotic value of $|\beta_k|^2$ increases. On the other hand with $\theta_0 = 0.1\,\pi$, the evolution of $|\beta_k|^2$ follows that for a quadratic potential, which is also analytically studied in Appendix 8.5.1.

The spikes in the evolution of $|\beta_k|^2$ seen in the plots, as well as the discontinuous jump at reheating, can be understood in terms of the frequency (387). In the asymptotic past, ω_k^2 is dominated by k^2. When the perturbation leaves the horizon during inflation, at $k = aH_{\rm inf}$, the frequency squared reduces to $\omega_k^2 \simeq -k^2$. This implies that right before the horizon exit the frequency squared has turned from positive to negative. This gives a divergence in $|\beta_k|^2$, since it is defined as in (139) with ω_k in the denominator. The spike after reheating has a similar explanation. During RD, $\omega_k^2 = k^2 + m_{\rm eff}^2 a^2$; the k^2 term is always positive, while $m_{\rm eff}^2$ could be either positive or negative, depending on the value of the cosine. If the initial field is close to the hilltop, then $m_{\rm eff}^2$ is originally negative. With the parameter choice in the plot ($m = k/a_{\rm reh} = 10^2\,\text{GeV}$), the tachyonic mass term dominates the frequency right after reheating. This implies that the frequency squared flips its sign immediately after reheating, causing the spike in $|\beta_k|^2$. There is another spike at the onset of the oscillations, depending on the initial displacement angle. In fact, when the background field starts oscillating, $m_{\rm eff}^2$ goes from negative to positive. Since $\omega_k^2 \simeq m_{\rm eff}^2 a^2$ at that time, it crosses zero, making $|\beta_k|^2$ diverge. The jump at reheating is instead caused by the discontinuity of the frequency ω_k, which arises due to a''/a suddenly vanishing upon instantaneous reheating.

However we remark that the spikes and jumps of $|\beta_k|^2$ appear only while adiabaticity is violated and hence $|\beta_k|^2$ cannot be interpreted as the particle number, as we will explain in the next subsection. The irregular behaviours are artifacts due to our definition of $|\beta_k|^2$, as well as the choice of the cosmological background, and hence should not have physical consequences. We actually show in Appendix 8.6 that a non-instantaneous reheating removes the jump of $|\beta_k|^2$, but does not alter the final value of $|\beta_k|^2$.

8.3.2.1 *Adiabaticity Condition*

We have seen that $|\beta_k|^2$ approaches a constant when the background field starts oscillating. In order to understand why this is the case, let us analyse the adiabaticity conditions

$$\left|\frac{\omega_k'}{\omega_k^2}\right|^2, \left|\frac{\omega_k''}{\omega_k^3}\right| \ll 1\,. \tag{399}$$

Here ω_k is the effective frequency associated with the mode, defined in (387). If ω_k is real and the adiabaticity condition holds, then the solution to the equation of motion for the perturbations should approach a plane wave solution. In particular, it implies that the WKB approximation holds so that the mode function can be written as

$$u_k(\tau) \simeq \frac{A_k}{\sqrt{2\omega_k(\tau)}}\, e^{-i\int^\tau \omega_k(\tau')d\tau'} + \frac{B_k}{\sqrt{2\omega_k(\tau)}}\, e^{i\int^\tau \omega_k(\tau')d\tau'}\,. \tag{400}$$

When this is the case, the time-dependent Bogoliubov coefficients α_k and β_k reduce to the C-numbers A_k and B_k, up to a time-dependent phase.

Let us analytically assess the adiabaticity condition for a quadratic potential, i.e. $m_{\rm eff}^2 = m^2$. In the dS epoch, the first adiabaticity parameter $|\omega_k'/\omega_k^2|$ is tiny before the mode exits the horizon, however when the mode is far outside the horizon then it settles to a constant value of $1/\sqrt{2}$. This can be shown by ignoring the axion mass which is much smaller than the inflationary Hubble scale, giving

$$\left|\frac{\omega_k'}{\omega_k^2}\right| \simeq \frac{1}{\sqrt{2}}\left|1-\frac{k^2}{2a^2H_{\rm inf}^2}\right|^{-3/2}\,. \tag{401}$$

The second adiabaticity parameter ω_k''/ω_k^3 exhibits a similar behaviour.

The adiabaticity condition becomes satisfied again after inflation when the axion field starts oscillating. During radiation domination, the first adiabaticity parameter reduces to

$$\frac{\omega_k'}{\omega_k^2} = \frac{a^3 H\, m^2}{\left(k^2+a^2m^2\right)^{3/2}}. \tag{402}$$

Given this result, there are two possible regimes:

$$\frac{\omega_k'}{\omega_k^2} \simeq \begin{cases} \frac{a^3 H\, m^2}{k^3} & k \gg a\, m, \\ \frac{H}{m} & k \ll a\, m. \end{cases} \tag{403}$$

We restrict ourselves to wave modes that are outside the horizon at the onset of the oscillations, i.e. $k < a_{\rm osc} m$. Hence after the oscillation begins, namely when $a > a_{\rm osc}$ and $H < m$, the adiabaticity parameter is given by the second line, which is smaller than unity. Therefore starting from that point the adiabaticity condition is always recovered. The behaviour long before $a_{\rm osc}$ depends on the actual value of k. The second adiabaticity parameter is

$$\frac{\omega_k''}{\omega_k^3} = \frac{m^2}{\left(k^2+a^2m^2\right)^2}\left(H^2a^4 - \frac{m^2H^2a^6}{k^2+a^2m^2}\right). \tag{404}$$

Considering again the two possible regimes, we have:

$$\frac{\omega_k''}{\omega_k^3} \simeq \begin{cases} \dfrac{m^2 a^4 H^2}{k^4} & k \gg a\, m, \\ \dfrac{k^2 H^2}{a^2 m^4} & k \ll a\, m. \end{cases} \tag{405}$$

Also in this case the condition is surely satisfied when $a > a_{\rm osc}$.

The above discussions apply similarly to the full cosine potential, for which we numerically checked with initial misalignment angles close to the hilltop. The behaviours of the adiabaticity parameters are the same while the axion is frozen by the Hubble friction. Soon after the axion starts to oscillate the adiabaticity parameters also oscillate, however, within a few e-folds the adiabaticity condition becomes satisfied.

8.3.2.2 *Enhancement in the Number of Particles*

In order to understand the enhancement in the beta coefficient due to the anharmonic effects, we show in Figure 18 (left, purple line) the value of $|\beta|^2$ in the asymptotic future as a function of the initial field value $\theta_0 = \bar{\phi}_0/f$. (The pink line will be explained in Section 8.3.2.4.) The asymptotic value of the Bogoliubov coefficient significantly increases as one approaches the hilltop at $\theta_0 = \pi$. This behaviour can be interpreted analysing the time at which the field starts oscillating. As we have seen in Section 8.2, increasing the initial field value delays the onset of the oscillations. Approaching the hilltop this delay becomes more and more evident. If we consider the field perturbation around a background value close to the minimum, the delay in the onset of the oscillation is too tiny to affect the evolution in time of $\delta\phi_k$. However, if the field perturbation is considered around a background field value close to the maximum of the potential, then the evolution in time of the perturbation changes dramatically. In fact, close to the hilltop even a small difference in the initial position leads to a huge difference in the time of the onset of the oscillations. This implies that patches of the Universe that differ by a tiny variation of the initial misalignment angle will start to oscillate at very different times, sourcing huge fluctuations. This in turn reflects into the modulus square of the mode functions, that enters directly into $|\beta_k|^2$. In the hypothetical situation where the angle is set initially to π, the field does not start oscillating at all. Hence $\delta\phi_k$ is going to become infinite, thus making $|\beta_k|^2$ divergent.

To better analyse the behaviour of $|\beta_k|^2$ near the hilltop it is worth working in terms of $\pi/(\pi - \theta_0)$. In terms of this variable, the hilltop at $\theta_0 = \pi$ is shifted to ∞. In Figure 18 (right, purple line), $|\beta_k|^2$ is reported in terms of this new variable. We find that the asymptotic value of $|\beta_k|^2$ grows towards the hilltop [4] as $(\pi - \theta_0)^{-2}$.

We should remark that the above discussions do not apply arbitrarily close to the hilltop. In particular if the initial displacement from the hilltop, $\pi - \theta_0$, is comparable to or smaller than the angular quantum fluctuation $\delta\theta$ (whose

4 A similar scaling was also found for the two-point correlator of the field fluctuations in the context of axionic curvatons [169].

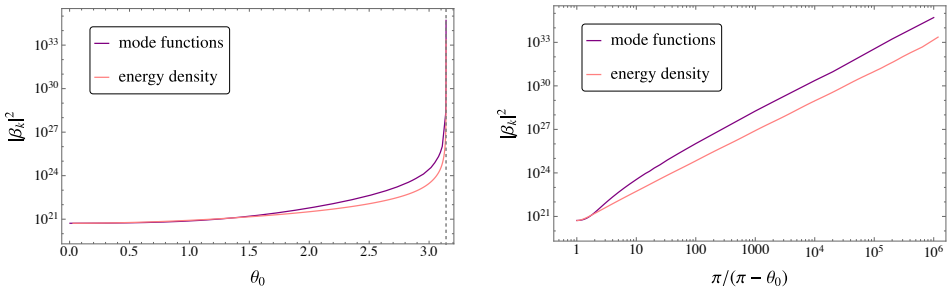


Figure 18: Asymptotic value of $|\beta_k|^2$ as functions of the initial displacement angle (left), and of $\pi/(\pi-\theta)$ (right). The parameters are chosen as $H_{\rm inf} = 10^8\,\text{GeV}$, $m = 10^2\,\text{GeV}$, and $k/a_{\rm reh} = 10^2\,\text{GeV}$. The purple line refers to $|\beta_k|^2$ computed through the mode functions. The pink line shows the second derivative of the axion density in terms of the initial field value, as given in the right-hand side of (417).

amplitude is of $H_{\rm inf}/f$), then the perturbative expansion around the classical background breaks down. In this regime the field can roll down to the other side of the hill in some patches of the universe, and give rise to axionic domain walls. In this work we do not consider such cases.

8.3.2.3 *Parameter Dependence*

Let us now study the dependence of $|\beta_k|^2$ on the parameters $H_{\rm inf}$, m, k. The dependence on the parameters can be derived analytically for a quadratic potential. The complete derivation is reported in Appendix 8.5.2, where we show that the asymptotic value of $|\beta_k|^2$ for a quadratic potential is given by

$$|\beta_k|^2 = \frac{1}{8\pi}\,\Gamma(1/4)^2\,\left(\frac{a_{\rm reh}}{k}\right)^3\,\frac{H_{\rm inf}^{7/2}}{\sqrt{m}}\,. \tag{406}$$

A physical interpretation of this result in terms of the energy density will be presented in Section 8.3.2.4. The dependence of $|\beta_k|^2 \propto k^{-3}$ shows the scale invariance of the perturbation.

The expression (406) applies for initial field values close to the minimum, such that the potential is well approximated by a quadratic. To understand the dependence on the parameters for field values where anharmonic effects are relevant, we have to rely on numerical simulations. The results are shown in Figure 19, where the asymptotic value of $|\beta_k|^2$ as a function of the initial misalignment angle is plotted. The different lines correspond to different choices for the Hubble rate, the axion mass, or the wave number; the horizontal dashed lines are the analytical value computed using (406). What we find is that $|\beta_k|^2$ always depends on the same combination of parameters as given in (406), which sets the overall normalization for $|\beta_k|^2$. Since the dependence of $|\beta_k|^2$ on k is the same, we can also see that the energy density remains scale independent when the anharmonic effects are taken into account. Moreover, we see that the shape of $|\beta_k|^2$ as a function of θ_0 is identical for each choice of the parameters. This indicates that the anharmonic enhancement of $|\beta_k|^2$ is determined only by the initial angle.

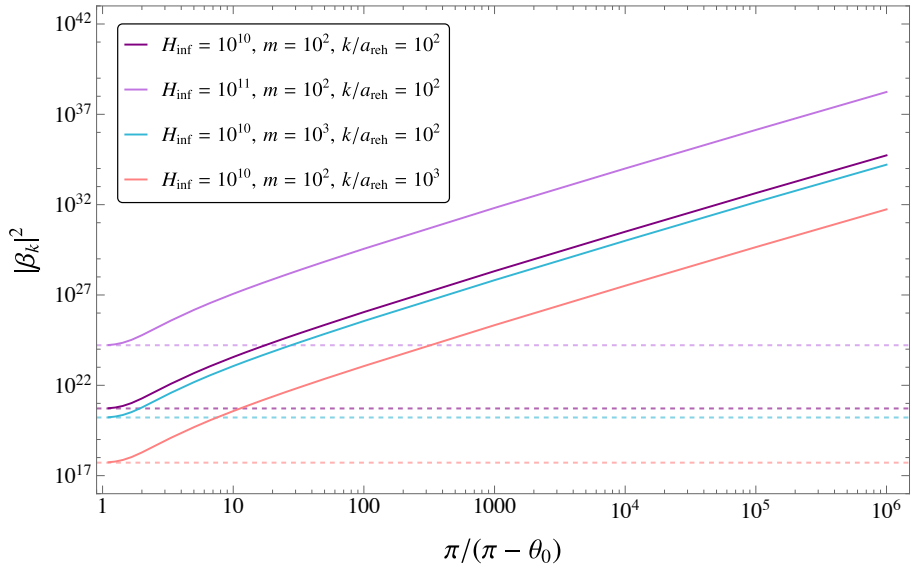


Figure 19: Asymptotic value of the Bogoliubov coefficient $|\beta_k|^2$ as a function of the axion misalignment angle θ_0. Colours denote different choices of the inflationary Hubble scale, axion mass, and the wave number upon reheating, as listed in the legend in units of GeV. Dashed horizontal lines denote the offset at $\theta_0 \to 0$, as given in (406).

The final value for $|\beta_k|^2$ also allows us to compute the number of axions today. From (148) (or (414)), the physical number density of axion particles that were quantum mechanically produced in the early universe is

$$n = \int \frac{dk}{k}\, n_k\,, \qquad n_k = \frac{k^3 |\beta_k|^2}{2\pi^2 a^3}\,, \tag{407}$$

where n_k denotes the number density of particles with comoving momentum $\sim k$. (It should be noted that the total number of axions is dominated by the zero mode axions classically produced from the vacuum misalignment.) Using the expression (406) for axions produced close to the potential minimum, and rewriting the redshift at instantaneous reheating in terms of the inflation scale as

$$\frac{a_{\rm today}}{a_{\rm reh}} \sim 10^{28} \left(\frac{H_{\rm inf}}{10^{12}\,{\rm GeV}}\right)^{1/2}\,, \tag{408}$$

the number density today is obtained as

$$n_{k\,{\rm today}} \sim 100\,{\rm cm}^{-3} \left(\frac{m}{1\,{\rm eV}}\right)^{-1/2} \left(\frac{H_{\rm inf}}{10^{12}\,{\rm GeV}}\right)^{2}\,. \tag{409}$$

8.3.2.4 *Alternative Calculation for* $|\beta_k|^2$

In order to understand the physics underlying the expression (406), let us present an alternative derivation of the asymptotic value of $|\beta_k|^2$ using the energy density of the axion field:

$$\rho = \frac{(\phi')^2 + \partial_i\phi\partial_i\phi}{2a^2} + V(\phi)\,. \tag{410}$$

Expanding this in terms of the field fluctuation $\delta\phi$, then the expectation value of the density operator in the initial vacuum defined in (148) is written as

$$\langle\rho\rangle = \bar{\rho} + \langle\rho_2\rangle + \sum_{n=3}^{\infty} \frac{d^n V(\bar{\phi})}{d\bar{\phi}^n} \frac{\langle\delta\phi^n\rangle}{n!} \,. \tag{411}$$

Here $\bar{\rho}$ is the energy density of the background field as given in (397), and we considered terms linear in $\delta\phi$ to have vanishing expectation values. The quadratic-order density operator ρ_2 is given by

$$\rho_2 = \frac{1}{2a^2}\left\{(\delta\phi')^2 + (\partial_i\delta\phi)(\partial_i\delta\phi) + a^2 m_{\rm eff}^2 \delta\phi^2\right\} \,, \tag{412}$$

whose vacuum expectation value is written in terms of the Bogoliubov coefficients as

$$\begin{aligned}\langle\rho_2\rangle = \frac{1}{2a^4}\int \frac{d^3k}{(2\pi)^3}\Bigg[|\omega_k|\left(|\beta_k|^2 + \frac{1}{2} - \frac{\alpha_k\beta_k + \alpha_k^*\beta_k^*}{2}\right) \\ + \frac{k^2 + a^2(m_{\rm eff}^2 + H^2)}{|\omega_k|}\left(|\beta_k|^2 + \frac{1}{2} + \frac{\alpha_k\beta_k + \alpha_k^*\beta_k^*}{2}\right) + iaH(\alpha_k\beta_k - \alpha_k^*\beta_k^*)\Bigg] \,.\end{aligned} \tag{413}$$

After the onset of the axion oscillations the effective mass asymptotes to the mass around the minimum, $m_{\rm eff} \simeq m$ ($\gg H, k/a$), and the frequency to $|\omega_k| \simeq am$. In this epoch (413) takes the form of

$$\langle\rho_2\rangle \simeq \frac{m}{a^3}\int \frac{d^3k}{(2\pi)^3}\left(|\beta_k|^2 + \frac{1}{2}\right) \,. \tag{414}$$

This is equivalent to the asymptotic value of the Hamiltonian density $\langle\mathcal{H}\rangle/a^4V$, cf. (148).

We can also compute the axion density by treating it as a purely classical quantity. For this, notice that the axion field during inflation follows a slow-roll attractor where the field velocity is set by the field value as $\phi' \propto -dV/d\phi$. Hence the asymptotic energy density can be considered to be uniquely determined by the axion field value at some initial time τ_i during inflation, i.e., $\rho = \rho(\phi_i)$. Then the spatial inhomogeneity of the asymptotic density can be understood to originate from that of the initial field, $\phi_i(\boldsymbol{x}) = \bar{\phi}_i + \delta\phi_i(\boldsymbol{x})$, where $\bar{\phi}_i$ is the average field value over the entire universe at τ_i, and $\delta\phi_i$ is the classical fluctuation around the average. (We are being somewhat sloppy and using the same notation as we used in (378) for splitting between the classical background and quantum fluctuations, but we stress that here everything is classical.) Expanding the asymptotic density in terms of $\delta\phi_i(\boldsymbol{x})$, and also taking a spatial average yields

$$\langle\rho(\phi_i)\rangle_{\rm avg} = \rho(\bar{\phi}_i) + \frac{\partial^2\rho(\bar{\phi}_i)}{\partial\bar{\phi}_i^2}\frac{\langle\delta\phi_i^2\rangle_{\rm avg}}{2} + \sum_{n=3}^{\infty}\frac{\partial^n\rho(\bar{\phi}_i)}{\partial\bar{\phi}_i^n}\frac{\langle\delta\phi_i^n\rangle_{\rm avg}}{n!} \,. \tag{415}$$

By identifying the spatially averaged quantities with the vacuum expectation values of the corresponding operators, we can equate (415) with (411). Moreover, the variance $\langle\delta\phi^2\rangle_{\rm avg}$ can be evaluated as the vacuum expectation

value of the quadratic operator, as shown in (164). Hence the second term of (415) is rewritten as

$$\frac{d^2\rho(\bar{\phi}_i)}{d\bar{\phi}_i^2}\frac{\langle\delta\phi_i^2\rangle_{\rm avg}}{2} \simeq \frac{1}{2}\frac{d^2\rho(\bar{\phi}_i)}{d\bar{\phi}_i^2}\int_{k\leq a_i H_{\rm inf}}\frac{d^3k}{(2\pi)^3}\frac{H_{\rm inf}^2}{2k^3}\,. \tag{416}$$

Here we ignored modes that are sub-horizon at the time τ_i, since the contributions from such modes should be renormalized and absorbed into the cosmological constant. Additionally, for the mode function during inflation, we substituted its value in the super-horizon limit for an effectively massless field, $|u_k|^2/a^2 \simeq H_{\rm inf}^2/2k^3$ (cf. $k \ll aH_{\rm inf}$ limit of (424) with $\nu = 3/2$).

Upon comparing (411) and (415), let us identify $\bar{\rho}$ with $\rho(\bar{\phi}_i)$, and further ignore the higher-order correlators. Then we can equate the second terms of each expression, namely, (414) and (416). Let us further suppose that this equality holds mode by mode, and also drop the $1/2$ in (414). Then we find a relation between the asymptotic value of the Bogoliubov coefficient, and the second-order derivative of the background energy density in terms of the initial field value,

$$|\beta_k|^2 \sim \frac{a^3 H_{\rm inf}^2}{4mk^3}\frac{\partial^2\rho(\bar{\phi}_i)}{\partial\bar{\phi}_i^2}\,. \tag{417}$$

Since the energy density after the axion started oscillating redshifts as $\rho \propto a^{-3}$, the right-hand side is actually time-independent.

If the initial field value is close to the potential minimum, i.e. $|\bar{\phi}_i| \ll f$, then the axion potential is approximately quadratic and the field begins a harmonic oscillation when $H \sim m$. Hence the asymptotic axion density can approximately be written as

$$\rho(\bar{\phi}_i) \sim \frac{1}{2}m^2\bar{\phi}_i^2\left(\frac{a_{\rm osc}}{a}\right)^3 \sim \frac{1}{2}m^{1/2}H_{\rm inf}^{3/2}\,\bar{\phi}_i^2\left(\frac{a_{\rm reh}}{a}\right)^3\,, \tag{418}$$

where upon moving to the far right-hand side we used $a_{\rm osc} \sim a_{\rm reh}(H_{\rm inf}/m)^{1/2}$. Plugging this into (417), we can estimate the Bogoliubov coefficient around the minimum as

$$|\beta_k|^2 \sim \frac{1}{4}\left(\frac{a_{\rm reh}}{k}\right)^3\frac{H_{\rm inf}^{7/2}}{m^{1/2}}\,. \tag{419}$$

This matches with the exact result (406) up to a numerical factor of order unity[5].

We have numerically computed both sides of (417); these are displayed as functions of the initial angle [6] in Figure 18, where the purple line shows the

5 The numerical factor of (406) can also be obtained from (417) by using the exact result for the asymptotic axion density [170] (see their Eq. (A3), and combine with $H = H_{\rm inf}(a_{\rm reh}/a)^2$):

$$\rho = \frac{[\Gamma(\frac{1}{4})]^2}{4\pi}m^{\frac{1}{2}}H_{\rm inf}^{\frac{3}{2}}\bar{\phi}_i^2\left(\frac{a_{\rm reh}}{a}\right)^3\,. \tag{420}$$

6 The background field $\bar{\phi}_i$ in (417) denotes the value after the wave mode of interest has left the horizon (cf. discussions below (416)), while in the plots we use $\theta_0 = \bar{\phi}_0/f$ which is the value when the mode is still deep inside the horizon. However we do not distinguish between $\bar{\phi}_i$ and $\bar{\phi}_0$, since the axion background is effectively frozen during inflation for our choice of parameters.

left-hand side, while the pink line shows the right-hand side. At $\theta_0 \lesssim 1$, where the potential can be approximated by a quadratic, the two results are in good agreement. In particular, both asymptote to the value of (406) as $\theta_0 \to 0$. Close to the hilltop, on the other hand, $|\beta_k|^2$ is consistently larger than the right-hand side of (417) by an order of magnitude. We have also checked that the θ_0-dependences of either sides of (417) are unaltered by changing the values of m, $H_{\rm inf}$, and k; hence the behaviours discussed above are also parameter-independent.

We should remark that our calculation incorporates axion self-interactions through the interaction between the homogeneous background field (zero mode) and the fluctuation mode, however we have ignored mode-mode interactions by expanding the action only up to quadratic order in the fluctuation. The relation (417) has also been derived by neglecting higher-order correlators. One would naively expect the mode-mode interactions to be suppressed by a hierarchical parameter choice such that $m \ll H_{\rm inf} \ll f$. However the uniform discrepancy between both sides of (417) at $\theta_0 \gtrsim 1$ may be implying the importance of the interactions between the fluctuation modes. We leave a detailed investigation of this for the future.

8.3.3 *Squeezing Parameters*

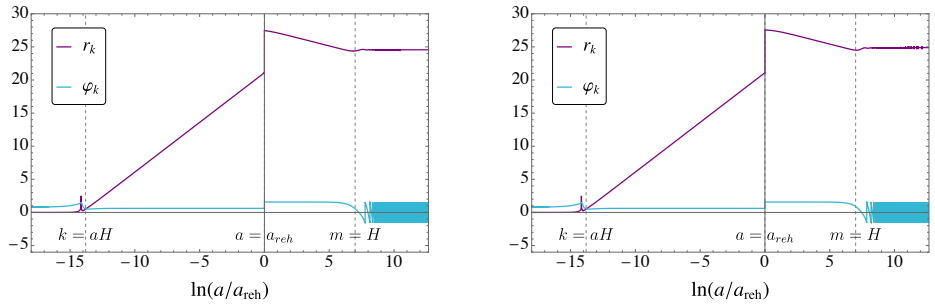
We can now proceed to the analysis of the squeezing parameters. Through relations (394), one gets the evolution in time of the squeezing parameters. The result is shown in Figure 20 for r_k and φ_k, which are the two parameters linked with physical quantities, as explained in Section 4.3. Their evolution is reported for four different values of the initial misalignment angle.

The r_k parameter is directly linked with the modulus square of the beta coefficient; we can therefore see an enhancement in its value towards the hilltop. r_k gives a measure of the stretching of the ellipse describing the phase space distribution of two conjugate variables, as explained in Section 4.3.2. If r_k increases, as observed taking into account the anharmonic effects, then the ellipse gets stretched along one of its axis, and the state described by the two conjugate variables becomes more and more squeezed. We therefore conclude that anharmonic effects give extra squeezing at the onset of the oscillations.

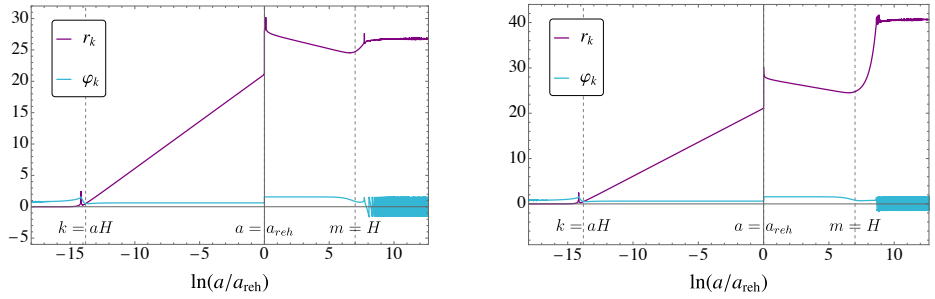
The angle φ_k is instead linked with the rotation of the ellipse in phase space. φ_k is constant until the mode exits the horizon, then shifts to another constant value after the horizon exit. When the background field starts oscillating, and the adiabaticity condition starts to hold, the phase starts to rotate. This behaviour is visible in Figure 20. The sharp lines are present since the phase is restricted to the range $-\pi \leq \varphi_k \leq \pi$. In phase space, the ellipse described by this phase is constantly rotating by this time dependent angle.

8.4 SUMMARY OF THE MAIN RESULTS

In this chapter, we have computed the time evolution of the Bogoliubov coefficients and the squeezing parameters for an axion-like field during inflation and radiation domination, keeping into account self-interactions. In particu-



(a) $\theta_0 = 0.1\,\pi$ **(b)** $\theta_0 = 0.4\,\pi$



(c) $\theta_0 = 0.8\,\pi$ **(d)** $\theta_0 = 0.999999\,\pi$

Figure 20: Time evolution of the squeezing parameters r_k and φ_k for different values of the initial misalignment angle. The parameters chosen for the evaluation are $H_{\rm inf} = 10^8\,\text{GeV}$, $m = 10^2\,\text{GeV}$, and $k/a_{\rm reh} = 10^2\,\text{GeV}$. The dashed vertical lines set the horizon exit ($k = aH$), reheating ($a = a_{\rm reh}$) and the onset of the oscillations of the background field ($m = H$).

lar we considered the non-trivial evolution of the background field. We have shown that the net number of particles created due to the expansion of the Universe, given by $|\beta_k|^2$, increases as the initial background field approaches the hilltop of the cosine potential. The r_k parameter determining the amount of squeezing increases accordingly. Hence we conclude that the self-interaction due to the cosine potential, and specifically the interaction between the perturbation and the non-trivial background field dynamics, gives rise to extra post-inflation squeezing.

An analytical expression for $|\beta_k|^2$ in terms of the relevant parameters of the system has also been found in the quadratic potential limit in (406). A full derivation has been carried out in terms of the analytical mode functions in Appendix 8.5.1. The expression (406) has also been confirmed via numerical computations to set the overall normalization of $|\beta_k|^2$. The behaviour of the final value of $|\beta_k|^2$ as a function of the initial displacement angle is not affected by the physical parameters $H_{\rm inf}$, m and k, provided the mode considered reenters the horizon after the background has started oscillating. Moreover the anharmonic enhancement of the squeezing is solely determined by the initial misalignment angle.

We have also derived a relation between the asymptotic values of the Bogoliubov coefficients, and the field derivatives of the background energy density,

as shown in (417). This relation exactly holds for small misalignment angles where the axion potential is well approximated by a quadratic, however we also found that it breaks down towards the hilltop. Here we note that in this paper we evaluated the effect of axion self-interactions through the interaction between the homogeneous background field and the fluctuation, while we have ignored interactions among the fluctuation modes. The breakdown of (417) towards the hilltop may be indicating that mode-mode couplings can further enhance axion squeezing. We leave an investigation of this effect for future work.

A connection with observables has also been pointed out. The net number of particles created by the expansion of the Universe is given by $|\beta_k|^2$, which is directly linked also to the parameter r_k and consequently to the amount of squeezing of the perturbations. The more particles are created, the more squeezed the state is. The other physically relevant squeezing parameter, i.e. the phase φ_k, is related with the power spectrum of the field fluctuations, as shown for the case of the inflaton perturbations in (166).

One interesting question left for future work is how we could observationally discern among the quantum or classical origin of the axion perturbations. The main problem in addressing this question is the fact that the two-point correlation functions of a squeezed state can be perfectly mimicked by a stochastic classical distribution. Despite this, a squeezed state is an intrinsically quantum state and in particular it is an entangled state. Hence one possible test of the quantum nature of the perturbations is a Leggett-Garg type experiment on the CMB. Indeed, contrary to the case of curvature perturbations for which $\pi_\zeta = \zeta'$ is vanishing on super-horizon scales, the conjugate momentum for an axion field is not vanishing. We have indeed shown that the phase φ_k oscillates in the late time limit, making the ellipse in phase space describing the system to rotate. This suggests that the time derivative of the perturbation is non-negligible, and hence axions may provide an ideal target for a cosmological Leggett-Garg experiment.

Another way to probe the nature of the primordial fluctuations is to consider interacting theories and compute higher order correlators, as shown in Chapter 7. Hence a careful analysis of the axion bispectrum might be enlightening. In order to compute the bispectrum of an axion field, the effect of the non-trivial background computed in this chapter will have to be taken into account.

8.5 APPENDIX A: QUADRATIC POTENTIAL

In this appendix we study a quadratic axion potential, and derive analytic solutions for the mode function, as well as the asymptotic values of the Bogoliubov coefficients. The analytical results presented coincide with the numerical results obtained for the full cosine potential in the limit of a small initial displacement angle, close to the minimum of the potential.

8.5.1 *Mode Functions*

The equation of motion for the mode function is given by (398), with $m_{\rm eff}$ replaced by a constant and positive mass m, as here we focus on a quadratic potential. Let us solve this equation in the dS and RD epochs, assuming the two epochs to be connected by an instantaneous reheating.

DS EPOCH With a constant Hubble rate $H = H_{\rm inf}$, the conformal time is related to the scale factor as

$$\tau = -\frac{1}{aH_{\rm inf}}. \tag{421}$$

Here we set the time at reheating as $\tau_{\rm reh} = -1/a_{\rm reh}H_{\rm inf}$. The equation of motion then reduces to the form,

$$u_k'' + \left\{k^2 + \frac{1}{\tau^2}\left(\frac{m^2}{H_{\rm inf}^2} - 2\right)\right\} u_k = 0\,. \tag{422}$$

Supposing $m^2/H_{\rm inf}^2 < 9/4$, the solution is given in terms of Hankel functions as,

$$u_k = (-\tau)^{\frac{1}{2}}\left\{c_1\, H_\nu^{(1)}(-k\tau) + c_2\, H_\nu^{(2)}(-k\tau)\right\}, \qquad \nu = \left(\frac{9}{4} - \frac{m^2}{H_{\rm inf}^2}\right)^{\frac{1}{2}}. \tag{423}$$

The two constants c_1 and c_2 can be fixed by requiring that the mode function approaches a positive frequency solution in the asymptotic past, and also that it satisfies the normalization condition (103). This yields, up to an unphysical phase,

$$u_k = \left(\frac{\pi}{4aH_{\rm inf}}\right)^{\frac{1}{2}} H_\nu^{(1)}\left(\frac{k}{aH_{\rm inf}}\right), \tag{424}$$

where we have rewritten the solution in terms of the scale factor.

RD EPOCH In a radiation-dominated universe where $H \propto a^{-2}$, the equation of motion can be rewritten as

$$\frac{d^2u_k}{dz^2} + \left(\frac{z^2}{4} + \frac{\kappa^2}{2\mu}\right) u_k = 0, \tag{425}$$

where

$$\kappa = \frac{k}{a_{\rm reh}H_{\rm inf}}, \quad \mu = \frac{m}{H_{\rm inf}}, \quad z = (2\mu)^{\frac{1}{2}}\frac{a}{a_{\rm reh}}. \tag{426}$$

Solutions to this equation are the parabolic cylinder functions,

$$u_k = c_3 D_{-\lambda}\left(e^{i\frac{\pi}{4}}z\right) + c_4 D_{\lambda-1}\left(e^{i\frac{3\pi}{4}}z\right), \qquad \lambda = \frac{1}{2} + \frac{i\kappa^2}{2\mu}. \tag{427}$$

The two constants c_3 and c_4 are fixed by imposing continuity of the solutions (424) and (427), as well as their time derivatives, at the time of reheating.

8.5.2 *Asymptotic* $|\beta_k|^2$

In order to evaluate the Bogoliubov coefficient $|\beta_k|^2$ in the asymptotic future, we introduce linear combinations of parabolic cylinder functions,

$$\mathcal{F}_+ = \frac{e^{-\frac{\pi\kappa^2}{8\mu}}}{(2\mu)^{\frac{1}{4}}(a_{\rm reh}H_{\rm inf})^{\frac{1}{2}}} D_{-\lambda}\left(e^{i\frac{\pi}{4}}z\right) , \tag{428}$$

$$\mathcal{F}_- = \frac{e^{\frac{3\pi\kappa^2}{8\mu}}}{(2\mu)^{\frac{1}{4}}(a_{\rm reh}H_{\rm inf})^{\frac{1}{2}}} \left\{ D_{\lambda-1}\left(e^{i\frac{3\pi}{4}}z\right) + \frac{(2\pi)^{\frac{1}{2}}e^{-i\frac{3\pi}{4}-\frac{\pi\kappa^2}{4\mu}}}{\Gamma(-\lambda+1)} D_{-\lambda}\left(e^{i\frac{\pi}{4}}z\right) \right\} , \tag{429}$$

and rewrite the mode function in the RD epoch (427) as

$$u_k = A_k\,\mathcal{F}_+ + B_k\,\mathcal{F}_- . \tag{430}$$

Here A_k and B_k are time-independent coefficients. The functions $\mathcal{F}_+$ and $\mathcal{F}_-$ are chosen such that in the asymptotic future, they respectively approach the WKB solutions with positive and negative frequencies:

$$\frac{e^{\mp i\int^\tau d\tilde{\tau}\,\omega_k(\tilde{\tau})}}{\sqrt{2\omega_k(\tau)}} \sim \frac{e^{\mp i\left(\frac{z^2}{4}+\text{const.}\right)}}{(2\mu)^{\frac{1}{4}}(a_{\rm reh}H_{\rm inf}\,z)^{\frac{1}{2}}} . \tag{431}$$

This can be checked by noting that for an argument w with a sufficiently large amplitude and $s \neq 0, 1, 2, \cdots$, the parabolic cylinder function is approximated by

$$D_s(w) \sim e^{-\frac{w^2}{4}} w^s - \frac{\sqrt{2\pi}}{\Gamma(-s)} e^{i\pi s+\frac{w^2}{4}} w^{-s-1} , \tag{432}$$

for $\pi/4 < \arg w < 5\pi/4$. For $|\arg w| < 3\pi/4$, the approximate expression is given only by the first term in the right hand side. Hence the amplitudes of the coefficients A_k and B_k in (430) match with those of the Bogoliubov coefficients α_k and β_k in the asymptotic future.

By matching the mode functions (424) and (430), as well as their time derivatives u_k' at $a = a_{\rm reh}$, the coefficient B_k can be obtained as,

$$B_k = \frac{\pi^{\frac{1}{2}}e^{i\frac{\pi}{4}-\frac{3\pi\kappa^2}{8\mu}}}{2^{\frac{5}{4}}\mu^{\frac{1}{4}}} \times \frac{\kappa H^{(1)}_{\nu+1}(\kappa)D_{-\lambda} - H^{(1)}_{\nu}(\kappa)\left\{(\frac{1}{2}+\nu+i\mu)D_{-\lambda} + e^{-i\frac{3\pi}{4}}\sqrt{2\mu}\,D_{-\lambda+1}\right\}}{iD_{-\lambda+1}D_{\lambda-1} + D_{-\lambda}\left\{D_\lambda + e^{-i\frac{\pi}{4}}\sqrt{2\mu}D_{\lambda-1}\right\}} . \tag{433}$$

Here the arguments of the parabolic cylinder functions are $e^{i\pi/4}\sqrt{2\mu}$ for $D_{-\lambda}$ and $D_{-\lambda+1}$, while $e^{i3\pi/4}\sqrt{2\mu}$ for D_λ and $D_{\lambda-1}$. This expression for B_k can

by simplified by first expanding in small κ, and then further simplifying the leading term by considering a small μ. This gives,[7]

$$B_k \sim -\frac{i\Gamma(\frac{1}{4})}{2^{\frac{3}{2}}\pi^{\frac{1}{2}}}\frac{1}{\kappa^{\frac{3}{2}}\mu^{\frac{1}{4}}}\,. \tag{436}$$

This gives a good approximation for (433) at $\kappa^2 \lesssim \mu \ll 1$; here note that $\kappa^2 \lesssim \mu$ is equivalent to $k \lesssim (aH)_{\rm osc}$. Hence for wave modes that are outside the Hubble horizon when the axion begins to oscillate during the RD epoch, the asymptotic value of the Bogoliubov coefficient is obtained as

$$|\beta_k|^2 \sim \frac{[\Gamma(\frac{1}{4})]^2}{8\pi}\left(\frac{a_{\rm reh}}{k}\right)^3\frac{H_{\rm inf}^{\frac{7}{2}}}{m^{\frac{1}{2}}}\,. \tag{437}$$

8.6 APPENDIX B: MORE REALISTIC MODELS FOR THE EVOLUTION OF THE UNIVERSE

In the results derived in this chapter, we assumed a pure dS spacetime followed by an RD spacetime, further assuming the reheating phase to be instantaneous. In this Appendix, we check that changing the evolution of the Hubble rate does not affect our main conclusions on the asymptotic value for $|\beta_k|^2$ and the squeezing parameters.

8.6.1 *Smooth Reheating*

We first smooth the Hubble rate evolution between the dS and RD epochs to see if our results are affected by a non-instantaneous reheating phase. The expression we use is the following:

$$H = H_{\rm inf}\,\frac{a_{\rm reh}^2}{a^2 + a_{\rm reh}^2} \tag{438}$$

We numerically solved the axion's equations of motion with the Hubble rate (438), and we found that it does not change the evolution of the background field nor the fluctuation's mode function. However it affects the evolution of β_k as shown in Figure 21. The behaviour of $|\beta_k|^2$ is modified near the reheating phase, but it coincides with the result from instantaneous reheating after a few e-folds. Hence the final value of $|\beta_k|^2$ is not affected by this modification to the Hubble evolution. This is because the post-inflation squeezing is determined by the field dynamics near the onset of the oscillations; the Hubble rates in

7 We use that the Hankel function of the first kind at $w \to 0$ asymptotes to

$$H_s^{(1)}(w) \sim -\frac{i}{\pi}\Gamma(s)\left(\frac{w}{2}\right)^{-s}\,, \tag{434}$$

for $\mathrm{Re}(s) > 0$. We also use

$$D_{\frac{1}{2}}(0) = \frac{2^{\frac{1}{4}}\pi^{\frac{1}{2}}}{\Gamma(\frac{1}{4})}\,, \quad D_{-\frac{1}{2}}(0) = \frac{\pi^{\frac{1}{2}}}{2^{\frac{1}{4}}\Gamma(\frac{3}{4})}\,. \tag{435}$$

(438) and (375) differ for a few e-folds around reheating, however they coincide by the time the oscillations begin.

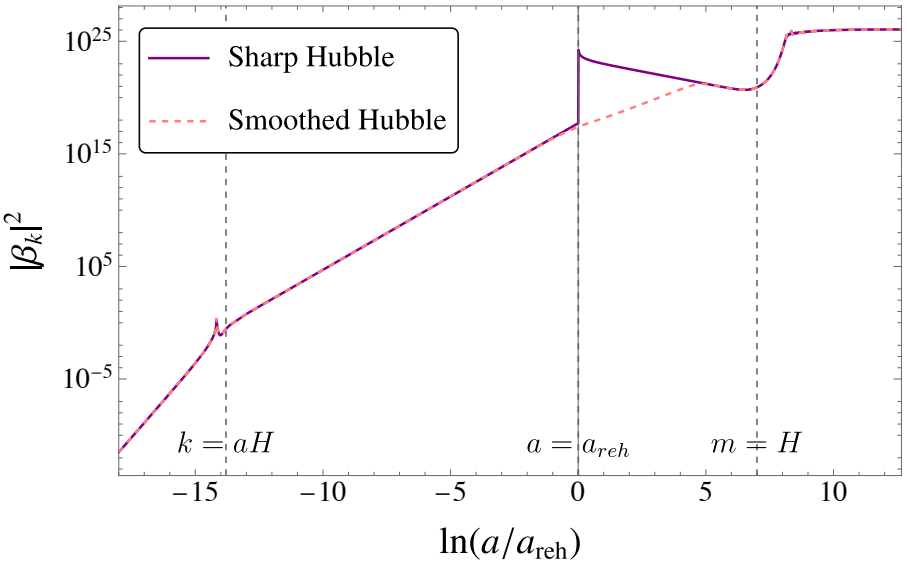


Figure 21: Time evolution of $|\beta_k|^2$ for instantaneous reheating (purple) and smooth reheating (pink dashed), for an initial angle $\theta_0 = 0.99\,\pi$. The values chosen for the parameters are $H_{\rm inf} = 10^8$ GeV, $m = 10^2$ GeV and $k/a_{\rm reh} = 10^2$ GeV.

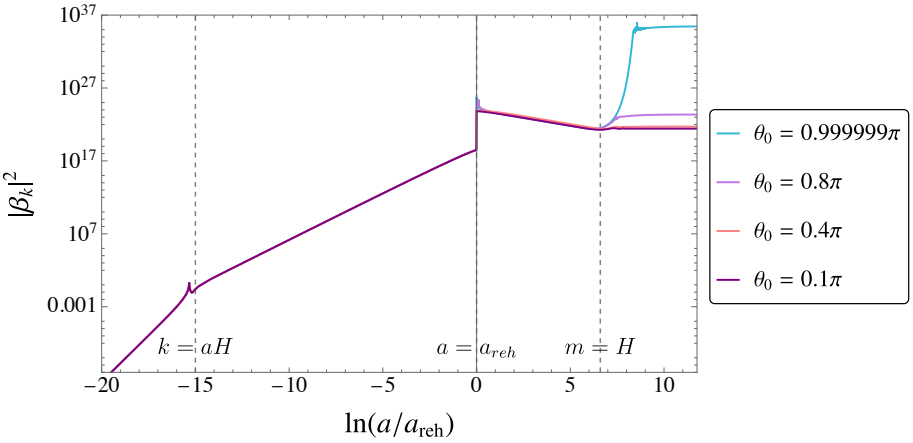


Figure 22: Time evolution of $|\beta_k|^2$ in a quasi de Sitter inflationary background, for different initial background field values. The parameters used are $m_\varphi = 10^8$ GeV, $m = 10^2$ GeV and $k/a_{\rm reh} = 10^2$ GeV.

8.6.2 *Single Field Inflation*

We now study a quasi de Sitter inflationary background, by considering a single-field inflation model with a quadratic potential

$$U = \frac{1}{2} m_\varphi^2 \, \varphi^2. \tag{439}$$

We assume that the background dynamics is completely determined by the inflaton, with the axion field being only a spectator field. We also suppose instantaneous reheating, followed by a period of radiation domination. Therefore the Hubble rate is now given by:

$$H = \begin{cases} m_\varphi \sqrt{\frac{1}{3} - \frac{2}{3} \ln\left(\frac{a}{a_{\rm reh}}\right)} & \text{inflation} \\ \frac{m_\varphi}{\sqrt{3}} \left(\frac{a}{a_{\rm reh}}\right)^{-2} & \text{RD} \end{cases} \tag{440}$$

In contrast to the exact dS background invoked before in the chapter, now the Hubble rate varies in time during inflation, with the inflation scale set by the inflaton mass. Upon computing the evolution of the axion fluctuations in the above cosmological background, we have chosen $m_\varphi = 10^8\,\text{GeV}$ (hence $H_{\rm inf} \sim 10^8\,\text{GeV}$), combined with $m = 10^2\,\text{GeV}$ and $k/a_{\rm reh} = 10^2\,\text{GeV}$; these parameters have the same order of magnitude as those in Figure 21. We checked that the mode function present similar behaviours as in the case of an exact dS spacetime. The results for the time evolution of $|\beta_k|^2$ are reported in Figure 22 for different initial misalignment angles. The general features of the evolution of $|\beta_k|^2$ are similar to those in Figure 21 for an exact dS spacetime followed by an instantaneous reheating; $|\beta_k|^2$ approaches a constant value after the onset of the oscillations, and its numerical value depends on the initial field.

From these analyses we conclude that our main conclusions for the axion squeezing are independent of the details of the inflation and reheating models.

9

CONCLUSIONS AND OUTLOOK

The narrative of this thesis revolves around a single unifying theme: finding a way to test the quantum nature of the cosmological perturbations. The primordial fluctuations are indeed always considered as arising from the quantum vacuum; however the CMB measurements are analyzed within a classical framework. Several questions then arise: are the cosmological perturbations really quantum? Did a classicalization process happen? Is there a way to test the quantumness of the perturbations? Answering these fundamental questions is a compelling task in modern cosmology. Numerous approaches have been explored in the literature, and this thesis provides an extensive review of the key findings from recent years. Additionally, this work advances this field of research by offering significant conclusions and introducing new opportunities for testing the quantum nature of the perturbations. Namely, we argued that a violation of the Leggett-Garg inequalities could be potentially tested from the CMB measurements. Furthermore, the detection of the bispectrum of both scalar and tensor perturbations could provide the definitive proof of the quantumness of the perturbations. Moreover, another potentially extremely useful tool has been analyzed, i.e. axion-like particles. These particles do not interact neither with other fields during inflation nor with the thermal bath after reheating; they could then evade the decoherence processes leading to the classicalization of the perturbations. Furthermore it has been proved that anharmonic effects greatly enhance both the number of particles created by the expanding Universe and the amount of squeezing of the perturbations. In Chapter 5 we have seen how the more squeezed the perturbations are the stronger the quantum effects are. Hence the effect of the non-trivial background due to the self-interactions of the axion field increases the quantumness of the fluctuations.

All these conclusions have been extensively explained in this thesis, together with a careful analysis of the pre-existing literature. A general introduction on Inflation and the theory of cosmological perturbations was given in Chapter 2 and Chapter 3.

In Chapter 4, the phenomenon of cosmological particle creation was analyzed. The concept of squeezing was introduced as a pivotal mechanism, revealing that the amplification of modes outside the horizon can be understood as the creation of particle pairs with opposite momenta due to the expansion of spacetime. The analysis demonstrated that the Hilbert space of cosmological perturbations could be effectively divided into sub-spaces corresponding to these particle pairs, evolving from a vacuum state to a two-mode squeezed state. This chapter laid the foundation for understanding the quantum evolution of perturbations in a cosmological setting.

Chapter 5 transitioned into a discussion on the partitions of Hilbert space and how physical quantities vary based on these partitions. It was revealed

that the classical stochastic description of the Wigner function could perfectly mimic the quantum perturbations' two-point functions, raising questions about the detectability of quantum signatures. The chapter critically assessed the positivity of the Wigner function, non-separability, and quantum discord as potential indicators of quantum characteristics in the cosmological context. This provided a bridge between classical stochastic processes and quantum phenomena, opening avenues for detecting quantum signatures in cosmological data.

The quantumness of perturbations was further explored in Chapter 6 through the lens of cosmological Bell inequalities. The introduction of pseudo-spin operators for continuous variable systems allowed for the construction of Bell inequality, whose violation has been proved for some values of the squeezing parameters. Additionally, the chapter presented the Leggett-Garg inequalities (LGI) as an alternative approach, overcoming observational challenges associated with Bell inequalities. The violation of LGI in the context of cosmological perturbations [28] was a significant finding, indicating that quantum phenomena may indeed be observable on cosmological scales.

In Chapter 7, the focus shifted beyond Gaussian fields to examine the effects of interactions, particularly through the study of non-Gaussianities and the bispectrum. The absence of poles in the bispectrum was identified as a clear quantum signature, suggesting that the primordial perturbations were not merely classical stochastic processes but had a quantum origin. The detailed computation of the bispectrum for primordial gravitational waves [31] further underscored the importance of non-Gaussianities as a tool for detecting quantum traces in the sky.

Chapter 8 delved into the evolution of axion-like particles in an expanding universe, focusing on the effect of self-interactions [39]. The chapter provided a detailed analysis of how self-interaction affects the evolution of these particles, with particular attention to the squeezing amplitude in relation to the initial misalignment angle of the axion field. The findings highlighted the critical role of anharmonic effects in enhancing the squeezing amplitude, which in turn makes the quantum effects stronger. The modified evolution of the Gaussian perturbations have also to be taken into account when studying perturbatively the non-Gaussianities of the system.

This body of work has provided significant insights into the quantum characteristics of cosmological perturbations, from the particle creation and squeezing mechanisms to the detection of quantum signatures through advanced mathematical frameworks. The study of Leggett-Garg inequalities [28], non-Gaussianities [31] and axion-like particles [39] has further expanded the potential for uncovering the quantum origins of the universe, presenting a comprehensive approach to understanding the early Universe's complexities. These findings contribute to the broader goal of bridging quantum mechanics and cosmology, offering a glimpse into the quantum underpinnings of the cosmos.

Several questions remain unanswered and deserve further scrutiny. For instance, the LGI have been computed for the cosmological perturbations during inflation, however the full evolution of the perturbations during radiation and

matter dominations has not been considered. Computing the evolution of the squeezing parameters in these eras of the Universe would allow a more direct comparison between the analytical results and the measurements on the CMB. In the final version of [28] the evolution of the perturbations after inflation will be taken into account.

Furthermore, concerning the study of non-Gaussianities much work still has to be done. One interesting development could be to check the cross-correlations between the two bispectra, computed in the classical and quantum approaches. Indeed, even if the poles in the folded configuration are present in both the cases, the two bispectra could in principle differ in the regions outside these poles. This computation is going to be added in [31] before its publication.

Another future development in the context of non-Gaussianities is the study of the bispectrum of axion fluctuations. The modified evolution of the Gaussian axion perturbations found in [39] has to be taken into account when applying the Green method to the study of the bispectrum. A full analysis of axions fluctuations could shed light on the observational tests of the quantum nature of primordial fluctuations. This is particularly relevant since recent developments have been done concerning the detection of axions and axion-like particles (see [171] for a review).

We finally mention that another interesting line of research which was not mentioned in this work concerns the analysis of the effects of primordial gravitational waves interacting with a gravitational interferometer. Indeed, exploiting the noise of primordial gravitational waves in interferometers, one could formulate a sophisticated measurement protocol to uncover their quantum properties [172–175].

BIBLIOGRAPHY

[1] David Polarski and Alexei A. Starobinsky. 'Semiclassicality and decoherence of cosmological perturbations'. Class. Quant. Grav. **13** (1996), pp. 377–392. arXiv:gr-qc/9504030.

[2] L. P. Grishchuk and Yu. V. Sidorov. 'Squeezed quantum states of relic gravitons and primordial density fluctuations'. Phys. Rev. D **42** (1990), pp. 3413–3421.

[3] L. P. Grishchuk. 'Signatures of quantum gravity in the large scale universe'. *4th Paris Cosmology Colloquium*. 1997, pp. 176–195. arXiv:gr-qc/9708070.

[4] L. P. Grishchuk. 'Relic gravitational waves and cosmology'. Phys. Usp. **48** (2005), pp. 1235–1247. arXiv:gr-qc/0504018.

[5] Claus Kiefer and David Polarski. 'Emergence of classicality for primordial fluctuations: Concepts and analogies'. Annalen Phys. **7** (1998), pp. 137–158. arXiv:gr-qc/9805014.

[6] Bruce Allen, Eanna E. Flanagan and Maria Alessandra Papa. 'Is the squeezing of relic gravitational waves produced by inflation detectable?' Phys. Rev. D **61** (2000), p. 024024. arXiv:gr-qc/9906054.

[7] Ivan Agullo, Béatrice Bonga and Patricia Ribes Metidieri. 'Does inflation squeeze cosmological perturbations?' JCAP **09** (2022), p. 032. arXiv:2203.07066.

[8] Jen-Tsung Hsiang and Bei-Lok Hu. 'No Intrinsic Decoherence of Inflationary Cosmological Perturbations'. Universe **8**.1 (2022), p. 27. arXiv:2112.04092.

[9] Jerome Martin and Vincent Vennin. 'Quantum Discord of Cosmic Inflation: Can we Show that CMB Anisotropies are of Quantum-Mechanical Origin?' Phys. Rev. D **93**.2 (2016), p. 023505. arXiv:1510.04038.

[10] L. Henderson and V. Vedral. 'Classical, quantum and total correlations'. J. Phys. A **34**.35 (2001), p. 6899. arXiv:quant-ph/0105028.

[11] Harold Ollivier and Wojciech H. Zurek. 'Quantum Discord: A Measure of the Quantumness of Correlations'. Phys. Rev. Lett. **88**.1 (2001), p. 017901. arXiv:quant-ph/0105072.

[12] Anindita Bera, Tamoghna Das, Debasis Sadhukhan, Sudipto Singha Roy, Aditi Sen(De) and Ujjwal Sen. 'Quantum discord and its allies: a review of recent progress'. Rept. Prog. Phys. **81**.2 (2017), p. 024001.

[13] Reinhard F. Werner. 'Quantum states with Einstein-Podolsky-Rosen correlations admitting a hidden-variable model'. Phys. Rev. A **40** (1989), pp. 4277–4281.

[14] Jerome Martin, Amaury Micheli and Vincent Vennin. 'Comparing quantumness criteria'. EPL **142**.1 (2023), p. 18001. arXiv:2211.10114.

[15] Konrad Banaszek and Krzysztof Wódkiewicz. 'Testing Quantum Nonlocality in Phase Space'. Phys. Rev. Lett. **82**.10 (1999), p. 2009.

[16] John F. Clauser, Michael A. Horne, Abner Shimony and Richard A. Holt. 'Proposed experiment to test local hidden variable theories'. Phys. Rev. Lett. **23** (1969), pp. 880–884.

[17] G. Gour, F.C. Khanna, A. Mann and M. Revzen. 'Optimization of Bell's inequality violation for continuous variable systems'. Physics Letters A **324**.5–6 (2004), pp. 415–419.

[18] David Campo and Renaud Parentani. 'Decoherence and entropy of primordial fluctuations II. The entropy budget'. Phys. Rev. D **78** (2008), p. 065045. arXiv:0805.0424.

[19] Jérome Martin and Vincent Vennin. 'Bell inequalities for continuous-variable systems in generic squeezed states'. Phys. Rev. A **93**.6 (2016), p. 062117. arXiv:1605.02944.

[20] Sayantan Choudhury, Sudhakar Panda and Rajeev Singh. 'Bell violation in the Sky'. Eur. Phys. J. C **77**.2 (2017), p. 60. arXiv:1607.00237.

[21] Jiunn-Wei Chen, Shou-Huang Dai, Debaprasad Maity, Sichun Sun and Yun-Long Zhang. 'Towards Searching for Entangled Photons in the CMB Sky'. Phys. Rev. D **99**.2 (2019), p. 023507. arXiv:1701.03437.

[22] Sugumi Kanno and Jiro Soda. 'Infinite violation of Bell inequalities in inflation'. Phys. Rev. D **96**.8 (2017), p. 083501. arXiv:1705.06199.

[23] Jerome Martin and Vincent Vennin. 'Obstructions to Bell CMB Experiments'. Phys. Rev. D **96**.6 (2017), p. 063501. arXiv:1706.05001.

[24] Jerome Martin and Vincent Vennin. 'Real-space entanglement of quantum fields'. Phys. Rev. D **104**.8 (2021), p. 085012. arXiv:2106.14575.

[25] H. S. Karthik, Akshata Shenoy Hejamadi and A. R. Usha Devi. 'Leggett-Garg inequalities and temporal correlations for a qubit under PT -symmetric dynamics'. Phys. Rev. A **103**.3 (2021), p. 032420. arXiv:1907.02879.

[26] Clive Emary, Neill Lambert and Franco Nori. 'Leggett–Garg inequalities'. Rept. Prog. Phys. **77**.1 (2013), p. 016001.

[27] Jerome Martin and Vincent Vennin. 'Leggett-Garg Inequalities for Squeezed States'. Phys. Rev. A **94**.5 (2016), p. 052135. arXiv:1611.01785.

[28] Valentina Danieli and Jerôme Martin. *Leggett-Garg Inequality Violation for the Cosmological Perturbations*. In preparation. 2024.

[29] R.L. Hudson. 'When is the wigner quasi-probability density non-negative?' Reports on Mathematical Physics **6**.2 (1974), pp. 249–252.

[30] Daniel Green and Rafael A. Porto. 'Signals of a Quantum Universe'. Phys. Rev. Lett. **124**.25 (2020), p. 251302. arXiv:2001.09149.

[31] Valentina Danieli, Nicola Bartolo, Sabino Matarrese, Angelo Ricciardone and Matteo Viel. *Quantum Signatures in Graviton Bispectrum*. In preparation. 2024.

[32] David Wands. 'Multiple field inflation'. Lect. Notes Phys. **738** (2008), pp. 275–304. arXiv:astro-ph/0702187.

[33] C. P. Burgess, R. Holman, G. Tasinato and M. Williams. 'EFT Beyond the Horizon: Stochastic Inflation and How Primordial Quantum Fluctuations Go Classical'. JHEP **03** (2015), p. 090. arXiv:1408.5002.

[34] Jerome Martin and Vincent Vennin. 'Observational constraints on quantum decoherence during inflation'. JCAP **05** (2018), p. 063. arXiv:1801.09949.

[35] Thomas Colas, Julien Grain and Vincent Vennin. 'Benchmarking the cosmological master equations'. Eur. Phys. J. C **82**.12 (2022), p. 1085. arXiv:2209.01929.

[36] C. P. Burgess, Thomas Colas, R. Holman, Greg Kaplanek and Vincent Vennin. 'Cosmic Purity Lost: Perturbative and Resummed Late-Time Inflationary Decoherence' (2024). arXiv:2403.12240.

[37] Cliff P. Burgess, R. Holman and D. Hoover. 'Decoherence of inflationary primordial fluctuations'. Phys. Rev. D **77** (2008), p. 063534. arXiv:astro-ph/0601646.

[38] C. P. Burgess, R. Holman, Greg Kaplanek, Jerome Martin and Vincent Vennin. 'Minimal decoherence from inflation'. JCAP **07** (2023), p. 022. arXiv:2211.11046.

[39] Valentina Danieli, Takeshi Kobayashi, Nicola Bartolo, Sabino Matarrese and Matteo Viel. 'Anharmonic effects on the squeezing of axion perturbations'. JCAP **04** (2024), p. 058. arXiv:2309.13112.

[40] Steven Weinberg. *Cosmology*. 2008.

[41] Daniel Baumann. *Cosmology*. Cambridge University Press, 2022.

[42] Edward W. Kolb and Michael S. Turner, eds. *THE EARLY UNIVERSE. REPRINTS*. 1988.

[43] Scott Dodelson. *Modern Cosmology*. Amsterdam: Academic Press, 2003.

[44] Sean M. Carroll. *Spacetime and Geometry: An Introduction to General Relativity*. Cambridge University Press, 2019.

[45] Albert Einstein. 'Die Feldgleichungen der Gravitation'. Sitzungsberichte der Königlich Preussischen Akademie der Wissenschaften (1915), pp. 844–847.

[46] Steven Weinberg. *Gravitation and Cosmology: Principles and Applications of the General Theory of Relativity*. New York: John Wiley and Sons, 1972.

[47] Edwin Hubble. 'A relation between distance and radial velocity among extra-galactic nebulae'. Proc. Nat. Acad. Sci. **15** (1929), pp. 168–173.

[48] N. Aghanim et al. 'Planck 2018 results. VIII. Gravitational lensing'. Astron. Astrophys. **641** (2020), A8. arXiv:1807.06210.

[49] Georges Lemaitre. 'A Homogeneous Universe of Constant Mass and Growing Radius Accounting for the Radial Velocity of Extragalactic Nebulae'. Annales Soc. Sci. Bruxelles A **47** (1927), pp. 49–59.

[50] Arno A. Penzias and Robert Woodrow Wilson. 'A Measurement of excess antenna temperature at 4080-Mc/s'. Astrophys. J. **142** (1965), pp. 419–421.

[51] R. H. Dicke, P. J. E. Peebles, P. G. Roll and D. T. Wilkinson. 'Cosmic Black-Body Radiation'. Astrophys. J. **142** (1965), pp. 414–419.

[52] P. A. R. Ade et al. 'Planck 2015 results. XVI. Isotropy and statistics of the CMB'. Astron. Astrophys. **594** (2016), A16. arXiv:1506.07135.

[53] N. Aghanim et al. 'Planck 2018 results. I. Overview and the cosmological legacy of Planck'. Astron. Astrophys. **641** (2020), A1. arXiv:1807.06205.

[54] N. Aghanim et al. 'Planck 2018 results. VI. Cosmological parameters'. Astron. Astrophys. **641** (2020). [Erratum: Astron.Astrophys. 652, C4 (2021)], A6. arXiv:1807.06209.

[55] Cyril Pitrou, Alain Coc, Jean-Philippe Uzan and Elisabeth Vangioni. 'Precision big bang nucleosynthesis with improved Helium-4 predictions'. Phys. Rept. **754** (2018), pp. 1–66. arXiv:1801.08023.

[56] Gianfranco Bertone, Dan Hooper and Joseph Silk. 'Particle dark matter: Evidence, candidates and constraints'. Phys. Rept. **405** (2005), pp. 279–390. arXiv:hep-ph/0404175.

[57] F. Zwicky. 'Die Rotverschiebung von extragalaktischen Nebeln'. Helv. Phys. Acta **6** (1933), pp. 110–127.

[58] Adam G. Riess et al. 'Observational evidence from supernovae for an accelerating universe and a cosmological constant'. Astron. J. **116** (1998), pp. 1009–1038. arXiv:astro-ph/9805201.

[59] S. Perlmutter et al. 'Measurements of Ω and Λ from 42 High Redshift Supernovae'. Astrophys. J. **517** (1999), pp. 565–586. arXiv:astro-ph/9812133.

[60] Alan H. Guth. 'The Inflationary Universe: A Possible Solution to the Horizon and Flatness Problems'. Phys. Rev. D **23** (1981). Ed. by Li-Zhi Fang and R. Ruffini, pp. 347–356.

[61] Andrei D. Linde. 'A New Inflationary Universe Scenario: A Possible Solution of the Horizon, Flatness, Homogeneity, Isotropy and Primordial Monopole Problems'. Phys. Lett. B **108** (1982). Ed. by Li-Zhi Fang and R. Ruffini, pp. 389–393.

[62] Andreas Albrecht and Paul J. Steinhardt. 'Cosmology for Grand Unified Theories with Radiatively Induced Symmetry Breaking'. Phys. Rev. Lett. **48** (1982). Ed. by Li-Zhi Fang and R. Ruffini, pp. 1220–1223.

[63] F. Lucchin and S. Matarrese. 'Power Law Inflation'. Phys. Rev. D **32** (1985), p. 1316.

[64] Jinn-Ouk Gong. 'Multi-field inflation and cosmological perturbations'. Int. J. Mod. Phys. D **26**.01 (2016), p. 1740003. arXiv:1606.06971.

[65] Oskar Klein. 'Quantum Theory and Five-Dimensional Theory of Relativity. (In German and English)'. Z. Phys. **37** (1926). Ed. by J. C. Taylor, pp. 895–906.

[66] W. Gordon. 'Der Comptoneffekt nach der Schrödingerschen Theorie'. Z. Phys. **40**.1 (1926), pp. 117–133.

[67] A. D. Dolgov and Andrei D. Linde. 'Baryon Asymmetry in Inflationary Universe'. Phys. Lett. B **116** (1982), p. 329.

[68] Jennie H. Traschen and Robert H. Brandenberger. 'Particle Production During Out-of-equilibrium Phase Transitions'. Phys. Rev. D **42** (1990), pp. 2491–2504.

[69] Andreas Albrecht, Paul J. Steinhardt, Michael S. Turner and Frank Wilczek. 'Reheating an Inflationary Universe'. Phys. Rev. Lett. **48** (1982), p. 1437.

[70] Lev Kofman, Andrei D. Linde and Alexei A. Starobinsky. 'Reheating after inflation'. Phys. Rev. Lett. **73** (1994), pp. 3195–3198. arXiv:hep-th/9405187.

[71] Lev Kofman, Andrei D. Linde and Alexei A. Starobinsky. 'Towards the theory of reheating after inflation'. Phys. Rev. D **56** (1997), pp. 3258–3295. arXiv:hep-ph/9704452.

[72] Mustafa A. Amin, Mark P. Hertzberg, David I. Kaiser and Johanna Karouby. 'Nonperturbative Dynamics Of Reheating After Inflation: A Review'. Int. J. Mod. Phys. D **24** (2014), p. 1530003. arXiv:1410.3808.

[73] R. K. Sachs and A. M. Wolfe. 'Perturbations of a cosmological model and angular variations of the microwave background'. Astrophys. J. **147** (1967), pp. 73–90.

[74] Viatcheslav F. Mukhanov and G. V. Chibisov. 'Quantum Fluctuations and a Nonsingular Universe'. JETP Lett. **33** (1981), pp. 532–535.

[75] V. F. Mukhanov and G. V. Chibisov. 'Energy of vacuum and the large-scale structure of the Universe.' Zhurnal Ehksperimental'noj i Teoreticheskoj Fiziki **83** (1982), pp. 475–487.

[76] Alexei A. Starobinsky. 'Dynamics of Phase Transition in the New Inflationary Universe Scenario and Generation of Perturbations'. Phys. Lett. B **117** (1982), pp. 175–178.

[77] Alan H. Guth and S. Y. Pi. 'Fluctuations in the New Inflationary Universe'. Phys. Rev. Lett. **49** (1982), pp. 1110–1113.

[78] James M. Bardeen, Paul J. Steinhardt and Micheal S. Turner. 'Spontaneous creation of almost scale-free density perturbations in an inflationary universe.' Phys. Rev. D **28** (1983), pp. 679–693.

[79] V. A. Rubakov, M. V. Sazhin and A. V. Veryaskin. 'Graviton Creation in the Inflationary Universe and the Grand Unification Scale'. Phys. Lett. B **115** (1982), pp. 189–192.

[80] Daniel Baumann. 'Inflation'. *Theoretical Advanced Study Institute in Elementary Particle Physics: Physics of the Large and the Small*. 2011, pp. 523–686. arXiv:0907.5424.

[81] Viatcheslav F. Mukhanov, H. A. Feldman and Robert H. Brandenberger. 'Theory of cosmological perturbations. Part 1. Classical perturbations. Part 2. Quantum theory of perturbations. Part 3. Extensions'. Phys. Rept. **215** (1992), pp. 203–333.

[82] Hideo Kodama and Misao Sasaki. 'Cosmological Perturbation Theory'. Progress of Theoretical Physics Supplement **78** (1984), pp. 1–166.

[83] James M. Bardeen. 'Gauge Invariant Cosmological Perturbations'. Phys. Rev. D **22** (1980), pp. 1882–1905.

[84] Andrew R. Liddle and D. H. Lyth. *Cosmological inflation and large scale structure*. 2000.

[85] L. P. Grishchuk and Jerome Martin. 'Best unbiased estimates for the microwave background anisotropies'. Phys. Rev. D **56** (1997), pp. 1924–1938. arXiv:gr-qc/9702018.

[86] P. A. R. Ade et al. 'Improved Constraints on Primordial Gravitational Waves using Planck, WMAP, and BICEP/Keck Observations through the 2018 Observing Season'. Phys. Rev. Lett. **127**.15 (2021), p. 151301. arXiv:2110.00483.

[87] Y. Akrami et al. 'Planck 2018 results. X. Constraints on inflation'. Astron. Astrophys. **641** (2020), A10. arXiv:1807.06211.

[88] N. D. Birrell and P. C. W. Davies. *Quantum Fields in Curved Space*. Cambridge Monographs on Mathematical Physics. Cambridge University Press, 1982.

[89] Viatcheslav Mukhanov and Sergei Winitzki. *Introduction to quantum effects in gravity*. Cambridge University Press, 2007.

[90] C. Lueders and J. E. Roberts. 'Local quasiequivalence and adiabatic vacuum states'. Commun. Math. Phys. **134** (1990), pp. 29–63.

[91] B. L. Hu, Gungwon Kang and A. Matacz. 'Squeezed vacua and the quantum statistics of cosmological particle creation'. Int. J. Mod. Phys. A **9** (1994), pp. 991–1008. arXiv:gr-qc/9312014.

[92] Esteban A. Calzetta and Bei-Lok B. Hu. *Nonequilibrium Quantum Field Theory*. Oxford University Press, 2009.

[93] Jerome Martin. 'Inflationary perturbations: The Cosmological Schwinger effect'. Lect. Notes Phys. **738** (2008), pp. 193–241. arXiv:0704.3540.

[94] Jerome Martin, Amaury Micheli and Vincent Vennin. 'Discord and decoherence'. JCAP **04**.04 (2022), p. 051. arXiv:2112.05037.

[95] Leonard Parker. 'Quantized fields and particle creation in expanding universes. 1.' Phys. Rev. **183** (1969), pp. 1057–1068.

[96] Carlton M. Caves and Bonny L. Schumaker. 'New formalism for two-photon quantum optics. 1. Quadrature phases and squeezed states'. Phys. Rev. A **31** (1985), pp. 3068–3092.

[97] Andreas Albrecht, Pedro Ferreira, Michael Joyce and Tomislav Prokopec. 'Inflation and squeezed quantum states'. Phys. Rev. D **50** (1994), pp. 4807–4820. arXiv:astro-ph/9303001.

[98] Amaury Micheli and Patrick Peter. 'Quantum cosmological gravitational waves?' (2022). arXiv:2211.00182.

[99] Jerome Martin, Vincent Vennin and Patrick Peter. 'Cosmological Inflation and the Quantum Measurement Problem'. Phys. Rev. D **86** (2012), p. 103524. arXiv:1207.2086.

[100] Julien Grain and Vincent Vennin. 'Canonical transformations and squeezing formalism in cosmology'. JCAP **02** (2020), p. 022. arXiv:1910.01916.

[101] E. Wigner. 'On the Quantum Correction For Thermodynamic Equilibrium'. Phys. Rev. **40** (5 1932), pp. 749–759.

[102] N. Mukunda, R. Simon and G. Sudarshan. 'Gaussian Wigner distributions in quantum mechanics and optics'. Phys. Rev. A **36** (1987), p. 3868.

[103] N. Mukunda, R. Simon and G. Sudarshan. 'Gaussian Wigner distributions: a complete characterization'. Phys. Lett. A **124** (1987), p. 223.

[104] W. Case. 'Wigner functions and Weyl transforms for pedestrians'. American Journal of Physics - AMER J PHYS **76** (2008).

[105] G. Adesso, S. Ragy and A. R. Lee. 'Continuous Variable Quantum Information: Gaussian States and Beyond'. Open Systems & Information Dynamics **21** (2014).

[106] Kenta Ando and Vincent Vennin. 'Bipartite temporal Bell inequalities for two-mode squeezed states'. Phys. Rev. A **102**.5 (2020), p. 052213. arXiv:2007.00458.

[107] M. Revzen, P. A. Mello, A. Mann and L. M. Johansen. 'Bell's inequality violation with non-negative Wigner functions'. Physical Review A **71**.2 (2005).

[108] R. Simon. 'Peres-Horodecki Separability Criterion for Continuous Variable Systems'. Phys. Rev. Lett. **84** (2000), pp. 2726–2729. arXiv:quant-ph/9909044.

[109] Gerardo Adesso and Animesh Datta. 'Quantum versus Classical Correlations in Gaussian States'. Phys. Rev. Lett. **105**.3 (2010), p. 030501.

[110] Paolo Giorda and Matteo G. A. Paris. 'Gaussian Quantum Discord'. Phys. Rev. Lett. **105**.2 (2010), p. 020503.

[111] Stefano Pirandola, Gaetana Spedalieri, Samuel L. Braunstein, Nicolas J. Cerf and Seth Lloyd. 'Optimality of Gaussian Discord'. Physical Review Letters **113**.14 (2014).

[112] J. S. Bell. 'On the Einstein-Podolsky-Rosen paradox'. Physics Physique Fizika **1** (1964), pp. 195–200.

[113] Alain Aspect, Philippe Grangier and Gerard Roger. 'Experimental realization of Einstein-Podolsky-Rosen-Bohm Gedankenexperiment: A New violation of Bell's inequalities'. Phys. Rev. Lett. **49** (1982), pp. 91–97.

[114] Alain Aspect, Jean Dalibard and Gerard Roger. 'Experimental test of Bell's inequalities using time varying analyzers'. Phys. Rev. Lett. **49** (1982), pp. 1804–1807.

[115] Gregor Weihs, Thomas Jennewein, Christoph Simon, Harald Weinfurter and Anton Zeilinger. 'Violation of Bell's inequality under strict Einstein locality conditions'. Phys. Rev. Lett. **81** (1998), pp. 5039–5043. arXiv:quant-ph/9810080.

[116] A. Einstein, B. Podolsky and N. Rosen. 'Can Quantum-Mechanical Description of Physical Reality Be Considered Complete?' Phys. Rev. **47** (10 1935), pp. 777–780.

[117] B. S. Cirelson. 'QUANTUM GENERALIZATIONS OF BELL'S INEQUALITY'. Lett. Math. Phys. **4** (1980), pp. 93–100.

[118] Zeng-Bing Chen, Jian-Wei Pan, Guang Hou and Yong-De Zhang. 'Maximal Violation of Bell's Inequalities for Continuous Variable Systems'. Phys. Rev. Lett. **88** (4 2002), p. 040406.

[119] Michael Revzen. 'The Wigner Function as Distribution Function'. Foundations of Physics **36** (2006), pp. 546–562.

[120] Jan-Åke Larsson. 'Bell Inequalities for Position Measurements'. Phys. Rev. A **70** (2004), p. 022102. arXiv:quant-ph/0310140.

[121] Llorenç Espinosa-Portalés and Vincent Vennin. 'Real-space Bell inequalities in de Sitter'. JCAP **07**.07 (2022), p. 037. arXiv:2203.03505.

[122] A. J. Leggett and Anupam Garg. 'Quantum mechanics versus macroscopic realism: Is the flux there when nobody looks?' Phys. Rev. Lett. **54** (1985), pp. 857–860.

[123] Tobias Fritz. 'Quantum correlations in the temporal Clauser – Horne – Shimony – Holt (CHSH) scenario'. New Journal of Physics **12**.8 (2010), p. 083055.

[124] Y. Akrami et al. 'Planck 2018 results. IX. Constraints on primordial non-Gaussianity'. Astron. Astrophys. **641** (2020), A9. arXiv:1905.05697.

[125] Kari Enqvist and Martin S. Sloth. 'Adiabatic CMB perturbations in pre - big bang string cosmology'. Nucl. Phys. B **626** (2002), pp. 395–409. arXiv:hep-ph/0109214.

[126] David H. Lyth, Carlo Ungarelli and David Wands. 'The Primordial density perturbation in the curvaton scenario'. Phys. Rev. D **67** (2003), p. 023503. arXiv:astro-ph/0208055.

[127] David H. Lyth and David Wands. 'Generating the curvature perturbation without an inflaton'. Phys. Lett. B **524** (2002), pp. 5–14. arXiv:hep-ph/0110002.

[128] Silvia Mollerach. 'Isocurvature Baryon Perturbations and Inflation'. Phys. Rev. D **42** (1990), pp. 313–325.

[129] Takeo Moroi and Tomo Takahashi. 'Effects of cosmological moduli fields on cosmic microwave background'. Phys. Lett. B **522** (2001). [Erratum: Phys.Lett.B 539, 303–303 (2002)], pp. 215–221. arXiv:hep-ph/0110096.

[130] N. Bartolo, S. Matarrese and A. Riotto. 'On nonGaussianity in the curvaton scenario'. Phys. Rev. D **69** (2004), p. 043503. arXiv:hep-ph/0309033.

[131] N. Bartolo, S. Matarrese and A. Riotto. 'Nongaussianity from inflation'. Phys. Rev. D **65** (2002), p. 103505. arXiv:hep-ph/0112261.

[132] N. Bartolo, E. Komatsu, Sabino Matarrese and A. Riotto. 'Non-Gaussianity from inflation: Theory and observations'. Phys. Rept. **402** (2004), pp. 103–266. arXiv:astro-ph/0406398.

[133] Daniel Babich, Paolo Creminelli and Matias Zaldarriaga. 'The Shape of non-Gaussianities'. JCAP **08** (2004), p. 009. arXiv:astro-ph/0405356.

[134] Eiichiro Komatsu and David N. Spergel. 'Acoustic signatures in the primary microwave background bispectrum'. Phys. Rev. D **63** (2001), p. 063002. arXiv:astro-ph/0005036.

[135] Francis Bernardeau and Jean-Philippe Uzan. 'NonGaussianity in multifield inflation'. Phys. Rev. D **66** (2002), p. 103506. arXiv:hep-ph/0207295.

[136] Francis Bernardeau and Jean-Philippe Uzan. 'Inflationary models inducing non-Gaussian metric fluctuations'. Phys. Rev. D **67** (2003), p. 121301. arXiv:astro-ph/0209330.

[137] Christian T. Byrnes and David Wands. 'Curvature and isocurvature perturbations from two-field inflation in a slow-roll expansion'. Phys. Rev. D **74** (2006), p. 043529. arXiv:astro-ph/0605679.

[138] Christian T. Byrnes, Ki-Young Choi and Lisa M. H. Hall. 'Conditions for large non-Gaussianity in two-field slow-roll inflation'. JCAP **10** (2008), p. 008. arXiv:0807.1101.

[139] Jussi Valiviita, Hooshyar Assadullahi, David Wands and David Wands. 'Primordial non-gaussianity from multiple curvaton decay'. *43rd Rencontres de Moriond: Cosmology*. Vietnam: The Gioi, 2008, pp. 279–282. arXiv:0806.0623.

[140] Filippo Vernizzi and David Wands. 'Non-gaussianities in two-field inflation'. JCAP **05** (2006), p. 019. arXiv:astro-ph/0603799.

[141] Laura E. Allen, Sujata Gupta and David Wands. 'Non-gaussian perturbations from multi-field inflation'. JCAP **01** (2006), p. 006. arXiv:astro-ph/0509719.

[142] Andrei D. Linde and Viatcheslav F. Mukhanov. 'Nongaussian isocurvature perturbations from inflation'. Phys. Rev. D **56** (1997), R535–R539. arXiv:astro-ph/9610219.

[143] Paolo Creminelli and Matias Zaldarriaga. 'Single field consistency relation for the 3-point function'. JCAP **10** (2004), p. 006. arXiv:astro-ph/0407059.

[144] Clifford Cheung, Paolo Creminelli, A. Liam Fitzpatrick, Jared Kaplan and Leonardo Senatore. 'The Effective Field Theory of Inflation'. JHEP **03** (2008), p. 014. arXiv:0709.0293.

[145] Paolo Creminelli, Alberto Nicolis, Leonardo Senatore, Max Tegmark and Matias Zaldarriaga. 'Limits on non-gaussianities from wmap data'. JCAP **05** (2006), p. 004. arXiv:astro-ph/0509029.

[146] Juan Martin Maldacena. 'Non-Gaussian features of primordial fluctuations in single field inflationary models'. JHEP **05** (2003), p. 013. arXiv:astro-ph/0210603.

[147] Viviana Acquaviva, Nicola Bartolo, Sabino Matarrese and Antonio Riotto. 'Second order cosmological perturbations from inflation'. Nucl. Phys. B **667** (2003), pp. 119–148. arXiv:astro-ph/0209156.

[148] Toby Falk, Raghavan Rangarajan and Mark Srednicki. 'The Angular dependence of the three point correlation function of the cosmic microwave background radiation as predicted by inflationary cosmologies'. Astrophys. J. Lett. **403** (1993), p. L1. arXiv:astro-ph/9208001.

[149] Alejandro Gangui, Francesco Lucchin, Sabino Matarrese and Silvia Mollerach. 'The Three point correlation function of the cosmic microwave background in inflationary models'. Astrophys. J. **430** (1994), pp. 447–457. arXiv:astro-ph/9312033.

[150] Xingang Chen. 'Primordial Non-Gaussianities from Inflation Models'. Adv. Astron. **2010** (2010), p. 638979. arXiv:1002.1416.

[151] Steven Weinberg. 'Quantum contributions to cosmological correlations'. Phys. Rev. D **72** (2005), p. 043514. arXiv:hep-th/0506236.

[152] Michael E. Peskin and Daniel V. Schroeder. *An Introduction to quantum field theory*. Reading, USA: Addison-Wesley, 1995.

[153] Arjun Berera. 'Warm inflation'. Phys. Rev. Lett. **75** (1995), pp. 3218–3221. arXiv:astro-ph/9509049.

[154] Diana Lopez Nacir, Rafael A. Porto, Leonardo Senatore and Matias Zaldarriaga. 'Dissipative effects in the Effective Field Theory of Inflation'. JHEP **01** (2012), p. 075. arXiv:1109.4192.

[155] Diana Lopez Nacir, Rafael A. Porto and Matias Zaldarriaga. 'The consistency condition for the three-point function in dissipative single-clock inflation'. JCAP **09** (2012), p. 004. arXiv:1206.7083.

[156] Gustavo Joaquin Turiaci and Matias Zaldarriaga. 'Non-Gaussianities in Dissipative EFT of Inflation Coupled to a Fluid' (2013). arXiv:1310.4531.

[157] Fernando C. Lombardo and Diana Lopez Nacir. 'Decoherence during inflation: The Generation of classical inhomogeneities'. Phys. Rev. D **72** (2005), p. 063506. arXiv:gr-qc/0506051.

[158] Patrick Martineau. 'On the decoherence of primordial fluctuations during inflation'. Class. Quant. Grav. **24** (2007), pp. 5817–5834. arXiv:astro-ph/0601134.

[159] David Campo and Renaud Parentani. 'Decoherence and entropy of primordial fluctuations. I: Formalism and interpretation'. Phys. Rev. D **78** (2008), p. 065044. arXiv:0805.0548.

[160] Andreas Ringwald. 'Exploring the Role of Axions and Other WISPs in the Dark Universe'. Phys. Dark Univ. **1** (2012), pp. 116–135. arXiv:1210.5081.

[161] David J. E. Marsh. 'Axions and ALPs: a very short introduction'. *13th Patras Workshop on Axions, WIMPs and WISPs*. 2018, pp. 59–74. arXiv:1712.03018.

[162] Jérôme Martin and Vincent Vennin. 'Non Gaussianities from Quantum Decoherence during Inflation'. JCAP **06** (2018), p. 037. arXiv:1805.05609.

[163] Aoumeur Daddi Hammou and Nicola Bartolo. 'Cosmic decoherence: primordial power spectra and non-Gaussianities'. JCAP **04** (2023), p. 055. arXiv:2211.07598.

[164] R. D. Peccei and Helen R. Quinn. 'CP Conservation in the Presence of Instantons'. Phys. Rev. Lett. **38** (1977), pp. 1440–1443.

[165] Steven Weinberg. 'A New Light Boson?' Phys. Rev. Lett. **40** (1978), pp. 223–226.

[166] Frank Wilczek. 'Problem of Strong P and T Invariance in the Presence of Instantons'. Phys. Rev. Lett. **40** (1978), pp. 279–282.

[167] Jondalar L. J. Kuß and David J. E. Marsh. 'Squeezing the Axion'. Open J. Astrophys. **4** (2021), p. 2021. arXiv:2106.03528.

[168] Sugumi Kanno and Jiro Soda. 'Squeezed quantum states of graviton and axion in the universe'. Int. J. Mod. Phys. D **31**.13 (2022), p. 2250098. arXiv:2112.14496.

[169] Masahiro Kawasaki, Takeshi Kobayashi and Fuminobu Takahashi. 'Non-Gaussianity from Curvatons Revisited'. Phys. Rev. D **84** (2011), p. 123506. arXiv:1107.6011.

[170] Takeshi Kobayashi, Riccardo Murgia, Andrea De Simone, Vid Iršič and Matteo Viel. 'Lyman-α constraints on ultralight scalar dark matter: Implications for the early and late universe'. Phys. Rev. D **96**.12 (2017), p. 123514. arXiv:1708.00015.

[171] Igor Garcia Irastorza. 'An introduction to axions and their detection'. SciPost Phys. Lect. Notes **45** (2022), p. 1. arXiv:2109.07376.

[172] Sugumi Kanno, Jiro Soda and Junsei Tokuda. 'Indirect detection of gravitons through quantum entanglement'. Phys. Rev. D **104**.8 (2021), p. 083516. arXiv:2103.17053.

[173] Daniel Carney, Holger Müller and Jacob M. Taylor. 'Using an Atom Interferometer to Infer Gravitational Entanglement Generation'. PRX Quantum **2**.3 (2021). [Erratum: PRX Quantum 3, 010902 (2022)], p. 030330. arXiv:2101.11629.

[174] Luca Abrahao, Francesco Coradeschi, Antonia Micol Frassino, Thiago Guerreiro, Jennifer Rittenhouse West and Enrico Schioppa Junior. 'The quantum optics of gravitational waves'. Class. Quant. Grav. **41**.1 (2024), p. 015029. arXiv:2308.12713.

[175] Daniel Carney, Valerie Domcke and Nicholas L. Rodd. 'Graviton detection and the quantization of gravity'. Phys. Rev. D **109**.4 (2024), p. 044009. arXiv:2308.12988.

COLOPHON

The cover is taken from a picture by:
Mike Zeng, for *Quanta Magazine*, an editorially independent online publication launched by the Simons Foundation in 2012;

www.quantamagazine.org

This document was typeset using the typographical look-and-feel `classicthesis` developed by André Miede. The style was inspired by Robert Bringhurst's seminal book on typography "*The Elements of Typographic Style*". `classicthesis` is available for both LaTeX and LyX:

`https://bitbucket.org/amiede/classicthesis/`

Final Version as of 20th September 2024 (`classicthesis`).